AMBIGUOUS POLYMERIC SURFACES FOR MARINE ANTI-FOULING APPLICATIONS

A Dissertation

Presented to the Faculty of the Graduate School

of Cornell University

In Partial Fulfillment of the Requirements for the Degree of

Doctor of Philosophy

by

Craig Jonathan Weinman

May 2009

AMBIGUOUS POLYMERIC SURFACES FOR MARINE ANTI-FOULING APPLICATIONS

Craig Jonathan Weinman, Ph. D.

Cornell University 2009

Marine biofouling is defined as the undesirable accumulation of biomacromolecules, microbial slimes, plants, and animals on a surface immersed in seawater. Due to the extra surface area and roughness generated by biofouling, vessels moving through the ocean require more energy to overcome frictional forces. Consequently, significant savings in both fuel consumption and emissions can be realized by combating biofouling. While traditional methods of biofouling control have generally incorporated ablative metallic biocide containing materials, these coatings are now being phased out due to their inherent risk to the environment. This has opened the door for the development of novel polymeric materials, dependant on a combination of surface chemistry and bulk modulus, as a means of marine fouling control.

This dissertation will explore the development, characterization and assay of several different multilayer polymeric coatings consisting of a relatively thick low modulus poly(styrene)-*block*-poly(ethylene-*ran*-butylene)-*block*-poly(styrene) (SEBS) thermoplastic elastomer base layer and a relatively thin surface active block copolymer (SABC) consisting of poly(styrene) and a functional block derived from either poly(acrylic acid) or poly(isoprene). Additionally, a fundamental study comparing the performance of surfaces functionalized with polymer brushes to surfaces functionalized with self-assembled monolayers will be presented.

Bulk chemical characterization of the materials produced will be related using methods including ^{1}H NMR spectroscopy, Fourier transform infrared (FTIR)

spectroscopy, elemental analysis, and gel permeation chromatography. Surface characterization of the materials produced meanwhile will be presented using X-ray photoelectron spectroscopy (XPS), dynamic water contact angle analysis, and near-edge X-ray adsorption fine structure (NEXAFS) measurements. Biofouling performance meanwhile will be evaluated using a combination of biofouling assays including settlement and release of the green alga *Ulva* and the diatom *Navicula* and tests of the adhesion characteristics of the protein bovine serum albumin (BSA). Correlations between surface chemistry, coating modulus, and fouling settlement and release behavior will be identified and specific conclusions on the fouling performance of these various coating formulations will be reported on.

BIOGRAPHICAL SKETCH

After graduating third in his class at Yorktown High School, in Yorktown Heights, New York, Craig Jonathan Weinman decided to attend a small, liberal arts college in Lexington, Virginia called Washington & Lee University. After flirting with the idea of studying Neuroscience and going Pre-Med, Craig decided to pursue a Bachelors of Science in Chemistry-Engineering, and graduated in 2003. While at Washington & Lee, he performed research in the area of immiscible polymer blends with Professor Kenneth Van Ness and quickly developed a desire to continue work in the field of polymer science. Fortunately, Craig also rekindled his love for the outdoors while spending four years in the beautiful Shenandoah Valley. In 2003, he moved to Ithaca, New York and began his studies at Cornell University in the Department of Materials Science & Engineering and started working towards a doctorate under the supervision of Professor Christopher Ober. While at Cornell, Craig's work has focused primarily on the development of marine antifouling and/or fouling-release coatings through the synthesis and functionalization of block copolymers through polymer analogous reactions. Of course it was hard to find time to do all of that research with the gorges and lakes of central New York to explore and the Catskills and Adirondacks a day trip away. It has been a long road, but the next chapter is already in place with a planned move to Chandler, Arizona and a job with a small company called Intel. The real concern of course is how will Craig ever find time to explore everything the western US has to offer?

To my wonderful, loving wife Caitlin who has done her best to be there every step of the way and my parents who apparently did a pretty good job!

ACKNOWLEDGMENTS

First, I would like to thank all of the Ober group members, past and present who have helped pave the way for this work and helped lay a great foundation to build upon. In particular I would like to thank Sitaraman Krishnan who spent more time than he ever should have walking me through things while I was just starting out, and Marvin Paik who is not just a great coworker and collaborator, but also a truly great and dear friend.

Additionally, I would like to mention that this work was supported in part by the United States Department of Defense's Strategic Environmental Research and Development Program (SERDP), grant WP #1454 with additional support from the Office of Naval Research (ONR) through award #N00014-02-1-0170. It has been an honor to be part of these broad, collaborative projects and I am thankful for all of the great, supportive people I have had a chance to work with at different institutions. Additionally, I would like to thank the staff who has helped along the way at the Cornell NanoScale Facility (CNF), Cornell Center for Materials Research (CCMR), and Nanobiotechnology Center (NBTC).

TABLE OF CONTENTS

LIST OF FIGURES

LIST OF TABLES

CHAPTER 1

BACKGROUND ON BIOFOULING WITH EMPHASIS ON MARINE APPLICATIONS

Abstract

Polymers containing tethered biocides, self-assembling polymers, nanostructured polymer thin films, and topographically patterned PDMS elastomers are being actively explored as advanced coatings for marine and biomedical applications. This introductory chapter highlights recent advances in the design and synthesis of polymeric materials that can resist fouling by biomolecules, cells and organisms. Current understanding of the mechanisms of anti-biofouling activity is also discussed.

Introduction

Anti-biofouling surfaces are key components of several current and forward technologies. Applications for anti-biofouling surfaces range from coatings for marine vessels[1-5] and biomedical implants,[6] to biosensors[7] and carriers for targeted drug delivery.[8-10] Due to the breadth of the field and since this thesis will focus primarily on the development of new anti-biofouling and fouling release coatings with regards to marine applications, the following review will focus chiefly on materials used in this sector.

For marine applications, the realm of anti-biofouling surfaces can be divided into three major subclasses. The first is ablative coatings that release toxic moieties such as tributyl tin (TBT) or copper through leaching, effectively poisoning and ultimately killing fouling organisms that come in contact with the local environment

of the coating. These coatings have been found to have several significant problems associated with them however, including lack of selectivity towards target organisms[11] and the resultant build up of toxins in the environment. Thus, tributyltin has already been banned most places in the world[12] and the marine community is already desperately seeking alternatives to copper based coatings fearing similar future action against them. For these reasons, ablative TBT and copper derived coatings will not be discussed further in this introductory chapter.

Another major class of antifouling coatings is those containing some tethered toxic biocidal chemical functionality capable of poisoning and/or disrupting fouling organisms. The advantage of these coatings over ablative systems is that the toxic moieties are not readily released into the environment, and thus can be more selective towards the organisms only interacting with the surface undergoing fouling. Several examples include polymers containing tethered quaternary ammonium groups,[13-15] and polymers containing tethered antibiotic compounds.[16-18] A few specific examples applied to marine biofouling as reported in literature will be examined in the following introductory chapter.

The final area of interest is coatings that control biofouling through non-toxic, passive means. Since this thesis will focus primarily on coatings derived to work in this fashion, the bulk of the following discussion will concern these materials. Many non-toxic antifouling surfaces are based on the minimization of intermolecular forces of interaction between extracellular biomolecules and the surface in question. This allows the facile removal of an adhered cell under low applied shear stresses. An alternative type of antifouling surface frequently referred to as a “stealth surface,” can actually remain undetected by cells in a biological environment and therefore is not prone to biofouling. To date, research on cell-material interactions has determined two main classes of non-toxic coatings capable of resisting biofouling. Hydrophobic

surfaces such as those of poly(dimethylsiloxane) (PDMS) are known to demonstrate robust fouling release properties, while hydrophilic surfaces of polymers such as poly(ethylene glycol) (PEG), distinguished by low values of polymer-water interfacial energy, show resistance to protein adsorption and cell adhesion. This value of interfacial energy between a surface and water is expected to play a very important role in bestowing antifouling characteristics to a surface.[19] Non-polar hydrophobic surfaces exhibit high values of interfacial energy with water. For instance, the interfacial energy of PDMS with water is about 52 mJ/m^2.[1] In comparison, the water interfacial energy of polar polymers such as PEG or poly(2-hydroxyethyl methacrylate) (PHEMA) is below 5 mJ/m^2.[20, 21] For this reason, when a hydrophobic surface comes in contact with a biological interface, amphiphilic biomolecules such as proteins readily adsorb on the surface to minimize this value of interfacial energy. Nonetheless, non-polar surfaces of elastomeric polymers such as PDMS have been widely explored as fouling release coatings since their low modulus in conjunction with their low values of surface energy allow the adhered fouling molecules or organisms to be readily detached from the surface at low forces of applied shear. In the case of hydrophilic surfaces however, the adsorption of biomolecules does not confer any significant thermodynamic advantage because the interfacial energy is already low. For this reason, these surfaces generally show resistance to protein adsorption and cellular adhesion.

Figure 1.1 depicts the general concept of an anti-biofouling surface using the example of zoospores of the marine green alga *Ulva*. *Ulva* is a ubiquitous, predominant fouling species in marine biofilms. Motile zoospores of *Ulva* are capable of swimming and exploring their environment using whip-like whiskers called flagella, actively seeking a suitable surface for settlement. Upon detection of a surface with desirable properties, the spore attaches to the substrate by its anterior flagellated end

and both adsorbs the flagella into the protoplasm and secretes a glycoprotein adhesive present in membrane bound cytoplasmic vesicles (depicted in Figure 1.1a).[22] Following spore settlement and attachment, germination gives rise to sporelings (young plants) which further adhere to the substrate using adhesives secreted by rhizoids. An anti-biofouling surface meanwhile can prevent detection of the surface by the *Ulva* zoospores and prevent subsequent settlement and attachment (Figure 1.1b). In the case of a fouling release surface (not pictured), easy release of the adhesive pad under low to moderate shear stresses generated by the flow of water past the surface or mechanical cleaning yields detachment of the fouling organisms from the substrate.

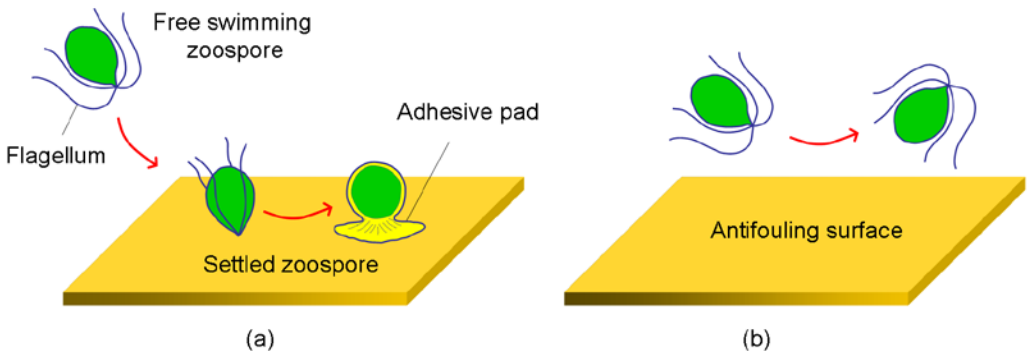

Figure 1.1. (a) Settlement and adhesion of a zoospore of the green alga *Ulva* on a surface prone to biofouling. (b) Spore behavior near an antifouling surface. Original figure from S. Krishnan, C. J. Weinman, C. K. Ober, *J. Mater. Chem.*, 2008, **18**, 3405 – Reproduced by permission of the Royal Society of Chemistry.

Current advances in macromolecular synthesis and self-assembly has led to the exploration of polymers and other novel materials for use as anti-biofouling surfaces. The performance of these surfaces is based on low interfacial energy with water, low intermolecular forces of interaction with biomolecules, or in some cases, both of these properties. The purpose of this introductory chapter will be to highlight novel polymer

and material architectures and surface modification strategies that impart antifouling or fouling release characteristics to a surface. Figure 1.2 summarizes the three major non-toxic approaches to make a surface resistant to biofouling. Much of this work is part of two major research efforts, one funded by the US Office of Naval Research (http://www.onr.navy.mil) and the other by the European Community through its AMBIO (Advanced Nanostructured Surfaces for the Control of Biofouling) program (http://www.ambio.bham.ac.uk)[23]. Both programs are actively studying new concepts in environmentally friendly fouling prevention, which are desperately required to replace traditional inherently toxic metal-based systems of fouling control.

The following introductory chapter will summarize different approaches taken by various research groups to combat the challenge of forming anti-biofouling and fouling release surfaces. Particular attention will be paid to the chemical structures produced and the various techniques utilized to demonstrate these surfaces' inherent anti-biofouling character. To facilitate understanding of the breadth of the fouling problem, an overview of the development of a marine biofouling community will also be presented. The performance evaluation of these antifouling polymers has been greatly facilitated by marine biologists including the research groups of Professor James Callow (University of Birmingham) which study settlement and adhesion of marine algae, and Professors Dean Wendt (California Polytechnic State University), Geoff Swain (Florida Institute of Technology), and Anthony Clare (New Castle University) who conduct laboratory and field assays involving barnacles and other marine organisms. While the primary focus of this introductory chapter will be on the role of materials chemistry in anti-biofouling, there are other promising antifouling approaches that rely solely on modifying the physical characteristics of the coating. A prominent outcome of the latter approach is a shark-skin inspired PDMS coating utilizing the Sharklet AF^{TM} microtopography. This approach was pioneered by the

research group of Professor Anthony Brennan (University of Florida).[24, 25] Several such 3D coatings (figure 2) based on microtopography manipulation will be further discussed.

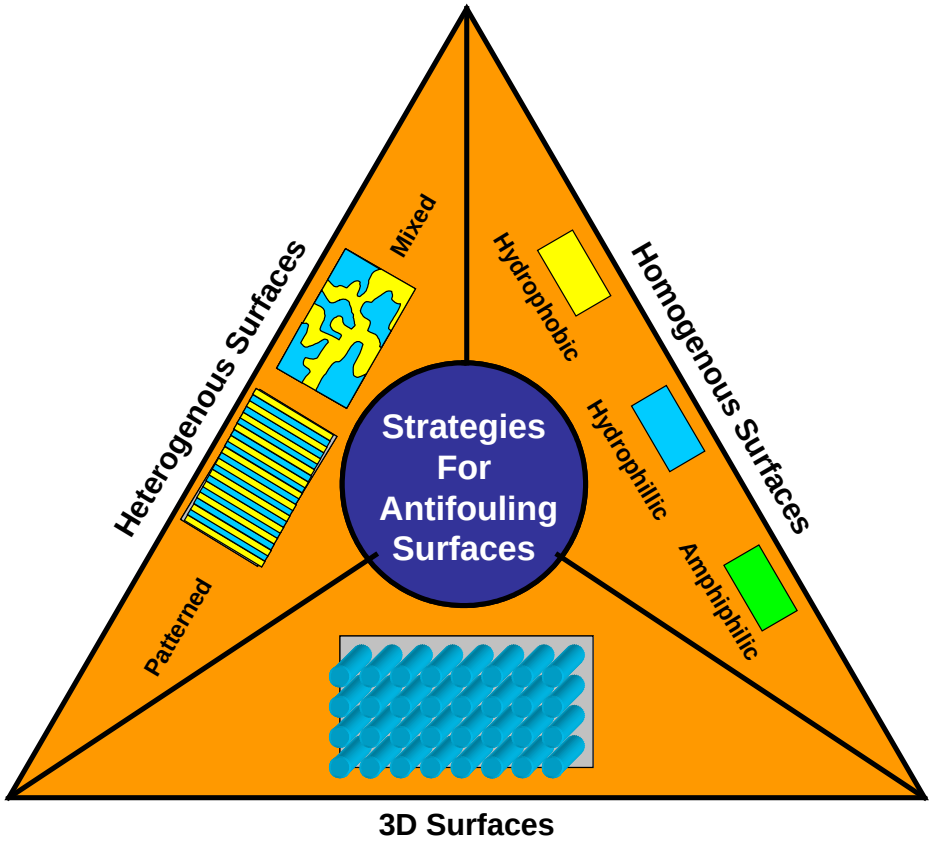

Figure 1.2. Three major approaches to producing anti-biofouling surfaces. Homogenous surfaces of hydrophilic (blue), hydrophobic (yellow), or amphiphilic (green) character can be utilized. Protein and cell resistant hydrophilic surfaces help to avoid the settlement of fouling organisms in the first place. The inherent "slipperiness" of non-polar low surface energy, hydrophobic coatings leads to facile release. In combination with low surface modulus, these coatings can aid the detachment of settled organisms under applied shear flow. Amphiphilic surfaces with chemical or textural complexity can effectively "confuse" fouling organisms into avoiding settlement and are effective against a vast range of biomolecules, cells, and organisms in a biological environment. Mixed or patterned surfaces of alternating hydrophobic and hydrophilic character can also be utilized due to their intricacy. Finally, 3D surfaces can be used to modify the surface of an anti-biofouling coating by control of surface topography. This factor can influence the ability of marine organisms to stick to the coating surface. Original figure from S. Krishnan, C. J. Weinman, C. K. Ober, *J. Mater. Chem.*, 2008, **18**, 3405 – Reproduced by permission of the Royal Society of Chemistry.

Marine Biofouling: Mechanisms and Consequences

Over 4000 different species of marine fouling organism have been identified.[26] While this number highlights the difficulties experienced in producing a universal coating system able to resist and/or release the broadest range possible of marine organisms, it is still a very small proportion relative to all known marine organisms. This is because only organisms that have adapted to tolerate wide fluctuations in environmental conditions such as temperature, water flow and salinity can effectively survive as fouling organisms.[27]

Four distinct steps have been identified in the development of a fully mature fouling community. Upon immersing a clean surface in water it adsorbs a "conditioning film" almost instantaneously consisting of various organic molecules such as polysaccharides, proteins and proteoglycans and possibly even inorganic compounds.[28, 29] Development of this conditioning film is primarily a physical process governed by forces such as Brownian motion, electrostatic interaction and van der Waals forces. Once modified with this conditioning film, a surface is rapidly colonized by bacteria and single-cell diatoms, both examples of primary fouling organisms. These species are first adsorbed onto the surface in primarily physical means, but once further colonization takes place by protozoa and algal spores, they become adhered with these organisms, creating a microbial biofilm.[30] The combination of biological adhesives, known as extracellular polymeric substances (EPS) and the roughness associated with irregular microbial colonies aids the trapping of further organisms and particles. This further growth and development of the biofilm leads to the final stage of fouling involving the settlement and growth of larger marine invertebrates in conjunction with the growth of seaweed or macroalgae. A schematic of the development of a marine biofouling community with regards to procession and time scale is depicted in Figure 1.3.

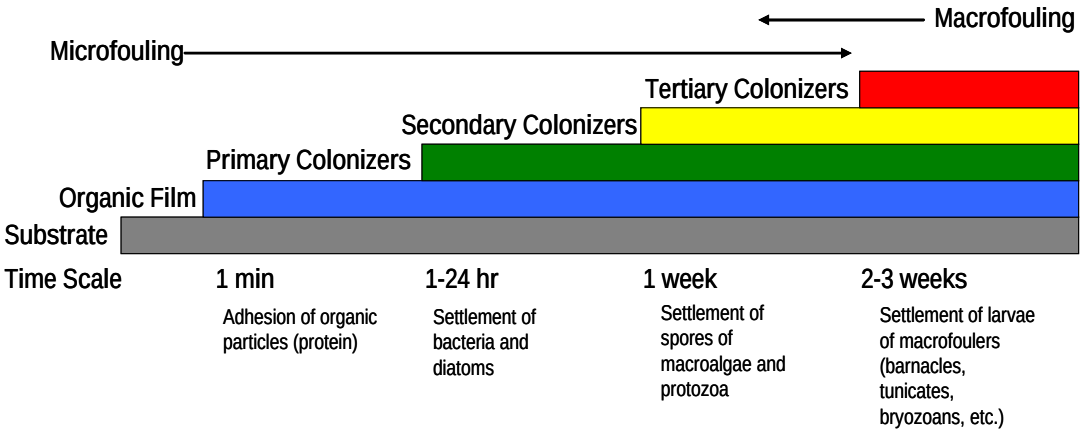

Figure 1.3. A schematic depiction of the development of a marine biofouling community from the initial physical adsorption of organic molecules to the development of a macrofouling community. Figure adapted from D. M. Yebra, S. Kiil, and K. Dam-Johansen, *Prog. Org. Coat.*, 2004, **50**, 75.

The final point to consider before moving onto exploration of specific routes taken to produce anti-biofouling coatings is the economic and environmental ramifications of the marine biofouling problem. The work of Townsin and Schultz examined the powering penalty associated with fouling, and while estimates vary depending on the model used, Schultz determined that powering penalties of up to 86% can be realized at cruising velocities.[31, 32] This clearly demonstrates both the fuel and emission savings that can be realized by combating the fouling problem to the best of our abilities, especially in this current society concerned both with finite energy reserves and global climate change due to green house gas emissions.

Anti-Biofouling Coatings Containing Tethered Biocides

Polymeric coatings functionalized with tethered biocidal moieties have been an active area of research as an alternative to metal based biocide containing ablative coatings. A major advantage to these compounds is that while TBT and copper based ablative coatings self-polish and release their biocidal groups into the environment,

these coatings only expose fouling organisms interacting at the surface-biology interface to these toxic biocides. Thus selectivity, a major issue of TBT and copper coatings is greatly improved.

Polycations with hydrophobic alkyl or benzyl side chains are known to have a disrupting effect on lipid bilayers, such as those of bacterial cells, in an aqueous environment.[33] Taking this into account, quaternary ammonium containing polymeric coatings have been used in many antimicrobial applications.[14, 34-37] Due to the significant role bacteria plays in the development of a marine biofilm, a natural extension of the use of quaternary ammonium containing polymers was to marine anti-biofouling applications.

Krishnan et al. examined the settlement, growth and release characteristics of *Ulva* and the detachment of *Navicula* on surfaces of a polystyrene-*block*-poly(4-vinylpyridine) copolymer quaternized with ω-6-perfluorooctyl-bromohexane and 1-bromohexane to obtain quaternized block copolymers with semifluorinated side chains (Figure 1.4a).[38] In a related study, Park et al. performed an analogous set of experiments on surfaces of an elastomeric polystyrene-*block*-poly(ethylene-*ran*-butylene)-*block*-polyisoprene copolymer with grafted quaternized side chains of ω-6-perfluorooctyl-bromohexane and 1-bromohexane (Figure 1.4b).[13] In both studies, *Ulva* spores were found to settle in very high amounts relative to control surfaces. Meanwhile, *Ulva* sporelings were found to not be released effectively from the surface of the quaternized triblock copolymer. It was hypothesized that the electrostatic interactions between the negatively charged spores and the positively charged surface was the reason for this high settlement of *Ulva* spores in conjunction with poor release of *Ulva* sporelings. In both cases, growth of individual *Ulva* sporelings was stunted and appeared to be disrupted. This may have been due to the chronic toxicity mediated by the quaternary ammonium component of the coating, but another possible

explanation was that the high settlement density of the spores simply led to competition for space and nutrients for the developing sporelings. Analysis of the removal of *Navicula* diatoms from both surfaces also demonstrated poor fouling release properties.

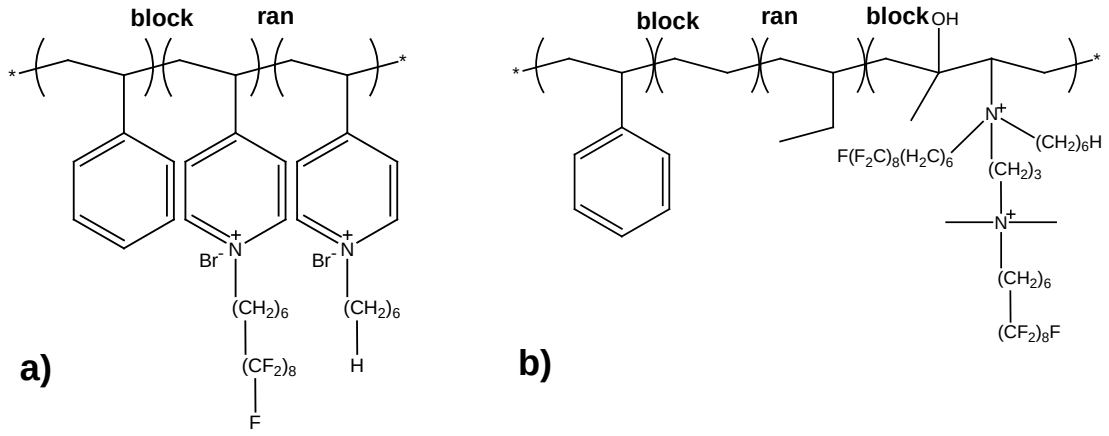

Figure 1.4. Chemical structures of (a) polystyrene-*block*-poly(4-vinylpyridine) copolymer quaternized with ω-6-perfluorooctyl-bromohexane and 1-bromohexane and (b) polystyrene-*block*-poly(ethylene-*ran*-butylene)-*block*-polyisoprene copolymer with grafted quaternized side chains of ω-6-perfluorooctyl-bromohexane and 1-bromohexane.

In a recent publication, Majumdar et al. reported on marine antifouling coatings consisting of tethered quaternary ammonium groups in a moisture curable cross-linked PDMS matrix.[15] The goal of this research was to combine the fouling release efficacy of PDMS with the antifouling character of the quaternary ammonium groups. The building block of this matrix is given in figure 1.5a. A statistical experiment design was used to identify optimum coating compositions and develop structure-property relationships due to the anticipated complexity of this system. Biofouling assays demonstrated that the optimized coating system demonstrated greater than an 80% reduction in retention of the marine bacteria *Cellulophaga lytica*

(*C. lytica*) and greater than a 90% reduction in biofilm growth for the diatom, *Navicula.*

Additionally, in a closely related parallel study, Majumdar et al. reported on a combinatorial high-throughput approach to produce and screen 75 different quaternary ammonium salt containing PDMS hybrid anti-fouling/fouling-release coatings.[39] As precursors for cross-linking reactions, three different silanol terminated PDMS precursors were selected: a low molecular weight sample of 2000 g/mol, an intermediate compound of 18000 g/mol, and a high molecular weight compound of 49000 g/mol. To impart functionality to the coatings, four different quaternary ammonium salt containing trimethoxysilanes were used. As depicted in figure 1.5b-1.5e, alkyl chain length of the quaternary ammonium salt was varied from a one carbon alkyl chain (C-1 QAS) to an 18 carbon alkyl chain (C-18 QAS). Surface characterization of the series of coatings found that in general, hydrophobicity and surface roughness increased with increasing incorporation of quaternary ammonium salt. Compositional variables that resulted in the lowest surface energies were found to possess the highest surface micro-roughness. Anti-fouling behavior meanwhile was highly dependent on which quaternary ammonium salt was utilized in the coating formulation. For the marine bacterium, *C. lytica*, C-18 QAS was found to be very effective in inhibiting bacterial biofilm development. However, only the C-14 QAS derived coatings were found to effectively inhibit the development of a *Navicula incerta* biofilm. With respect to fouling release of sporelings of the green alga *Ulva*, several of the coatings based on the C-18 QAS demonstrated higher sporeling removal than the commercially-available PDMS fouling-release coating Intersleek. These coatings also demonstrated a high degree of nano-roughness, suggesting a correlation between nano-roughness and fouling release efficacy.

Finally, Ye et al. explored the characterization and marine fouling behavior of two additional cross-linked PDMS matrices with tethered biocidal functionality.[40] Particular focus was given to the use of sum frequency generation (SFG) vibrational spectroscopy, a technique capable of studying polymer surface structures at the molecular level in chemical environments including water. This technique is unique since unlike many other surface characterization techniques, such as X-ray photoelectron spectroscopy (XPS) and near-edge X-ray adsorption fine structure (NEXAFS), high vacuum is not required for operation. Two different biocidal moieties for incorporation into PDMS were selected, 5-chloro-2-(2,4-dichlorophenoxy)phenol (triclosan) and the quaternary ammonium containing group, tetradecyldimethyl(3-trimethoxysilylpropyl)ammonium chloride (C-14 QAS). Figure 5f depicts the curing agent synthetic precursor used to incorporate triclosan into a PDMS matrix, while figure 5c shows the precursor used to incorporate the C-14 QAS biocidal moieties. SFG indicated segregation of the triclosan moieties to the surface when the bulk concentration of triclosan incorporated in the PDMS matrix exceeded 8.75% by weight, while C-14 QAS was found to segregate to the surface after 5% incorporation by weight. While antifouling assays for the triclosan containing PDMS coating material were not expressly reported, the C-14 QAS containing PDMS demonstrated very little reduction in the growth of *C. lytica* marine bacteria. *Navicula* diatoms however showed contrary behavior with biofilm growth and retention being reduced proportionally as the amount of C-14 QAS incorporated by weight increased. The maximum reduction in *Navicula* biofilm growth and retention, ca. ~65%, was demonstrated for a PDMS coating with 18.7% incorporation of C-14 QAS by weight.

Figure 1.5. Structures of precursor functional groups used in part to form cross-linked PDMS matrices with tethered biocidal functionality: (a) Methylhydrosiloxane-dimethylsiloxane copolymer with grafted quaternary ammonium groups used to form a cross-linked PDMS matrix with quaternary ammonium functionality. (b-e) Functional precursors to forming cross-linked PDMS matrix with (b) n-trimethoxysilypropyl-N,N,N-trimethylammonium chloride (C-1 QAS), (c) tetradecyldimethyl(3-trimethoxysilylpropyl) ammonium chloride (C-14 QAS), (d) octadecyldimethyl(3-trimethoxysilylpropyl) ammonium chloride (C-18 QAS), and (e) n-(trimethoxysilyethyl)benzyl-N,N,N-trimethyl ammonium chloride (Ph QAS) groups. (f) Curing agent with the biocide 5-chloro-2-(2,4-dichlorophenoxyl)phenol (triclosan) incorporated.

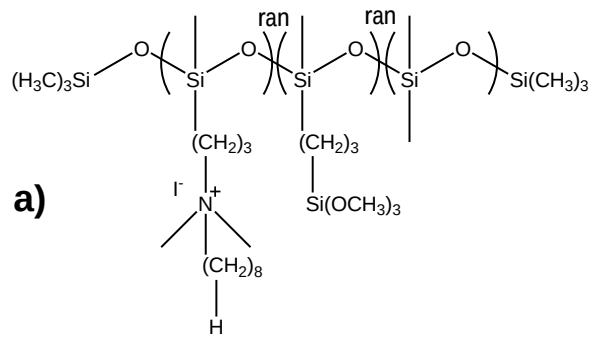
ran
ran
(H3C)3Si
O
Si
O
Si
O
Si
O
Si(CH3)3
(CH2)3
(CH2)3
I-
N+
Si(OCH3)3
(CH2)8
H

a)

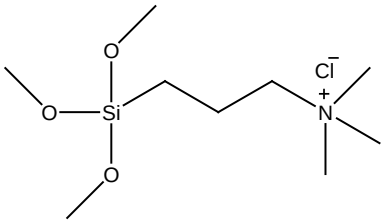
O
Si
O
O
Cl−
+
N

b)

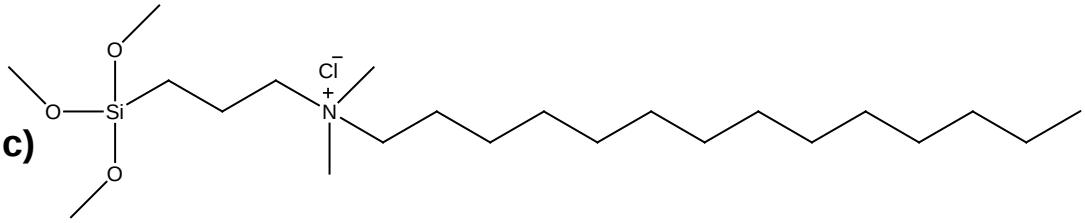
O
Si
O
O
Cl−
+
N

c)

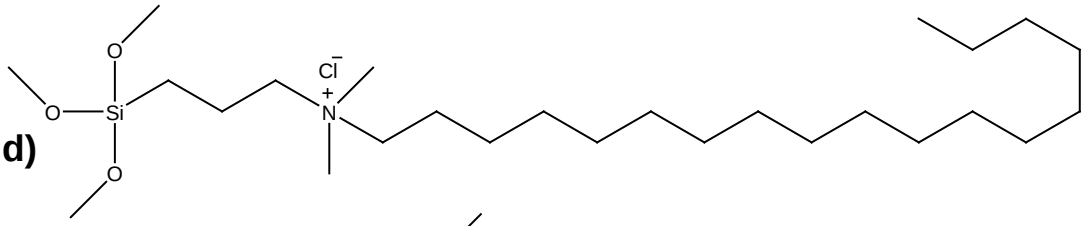
O
Si
O
O
Cl−
+
N

d)

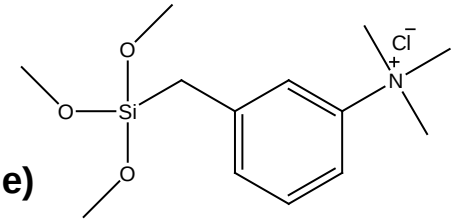
O
Si
O
O
Cl−
+
N

e)

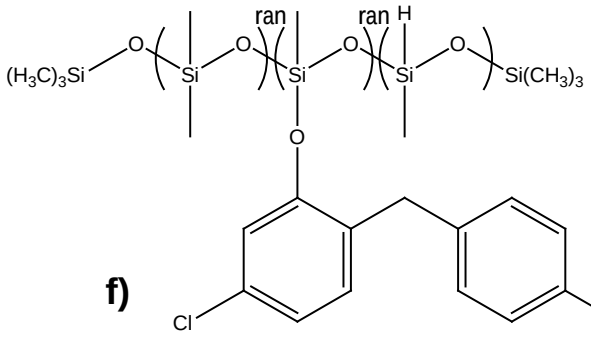
ran
ran
H
(H3C)3Si
O
Si
O
Si
O
Si
O
Si(CH3)3
O
Cl
Cl

f)

Liquid Crystalline Block Copolymers with Semifluorinated Side Chains

The molecular self-assembly of block copolymers with liquid crystalline semifluorinated alkyl side chains can be utilized to form a highly non-polar hydrophobic surface possessing a very low value of surface energy. The block copolymer depicted in figure 6 consists of a polystyrene block that imparts solubility to the fluorinated polymer in common organic solvents, and also acts as a compatibilizer when the surface-active block copolymer is blended with a relatively inexpensive commercial poly(styrene)-*block*-poly(ethylene-*ran*-butylene)-*block*-poly(styrene) (SEBS) thermoplastic elastomer in the coating formulation. The second block meanwhile is derived from the modification of 1,2-polyisoprene by hydroboration and subsequent oxidation followed by a catalyzed coupling reaction.[41]

The fluorinated block, possessing mesogenic semifluorinated alkyl side chains, preferentially segregates to the air-polymer interface because of the low surface energy of the perfluoromethyl head groups. The formation of a thermally stable smectic mesophase at the surface (and in the bulk)[42] prevents molecular restructuring when the coating is immersed in water at ambient temperatures. This is significant since molecular reconstruction is often a problem when a highly hydrophobic polymer surface is immersed in water. This restructuring occurs to position the more polar groups of the polymer at the polymer-water interface, thereby lowering the interfacial energy. For these liquid crystalline polymers however, the energy penalty of disrupting the fluoroalkyl smectic mesophase precludes such restructuring. Coatings prepared from blends of the fluorinated polymer and a SEBS triblock hydrocarbon polymer showed excellent release of the marine green alga *Ulva.* Although high settlement of algal zoospores was expected due to hydrophobic interactions, polymers with semifluorianted alkyl side chains consistently (and unexpectedly) showed lower settlement than Silastic-T2 PDMS coatings used as controls. As expected however, the

hydrophobic fluorinated surfaces were not resistant to protein adsorption[43] and demonstrated poor release of *Navicula* diatoms, which typically adhere strongly to hydrophobic substrates.[41]

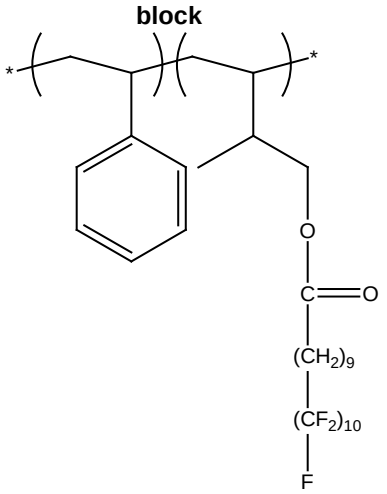

Figure 1.6. Sample structure of a block copolymer derived from poly(styrene)-*block*-poly(isoprene) with liquid crystalline semifluorinated alkyl side chains that form a self-assembled monolayer of non-polar fluoroalkyl groups at the surface of the coating.

Block Copolymers with Environmentally Responsive Amphiphilic Side Chains

Block copolymers derived from poly(styrene)-*block*-poly(acrylic acid) with perfluoroalkyl tagged oligoethylene glycol group as side chains (depicted in Figure 1.7a) were also used in studies of novel anti-biofouling polymeric coatings.[44] Following spray coating of the polymer and annealing in air, X-ray absorption studies indicated that the PEGylated block migrated to the surface of the coating due to the presence of the low-energy perfluoroalkyl groups in the side chains. Further surface enrichment by the PEGylated block occurred when the coating was immersed in an aqueous environment. The polymer-water interfacial energy was determined to be ca. ~ 4 mJ/m^2. The side chains did not exhibit liquid crystalline mesophase formation, possibly due to the dispersion in the number of ethylene glycol and perfluoroethyl

groups incorporated in each side chain. This molecular architecture allowed for a chemically dynamic surface capable of a facile switch in surface wettability. By combining the non-adhesive properties of non-polar fluoroalkyl groups with the antifouling characteristics of hydrophilic PEGylated groups, weak adhesion of both *Ulva* and *Navicula* was realized[44] in conjunction with low settlement density of barnacle cyprid larvae[45] and excellent resistance to protein adsorption. Tapping mode scanning force microscopy indicated that the amphiphilic block copolymer surfaces used in the marine biofouling assays were topographically smooth and compositionally uniform, with a lamellar morphology parallel to the substrate. The uniform nature of these antifouling surfaces is an important distinction from the hyperbranched copolymers discussed later.

Nanostructured Films of Amphiphilic Fluorinated Block Copolymers

Martinelli et al. recently reported on block copolymers synthesized using atom transfer radical polymerization consisting of a polystyrene block combined with a block of polystyrene carrying an amphiphilic polyoxyethylene-polytetrafluoroethylene chain side group, depicted in Figure 1.7b.[46] These block copolymers, either alone, or in a blend with 10% commercial poly(styrene)-*block*-poly(ethylene-*ran*-butylene)-*block*-poly(styrene) (SEBS) were analyzed by a combination of bulk and surface characterization techniques including angle resolved X-ray photoelectron spectroscopy, atomic force microscopy, size exclusion chromatography and NMR spectroscopy. The outer film surface was found to be enriched with perfluorinated groups and AFM analysis demonstrated the presence of well-defined compositional dependent morphological features. After immersion in water however, underwater AFM provided evidence of a transformation to a mixed surface structure in which the nanoscale heterogeneity and topography were increased. Bilayer coatings for biofouling assays

were prepared in a manner similar to those previously reported by Ober et al.[13, 14, 41, 44, 45] The intrinsic ability of the coatings to resist the settlement and reduce the adhesion strength of the green alga *Ulva* and the diatom, *Navicula* was tested. The amphiphilic nature of the copolymer coatings resulted in different results with regards to the two different organisms. *Ulva* were found to adhere least to coatings richest in the amphiphilic polystyrene component, with removal being maximal at intermediate degrees of incorporation the amphiphilic block. All of the test coatings performed better than the PDMS control. *Navicula* meanwhile adhered less strongly to coatings with a lower amount of incorporation of the amphiphilic side chains. This indicated that the molecular and nanoscale ambiguity of the amphiphilic surface lowered the driving forces for the adsorption of the adhesives secreted by the fouling organisms.

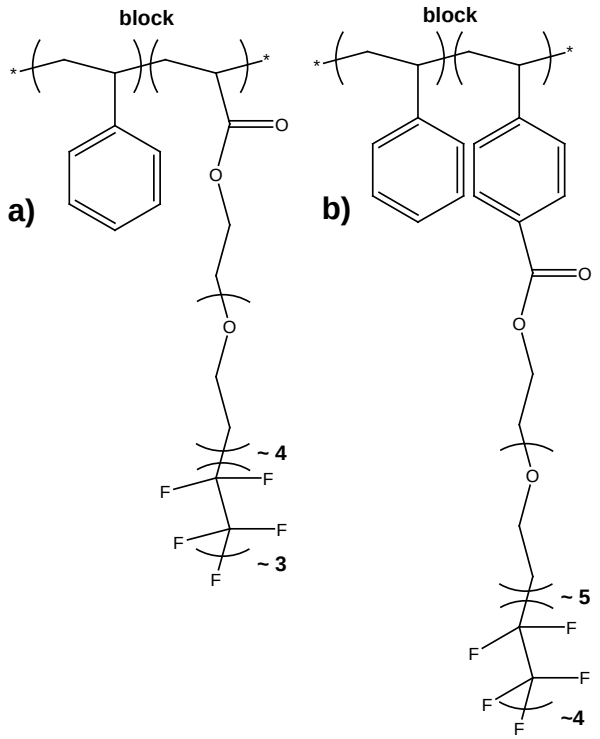

Figure 1.7. (a) Poly(styrene)-*block*-poly(acrylic acid) derived antifouling and fouling release block copolymer with amphiphilic PEGylated fluoroalkyl side chains. (b) Fouling-release block copolymer derived from polystyrene and polystyrene with amphiphilic polyoxyethylene-polytetrafluoroethylene side chains.

Perfluoropolyether-Based Random Terpolymers

Yarbrough et al. demonstrated fluorinated polymer coatings lacking liquid crystalline mesophases that still demonstrated promising fouling release of *Ulva* spores.[47] Perfluoropolyether derived random terpolymers depicted in Figure 8 were prepared. These terpolymers were coated on substrates and subsequently crosslinked. To inhibit surface restructuring of the coating in water, and thus retain its non-polar nature, photoacid-catalyzed epoxide ring-opening curing of the glycidyl methacrylate groups was performed. While these coatings showed good removal of *Ulva* spores under applied shear in a water flow channel after one hour of incubation, the release of *Ulva* sporelings following a week of growth was quite poor. It can be inferred that this was possibly due to the reorganization of polar groups to the surface of the coatings during this longer duration of immersion in an aqueous environment.

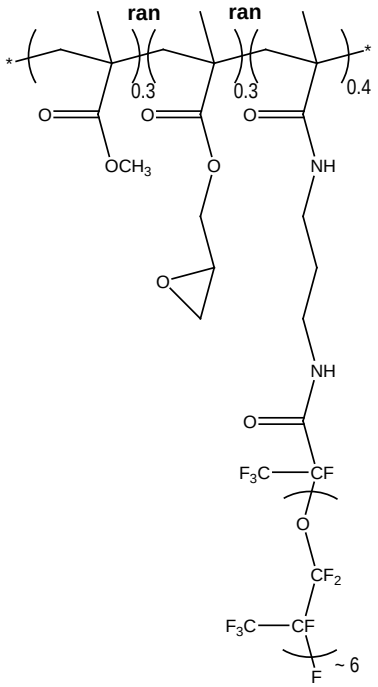

Figure 1.8. Perfluoropolyether-based random terpolymer used to form photo-crosslinkable fouling release coatings.

PEGylated Polymers

The antifouling properties of PEGylated polymers are well documented in the current literature.[2, 48, 49] In marine fouling settlement and release studies, polystyrene block copolymers with methoxy-terminated PEG side chains showed significantly weaker cell adhesion of *Navicula* diatoms compared to control surfaces of PDMS.[41] Diatoms adhere strongly to hydrophobic surfaces. This renders commercial PDMS based coatings particularly susceptible to accumulation of diatom slimes. Thus, developing coating systems capable of resisting diatom fouling is a very important area of marine biofouling research. A recent advance in hydrophilic PEGylated coatings involves the use of bio-inspired polymers prepared from methoxy-terminated PEG and the adhesive amino acid $_{L}$-3,4-dihydroxyphenylalanine (DOPA).[50] This approach involves conjugating mimics of mussel adhesive proteins with known antifouling polymers to confer even stronger antifouling properties to the surface. The catechol side groups of DOPA can form moisture resistant bonds with a variety of substrates including metals, glass, and plastics.[51, 52] Titanium surfaces coated with the DOPA containing polymer shown in Figure 1.9a were found to have good antifouling and fouling release properties in marine biofouling assays with respect to both green algal spores and diatoms.[50] Additional testing also demonstrated the resistance of these surfaces to protein and mammalian cell fouling.[53]

Dendrimers and hyperbranched polymers have also been used to generate PEGylated antifouling surfaces. The use of antifouling polymers to prevent fouling of water filtration membranes is another area of research with significant work being dedicated to it.[54, 55] Zhao et al. found that membranes prepared from blends of the hydrophobic polymer poly(vinylidene fluoride) (PVDF) and a hyperbranched amphiphilic polymer with hydrophilic PEG grafts, depicted in Figure 1.9b, showed significantly lower protein adsorption than pure PVDF membranes.[56] An additional

advantageous effect of this approach was that the enhanced hydrophilicity of the blended polymer system enhanced water flux characteristics through the membrane.

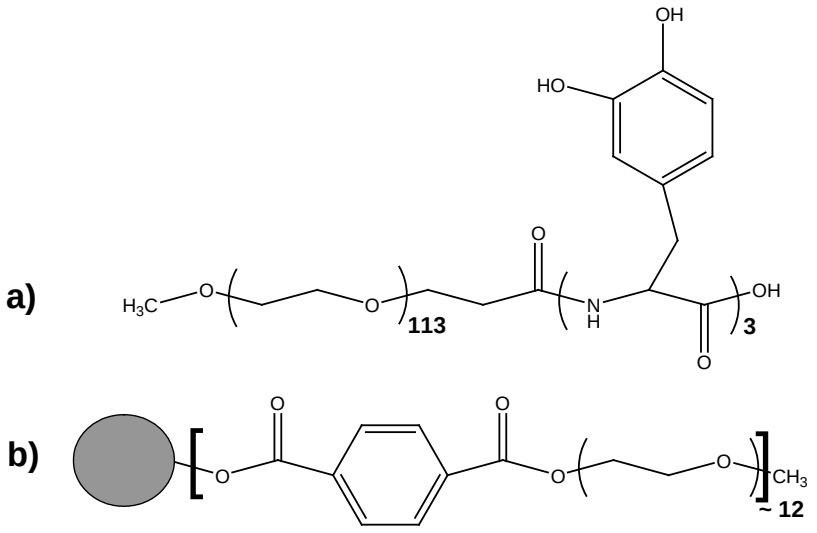

Figure 1.9. a) Mussel adhesive inspired methoxy-terminated PEG grafted to DOPA tripeptide antifouling polymer. b) Schematic representation of amphiphilic hyperbranched-star polymer consisting of grafted methoxy-terminated PEG attached to a hyperbranched polyester molecule.

Prior studies have indicated that as long as a surface is completely covered by ethylene glycol groups, the PEG chain length and the entropic effects associated with the molecular architecture will not have a strong influence on the antifouling properties of a PEG surface. Complete surface coverage by PEG can be obtained if the distance between the attachment sites of the PEG grafts is less than the radius of gyration of the PEG in solution.[57, 58] This condition can be achieved when the grafting density lies in the polymer brush regime. Comb-like architectures with a high grafting density of PEG along the polymer back-bone readily achieve this structure.[41] Thus, the main advantage of utilizing longer PEG grafts, comb like polymers with PEGylated

side chains, PEGylated polymer brushes, or dendritic PEG containing architectures is the formation of a dense, defect-free coating of ethylene glycol groups at the surface.

Self-assembled monolayers (SAMs) consisting of only a few ethylene glycol units per molecule have demonstrated extremely good resistance to adsorption of a wide variety of proteins.[59] Such experiments support the hypothesis that the formation of a hydration layer near a hydrophilic surface such as PEG is the basis for protein adsorption resistance. This is in opposition to the steric repulsion mechanism that has been speculated to be the cause of protein adsorption resistance for longer PEG chains. In recent work, Heuberger et al. found that the water content inside hydrated surface-grafted PEG chains is over 80 percent by volume using a combination of a quartz crystal microbalance and extended surface forces apparatus.[60, 61] It was proposed that the excellent protein resistance properties of this type of hydrophilic surface could be attributed to the high degree of organization in the PEG-water complex. Adsorption of protein onto such a surface requires disruption of this complex and would be both thermodynamically and kinetically unfavorable.

In contrast, Jiang et al. present findings in support of the steric repulsion mechanism of protein adsorption resistance for PEG. Hyperbranched PEG-like structures depicted in Figure 1.10 were synthesized on the surface of silicone elastomers and their antifouling characteristics were compared with those of linear PEG grafts.[62] While both of these surfaces were expected to be significantly hydrated due to densely packed hydroxyl and PEG groups on the surface, the linear PEG molecules were found to be much more effective in preventing bacterial attachment than the branched structures. This effect was attributed to the differences in the magnitudes of steric repulsion between the linear and branched molecular arrangements. Protein adsorption assays between linear and branched PEG

architectures were not reported however and are sorely needed to help clarify the validity of this hypothesis.

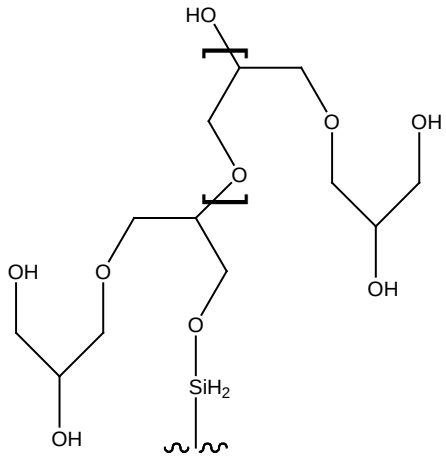

Figure 1.10. Antifouling PEG-like hyperbranched polymer produced on the surface of silicone elastomer. Linear PEG grafts were also attached to the hydroxyl groups to obtain PEGylated surfaces for comparison.

Another possible mechanism for protein adsorption resistance of PEG was suggested by Benhabbour et al. in a recent study where a thiol-terminated poly(ethylene glycol) (HS-PEG_{650}-OH) was attached to gold coated silicon wafers.[63] The terminal PEG OH groups were functionalized with aliphatic polyester dendrons of generations 1 to 4. Despite the fact that dendronization of the PEGylated surfaces resulted in an increase in surface hydrophilicity, protein adsorption actually increased. This led to the proposal that PEG chain flexibility is one of the primary factors in the mechanism of protein resistance as it was theorized that chain flexibility was impeded by the introduction of the dendrons with multiple peripheral OH groups. The interaction of these OH groups with the underlying PEG was believed to lower the conformational flexibility of the PEG grafts, reducing protein adsorption resistance.

In summary, PEGylated polymers currently form some of the best performing surfaces with regards to protein adsorption and adhesion resistance. Their long-term

stability in a biological environment is a crucial part of their use as practical antifouling coatings. Sharma et al. found that silicon surfaces modified with PEG retained protein and cell adhesion resistance even after four weeks of immersion in a PBS buffer solution (pH 7.4) maintained at 37 °C in 5% CO_2.[64] To date however, limited studies have been conducted that investigate the durability of PEG coatings in a marine environment, and more are sorely needed. It is known that polyethers and many other hydrophilic polymers can readily undergo oxidative degradation and chain cleavage.[65] Thus, many alternatives to PEG-based antifouling coatings are currently being research.

Hydrogels as Anti-Fouling Materials

Rasmussen et al. examined the settlement of cultured barnacle larvae, *Balanus amphitrite*, on a series of four different non-solid hydrogels.[66] Gels consisting of alginate (highly anionic), chitosan (highly cationic), polyvinyl alcohol substituted with light-sensitive stilbazolium groups (PVA-SbQ, very low cationic) and agarose (neutral) were selected. Polystyrene was used as a solid reference surface control. Barnacle settlement was tested directly on the different test materials, followed by a quality test of the non-settled larvae. All four gels inhibited barnacle settlement relative to polystyrene controls. Most notably, gels consisting of 2.5% PVA-SbQ and 0.5% agarose showed the most promising antifouling properties. Metamorphosis of barnacle larvae was clearly inhibited on the 2.5% PVA-SbQ gels. For the 0.5% agarose gels, only 10% of the larvae settled after 8 days. For alginate gels and 2% chitosan gels, less than 40% settlement of barnacle larvae occurred.

In a later study, Cowie et. al examined the use of poly(2-hydroxyethyl methacrylate) (PHEMA) hydogels to prevent marine fouling on the optical windows of marine underwater sensors.[67] PHEMA hydrogels loaded with the biocides

benzalkonium chloride (BAC) and dicocodimethylammonium chloride (Arquad 2C-75) were tested in conjunction with unloaded PHEMA hydrogels and poly(methylmethacrylate) (PMMA) control surfaces. While the Arquad 2C-75 loaded hydrogels were particularly effective at resisting fouling, both the PMMA control surfaces and the unloaded PHEMA hydrogels fouled heavily. This indicated that the inherent softness and hydrophilicity of the hydrogel alone was not enough to render it resistant to marine biofouling.

To improve on this previous work, Ekblad et al. devised a way to produce thin, yet robust PEG-containing hydrogel coatings with low protein adsorption to provide surfaces for the evaluation of biofouling resistance.[68] The method of preparation of these materials from UV-initiated free radical polymerization of 2-hydroxyethyl methacrylate (HEMA) and a PEG methacrylate, with an average PEG chain length of 10 units (PEG10MA) was previously reported in Larsson et al.[69] Hydrogel coated glass slides were used in laboratory assays with a range of common fouling organisms including the marine algae *Ulva* and *Navicula*, two species of marine bacteria, *Cobetia marina* and *Marinobacter hydrocarbonclasticus*, and the barnacle cyprid larvae, *Balanus amphitrite*. Additionally, biofouling assays using the fresh water bacterium, *Pseudomonas fluorescenes*, were conducted. Physicochemical properties of the coatings were investigated using contact angle measurements, infrared spectroscopy, and ellipsometry, with a special emphasis paid to determining the stability of the hydrogel in both the short and long-term upon immersion in artificial sea water.

Short term stability testing by goniometry and ellipsometry measurements of the PEG-containing hydrogel coatings immersed in artificial sea-water indicated that there were no statistically significant changes in the hydrogel thickness or contact angles during a period of 7 days. Long-term stability testing performed using IR spectroscopy and ellipsometry on PEG-containing hydrogel coatings immersed in

artificial sea water for a six month period indicated that approximately 95% of the hydrogel remained and protein adsorption resistance with regards to fibrinogen adsorption was preserved. This finding was surprising since it is well known that PEG can undergo oxidative degradation when exposed to oxygen and elevated temperatures or light.[70, 71] One possible reason given for the stability of these hydrogel films was the lack of dissolved organic species in the artificial sea water since PEG can be oxidized enzymatically.[72] Another possible reason was the presence of cross-links formed during the UV-irradiation process.[73]

Biological assays performed with *Ulva* spores indicated that while settlement was greatly reduced with only 5% to 6% settlement relative to glass controls, the hydrogels did not function as fouling-release materials with regards to *Ulva* spores. *Navicula* diatoms meanwhile demonstrated a much lower adhesion than glass controls and were generally easily removed (74% removal at 53 Pa water shear stress) under applied water flow. Settlement assays on the hydrogel coatings for barnacle larvae of *Balanus amphitrite* demonstrated that settlement on the hydrogel coatings never exceeded 21% that of glass. Similarly, settlement for all three types of bacteria that were tested were significantly less than that on glass controls, and between 73% and 88% of the bacteria was efficiently removed under applied water shear in a flow channel. Additional testing with ocean immersion field trials is planned to see if these positive laboratory assay results can be expanded upon.

Hyperbranched Amphiphilic Fluoropolymers

Gudipati et al. investigated surfaces hyperbranched network polymers containing discrete fluorinated and PEGylated groups based on the hypothesis that nanoscale heterogeneities in topography and composition would create a surface unfavorable with regards to protein adsorption.[74] An optimal composition of 55 weight percent fluorinated hydrophobic monomer and 45 weight percent hydrophilic PEGylated monomer in the resultant polymer was identified as giving the best protein adsorption resistance behavior in conjunction with the best fouling release of *Ulva* spores and sporelings.

In related work, Powell et al. reported the synthesis of hyperbranched fluoropolymers using atom transfer radical polymerization of an amphiphilic inimer.[75] They proposed that a coating prepared using the resulting polymer would have surface heterogeneities small enough in size to enhance resistance to protein adsorption and cell adhesion. Even though a textured surface is expected to provide a greater surface area for interaction with proteins and thus would be detrimental to antifouling activity, the primary idea driving the development of hyperbranched amphiphilic polymer coatings is that the nonuniformity of surface characteristics would actually impact the ability of a protein molecule to adsorb and unfold on a surface. For this hypothesis to be valid, the size of the surface heterogeneities must be below the size of protein molecules, on the order of 1 to 10 nm in range. To date, definitive evidence for the fact that a nanoscale variation in surface topography and chemistry can impart superior resistance to protein adsorption versus a topographically smooth and chemically uniform surface is still lacking. Nonetheless, a recent study has demonstrated that marine organisms (which are obviously on a much larger length scale than protein molecules) are capable of discriminating between surface domains of different wettability and of a specific size in the micrometer range.[76]

Patterned Fluorinated and PEGylated Monolayer Surfaces

To facilitate the design of "ambiguous" surfaces made to present both hydrophobic and hydrophilic domains to fouling organisms, Finlay et al. produced an array of squares containing alternating fluorinated monolayer and PEGylated monolayer stripes of different widths on either a uniform fluorinated monolayer or PEGylated monolayer background.[76] Molecular vapor deposition of fluorooctatrichlorosilane (FOTS) was combined with standard lithographic techniques and subsequent chemical back-filling with a PEGylated silane to produce these patterned features. Square arrays measured 1 cm x 1 cm, and stripes with widths of 500, 200, 100, 50, 20, 5, and 2 μm were examined. *Ulva* spores were found to be selective in choosing where to settle, settling at higher densities on fluorinated stripes compared to PEGylated stripes. However, the magnitude of the settlement response was found to be highly dependent on both the width of the stripes and the chemistry of the background with settlement on fluorinated stripes narrower than 20 μm similar to that experienced for the PEGylated background. This suggests that at some critical dimension below 20 μm, the *Ulva* spores were no longer able to distinguish the difference between the fluorinated and PEGylated features, regarding the surface as pure PEG.

Zwitterionic Polymers

Inspired by the natural anti-biofouling properties of cell membranes, polymers incorporating zwitterionic moieties such as phosphatidylcholines[77, 78] are promising anti-biofouling surfaces. Kitano et al. used controlled radical polymerization to polymerize methacrylate monomers with different pendant zwitterionic groups using disulfide carrying N,N-diethyldithiocarbamoyl derivatives as chain transfer agents.[79] A gold surface was incubated with an aqueous solution containing the resultant

telomers (depicted in Figure 1.11a) and self assembled monolayers were formed as confirmed by cyclic voltammetric measurements and contact angle analysis. These surfaces were found to be resistant to non-specific adsorption of proteins through the use of cyclic voltammetry and localized surface plasmon resonance absorption spectroscopy. Additional work by Kitano et al. on carboxybetaine containing zwitterionic polymers using Raman spectroscopy and attenuated total reflection infrared spectroscopy demonstrated that the surfaces of zwitterionic polymers did not upset the native hydrogen bonded network of water molecules present in the vicinity of the surface.[80] This is in stark contrast to the ionic groups and counterions of polyelectrolytes such as poly(sodium acrylate) and poly(sodium ethylenesulfonate) that strongly perturb the structure of water in their presence. This demonstrated that the existence of a native hydrogen bonded network of water near a surface is likely a necessary feature for antifouling and biocompatible characteristics.

Chen et al. explored the protein resistance properties of self-assembled monolayers containing phosphorylcholine moieties and inferred that their balanced charge and minimized dipole gave them a strong hydration capacity via electrostatic interactions. This was believed to be the primary factor behind their antifouling behavior.[81] Follow up work established the superior fouling resistance of oligo(phosphorylcholine) SAMs (despite the presence of negative charge) using a surface plasmon resonance sensor.[82]

Chang et al. reported on the protein resistance of coatings formed from the modification of SAMs with a poly(propylene oxide)-*block*-poly(sulfobetaine methacrylate) copolymer.[83] Subsequently, Zhang et al. prepared zwitterionic polymer brushes from sulfobetaine methacrylate and carboxybetaine methacrylate monomers (Figure 1.11b and 1.11c) on glass slides using atom transfer radical polymerization and found that the zwitterionic polymer brushes reduced fibrinogen adsorption to a

level comparable to that for PEGylated surfaces. Additionally, elevated resistance to adhesion of bovine aortic endothelial cells was demonstrated for these zwitterionic polymer brushes.[84] In follow up work by Cheng et al. the same zwitterionic polymeric brushes synthesized from sulfobetaine methacrylate resisted biofilm formation by both Gram positive and Gram negative bacteria.[85] Furthermore, Ladd et al. demonstrated their resistance to non-specific protein adsorption from human blood serum and plasma.[86] Finally, these zwitterionic polymer brush surfaces are being evaluated for marine anti-biofouling and fouling-release performance as part of the ONR coatings program and initial testing has identified their potential with regards to *Ulva* spore settlement and release in conjunction with sporeling growth and release. However, to date no formally reported results have been published.

This work on zwitterionic anti-biofouling materials by Jiang and coworkers has also recently led to the development of a new class of anti-biofouling polymers utilizing the concepts learned through molecular level study of the nonfouling character of zwitterionic polymeric materials.[87] Polyampholytes are a large group of polymers possessing both positively and negatively charged chemical moieties. Copolymer hydrogels were prepared from the combination of positively charged compounds such as aminoethyl methacrylate hydrochloride with negatively charged compounds 2-carboxyethyl acrylate and 3-sulfopropyl methacrylate potassium salt. Resistance to protein adsorption on the order of that seen for PEG and zwitterionic sulfobetaine methacrylate was demonstrated. This led to the inference that the close proximity of amino and carboxylic acid groups in the copolymer allow it to behave similar to zwitterions in ionic character and that strong hydration of the copolymer through ionic solvation is the key to polyampholyte nonfouling properties. This work has also been extended to the polymer brush regime by Bernards et al. who reported on the nonfouling character of statistical copolymer brushes of positively charged

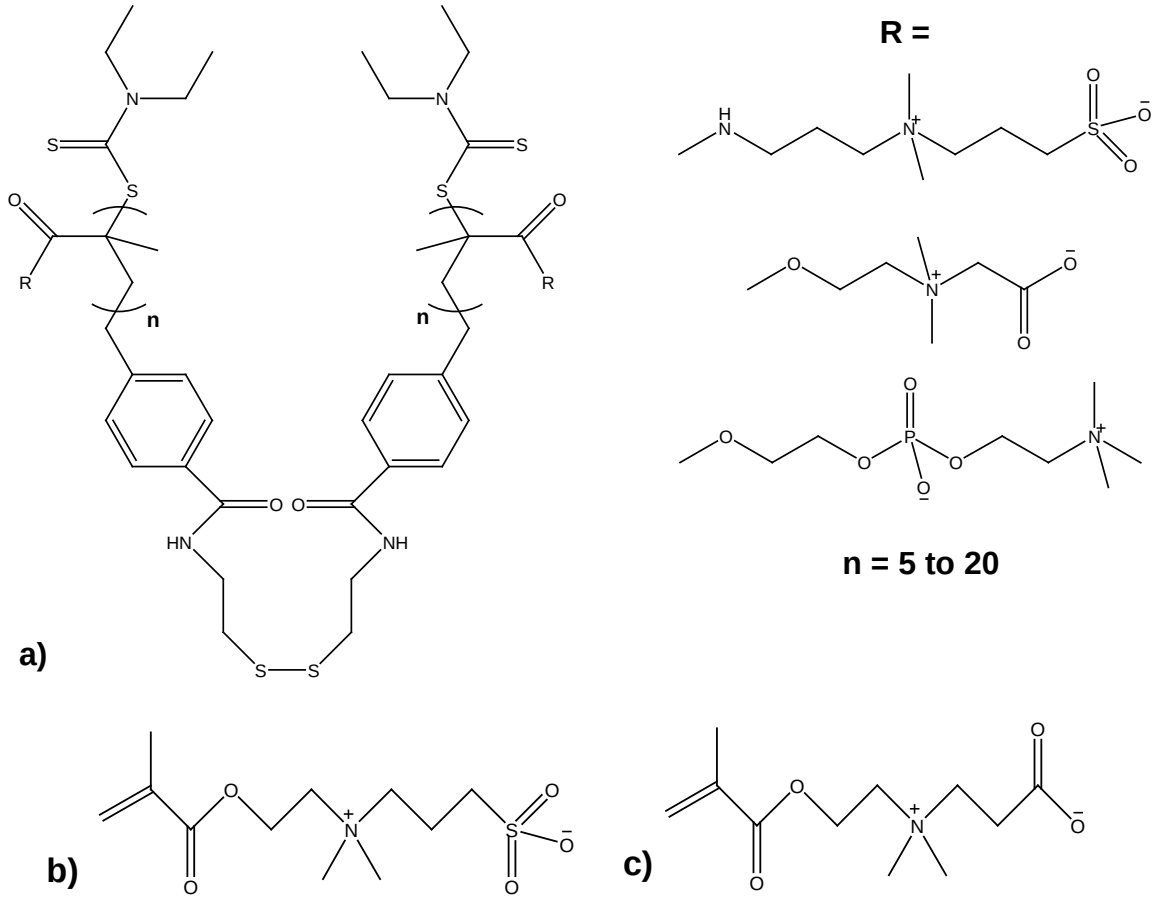

Figure 1.11. a) Antifouling telomers synthesized by controlled radical polymerization with zwitterionic side chains. A disulfide group is present to facilitate the attachment of the telomers to a gold substrates for self-assembled monolayer formation. b) Sulfobetaine methacrylate and c) Carboxybetaine methacrylate used for forming zwitterionic polymer brushes.

[2-(methacryloxy)ethyl] trimethyl ammonium chloride and negatively charged 3-sulfopropyl methacrylate potassium salt.[88] The best overall performance with regards to protein adsorption resistance was demonstrated for the copolymer brushes formed from a 1:1 homogenous reaction mixture of the two oppositely charged monomers.

Polymers with Oligosaccharide Grafts

Holland et al. introduced biomimetic non-adhesive glycocalyx-like surfaces by using surfactant polymers containing grafted oligosaccharide groups.[89] The glycocalyx is the extracellular polysaccharide matrix that prevents non-specific interactions of a cell with other cells and proteins. When a graphite surface was modified with the oligosaccharide grafted surfactant polymer, non-specific protein adsorption was found to be reduced by at least 90% relative to controls. In later work, Zhu and Marchant designed and synthesized maltose dendrons and attached them to a poly(vinylamine) backbone, depicted in Figure 1.12, to create a dense canopy of a protective glycocalyx-like saccharide coating over a biomaterials surface.[90] The dendritic architecture of the molecules enabled a high degree of surface coverage by glycosylated moieties, eliminating potential defect areas. Furthermore, it was demonstrated that these coatings successfully suppressed platelet adhesion, validating their ability to resist non-specific adsorption.

Xerogel Coatings

Xerogels are glass-like cross-linked networks derived from a sol-gel process. Tang et al. investigated marine organism settlement and adhesion properties of xerogels with tailored wettability.[91] These xerogels were prepared by combining the tetraethoxysilane precursor with other alkoxysilane precursors containing the non-polar n-propyl, n-octyl and 3,3,3-trifluoropropyl groups and the polar ethylenediamine groups, depicted in Figure 1.13. Coatings incorporating the n-propyl group showed the best removal of *Ulva* spores while coatings incorporating the n-octyl groups showed the highest removal of eight-day old *Ulva* sporelings. The xerogel coatings incorporating the semifluorinated n-propyl groups showed a higher settlement of both *Ulva* zoospores and barnacle cyprid larvae. Surprisingly, the fluorinated coatings only

showed moderate release of *Ulva* spores and sporelings, lower than or similar to xerogels containing both the n-propyl and n-octyl groups. Additionally, the fluorinated coatings did not effectively release juvenile barnacles, with only the xerogel coating derived from n-octyl groups functioning as a fouling release material with respect to this assay. When compared to the facile release of *Ulva* from liquid crystalline polymers with semifluorinated side chains,[41, 43] these results suggest that the liquid crystallinity and self-assembly of the relatively long semifluorinated alkyl side chains[92] may play an important role in fouling release performance.

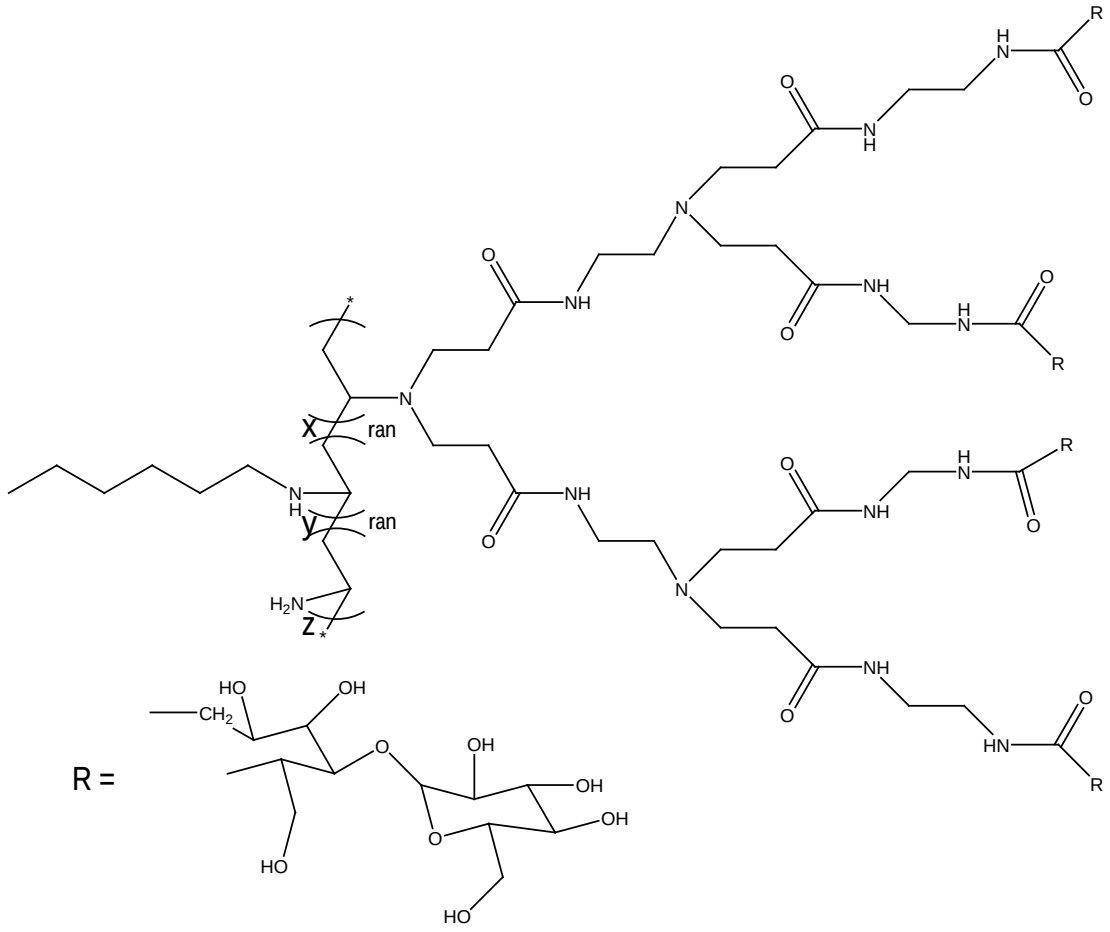

Figure 1.12. Dendritic antifouling polymer capable of resisting non-specific adsorption with glycodendron grafts.

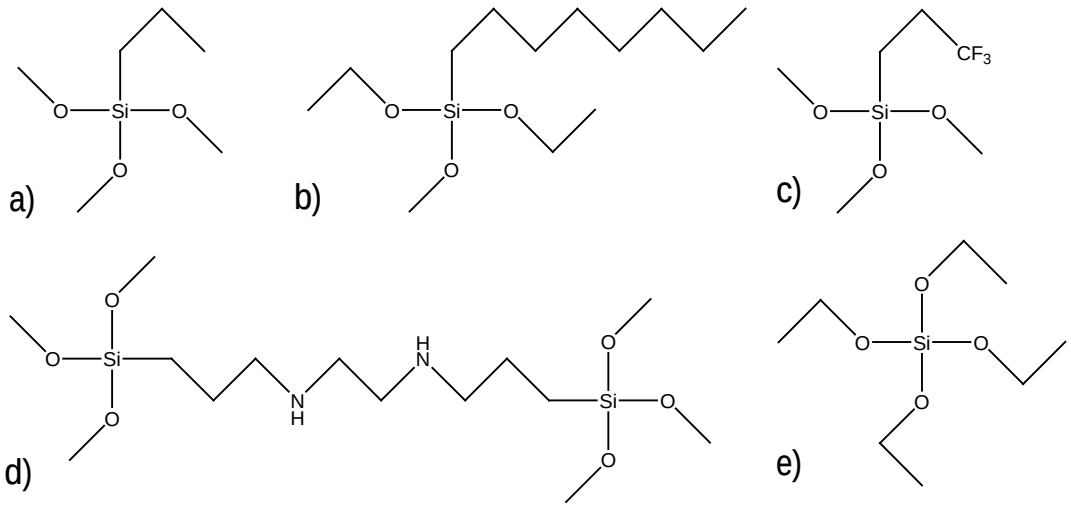

Figure 1.13. Precursor molecules used in sol-gel synthesis of xerogel anti-fouling coatings. a) n-propyltrimethoxysilane, b) n-octyltrimethoxysilane, c) 3,3,3-trifluoropropyltrimethoxysilane, d) bis[3-(trimethoxysilyl)propyl]-ethylenediamine, and e) tetraethoxyosilane.

Micro-Engineered PDMS Elastomeric Coatings

A series of studies have been published by Brennan and coworkers exploring the response of biological organisms to micropatterned PDMS elastomers. Callow et al. explored the settlement response of *Ulva* spores to two different topographic feature sets of varying dimensions: a series of 5 or 1.5 μm deep valleys with valley floors and ridges varying between 5 and 20 μm in width and circular pillars of 5 μm diameter, 5 or 1.5 μm in height spaced 5 to 20 μm apart.[93] The features were arranged in blocks to present the spores with a "choice" of where to settle. Spores were found to settle preferentially in the valleys and adjacent to the pillars. As the width of the valley decreased, the number of settled spores significantly increased. Settlement was generally lower for lower profile features. Silica beads of similar dimensions to the body of the spores were utilized to determine whether the spatial orientation between

the settled spores and the topographic features were a consequence of active settlement behaviors. It was determined that the spores were able to generally discern the difference between the silica beads and other spores, favoring gregarious settlement, which is energetically favorable through minimization of the force of adhesion.

In a follow up study by Hoipkemeier-Wilson et al. in which varying additions of non-network forming PDMS based oils were incorporated with similar microtopographies to those previously studied, *Ulva* spore settlement density was found to be greatly reduced on many of the surfaces with topographic features.[94] This was particularly true for the 5 μm wide and deep channels. This contrasted the smooth PDMS surfaces which showed no marked difference in settlement with the incorporation of oils. It was hypothesized that this effect was due to "oil in-filling" in which the oils would segregate to the bottom of the topographical features as determined primarily by molecular weight and viscosity. This effectively acted to reduce the profile of the patterned features.

To try to improve on these previous studies, Carman et al. introduced PDMS with biomimetic topography inspired by the skin of sharks called "Sharklet AF^{TM}."[24] The settlement of *Ulva* spores was evaluated on these surfaces and was found to be reduced by ~ 85% on the finer (ca. 2 μm) and more complex topographies relative to that on smooth PDMS. Spores avoided the 2 μm channels and were largely confined to defects and slightly wider spaces located between adjacent Sharklet AF^{TM} diamonds. To the best of our knowledge, this was the first demonstration of an engineered microtopography inhibiting the settlement of spores of a marine alga reported in the literature.

The next iteration of this work by Schumacher et al. saw the introduction of other regular PDMS microtopography patterns at the 2 μm length scale for antifouling

evaluation.[25] Features of this size are on the order of the dimensions of the spore body, and thus were expected to disrupt settling behavior. The Sharklet AF™ topography was tested in conjunction with hexagonally packed 2 μm diameter circular pillars, 2 μm wide ridges separated by 2 μm channels and a novel pattern combining 10 μm equilateral triangles with 2 μm diameter circular pillars. A dimensionless ratio known as the engineered roughness index (ERI) was introduced to provide a more comprehensive quantitative description of engineered surface topography expanding on Wenzel's roughness factor (the ratio of the actual surface area to the projected planar surface area). Spore settlement was found to generally decrease with increasing ERI. The 2 μm circular pillars (ERI = 5.0) and 2 μm wide ridges (ERI = 6.1) reduced settlement by 36% and 31% respectively relative to a smooth PDMS control. The new multi-feature topography consisting of 2 μm diameter circular pillars and 10 μm equilateral triangles (ERI = 8.7) reduced spore settlement by 58%. The Sharklet AF™ microtopography meanwhile yielded the largest reduction in spore settlement density, 77%. This work led to a hypothesis that to optimize resistance to *Ulva* spore settlement, topographical features must be of sufficient spacing to prevent spores from settling between them and sufficient size to allow a spore to settle fully on them. Furthermore, if a spore settles in such a way that it forms a bridge between two features, it must not be able to contact the floor between them.

Extension of the use of Sharklet AF™ to the inhibition of growth of a bacterial biofilm of *Staphylococcus aureus* was demonstrated in later work by Chung et al.[95] Despite the fact that the length scale of the bacteria was only on the order of ~ 1-2 μm, lower than the critical dimensions of the Sharklet AF™ pattern, it was hoped that the further colonization of additional bacteria and subsequent formation of a biofilm could be disrupted. It was found that while the smooth PDMS surface exhibited early-stage biofilm colonies at 7 days and mature biofilms at 14 days, the topographically

patterned surface did not demonstrate evidence of early biofilm colonization until day 21, clearly inhibiting the development of the colonies of *S. aureus*. The extension of the Sharklet AF^{TM} microtopography to inhibition of barnacle cyprid larvae of *Balanus amphitrite* has also recently been demonstrated.[96] A range of length scales was examined and in this case the optimal feature size was found to be 20 μm in width and 40 μm deep, reducing settlement by 97% relative to smooth PDMS controls. This led to the idea to try to superimpose smaller topographical features onto larger ones in hopes of being able to repel a wider range of fouling organisms. Work is currently on-going in this area.

Siloxane-Polyurethane and Siloxane-Acrylic-Polyurethane Polymers

Siloxane-polyurethane block copolymers have been explored as alternatives to pure PDMS coatings for use as marine fouling release materials.[97, 98] PDMS has poor mechanical durability and weakly adheres to most substrates, especially when mixed with fillers. Thus, the incorporation of polyurethane materials with better adhesive and mechanical properties was seen as a way to overcome these two short-comings. Ekin et al. have synthesized block copolymers consisting of PDMS and poly(ε-caprolactone) as shown in Figure 1.14a and 1.14b. Polyurethane coatings were formulated using a trifunctional alcohol (polycaprolactone triol) and an isocyanurate as depicted in Figure 1.14c and 1.14d.[98] Poly(ε-caprolactone) was incorporated to increase the compatibility between PDMS and polyurethane. Using a high-throughput combinatorial synthetic approach, they produced a series of 288 coating formulations containing different molecular weights of the PDMS block and different degrees of polymerization of the ε-caprolactone monomer. This sample library was then down-selected to eight coatings following initial screening. Analysis was then performed using a combination of bulk and surface characterization techniques in conjunction

with biofouling assays for bacteria (*C. lytica, Halomonus pacifica*), green algae (*Ulva*) and barnacles (*balanus amphitrite*). The combinatorial approach enabled the identification of coating formulations that showed better fouling release than PDMS controls (Silastic T2 and DC 3140). Coatings prepared using hydroxyalkyl carbamate terminated PDMS (the linear precursors) showed lower adhesion of barnacles than those prepared using the dihydroxyalkyl carbamate-terminated PDMS (the branched precursors). Lower molecular weight PDMS generally showed higher removal of soft fouling (bacterial and algal biofilms) than higher molecular weight PDMS. The opposite trend was seen in barnacle adhesion assays.

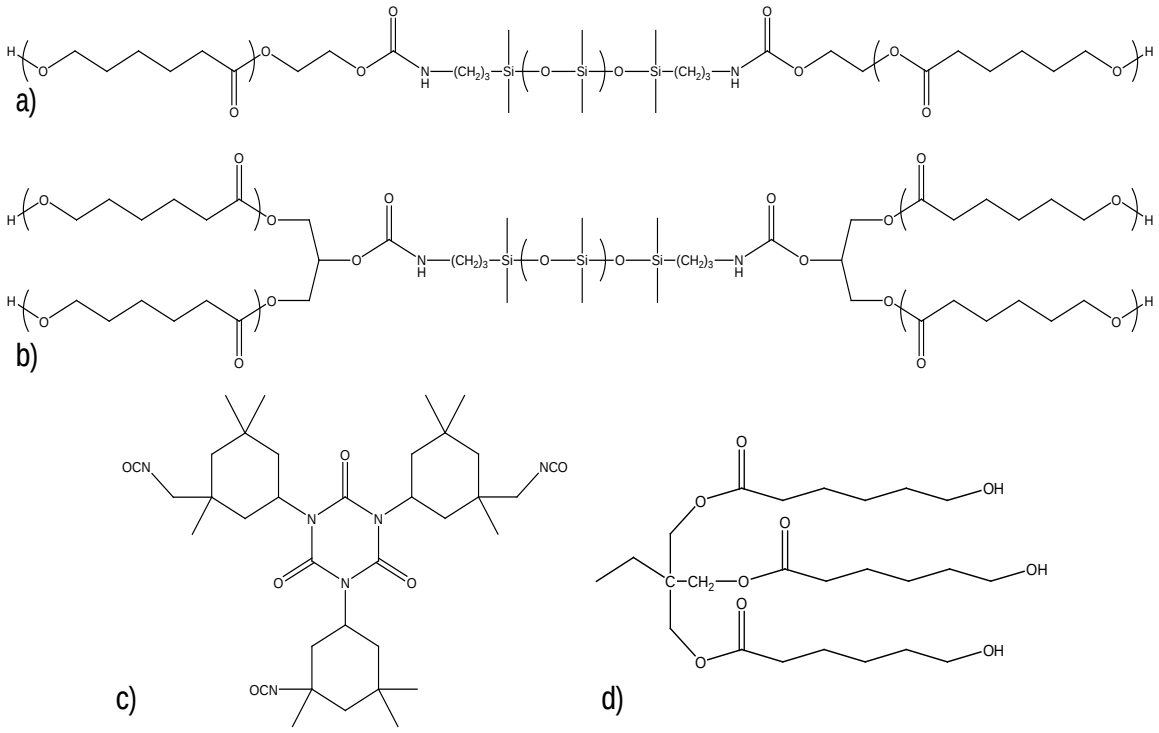

Figure 1.14. Formulation ingredients used to synthesize siloxane-polyurethane block copolymers. a) Linear block copolymer consisting of PDMS and poly(ε-caprolactone) and b) branched block copolymer consisting of PDMS and poly(ε-caprolactone). The isocyanurate (c) and trifunctional alcohol (d) used to form polyurethane coatings are also depicted.

A similar study was conducted where a terpolymer consisting of specific amounts of n-butyl acrylate, n-butyl methacrylate, and 2-hydroxyethyl acrylate was used as a polyol to fabricate siloxane-acrylic-polyurethane coatings when combined with 3-aminopropyl terminated PDMS and an aliphatic polyisocyanate.[97] Using combinatorial techniques, the compositions of the three monomers in the polyol precursor were systematically varied and siloxane-acrylic-polyurethane formulations resulting in better release of *Navicula* diatoms and *Ulva* sporelings than control PDMS surfaces were identified. It was determined that generally increasing the n-butylacrylate and 2-hydroxyethylacrylate composition in the acrylic polyol improved fouling release of both *Navicula* diatoms and *Ulva* sporelings.

PDMS Derived Coatings Filled with Carbon Nanotubes and Natural Sepiolites

Beigbeder et al. have recently reported on the development of PDMS coatings filled with low levels of two different nanofillers.[99] Either multiwall carbon nanotubes (MWCNT) or natural sepiolite (NS) (a microcrystalline-hydrated magnesium silicate, chemical structure $Si_{12}Mg_8O_{30}(OH)_4(H_2O)_4 \cdot 8H_2O$, exhibiting a microfibrous morphology) were used. The antifouling and fouling-release behavior of these coatings were explored through laboratory assays involving the representative soft fouling organisms, *Ulva* and the representative hard fouling organism, *Balanus amphitrite*. The bulk properties of the coatings appeared unchanged by the addition of low amounts of nanofiller (up to 0.2%). The surface properties of the coatings were found to be different however, with the filled coatings retaining more of their hydrophobicity upon immersion in water. While the removal of both *Ulva* zoospores and sporelings was generally increased for both the MWCNT and NS filled coatings, the most profound effect demonstrated in this study was the drastic reduction of adhesion strength of adult barnacles growing on PDMS elastomer containing a small

amount (0.05%) of MWCNT. This demonstrated that independent of bulk properties, the surface properties affect settlement and more pointedly, the fouling-release behavior of the filled materials.

Phosphazene Polymers

Polyphosphazenes consist of an inorganic –P=N- backbone with organic groups linked covalently to the phosphorous atoms. Poly[bis(2,2,2-trifluoroethoxy)phosphazene] (PTFEP) is known to be nonthrombogenic in nature.[100, 101] This hydrophobic, fluorinated phosphazene polymer, possessing an advancing water contact angle of about 110°, is not inherently antifouling in nature however. Rather, the resistance to platelet adhesion is derived from the adsorption of a "conditioning film" of human serum albumin. Once this conditioning film is in place, its presence is what actually prevents the adsorption of fibrinogen and fibronectin.[102] When compared to control surfaces including poly(methylmethacrylate), silicone, 3-aminopropyltrimethoxysilane SAM, and octyltrichlorosilane SAM, Welle et al. found that a PTFEP surface showed the highest adsorption of human serum albumin and the lowest adsorption of human fibrinogen from a 10% solution of human plasma in phosphate buffer saline.[102] This indicates that the biocompatibility and antifouling property of this hydrophobic PTFEP polymer is due to a competitive adsorption of albumin that passivates the surface with respect to other proteins. This suggests that similar effects must be anticipated and taken into account with regards to long term antifouling and fouling-release properties of polymeric coatings since similar conditioning films may develop depending on what the coatings are exposed to in their local environment.

Polyoxazoline Polymers

Polyoxazolines, a well known and widely studied group of polymers, have received renewed interest as biomaterials.[103] These polymers are hydrophilic and relatively non-toxic and have promise as antifouling coatings for biomedical applications. Konradi et al. have investigated the antifouling properties of side-chain polymers with poly (2-methyl-2-oxazoline) (PMOXA) side chains and a polycationic poly($_L$-lysine) (PLL) backbone, depicted in figure 1.15.[65] These polymers were designed to be analogous to the PEG-based side chain polymers previously studied by Kenausis et al.[58] The PLL-g-PMOXA copolymers are spontaneously adsorbed onto metal oxide surfaces through ionic interactions between the positively charged primary amine groups of the PLL with the negatively charged metal oxide surface. With optimal side chain grafting density, the resulting adsorbed monolayer of the PLL-g-PMOXA copolymer was able to eliminate protein adsorption from full human serum to less than 2 ng/cm^2. This was equivalent to the protein repellant properties of the best PEG-based coatings. Care must be taken however since coatings that are physically bound to substrates solely via electrostatic interactions are prone to desorption at high salt concentrations.[65] Thus, covalent attachment is preferred.

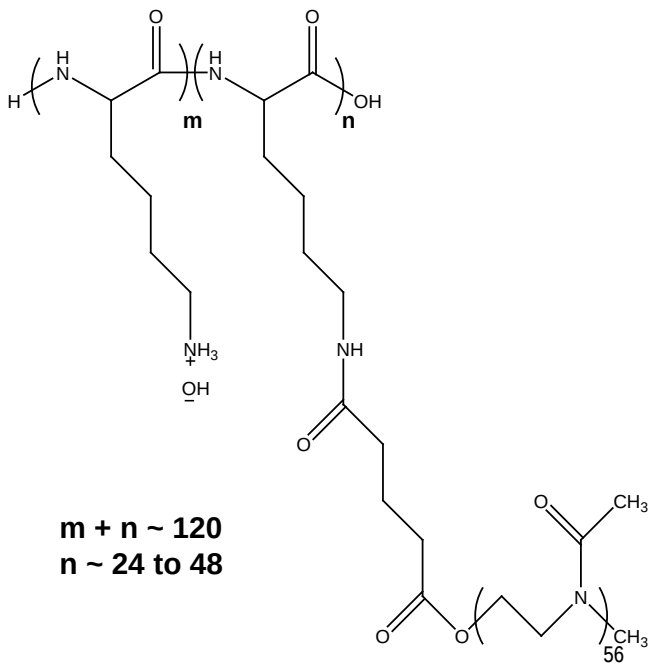

Figure 1.15. Poly($_L$-lysine)-*graft*-poly(2-methyl-2-oxazoline), a known anti-fouling polymer for biomedical applications.

In Conclusion

This introductory chapter has discussed and examined a wide range of polymeric coatings with promising anti-biofouling and fouling release properties. With an increasing focus on environmentally friendly non-toxic marine coatings, a large number of non-toxic polymer systems have been designed and evaluated in biofouling assays. When additional systems are analyzed from the closely related biomedical field, the shear number of different potential approaches to inhibiting and releasing fouling is truly vast. Based on the set of experimental data that has been reported thus far, certain generalizations can be made regarding the anti-biofouling performance of these various coatings. Hydrophilic PEGylated polymers, zwitterionic polymers, and polymers incorporating oligosaccharide moieties are inherently anti-biofouling in nature, resisting protein adsorption and cell settlement and adhesion. Hydrophobic PDMS and fluoropolymer surfaces are generally not resistant to protein

adsorption (and may actually encourage it), but are non-adhesive to cells and organisms because of their non-polar nature. Engineered microtopographies have been demonstrated as a way to impart settlement resistance to these materials however, especially when targeted towards specific organisms. Amphiphilic polymers meanwhile, incorporating hydrophilic PEGylated groups and hydrophobic fluorinated groups have shown anti-biofouling and fouling release properties comparable to or better than the widely used PDMS elastomers.

Because of their relatively low cost, there is significant ongoing effort in improving the anti-biofouling properties of PDMS elastomers, especially against diatom biofilms to which they are particularly susceptible. Additionally, increasing the yield strength and toughness of PDMS elastomers is of great importance if they are expected to endure a desirable service life in a marine environment. Meanwhile, it has been demonstrated that the cost of the relatively expensive fluorinated polymers can be controlled by blending with an inexpensive polymer since surface segregation of the low-energy fluoroalkyl group allows blending. This is another viable approach for creating anti-biofouling coatings.

Zwitterionic polymers and poly(ampholytes) are a unique class of charged polymers that show reduced protein adsorption and cell adhesion. Currently on-going work is focused on transferring success with these materials in the biomedical field to marine applications. Other ionically charged polymers such as those consisting of pyridinium groups[14] are not resistant to protein adsorption because of electrostatic interactions and in fact, adhesion and close contact of cells with surfaces of pyridinium polymers and other polycations[35] are believed to be important factors in their antimicrobial activity.

The future direction of anti-biofouling research should focus on correlating molecular level details of a surface with anti-biofouling behavior while establishing a

fundamental understanding of anti-biofouling and fouling release mechanisms. Understanding why certain organisms such as diatoms adhere strongly to non-polar PDMS coatings (which are otherwise non-adhesive in nature) will require knowledge on the role of mechanical properties of the coating on fouling release and the chemical composition of the adhesive matrices secreted by these organisms. Additionally, since very few anti-biofouling moieties show efficacy towards a wide range of organisms, more universal fouling release and control materials are needed, perhaps through the combination of multiple material approaches.

The following dissertation will focus primarily on the final concern voiced here, specifically the need for materials with more robust antifouling and fouling release properties towards as wide a range of organisms as possible. The majority of the work will be focused around the use of a flexible multilayer coating system consisting of a thick layer of a polystyrene-*block*-poly(ethylene-*ran*-butylene)-*block*-polystyrene (SEBS) thermoplastic elastomer and a thin layer of a styrenic surface active block copolymer (SABC). The SEBS thermoplastic elastomer base layer can be used to control the bulk modulus of the coating while the surface active block copolymer is used to control surface chemistry and functionality. Through this two pronged approach, we are able to tune bulk modulus through exploration of different thermoplastic elastomers, and surface chemistry through the use of different SABCs. Amphiphilic diblock SABCs derived from a polystyrene-*block*-poly(acrylic acid) precursor were explored in addition to three different classes of amphiphilic triblock SABCs derived from a polystyrene-*block*-poly(ethylene-*ran*-butylene)-*block*-poly(isoprene) precursor. Both approaches are profiled in Figure 1.16.

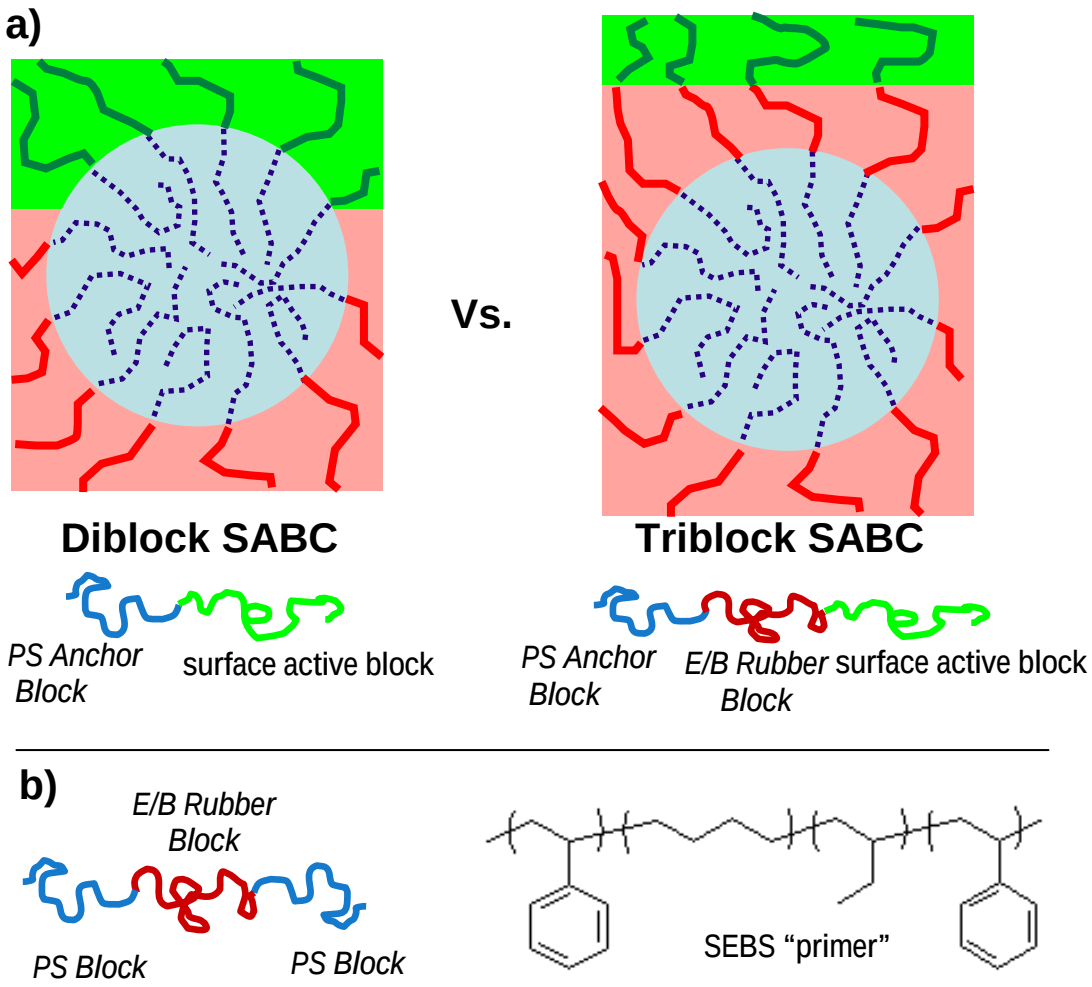

Figure 1.16. a) Schematic representation of multilayer coating system using both diblock SABCs and triblock SABCs. b) Schematic representation and chemical structure of polystyrene-*block*-poly(ethylene-*ran*-butylene)-*block*-polystyrene base layer.

Additionally, the effect of coating modulus will be explored using two different SEBS thermoplastic elastomer base layers with elastic modulii values varying by an order of magnitude while controlling the SABC top layer. Finally, a fundamental study using hydrophobic and hydrophilic self assembled monolayers (SAMs) and hydrophobic and hydrophilic polymer brushes to examine the fouling interactions of the green alga *Ulva* and *Navicula* diatoms will be reported on.

REFERENCES

1 S. Krishnan, C. J. Weinman, and C. K. Ober, *J. Mater. Chem.*, 2008, **18**, 3405.

2 T. Vladkova, *Journal of the University of Chemical Technology and Metallurgy*, 2007, **42**, 239.

3 D. M. Yebra, S. Kiil, and K. Dam-Johansen, *Prog. Org. Coat.*, 2004, **50**, 75.

4 L. D. Chambers, K. R. Stokes, F. C. Walsh, and R. J. K. Wood, *Surf. Coat. Technol.*, 2006, **201**, 3642.

5 J. Genzer and K. Efimenko, *Biofouling*, 2006, **22**, 339.

6 C. Werner, M. F. Maitz, and C. Sperling, *J. Mater. Chem.*, 2007, **17**, 3376.

7 N. Wisniewski and M. Reichert, *Colloids and Surfaces B: Biointerfaces*, 2000, **18**, 197.

8 J. M. Harris and R. B. Chess, *Nature Reviews Drug Discovery*, 2003, **2**, 214.

9 H. Otsuka, Y. Nagasaki, and K. Kataoka, *Advanced Drug Delivery Reviews*, 2003, **55**, 403.

10 V. P. Torchilin, *AAPS Journal*, 2007, **9**, E127.

11 L. Chromy and K. Uhacz, *Journal of the Oil and Colour Chemists' Association*, 1978, **61**, 39.

12 R. F. Brady, *Journal of Protective Coatings & Linings*, 2003, **20**, 33.

13 D. Park, J. A. Finlay, R. J. Ward, C. J. Weinman, S. Krishnan, M. Y. Paik, K. E. Sohn, M. E. Callow, J. A. Callow, D. L. Handlin, C. L. Willis, D. A. Fischer, E. R. Angert, E. J. Kramer, and C. K. Ober, *manuscript in preparation*.

14 S. Krishnan, R. J. Ward, A. Hexemer, K. E. Sohn, K. L. Lee, E. R. Angert, D. A. Fischer, E. J. Kramer, and C. K. Ober, *Langmuir*, 2006, **22**, 11255.

15 P. Majumdar, E. Lee, N. Patel, S. J. Stafslien, J. Daniels, and B. J. Chisholm, *Journal of Coatings Technology and Research*, 2008, **5**, 405.

16 N. Aumsuwan, R. Danyus, S. Heinhorst, and M. W. Urban, *Biomacromolecules*, 2008, **9**, 1712.

17 N. Aumsuwan, S. Heinhorst, and M. W. Urban, *Biomacromolecules*, 2007, **8**, 3525.

18 N. Aumsuwan, S. Heinhorst, and M. W. Urban, *Biomacromolecules*, 2007, **8**, 713.

19 E. A. Vogler, in 'Water', ed. M. Morra, New York, 2001.

20 J. D. Andrade, R. N. King, D. E. Gregonis, and D. L. Coleman, *J. Polym. Sci. Polym. Symp.*, 1979, **66**, 313.

21 Y. Ikada, in 'Water', ed. M. Morra, New York, 2001.

22 M. E. Callow and J. A. Callow, *Biologist*, 2002, **49**, 1.

23 A. Rosenhahn, T. Ederth, and M. E. Pettitt, *Biointerphases*, 2008, **3**, IR1.

24 M. L. Carman, T. G. Estes, A. W. Feinberg, J. F. Schumacher, W. Wilkerson, L. H. Wilson, M. E. Callow, J. A. Callow, and A. B. Brennan, *Biofouling*, 2006, **22**, 11.

25 J. F. Schumacher, M. L. Carman, T. G. Estes, A. W. Feinberg, L. H. Wilson, M. E. Callow, J. A. Callow, J. A. Finlay, and A. B. Brennan, *Biofouling*, 2007, **23**, 55.

26 C. D. Anderson and J. E. Hunter, NAV2000, Venice, 2000.

27 S. N. Ghiya, *Paintindia*, 1987, 19.

28 S. Abarzua and S. Jakubowsky, *Mar. Ecol. Prog. Ser.*, 1995, **123**, 301.

29 M. E. Callow and R. L. Fletcher, *Int. Biodeter. Biodegre.*, 1994, **34**, 333.

30 A. S. Clare, D. Rittschof, D. J. Gerhart, and J. S. Maki, *Invertebr. Reprod. Dev.*, 1992, **22**, 67.

31 R. L. Townsin, *Biofouling*, 2003, **19 (Supplement)**, 9.

32 M. P. Schultz, *Biofouling*, 2007, **23**, 331.

33 T. Ikeda, B. Lee, H. Yamaguchi, and S. Tazuke, *Biochim. Biophys. Acta, Biomembranes*, 1990, **1021**, 56.

34 D. Park, J. Wang, and A. M. Klibanov, *Biotechnology Progress*, 2006, **22**, 584.

35 P. Kurt, L. Wood, D. E. Ohman, and K. J. Wynne, *Langmuir*, 2007, **23**, 4719.

36 J. Huang, H. Murata, R. R. Koepsel, A. J. Russell, and K. Matyjaszewski, *Biomacromolecules*, 2007, **8**, 1396.

37 J. Lin, S. Qiu, K. Lewis, and A. M. Klibanov, *Biotechnology and Bioengineering*, 2003, **83**, 168.

38 S. Krishnan, J. A. Finlay, A. Hexemer, N. Wang, C. K. Ober, E. J. Kramer, M. E. Callow, J. A. Callow, and D. A. Fischer, *Polym. Prepr. (Am. Chem. Soc., Div. Polym. Chem)*, 2005, **46**, 1248.

39 P. Majumdar, E. Lee, N. Patel, K. Ward, S. J. Stafslien, J. Daniels, B. J. Chisholm, P. Boudjouk, M. E. Callow, J. A. Callow, and S. E. M. Thompson, *Biofouling*, 2008, **24**, 185.

40 S. Ye, A. McClelland, P. Majumdar, S. J. Stafslien, J. Daniels, B. Chisholm, and Z. Chen, *Langmuir*, 2008, **24**, 9686.

41 S. Krishnan, N. Wang, C. K. Ober, J. A. Finlay, M. E. Callow, J. A. Callow, A. Hexemer, K. E. Sohn, E. J. Kramer, and D. A. Fischer, *Biomacromolecules*, 2006, **7**, 1449.

42 P. Busch, S. Krishnan, M. Y. Paik, G. E. S. Toombes, D.-M. Smilgies, S. M. Gruner, and C. K. Ober, *Macromolecules*, 2007, **40**, 81.

43 J. P. Youngblood, L. Andruzzi, C. K. Ober, A. Hexemer, E. J. Kramer, J. A. Callow, J. A. Finlay, and M. E. Callow, *Biofouling*, 2003, **19**, 91.

44 S. Krishnan, R. Ayothi, A. Hexemer, J. A. Finlay, K. E. Sohn, R. Perry, C. K. Ober, E. J. Kramer, M. E. Callow, J. A. Callow, and D. A. Fischer, *Langmuir*, 2006, **22**, 5075.

45 C. J. K. Weinman, S.; Park, D.; Paik, M. Y.; Wong, K., Fischer, D. A.; Handlin, D. A., Kowalke, G. L.; Wendt, D. E.; Sohn, K. E.; Kramer, E. J.; Ober, C. K., *PMSE Preprints*, 2007, **96**, 597.

46 E. Martinelli, S. Agostini, G. Galli, E. Chiellini, A. Glisenti, M. E. Pettiitt, M. E. Callow, J. A. Callow, K. Graf, and F. W. Bartels, *Langmuir*, 2008, **24**, 13138.

47 J. C. Yarbrough, J. P. Rolland, J. M. DeSimone, M. E. Callow, J. A. Finlay, and J. A. Callow, *Macromolecules*, 2006, **39**, 2521.

48 H. Ma, J. Hyun, P. Stiller, and A. Chilkoti, *Advanced Materials*, 2004, **16**, 338.

49 S. Schilp, A. Kueller, A. Rosenhahn, M. Grunze, M. E. Pettitt, M. E. Callow, and J. A. Callow, *Biointerphases*, 2007, **2**, 143.

50 A. Statz, J. A. Finlay, J. Dalsin, M. E. Callow, J. A. Callow, and P. B. Messersmith, *Biofouling*, 2006, **22**, 391.

51 M. Yu and T. J. Deming, *Macromolecules*, 1998, **31**, 4739.

52 H. Yamamoto, *J. Adhes. Sci. Tech.*, 1987, **1**, 177.

53 J. L. Dalson and P. B. Messersmith, *Materials Today*, 2005, **8**, 38.

54 A. G. Fane, W. Xi, and R. Wang, *Interface Science and Technology*, 2006, **10**, 109.

55 G. Pearce, *Filtration & Separation*, 2007, **44**, 30.

56 Y.-H. Zhao, B.-K. Zhu, L. Kong, and Y.-Y. Xu, *Langmuir*, 2007, **23**, 5779.

57 R. Michel, S. Paschle, M. Textor, and D. G. Castner, *Langmuir*, 2005, **21**, 12327.

58 G. L. Kenausis, J. Voeroes, D. L. Elbert, N. Huang, R. Hofer, L. R. Taylor, M. Textor, J. A. Hubbell, and N. D. Spencer, *Journal of Physical Chemistry B*, 2000, **104**, 3298.

59 K. L. Prime and G. M. Whitesides, *J. Am. Chem. Soc.*, 1993, **115**, 10714.

60 M. Heuberger, T. Drobek, and N. D. Spencer, *Biophysical Journal*, 2005, **88**, 495.

61 M. Heuberger, T. Drobek, and J. Voeroes, *Langmuir*, 2004, **20**, 9445.

62 H. Jiang, S. Manolache, A. C. Wong, and F. S. Denes, *Journal of Applied Polymer Science*, 2006, **102**, 2324.

63 S. R. Benhabbour, L. Liu, H. Sheardown, and A. Adronov, *Macromolecules*, 2008, **41**, 2567.

64 S. Sharma, R. W. Johnson, and T. A. Desai, *Langmuir*, 2004, **20**, 348.

65 R. Konradi, B. Pidhatika, A. Muhlebach, and M. Textor, *Langmuir*, 2008, **24**, 613.

66 K. Rasmussen, P. R. Willemsen, and K. Ostgaard, *Biofouling*, 2002, **18**, 177.

67 P. R. Cowie, M. J. Smith, F. Hannah, M. J. Cowling, and T. Hodgkeiss, *Biofouling*, 2006, **22**, 173.

68 T. Ekblad, G. Bergstrom, T. Ederth, S. L. Conlan, R. Mutton, A. S. Clare, S. Wang, Y. Liu, Q. Zhao, F. D'Souza, G. T. Donnelly, P. R. Willemsen, M. E. Pettitt, M. E. Callow, J. A. Callow, and B. Liedberg, *Biomacromolecules*, 2008, **9**, 2775.

69 A. Larsson, T. Ekblad, O. Anderson, and B. Liedberg, *Biomacromolecules*, 2007, **8**, 287.

70 S. Han, C. Kim, and D. Kwon, *Polymer*, 1997, **38**, 317.

71 S. Morlat and J. L. Gardette, *Polymer*, 2003, **44**, 7891.

72 F. Kawai, *Applied microbiology and biotechnology*, 2002, **58**, 30.

73 A. Larsson and B. Liedberg, *Langmuir*, 2007, **23**, 11319.

74 C. S. F. Gudipati, J. A.; Callow, J. A.; Callow, M. E.; Wooley, K. L., *Langmuir*, 2005, **21**, 3044.

75 K. T. Powell, C. Cheng, and K. L. Wooley, *Macromolecules*, 2007, **40**, 4509.

76 J. A. Finlay, S. Krishnan, M. E. Callow, J. A. Callow, R. Dong, N. Asgill, K. Wong, E. J. Kramer, and C. K. Ober, *Langmuir*, 2008, **24**, 503.

77 K. Ishihara, R. Araguaki, U. Tomoko, A. Watanabe, and N. Nakabayashi, *Journal of Biomedical Materials Research*, 1990, **24**, 1069.

78 J. A. Hayward and D. Chapman, *Biomaterials*, 1984, **5**, 135.

79 H. Kitano, A. Kawasaki, H. Kawasaki, and S. Morokoshi, *Journal of Colloid and Interface Science*, 2005, **282**, 340.

80 H. Kitano, S. Tada, T. Mori, K. Takaha, M. Gemmei-Ide, M. Tanaka, M. FUkuda, and Y. Yokoyama, *Langmuir*, 2005, **21**, 11932.

81 S. Chen, J. Zheng, L. Li, and S. Jiang, *J. Am. Chem. Soc.*, 2005, **127**, 14473.

82 S. Chen, L. Liu, and S. Jiang, *Langmuir*, 2006, **22**, 2418.

83 Y. Chang, S. Chen, Z. Zhang, and S. Jiang, *Langmuir*, 2006, **22**, 2222.

84 Z. Zhang, T. Chao, S. Chen, and S. Jiang, *Langmuir*, 2006, **22**, 10072.

85 G. Cheng, Z. Zhang, S. Chen, J. D. Bryers, and S. Jiang, *Biomaterials*, 2007, **28**, 4192.

86 J. Ladd, Z. Zhang, S. Chen, J. C. Hower, and S. Jiang, *Biomacromolecules*, 2008, **9**, 1357.

87 S. Chen and S. Jiang, *Advanced Materials*, 2008, **20**, 335.

88 M. T. Bernards, G. Cheng, Z. Zheng, S. Chen, and S. Jiang, *Macromolecules*, 2008, **41**, 4216.

89 N. B. Holland, Y. Qiu, M. Ruegsegger, and R. E. Marchant, *Nature*, 1998, **392**, 799.

90 J. Zhu and R. E. Marchant, *Biomacromolecules*, 2006, **7**, 1036.

91 Y. Tang, J. A. Finlay, G. L. Kowalke, A. E. Meyer, F. V. Bright, M. E. Callow, J. A. Callow, D. E. Wendt, and M. R. Detty, *Biofouling*, 2005, **21**, 59.

92 S. Krishnan, Y.-J. Kwark, and C. K. Ober, *Chemical Record*, 2004, **4**, 315.

93 M. E. Callow, A. R. Jennings, A. B. Brennan, C. E. Seegert, A. Gibson, L. Wilson, A. Feinberg, R. Baney, and J. A. Callow, *Biofouling*, 2002, **18**, 237.

94 L. Hoipkemeier-Wilson, J. F. Schumacher, M. L. Carman, A. L. Gibson, A. W. Feinberg, M. E. Callow, J. A. Finlay, J. A. Callow, and A. B. Brennan, *Biofouling*, 2004, **20**, 53.

95 K. K. Chung, J. F. Schumacher, E. M. Sampson, R. A. Burne, P. J. Antonelli, and A. B. Brennan, *Biointerphases*, 2007, **2**, 89.

96 J. F. Schumacher, N. Aldred, M. E. Callow, J. A. Finlay, J. A. Callow, A. S. Clare, and A. B. Brennan, *Biofouling*, 2007, **23**, 307.

97 R. J. Pieper, A. Ekin, D. C. Webster, F. Casse, J. A. Callow, and M. E. Callow, *Journal of Coatings Technology and Research*, 2007, **4**, 453.

98 A. Ekin, D. C. Webster, J. W. Daniels, S. J. Stafslien, F. Casse, J. A. Callow, and M. E. Callow, *Journal of Coatings Technology and Research*, 2007, **4**, 435.

99 A. Beigbeder, P. Degee, S. L. Conlan, R. J. Mutton, A. S. Clare, M. E. Pettitt, M. E. Callow, J. A. Callow, and P. Dubois, *Biofouling*, 2008, **24**, 291.

100 D. R. Tur, V. V. Korsak, S. V. Vinogradova, N. B. Dobrova, S. P. Novikova, M. B. Il'ina, and E. S. Sidorenko, *Acta Polymerica*, 1985, **36**, 627.

101 S. Satzl, C. Henn, P. Christoph, P. Kurz, U. Stampfl, S. Stampfl, F. Thomas, B. Radeleff, I. Berger, M. Grunze, and G. M. Richter, *Investigative Radiology*, 2007, **42**, 303.

102 A. Welle, M. Grunze, and D. Tur, *Journal of Colloid and Interface Science*, 1998, **197**, 263.

103 N. Adams and U. S. Schubert, *Advanced Drug Delivery Reviews*, 2007, **59**, 1504.

CHAPTER 2

PROTEIN ADSORPTION RESISTANCE OF ANTI-BIOFOULING BLOCK COPOLYMERS CONTAINING AMPHIPHILIC SIDE CHAINS*

*Adapted from C. J. Weinman, N. Gunari, S. Krishnan, R. Dong, M. Y. Paik, K. E. Sohn, G. C. Walker, E. J. Kramer, D. A. Fischer, and C. K. Ober. *To be submitted: Soft Matter*.

Abstract

Surface active block copolymers (SABCs) with amphiphilic side chains containing ethoxylated fluoroalkyl groups have previously demonstrated advantageous properties with regards to marine fouling resistance and release. While it was previously postulated that the ability of the block copolymer surface to undergo an environmentally-dependent transformation in surface chemistry aided this behavior, protein adsorption characteristics of the surface were never explored. This study aims to expand our knowledge of how a protein interacts with the amphiphilic surface active block copolymer in an aqueous environment through experiments with bovine serum albumin (BSA), a widely utilized test protein. Fluorescence microscopy analysis using BSA labeled with fluorescein isothiocyanate (BSA-FITC) was performed on a SABC test surface to establish the polymer's protein adsorption resistance. Additionally, atomic force microscopy (AFM) based chemical force microscopy (CFM) was utilized to examine the force of adhesion of an AFM tip functionalized with strands of BSA protein with the SABC. 58% of the adhesion force measurements for the BSA coated AFM tip interacting with the surface of the amphiphilic SABC demonstrated no measurable force of adhesion in phosphate buffered saline (PBS). Furthermore, no measurements of force of adhesion were made in excess of 0.15 nN. This was in stark contrast to the non-zero mean adhesion force seen for several control surfaces in PBS.

Introduction

Anti-biofouling surfaces are of particular interest due to their wide range of applications from prevention of marine biofouling[1-5] to use in biomedical implants[6]. Generally, antifouling surfaces are based on the minimization of intermolecular forces between an interacting biomolecule and a surface. Hydrophobic surfaces such as

poly(dimethylsiloxane) (PDMS) are known to easily release biofouling under applied shear while hydrophilic polymers such as poly(ethylene glycol) (PEG), which possess a low polymer-water interfacial energy, demonstrate excellent resistance to protein adsorption and cell adhesion. Figure 2.1 depicts an amphiphilic block copolymer that was previously synthesized by Krishnan et al. and evaluated as an anti-fouling material against *Ulva* sporelings, *Navicula* diatoms and barnacle cyprid larvae[7, 8]. This material was found to perform very well against a wide range of fouling organisms, leading to the hypothesis that the chemical ambiguity and dynamic structure of the surface lowered the entropic and enthalpic driving forces for the adsorption of adhesive macromolecules associated with cellular adhesion[9]. Our previous studies did not examine forces of interaction of proteins with this polymeric surface however. Knowledge of this behavior will aid better understanding of the anti-biofouling performance of such coatings.

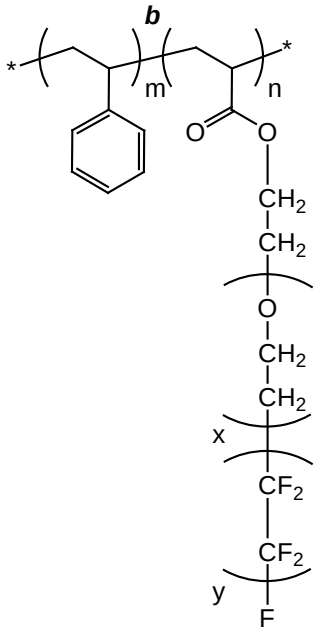

Figure 2.1. Schematic of polystyrene-*block*-poly(ethoxylated fluoroalkyl acrylate), PS-*b*-PAA-AMP.

Protein adsorption behavior of a given material depends primarily on surface free energy and chemical functionality.[10, 11] Multitudes of previous studies have been conducted on the protein adsorption characteristics of hydrophobic and hydrophilic self-assembled monolayers (SAMs) in conjunction with both grafted polymer brushes and polymeric thin films. In general, hydrophilic surfaces such as those containing poly(ethylene glycol) (PEG) or poly(ethylene oxide) (PEO) offer excellent resistance to protein adsorption and cellular adhesion.[12-14] In marked contrast, however, hydrophobic surfaces have demonstrated a tendency to adsorb proteins at elevated levels.[15, 16] Thus, the protein adsorption behavior of an amphiphilic material capable of presenting both hydrophobic and hydrophilic moieties is of great interest.

Atomic force microscopy (AFM)[17] with chemically modified tips is a dynamic analytical technique that can be used to determine adhesion forces between the functionalities on the tips and surfaces of interest. In previous studies, this technique has been used to map the spatial arrangement of chemical functional groups on a lithographically patterned SAM surface,[18] probe the adhesion of grafted macromolecules,[19] examine single molecule bond strengths,[20] determine the adhesion properties of a range of surfaces,[21, 22] study the role of temperature and media on intermolecular interactions involving hydrogen bonds,[23] and measure the elastic modulus of compliant surfaces.[24] The technique has been covered extensively in reviews and has a wide range of applications.[25-30] Further illustrating the breadth of applications of this technique, a recent study even reported on the use of chemical force microscopy to analyze the force of adhesion associated with a single spatula of a gecko's toe.[31] While chemical force microscopy has been used previously in the realm of biofouling research to probe the interaction between PDMS and *Ulva* spore adhesion,[32] to the best of our knowledge the interaction of protein with the surface of a specially tailored antifouling polymer has never been expressly examined before.

In this report, we begin with a description of the synthesis of the block copolymer and the preparation of surfaces, specifically focusing on changes in the synthetic scheme from the previous work reported by Krishnan et al.[7] Subsequently, a brief discussion of surface properties as determined by dynamic water contact-angle analysis, near-edge X-ray adsorption fine structure (NEXAFS) spectroscopy, and AFM imaging will be described. Finally, significant attention is paid to both protein adsorption experiments and chemical force microscopy conducted with bovine serum albumin (BSA) performed on surfaces of the amphiphilic block copolymer and several controls.

Experimental Section:

Materials

Polystyrene-*block*-poly(ethoxylated fluoroalkyl acrylate), PS-*b*-PAA-AMP, was prepared in a manner analogous to that previously reported.[7, 8] Styrene (FW 104.15, Aldrich, 99%) was agitated with an excess of basic alumina to remove the 4-*tert*-butylcatechol inhibitor. *Tert*-butyl acrylate (tBA, FW 128.17, Aldrich, 98%) containing 10-20 ppm of monomethyl ether hydroquinone as inhibitor was agitated with an excess of inhibitor remover (Aldrich) and filtered. The tBA monomer was then dried over sodium sulfate and distilled under vacuum. Copper(I) bromide (CuBr, FW 143.45, Aldrich, 99.999%), copper(II) bromide ($CuBr_2$, FW 223.35, Aldrich, 99.999%), 1,1,4,7,7-pentamethyldiethylene-triamine (PMDETA, $[(CH_3)_2NCH_2CH_2]_2NCH_3$, FW 173.30, Aldrich, 99%), methyl 2-bromopropionate (MBP, $CH_3CHBrCOOCH_3$, FW 167.00, Aldrich, 98%), 1,3-dicyclohexylcabrodiimide (DCC, $C_6H_{11}N=C=NC_6H_{11}$, FW 206.33, Aldrich, 99%), 4-(dimethylamino)pyridine (DMAP, $(CH_3)_2NC_5H_4N$, FW 122.17, Aldrich 99%), acetone (99.5%), anhydrous pyridine (99.8%), and anhydrous tetrahydrofuran (THF)

were obtained from Sigma-Aldrich and used without further purification. The ethoxylated fluoroalkyl surfactant Zonyl FSO-100, $F(CF_2CF_2)_y(CH_2CH_2O)_xCH_2CH_2OH$ (x = 0-15 and y = 1-7) (registered trademark of E.I. du Pont de Nemours & Co., Inc.; CAS no 122525-99-9), also was purchased from Sigma-Aldrich and used as received. Bovine serum albumin labeled with fluorescein isothiocyanate (BSA-FITC) was purchased from Sigma-Aldrich. 1,4-Dioxane, methanol, hydrochloric acid (37%) and all other reagents were used as received. The PBS buffer solution was prepared in water to yield 0.050 M phosphate buffer, 0.150 M sodium chloride, and a pH of 7.4 at 25 °C. Polystyrene-*block*-poly(ethylene-*co*-butylene)-*block*-polystyrene (SEBS) triblock thermoplastic elastomer (Kraton G1652M) was generously provided by Kraton Polymers.

Polymer Synthesis and Characterization

The synthetic scheme used closely followed the multi-step scheme previously reported in Krishnan et al.,[7] with modifications to the stoichiometry to effectively scale-up the amount of material synthesized by a factor of three or greater[8]. The synthetic scheme is illustrated in Figure 2.2. *Tert*-butyl acrylate (30.80 g) mixed with 9 mL of acetone, degassed by bubbling Ar, was combined with 0.42 g of PMDETA, 0.345 g CuBr and 0.027 g $CuBr_2$ and reacted at 60 °C for 6 h. The crude product was dissolved in diethyl ether and precipitated in an equivolume mixture of water and methanol. The product was collected, dissolved again in diethyl ether and reprecipitated. 17.75 g of bromine-terminated poly(*t*BA) macroinitiator (I) was produced with a molecular weight of 5500 g/mol and a polydispersity index of 1.10. Subsequently, polystyrene-*block*-poly(*t*BA) (II) was produced by sequential atom transfer radical polymerization (ATRP) reaction of styrene. 14 g of (I) was dissolved in 69.26 g of degassed styrene. 0.950 g of CuBr and 1.15 g of PMDETA was added to

the mixture. The reaction mixture was heated at 100 °C for 90 minutes, allowed to cool, diluted in THF and precipitated in cold methanol. The sample was collected and reprecipitated from THF in cold methanol. 62.80 g of (II) were produced with a polydispersity index of 1.17. The degrees of polymerization of the polystyrene and poly(*t*BA) blocks were found to be (m =) 369 and (n =) 43 respectively by performing integration of the relevant ^{1}H NMR spectra (data not shown). This corresponded to a polystyrene block weight of 38,000 g/mol. The poly(*t*BA) block was then deprotected quantitatively to poly(acrylic acid) (PAA) using hydrochloric acid, resulting in a PAA block weight of 3000 g/mol. Deprotection was done by dissolving 20 g of (II) in 200 mL 1,4-dioxane and adding ~10 mL of concentrated HCl to the reaction mixture. The mixture was then refluxed at 100° C for 6 hr and precipitated in an ice/water mixture. The reaction yielded 17.15 g of polystyrene-*block*-poly(acrylic acid) (III), PS-*b*-PAA. Finally, to synthesize polystyrene-*block*-poly(fluoroalkyl ethoxylated acrylate) (IV), PS-*b*-PAA-AMP, PS-*b*-PAA (10 g) was dissolved in 50 mL of pyridine (20% w/v). In a separate flask, DCC (12.61 g), DMAP (0.94 g), and Zonyl FSO-100 (28 g) were dissolved in 300 mL of THF. The THF solution was then added drop-wise to the polymer containing pyridine solution and mixed vigorously for 96 h (4 days). Upon completion, the reaction solution was filtered to remove insoluble dicyclohexylurea byproduct, concentrated under reduced pressure, and the polymer was recovered by precipitation in cold methanol (~0 °C). Further purification was accomplished by subsequently precipitating the polymer from THF into cold methanol twice.

^{1}H NMR for PS-*b*-PAA-AMP (300 MHz, $CDCl_3$, δ): 6.6 and 7.1 (5H styrene); 4.18 (br s, 2H, -$COOCH_2$-); 3.77 (t, 2H, -$COOCH_2CH_2$); 3.64 (br s, -CH_2CH_2O-), 2.42 (m, -CH_2CF_2-), 1.86, 1.45 (backbone). IR (dry film) υ_{max} (cm $^{-1}$): 3028 (C-H stretching, aromatic); 2920 (C-H stretching, backbone); 1736 (C=O stretching, ester); 1603 (C=C stretching, aromatic); 1493, 1452 (C-H bending, backbone); 1420-985 (C-

F stretching); 762 and 702 (C-H bending, aromatic). These results were generally consistent with results previously reported.

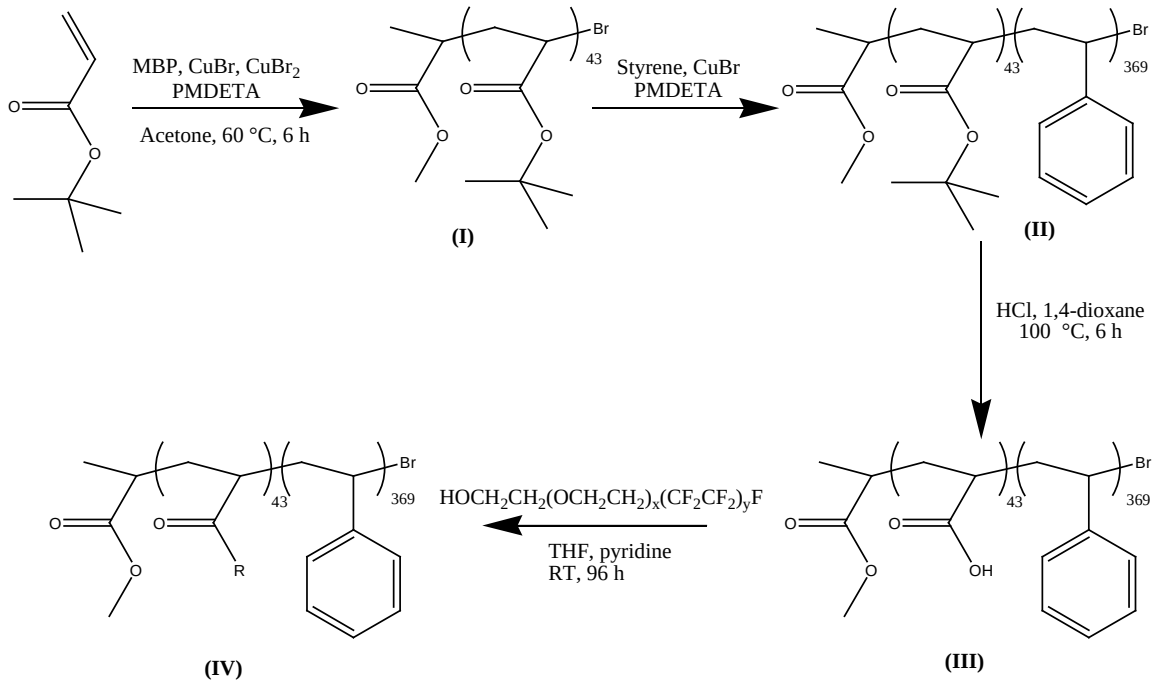

Figure 2.2. Synthetic scheme used to produce PS-*b*-PAA-AMP surface active block copolymer.

Gel permeation chromatography of a THF solution of polymers (1 mg/mL) was carried out using four Waters Styragel HT columns operating at 40 °C in conjunction with Waters 490 ultraviolet (λ = 254 nm) and Waters 410 refractive index detectors. The molecular weight range of the columns was from 500 to 10^7 g/mol. THF was used as the eluent at a flow rate of 1 mL/min, and toluene was used as a marker for flow calibration. The IR spectra of the polymers cast as films from TFT solution on sodium chloride plates was collected using a Mattson 2020 Galaxy Series FTIR spectrometer. ^{1}H NMR spectra were recorded using a Varian Gemini spectrometer with deuterated solvents.

Surface Preparation and Characterization

Surfaces for NEXAFS spectroscopy, contact angle measurement, AFM imaging, BSA protein adsorption testing, and BSA adhesion force measurements were prepared on silicon wafers by spin-coating 3% (w/v) solutions of PS_{38K}-*b*-PAA_{3K}-AMP in TFT at 2500 rpm using a Cee model 100CB spin coater. SEBS control surfaces were prepared in an analogous fashion using toluene as a solvent. All surfaces prepared for study were annealed in a vacuum oven at reduced pressure at 120 °C for at least 12 h followed by slow cooling to room temperature.

Contact angles were measured using an NRL contact angle goniometer (Ramé-Hart model 100-00) at room temperature. Dynamic water contact angle measurements were performed by the addition and retraction of a drop of water on the surface.

NEXAFS experiments were carried out on the U7A NIST/Dow materials characterization end-station at the National Synchrotron Light Source at Brookhaven National Laboratory (BNL). The general underlying principles of NEXAFS and a description of the beam line at BNL have been previously reported on.[33, 34] The partial-electron-yield (PEY) signal was collected using a channeltron electron multiplier with an adjustable entrance grid bias (EGB). Data was reported for a grid bias of -150 V. The channeltron PEY detector was positioned in the equatorial plane of the sample chamber and at an angle of 36° relative to the incoming X-ray beam. The PEY C 1s spectra were normalized by subtracting a linear pre-edge baseline and setting the edge jump to unity at 320 eV.[35] The photon energy was calibrated by adjusting the peak position of the lowest π* phenyl resonance from polystyrene to 285.5 eV.[36]

AFM Imaging

Intermittent contact mode (tapping mode) AFM images were obtained both in air and phosphate-buffered saline (PBS) buffer solution employing a MFP 3D microscope from Asylum Research, Santa Barbara, CA. V-shaped silicon nitride cantilevers (MLCT-AUNM) purchased from Veeco, Camarillo, CA with nominal spring constants of ~0.5 N/m were used for force measurement.

BSA Protein Adsorption Testing

0.5 mg of bovine serum albumin (BSA) labeled with fluorescein isothiocyanate (BSA-FITC) was dissolved in 5 mL of sea water (sea salt dissolved in deionized water). PS-*b*-PAA-AMP and a control of polystyrene-*block*-poly(ethylene-*ran*-butylene)-*block*-polystyrene (SEBS) were each spun-coat on a silicon wafer. Additionally, an uncoated silicon wafer, cleaned for 2 minutes with a Harrick PDC-32G oxygen plasma cleaner was used as a control. The three silicon wafers were then incubated in BSA-FITC solution in a dark room for two hours and rinsed with deionized water thoroughly afterwards. Fluorescence microscopy was performed using an Olympus BX51 upright microscope with a 40x UPlan Fluorite 40x dry objective (N.A. 0.75). Images were acquired using a Roper CoolSnap HQ CCD camera and Image Pro image acquisition and processing software. Fluorescein and FITC were observed with a 450 nm excitation and 550 nm emission filter set. False color fluorescence images subsequently reported here were processed using the ImageJ 1.36b software.

Adhesion Force Measurements of BSA

All measurements were obtained using an Asylum Research molecular force probe MFP-3D commercial AFM microscope. Bovine serum albumin (BSA) coated

AFM tips purchased from Novascan Technologies, Inc., Ames, IA were used for all measurements exhibiting a nominal spring constant of ~50 pN/nm. Prior to measurements, the spring constant was determined using the thermal noise method.[37] The resulting force-extension curves were analyzed with custom analysis software (Igor Pro, Wavemetrics). All experiments were carried out in PBS buffer at room temperature. A small number of force plots are obtained per tip as the AFM tips can get contaminated by the polymer which would affect the results. A total of 60 force plots were obtained from each AFM tip: 20 for a glass control, 20 for PS-*b*-PAA-AMP, and 20 for a SEBS control, in the order listed.

Results and Discussion:

Polymer Synthesis and Characterization

This work makes use of the synthetic strategy developed for polystyrene-*block*-poly(acrylic acid) block copolymer first reported by Davis and Matyjaszewski[38] while producing a PEGylated and semifluorinated polymer very closely related to that previously detailed by Krishnan, et al.[7] A new block copolymer, manifesting a cylindrical microstructure in thin films, was synthesized to probe previously unanswered questions about the ability of the nanostructured amphiphilic surface to resist protein adsorption and adhesion. Following synthesis of the PS-*b*-P*t*BA precursor, the subsequent quantitative hydrolysis to PS-*b*-PAA followed by esterification attachment of the ethoxylated fluoroalkyl side groups led to a high degree of attachment of amphiphilic units. Attachment was found to be on the order of 90 %, when calculated using integration of ^{1}H NMR spectra from the ratios of $-COOCH_2CH_2-$ protons of the side chains and the aromatic protons of the styrene. The GPC molecular weight distributions of the P*t*BA macroinitiator, PS-*b*-PtBA and the block copolymer with ethoxylated fluoroalkyl side chains, PS-*b*-PAA-AMP

demonstrated that all of the polymers had relatively low dispersity as expected. The degree of polymerization of the P*t*BA block was determined to be 43 through ^{1}H NMR by comparing the integration of the backbone >CH− and terminal >CH−Br peaks. Additionally, by examining the ^{1}H NMR spectra of the PS-*b*-PtBA block copolymer and comparing the integration of the aromatic protons (associated with the PS block) to that of all protons present, the degree of polymerization of the PS block was found to be about 369.

Surface Characterization

The advancing and receding water contact angles of PS-*b*-PAA-AMP were (86 ± 2)° and (41 ± 2)° respectively. The large contact angle hysteresis value (45°) is consistent with a dynamic surface capable of surface reconstruction. Figure 2.3 shows the NEXAFS spectrum of a PS-*b*-PAA-AMP surface prepared on silicon as described above at an angle of 50˚ between the surface and the soft X-ray beam. The sample was annealed in a vacuum oven under reduced pressure at 120 °C for 12 h. The NEXAFS spectra were generally consistent with surfaces previously reported.[7] The phenyl ring C 1s → $\pi^*_{C=C}$ resonance associated with polystyrene occurs at 285.5 eV.[34] Other peak assignments can be based on calibrated NEXAFS spectra of poly(ethylene oxide) and poly(methyl methacrylate) as discussed in Krishnan et al.[7] The resonance at 287.7 eV, which appears as a shoulder on a larger peak, is attributed to the 1s → σ^*_{C-H} transitions. The large resonance peak at 289 eV can be attributed to the 1s → $\pi^*_{C=O}$ transition. Finally, the σ^*_{C-F}, σ^*_{C-O}, and σ^*_{C-C} transitions related to the ethoxylated fluoroalkyl side chains result in resonance peaks at 293 and 295.8 eV. Thin films prepared using solutions of the block copolymer in either TFT or chloroform showed identical NEXAFS spectra, indicating that the surface morphologies obtained after

thermal annealing were equilibrium morphologies independent of processing conditions.

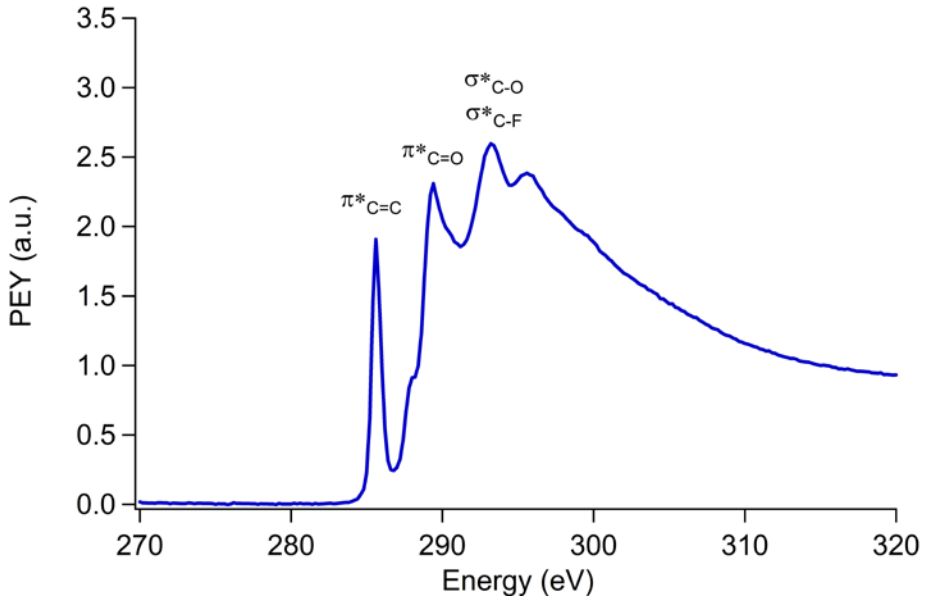

Figure 2.3. NEXAFS spectrum of a spin-coated surface of PS-*b*-PAA-AMP polymer on a silicon wafer after annealing at 120 °C for 12 hr at an angle of 50˚ between the surface and the soft X-ray beam with major resonance transition peaks labeled.

AFM Imaging

Thermally annealed thin films on silicon substrates were used for atomic force microscopy. AFM imaging of the PS-*b*-PAA-AMP sample taken in both an air and water environment are depicted in Figure 2.4. Phase images taken in both air and water showed a surface uniformly covered by PS-*b*-PAA-AMP with evidence of a cylindrical type morphology demonstrating regular domain spacing for both samples. When estimated for the surface immersed in water, the domain spacing was found to be on the order of 35 nm.

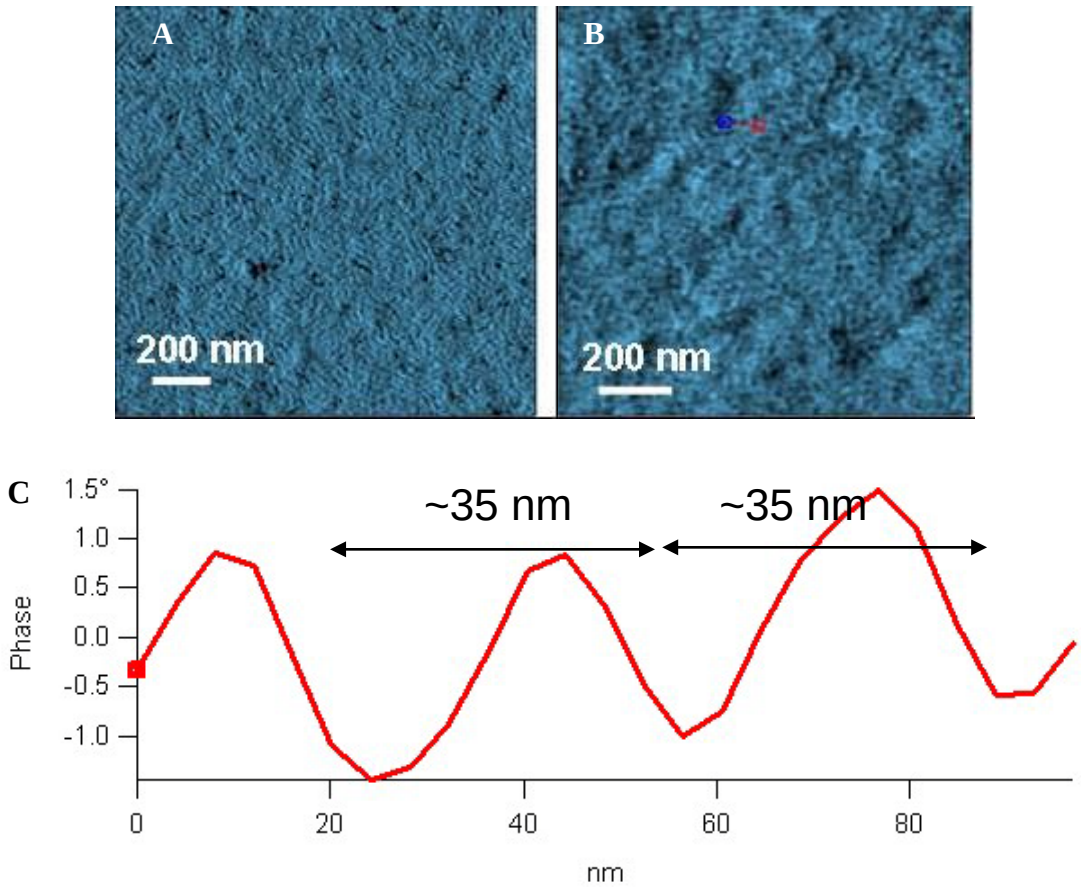

Figure 2.4. AFM phase images of PS-*b*-PAA-AMP taken both in air (A) and in water (B). Line scan from the water phase image (C) depicts evidence supporting a domain size on the order of 35 nm in the water-swollen film.

Fluorescence Microscopy of BSA-FITC Incubated Samples

As depicted in Figure 2.5, the PS-*b*-PAA-AMP sample was found to strongly resist adsorption of bovine serum albumin, especially when compared to the SEBS control. The measured surface concentration of adsorbed BSA-FITC was about eight-fold higher on a Si/SiO_2 surface than on the PS-*b*-PAA-AMP coated wafer. Care needs to be taken in comparing these measurements however since silicon has previously been found to quench the fluorescence of fluorescein.[15] More conclusively, fluorescence intensity of the adsorbed protein on the SEBS control was found to be 50 times greater than that experienced on the PS-*b*-PAA-AMP coated wafer (100 to 2).

This result is particularly striking since SEBS has been used as the base layer of a multi-layer polymeric marine-anti-fouling system.[7, 8, 39-41] This result clearly demonstrates the large difference in protein adsorption properties between the base layer and the surface active block copolymer layers of the previously explored multi-layer polymeric anti-fouling systems and also supports the inference made previously that upon immersion in water the surface of PS-*b*-PAA-AMP is able to reconstruct, bringing the protein adsorption resistant PEG groups to the surface.[7] The relatively high protein adsorption on SEBS is consistent with the hydrophobic nature of its surface.[2] The advancing water contact angle on SEBS is about 104° characterizing its hydrophobicity,[40] while the PS-*b*-PAA-AMP coated surfaces and Si/SiO_2 surfaces are water-wettable and fairly inert to protein adsorption. These results for BSA adsorption correlate to those observed for hydrophobic and hydrophilic SAMs in a recent study by Finlay et al.[42] Although both PS-*b*-PAA-AMP and Si/SiO_2 surfaces are hydrophilic, the improved protein resistance of the amphiphilic block copolymer surface over a bare silicon substrate is notable.

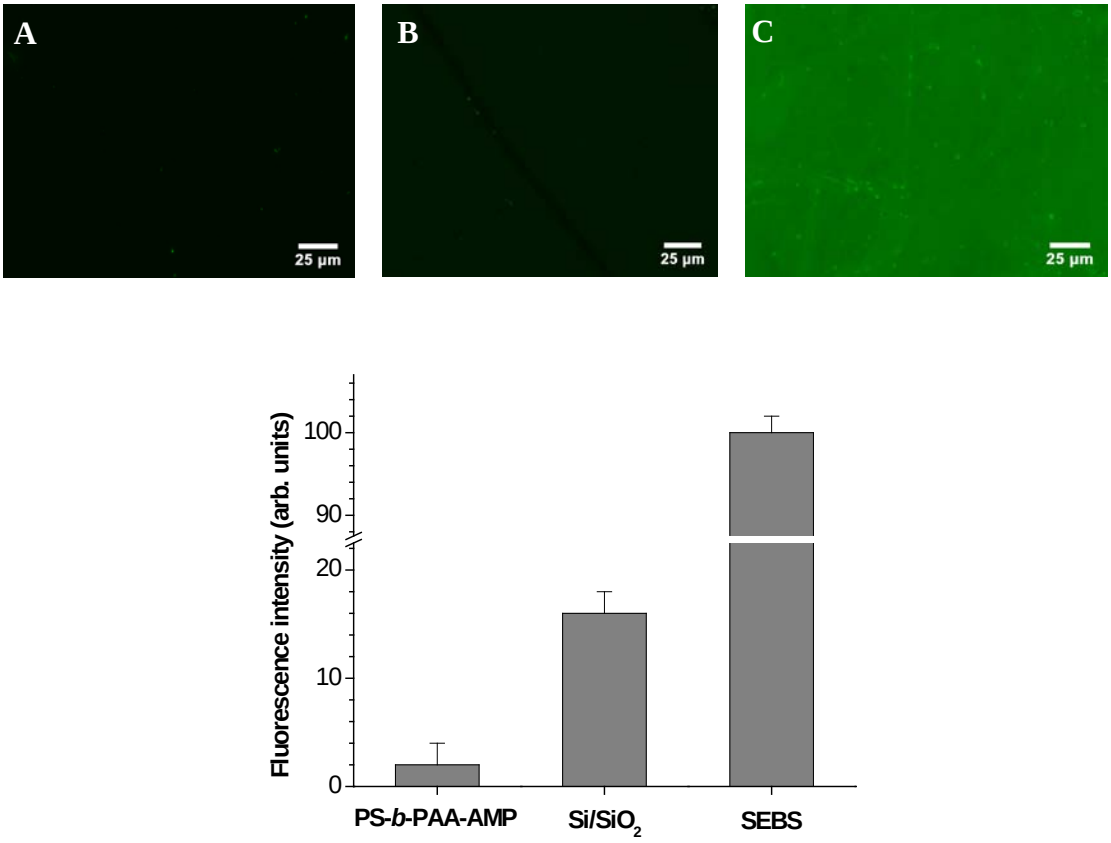

Figure 2.5. Fluorescence microscopy intensity results of BSA-FITC incubated samples. PS-*b*-PAA-AMP (A), the plain silicon wafer (Si/SiO_2) (B), and the SEBS control (C) are all pictured. The bar graph gives the relative fluorescence intensity of the three samples when the SEBS control is normalized to 100.

Adhesion Force Measurement of BSA

Adhesion force measurements taken using BSA coated AFM tips demonstrated a striking contrast between the interactions of BSA with surfaces of PS-*b*-PAA-AMP and glass and SEBS controls. Figure 2.6 gives typical force-extension profiles and force histograms when a BSA coated AFM tip interacts with a glass substrate, a SEBS surface, and a surface coated with PS-*b*-PAA-AMP. As expected, non-zero mean adhesion forces are seen for both SEBS (3.8 ± 1.1 nN) and glass (0.44 ± 0.1 nN). In stark contrast however, 58% of the adhesion force measurements for the BSA coated

tip interacting with the surface of PS-*b*-PAA-AMP demonstrated no measurable force of adhesion. Additionally, no measurements of force of adhesion were made in excess of 0.15 nN. These results are summarized in Figure 2.7.

Instantaneous measurements of adhesion force (in this case for tip-surface interaction times on the order of 0.1 s) can be misleading however. Proteins require time to attain an equilibrium conformation on a surface. Previously, Mondon et al. observed BSA to obtain a plateau maximum adhesion force after interacting for ca. ~ 2 s with a titanium surface.[43] Similar plateau maximum adhesion force behavior was seen for BSA on low density polyethylene with a range of wettability characteristics in a recent study by Xu et al.[44] To examine the time dependency of the force of adhesion of BSA with the surface of PS-*b*-PAA-AMP, the adhesion force of the BSA coated AFM tip was measured as a function of time. As depicted in figure 2.8, it was determined that a plateau adhesion force of roughly 300 pN was measured after 5 s of interaction, only increasing to ca. ~ 315 pN after 10 s of interaction. This further highlights the difference between the SEBS and PS-*b*-PAA-AMP surfaces since the SEBS surface shows a force of adhesion after only 0.1 s of interaction over ten times greater than that experienced for PS-*b*-PAA-AMP after 10 s of interaction. Clearly, these results in tandem further demonstrate the significant ability of PS-*b*-PAA-AMP to resist adsorption of proteins.

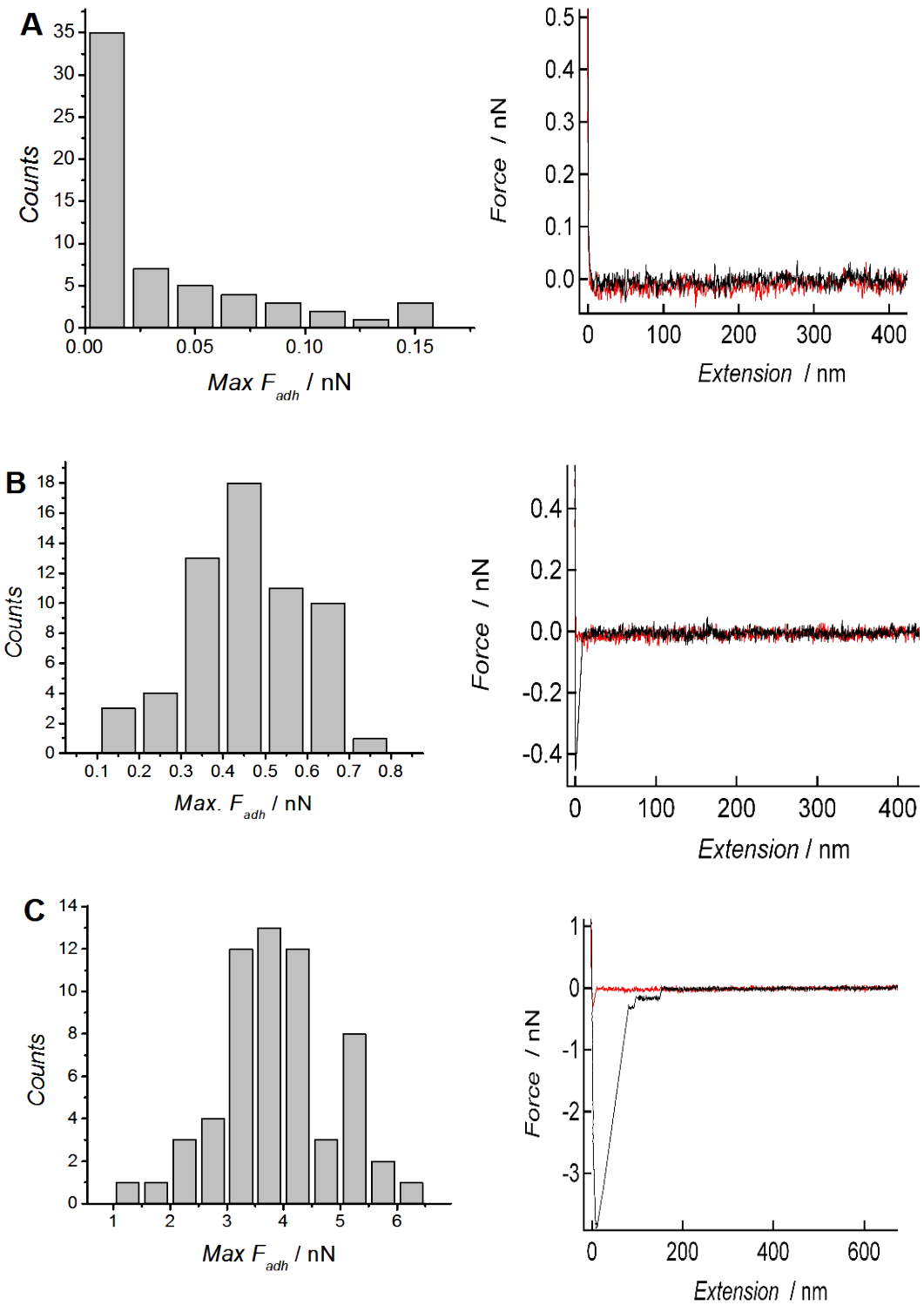

Figure 2.6. Force-extension profiles showing a typical adhesion force when a BSA coated AFM tip interacts with PS-*b*-PAA-AMP (A), a glass substrate (B), and SEBS coated substrate (C). In addition, the adhesion force histograms are given which can be used to determine the mean force of adhesion.

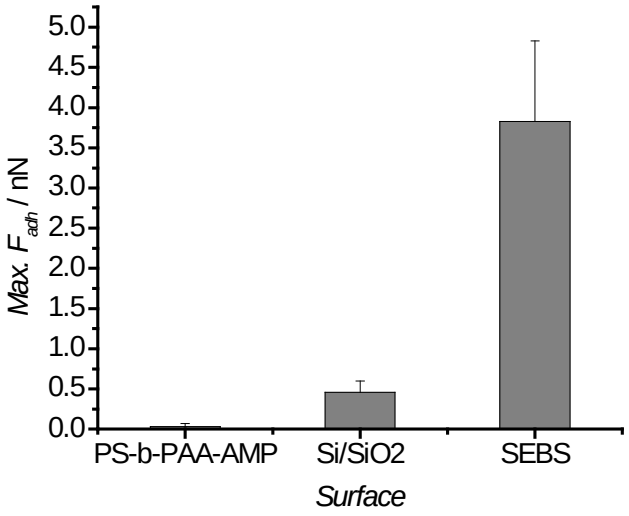

Figure 2.7. Average maximum measured force of adhesion for a BSA coated AFM tip while interacting with surfaces of PS-*b*-PAA-AMP, glass (Si/SiO_2) and SEBS.

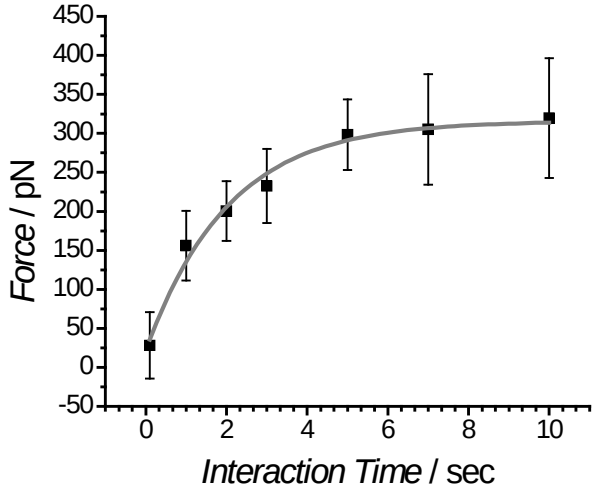

Figure 2.8. Maximum adhesion force of a BSA coated AFM tip as a function of interaction time on the substrate coated with PS-*b*-PAA-AMP.

Conclusions

A block copolymer containing grafted amphiphilic ethoxylated fluoroalkyl side chains that was previously demonstrated to be anti-biofouling was evaluated for protein adsorption and adhesion resistance against bovine serum albumin (BSA). Using fluorescence microscopy, surfaces were found to be extremely resistant to protein adsorption when compared to several controls. Additionally, AFM experiments using chemical force microscopy demonstrated the very weak force of adhesion between BSA molecules and surfaces coated with the amphiphilic block copolymer. This analysis helped to further our understanding of the anti-biofouling character of this material by confirming its anticipated propensity to resist protein adsorption.

Acknowledgements

This research was supported by the Office of Naval Research grants N00014-02-1-0170 to C. K. O. and E. J. K. and N00014-02-1-0327 to G. C. W. The Department of Defense's Strategic Environmental Research and Development Program (SERDP) grant WP-1454 to C.K.O.is also gratefully acknowledged. KES and EJK acknowledge partial support from an NSF Graduate Fellowship and the NSF Polymers Program (DMR-0704539). The NEXAFS experiment was done at the National Synchrotron Light Source at Brookhaven National Laboratory, which is supported by the U. S. Department of Energy, Division of Materials Science and Division of Chemical Sciences.

REFERENCES

1 T. Vladkova, *Journal of the University of Chemical Technology and Metallurgy*, 2007, **42**, 239.

2 S. Krishnan, C. J. Weinman, and C. K. Ober, *J. Mater. Chem.*, 2008, **18**, 3405.

3 J. Genzer and K. Efimenko, *Biofouling*, 2006, **22**, 339.

4 L. D. Chambers, K. R. Stokes, F. C. Walsh, and R. J. K. Wood, *Surf. Coat. Technol.*, 2006, **201**, 3642.

5 D. M. Yebra, S. Kiil, and K. Dam-Johansen, *Prog. Org. Coat.*, 2004, **50**, 75.

6 C. Werner, M. F. Maitz, and C. Sperling, *J. Mater. Chem.*, 2007, **17**, 3376.

7 S. Krishnan, R. Ayothi, A. Hexemer, J. A. Finlay, K. E. Sohn, R. Perry, C. K. Ober, E. J. Kramer, M. E. Callow, J. A. Callow, and D. A. Fischer, *Langmuir*, 2006, **22**, 5075.

8 C. J. K. Weinman, S.; Park, D.; Paik, M. Y.; Wong, K., Fischer, D. A.; Handlin, D. A., Kowalke, G. L.; Wendt, D. E.; Sohn, K. E.; Kramer, E. J.; Ober, C. K., *PMSE Preprints*, 2007, **96**, 597.

9 F. Y. Lin, W.-Y. Chen, and M. T. W. Hearn, *J. Mol. Recognit.*, 2002, **15**, 55.

10 C. D. Tidwell, S. I. Ertel, B. D. Ratner, B. J. Tarasevich, S. Atre, and D. L. Allara, *Langmuir*, 1997, **13**, 3404.

11 E. Ostuni, L. Yan, and G. M. Whitesides, *Colloids Surf., B*, 1999, **15**, 3.

12 S. Herrwerth, E. Wolfgang, S. Reinhardt, and M. Grunze, *J. Am. Chem. Soc.*, 2003, **125**, 9359.

13 L. Li, S. Chen, J. Zheng, B. D. Ratner, and S. Jiang, *J. Phys. Chem. B*, 2004, **109**, 2934.

14 K. L. Prime and G. M. Whitesides, *J. Am. Chem. Soc.*, 1993, **115**, 10714.

15 S. C. Follstaedt, J. A. Last, D. K. Cheung, P. L. Gourley, and D. Y. Sasaki, *Sandia Report*, 2000.

16 S. Ge, K. Kojio, A. Takahara, and T. Kajiyama, *J. Biomater. Sci. Polymer Edn.*, 1998, **9**, 131.

17 G. Binnig, C. F. Quate, and C. Gerber, *Phys. Rev. Lett.*, 1986, **56**, 930.

18 C. D. Frisbie, L. F. Rozsnyai, A. Noy, M. S. Wrighton, and C. M. Lieber, *Science*, 1994, **265**, 2071.

19 B. B. Akhremitchev, J. E. Bemis, S. Al-Maawali, Y. Sun, L. Stebounova, and G. C. Walker, *Biofouling*, 2003, **19 (Supplement)**, 99.

20 J. Gu, Z. Xiao, C.-M. Yam, G. Qin, M. Deluge, S. Boutet, and C. Cai, *Biophysical Journal*, 2005, **89**, L31.

21 B. B. Akhremitchev, B. K. Mohney, K. Marra, T. M. Chapman, and G. C. Walker, *Langmuir*, 1998, **14**, 3976.

22 T. Eastman and D.-M. Zhu, *Langmuir*, 1996, **12**, 2859.

23 A. Noy, S. Zepeda, C. A. Orme, Y. Yeh, and J. J. D. Yoreo, *J. Am. Chem. Soc.*, 2003, **125**, 1356.

24 Y. Sun, B. Akhremitchev, and G. C. Walker, *Langmuir*, 2004, **20**, 5837.

25 H. Clausen-Schaumann, M. Seitz, R. Krautbauer, and H. E. Gaub, *Current Opinion in Chemical Biology*, 2000, **4**, 524.

26 A. Janshoff, M. Neitzert, Y. Oberdörfer, and H. Fuchs, *Angew. Chem. Int. Ed.*, 2000, **39**, 3212.

27 M. Seitz, *Nanobiotechnology*, 2004, 404.

28 T. Hugel and M. Seitz, *Macromolecular Rapid Communications*, 2001, **22**, 989.

29 M. Taylor, A. J. Urquhart, D. G. Anderson, P. M. Williams, R. Langer, M. R. Alexander, and M. C. Davies, *Macromolecular Rapid Communications*, 2008, **29**, 1298.

30 D. Alsteens, E. Dague, P. G. Rouxhet, A. R. Baulard, and Y. F. Dufrene, *Langmuir*, 2007, **23**, 11977.

31 W. Sun, P. Neuzil, T. S. Kustandi, S. Oh, and V. D. Samper, *Biophysical Journal*, 2005, **89**, L14.

32 G. C. Walker, Y. Sun, S. Guo, J. A. Finlay, M. E. Callow, and J. A. Callow, *The Journal of Adhesion*, 2005, **81**, 1101.

33 M. Y. Paik, S. Krishnan, F. You, X. Li, A. Hexemer, Y. Ando, S. H. Kang, D. A. Fischer, E. J. Kramer, and C. K. Ober, *Langmuir*, 2007, **23**, 5110.

34 J. Genzer, E. Sivaniah, E. J. Kramer, J. Wang, H. Köerner, K. Char, C. K. Ober, B. M. DeKoven, R. A. Bubeck, D. A. Fischer, and S. Sambasivan, *Langmuir*, 2000, **16**, 1993.

35 M. G. Samant, J. Stöhr, H. R. Brown, and T. P. Russell, *Macromolecules*, 1996, **29**, 8334.

36 Y. Liu, T. P. Russell, M. G. Samant, J. Stöhr, H. R. Brown, A. Cossy-Favre, and J. Diaz, *Macromolecules*, 1997, **30**, 7768.

37 J. L. Hutter and J. Bechhoefer, *Rev. Sci. Instrum.*, 1993, **64**, 1868.

38 K. A. Davis and K. Matyjaszewski, *Macromolecules*, 2001, **34**, 2101.

39 S. Krishnan, N. Wang, C. K. Ober, J. A. Finlay, M. E. Callow, J. A. Callow, A. Hexemer, K. E. Sohn, E. J. Kramer, and D. A. Fischer, *Biomacromolecules*, 2006, **7**, 1449.

40 S. Krishnan, R. J. Ward, A. Hexemer, K. E. Sohn, K. L. Lee, E. R. Angert, D. A. Fischer, E. J. Kramer, and C. K. Ober, *Langmuir*, 2006, **22**, 11255.

41 J. P. Youngblood, L. Andruzzi, C. K. Ober, A. Hexemer, E. J. Kramer, J. A. Callow, J. A. Finlay, and M. E. Callow, *Biofouling*, 2003, **19**, 91.

42 J. A. Finlay, S. Krishnan, M. E. Callow, J. A. Callow, R. Dong, N. Asgill, K. Wong, E. J. Kramer, and C. K. Ober, *Langmuir*, 2008, **24**, 503.

43 M. Mondon, S. Berger, and C. Ziegler, *Analytical and Bioanalytical Chemistry*, 2003, **375**, 849.

44 L.-C. Xu and C. A. Siedlecki, *Biomaterials*, 2007, **28**, 3273.

CHAPTER 3

ABC TRIBLOCK SURFACE ACTIVE BLOCK COPOLYMERS WITH GRAFTED ETHOXYLATED FLUOROALKYL AMPHIPHILIC SIDE CHAINS FOR MARINE ANTI-FOULING AND FOULING-RELEASE APPLICATIONS

Abstract

An amphiphilic triblock surface active block copolymer (SABC) possessing ethoxylated fluoroalkyl side chains was synthesized through the chemical modification of a polystyrene-*block*-poly(ethylene-*ran*-butylene)-*block*-poly(isoprene) polymer precursor. Bilayer coatings on glass slides consisting of a thin layer of the amphiphilic SABC spray coated on a thick layer of a polystyrene-*block*-poly(ethylene-*ran*-butylene)-*block*-polystyrene (SEBS) thermoplastic elastomer were prepared for biofouling assays of the green alga *Ulva* and the diatom *Navicula*. Dynamic water contact angle analysis and X-ray photoelectron spectroscopy (XPS) were used to characterize the surfaces. Additionally, the effect of bulk elastic modulus of the coating on fouling settlement and release properties of the green alga *Ulva* was examined through the use of two different SEBS thermoplastic elastomers possessing values of modulus an order of magnitude in difference. While the amphiphilic SABC was found to both deter settlement by and easily release the green alga *Ulva* when used with both the “high” and “low” modulus SEBS base layers, release characteristics were particularly robust for the “low” modulus SEBS base layer. This was true even at the lowest measured applied water jet pressure of 19 kPa, resulting in ca. ~ 87% removal of biomass. Since knowledge of any correlation between coating elastic modulus and fouling release of “soft” fouling organisms reported in literature is extremely limited, this result was particularly striking. Furthermore, this result

demonstrates the ability to now also tune the elastic modulus of the base layer for this flexible multilayer coating system that has previously been used with different SABC chemistries. The realization of facile release of *Navicula* diatoms further highlights the potential of this amphiphilic triblock hybrid antifouling/fouling-release copolymer.

Introduction

Marine biofouling is defined as the build up of microbial slimes, plants and animals on any surface immersed in seawater.[1] Due to the extra roughness and surface area imparted by the accumulation of biofouling, and the resultant increase in frictional forces that a seafaring vessel must overcome, it is an extremely costly problem for nautical interests.[2] In a recent study by Schultz, it was suggested that a powering penalty of up to 86% can be realized at cruising velocities when a ship is heavily fouled with calciferous organisms, such as barnacles.[3] This clearly suggests that a significant reduction in fuel consumption and emissions can be realized through successful control of biofouling. The realization of these goals is ever more critical in the current geopolitical climate concerned with dwindling energy resources and global climate change.

To date the most effective method of marine biofouling control has been the use of ablative organometallic coatings that leach a potent biocide, tributyl tin (TBT). Unfortunately, TBT containing coatings were found to be extremely harmful to the environment and do not exhibit the necessary degree of selectivity towards target organisms.[4] Consequently, they have already been banned most places in the world.[5] This has left the marine community scrambling for an alternative to TBT based coatings with similar performance. Environmentally friendly alternatives are desperately being sought and several recent reviews have focused on the various approaches being pursued.[6-10]

Most of the alternative coatings developed for marine anti-fouling and/or fouling release that have been reported in literature have incorporated novel polymeric materials. Specific attention has been placed on controlling the wettability and surface energy of coatings through tuning of surface chemistry, with successful antifouling and/or fouling-release behavior demonstrated for both hydrophobic and hydrophilic systems.[7] The bulk modulus of a coating is also of significant interest, with more compliant systems traditionally showing reduced settlement and more facile release of fouling organisms.[11-13] Thus, hydrophobic poly(dimethyl siloxane) (PDMS) based coating systems have shown extremely robust fouling release performance due to their combination of low surface energy and elasticity.[14-16] Nevertheless, PDMS derived coatings are still particular susceptible to fouling by diatom slimes[17] and concerns also exist about their long term durability. On the opposite side of the wettability spectrum, hydrophilic coatings incorporating poly(ethylene glycol) (PEG) moieties, known for their exceptional resistance to protein adsorption and cell adhesion,[18-20] have also demonstrated resistance to settlement by and elevated release of marine fouling organisms.[20-22]

This realization of desirable fouling behavior on both sides of the wettability spectrum has led several groups of researchers to the development of ambiguous, amphiphilic coating materials incorporating both hydrophobic and hydrophilic moieties. Motivation has been driven by the desire to produce a universal anti-fouling and/or fouling-release coating capable of both resisting settlement by and readily releasing as wide a range of fouling organisms as possible. With this in mind, Gudipati et al. produced surface tethered hyperbranched polymers containing both fluorinated and PEGylated groups. These materials were characterized by both low protein adsorption and high fouling release at an optimal composition of hydrophobic and hydrophilic monomers.[23] More recently, Ober and coworkers reported on the

development of a poly(styrene)-*block*-poly(acrylic acid) derived surface active block copolymer with amphiphilic ethoxylated fluoroalkyl side chains capable of both resisting and releasing *Ulva* and *Navicula*, and also deterring barnacle settlement.[24, 25] Additionally, a similar functionalized amphiphilic poly(styrene) block copolymer containing ethoxylated fluoroalkyl side chains has been reported by Martinelli et al. with further promising algal settlement and release results.[26]

This work will specifically aim to report on further developments to the multilayer polymeric coating approach taken by Ober and coworkers to produce antifouling and/or fouling-release coatings. In this body of work, bulk coating modulus has been controlled by the use of a thick layer of the thermoplastic elastomer poly(styrene)-*block*-poly(ethylene-*ran*-butylene)-*block*-poly(styrene) (SEBS), with a mechanically tethered thin layer of a styrenic surface active block copolymer (SABC) imparting chemical functionality to the surface. Previous work has focused on the synthesis of hydrophobic and hydrophilic side chain polymers derived from poly(styrene)-*block*-poly(isoprene),[21, 22] amphiphilic side chain polymers derived from poly(styrene)-*block*-poly(acrylic acid),[24, 25] and antimicrobial polymers formed from poly(styrene)-*block*-poly(4-vinylpyridine).[27, 28] This work however will focus on the synthesis and characterization of a new poly(styrene)-*block*-poly(ethylene-*ran*-butylene)-*block*-poly(isoprene) derived system specifically designed with optimization of the surface segregation of side chain functional moieties in mind. This can be achieved through the presence of a 25,000 g/mol poly(ethylene-*ran*-butylene) block that serves as a "molecular spacer" that should theoretically allow the functionalized isoprene block a greater ability to explore its conformational space and segregate to the surface. Synthesis and characterization of an amphiphilic triblock SABC containing ethoxylated fluoroalkyl side chains will be described, further building on the work reported in Weinman et al.[29] Particular attention will be paid to surface

characterization of the resultant SABCs using dynamic water contact angle analysis and X-ray photoelectron spectroscopy (XPS). The use of two different SEBS thermoplastic elastomer base layers with Young's modulus values varying by an order of magnitude and the combined effect of coating modulus and surface chemistry with regards to both settlement and release of the green alga *Ulva* and *Navicula* diatoms will also be explored.

Experimental Section:

Materials

The polystyrene$_{8K}$-*block*-poly(ethylene-*ran*-butylene)$_{25K}$-*block*-polyisoprene$_{10K}$ (PS_{8K}-*b*-$P(E/B)_{25K}$-*b*-PI_{10K}) triblock precursor copolymer was produced using anionic polymerization and subsequent catalytic hydrogenation by Kraton Polymers at large scale (~ 0.5 kg) to facilitate preparation of SABCs.

3-*meta*-Chloroperoxybenzoic acid (*m*CPBA, ClC_6H_4COOOH, FW 172.57, 77%), boron trifluoride diethyl etherate (BF_3•Et_2O, BF_3•$O(CH_2CH_3)_2$, FW 141.93, 99.9%), and the ethoxylated fluoroalkyl surfactant, Zonyl FSO-100 (registered trademark of E. I. du Pont de Nemours & Co., Inc., $F(CF_2CF_2)_y(CH_2CH_2O)_xCH_2CH_2OH$, x = 0-15 and y = 1-7, average $M_n \approx 725$ g/mol) were also purchased from Sigma Aldrich and used as received in the modification of the PS-*b*-P(E/B)-*b*-PI triblock precursor polymers. Anhydrous chloroform ($CHCl_3$) and α,α,α-trifluorotoluene (TFT) were purchased from Sigma Aldrich and used with no further purification. Chloroform, dichloromethane (CH_2Cl_2), methanol (CH_3OH), toluene, 6.25 N sodium hydroxide (NaOH), 96% sulfuric acid (H_2SO_4), 30 wt % hydrogen peroxide (H_2O_2) in water, 95% ethanol (CH_3CH_2OH) and all other reagents were used as received.

3-(Glycidoxypropyl)-trimethoxysilane (GPS, 99%) was purchased from Gelest and used as received. Two separate commercially available polystyrene-*block*-poly(ethylene-*ran*-butylene)-*block*-polystyrene (SEBS) ABA triblock thermoplastic elastomers, having different chemical and bulk properties (Kraton G1652 and Kraton MD6945) and SEBS grafted with maleic anhydride (MA-SEBS, Kraton FG1901X) were generously provided by Kraton Polymers.

Polymer Synthesis and Characterization

The amphiphilic surface active block copolymer was produced through a straight-forward two step modification of the Kraton PS_{8K}-*b*-$P(E/B)_{25K}$-*b*-PI_{10K} precursor polymer depicted in Figure 3.1, in similar fashion to that previously reported in Weinman et al.[29] Functionalization of the PI block of the triblock precursor was achieved through epoxidation of the residual unsaturated alkene groups in the polymer back-bone followed by subsequent catalytic ring-opening etherification reactions using non-ionic surfactant alcohols carrying amphiphilic functionality.

In a typical epoxidation reaction, the PS_{8K}-*b*-$P(E/B)_{25K}$-*b*-PI_{10K} SABC precursor polymer (5 g, 14.5 mmol of reactive isoprene sites) was dissolved in 100 mL of dichloromethane in a round bottomed flask. 3-chloroperoxybenzoic acid (*m*CPBA, 3.9 g, 17.4 mmol) was added to the mixture, and the solution was stirred vigorously for 5 hours at room temperature. Subsequently, the polymer was precipitated in methanol, collected by filtration, and reprecipitated from dichloromethane to remove residual *m*CPBA and its respective byproducts. The white, rubbery product was dried at room temperature under reduced pressure for 48 hours to remove remaining solvent.

^{1}H NMR for epoxidized PS_{8K}-*b*-$P(E/B)_{25K}$-*b*-PI_{10K} (300 MHz, $CDCl_3$, δ): 6.57, 7.07, (5H, styrene), 2.66 (br s, 1H, epoxidized isoprene, -CH_2**H**$COC(CH_3)CH_2$-), 0.80, 1.07, 1.22, 1.45, 1.57 (back-bone). IR (dry film) υ_{max} (cm $^{-1}$): 2925, 2850 (C-H

stretching); 1470 (C-H bending); 1070 (C-O stretching); 880 (C-O-C stretching); 700 (C-H bending, aromatic).

To produce ether-linked amphiphilic side chain surface active block copolymers, 2.1 g of epoxidized PS_{8K}-*b*-$P(E/B)_{25K}$-*b*-PI_{10K} (5.8 mmol of epoxide) was taken in a round bottom flask in conjunction with a four times molar excess (23.2 mmol) of the side-chain precursor ethoxylated fluoroalkyl surfactant alcohol. The reactants were purged with argon, and subsequently dissolved in ca. ~ 150 mL of anhydrous chloroform. Activated molecular sieves were added to the reaction mixture and it was allowed to sit for ca. ~ 12 h to optimize the up-take of water. Etherification was performed through the addition of boron trifluoride diethyl etherate catalyst (0.345 g, 2.4 mmol) followed by vigorous stirring at room temperature for at least 48 hours. Following the reaction, 6.25 N sodium hydroxide was added to quench any residual boron catalyst and the reaction mixture was concentrated under reduced pressure using a rotary evaporator. The resultant SABC was precipitated into methanol and the yellow rubbery product was collected by filtration and subsequently reprecipitated twice from chloroform to remove additional residual amphiphilic surface active side-chain alcohol. Finally, the finished sample was dried under reduced pressure at room temperature for 48 hours to fully remove residual solvent.

^{1}H NMR for PS_{8K}-*b*-$P(E/B)_{25K}$-*b*-PI_{10K} functionalized with Zonyl FSO-100 ethoxylated fluoroalkyl surfactant side chains (300 MHz, $CDCl_3$, δ): 6.56, 7.07, (5H, styrene), 3.77 (t, 2H, -OCH_2**CH_2**OH), 3.64 (br s, ~14H, –CH_2**CH_2**O(**CH_2CH_2**O)$_{\sim 2.5}$**CH_2**CH_2OH-); 2.42 (m, 2H, -**CH_2**CF_2); 0.82, 1.06, 1.23, 1.72 (back-bone). IR (dry film) υ_{max} (cm $^{-1}$): 3500 (O-H stretching); 2930, 2855 (C-H stretching); 1465, 1380 (C-H bending); 1245, 1220 (C-F stretching), 1150, 1135 (C-O stretching); 700 (C-H bending, aromatic).

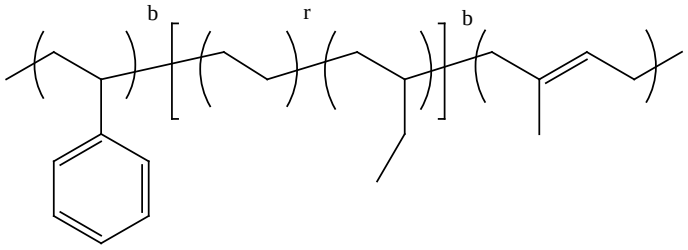

PS-*b*-P(E/B)-*b*-PI Triblock Copolymer

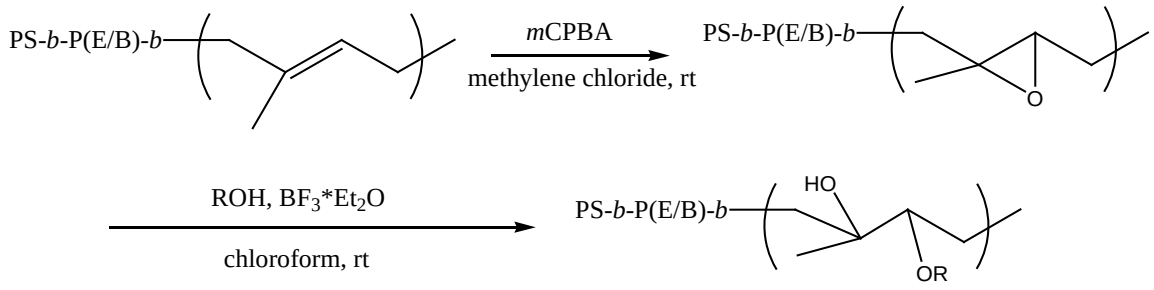

Figure 3.1. Synthesis of ether-linked surface active triblock copolymers containing ethoxylated fluoroalkyl derived side chains. ROH = $F(CF_2CF_2)_y(CH_2CH_2O)_xCH_2CH_2OH$, x = 0-15 and y = 1-7, average $M_n \approx 725$ g/mol).

^1H and ^{19}F NMR spectra were recorded using a Varian Gemini spectrometer with deuterated chloroform. The IR spectrum of the polymer cast as a film from THF solution on a sodium chloride plate was collected using a Mattson 2020 Galaxy Series FTIR spectrometer. Gel permeation chromatography of a THF solution of polymers (1 mg/mL) was carried out using four Waters Styragel HT columns operating at 40 °C in conjunction with Waters 490 ultraviolet ($\lambda = 254$ nm) and Waters 410 refractive index detectors. The molecular weight range of the columns was from 500 to 10^7 g/mol. THF was used as the eluent at a flow rate of 1 mL/min, and toluene was used as a marker for flow calibration.

Surface Preparation and Characterization

Surfaces for XPS and dynamic water contact angle analysis were prepared on silicon wafers by spin-coating 3% (w/v) solutions of SABCs in TFT at 2000 rpm for 60 seconds. All surfaces prepared for study were annealed in a vacuum oven at reduced pressure at 120 °C for at least 12 h followed by slow cooling to room temperature.

XPS measurements were performed using a Kratos Axis Ultra Spectrometer (Kratos Analytical, Manchester, UK) with a monochromatic Al Kα X-ray source (1486.6 eV) operating at 225 W under a vacuum of 1.0 × 10-8 Torr. Charge compensation was carried out by injection of low-energy electrons into the magnetic lens of the electron spectrometer. The pass energy of the analyzer was set at 40 eV for high-resolution spectra and 80 eV for survey scans, with energy resolutions of 0.05 and 1 eV, respectively. The spectra were analyzed using Casa XPS v.2.3.12Dev4 software. The C-C peak at 285 eV was used as the reference for binding energy calibration.

Water contact angles were measured using a contact angle goniometer (AST Products, Inc. model VCA Optima XE) at room temperature. Dynamic water contact angle measurements were performed through the addition and retraction of a small drop of water (ca. ~ 2 μL) on the surface. The advancing and receding contact angle behavior was digitally recorded and image analysis software was used to measure the angles.

Stress-Strain Analysis of SEBS Base Layers

Samples of the Kraton G1652 and Kraton MD6945 SEBS thermoplastic elastomers were pressed at 100 °C between teflon paper to 0.5 mm thickness and then

cut into dog bones. The samples were then monotonically stretched to fracture using an Instron (Norwood, MA) 1123 testing machine. All stress-strain curves were recorded at room temperature. Elastic modulus values were estimated for each sample by examining the slope of the stress-strain curve in the elastic deformation region.

Preparation of Surfaces for Biofouling Assay

Glass slides for biofouling assays with both the green alga *Ulva* and *Navicula* diatoms were prepared as previously reported for the amphiphilic SABC using either Kraton G1652 or Kraton MD6945 SEBS as a thermoplastic elastomer base layer when forming the multilayer coating.[27] The rationale behind testing MD6945 in addition to G1652 (which has typically been used in this work) was that the elastic modulus of MD6945 is very similar to that of PDMS, known to possess excellent fouling release properties due to a combination of both its surface energy and its low modulus.[10, 13, 15, 30] The elastic modulus of G1652 meanwhile is still roughly an order of magnitude greater than that of PDMS. By using the same SABC top layer while varying the thermoplastic elastomer base layer, a direct comparison of the fouling settlement and release behavior obtained by varying the modulus of the base was possible. For all biofouling assays, glass microscope slides coated with a polydimethylsiloxane elastomer (PDMS), Silastic® T2 (Dow Corning) prepared as described by Schumacher et al.[31] and G1652 SEBS were used as standards. MD6945 controls were also included where applicable. PDMS was used as a control due to excellent release properties against macrofouling organisms such as *Ulva* sporelings, while the G1652 and MD6945 base layers were used to highlight the differences in performance between the base layer when used alone and as part of the multilayer coatings.

Settlement of *Ulva* Zoospores and Strength of Attachment of *Ulva* Sporelings

Nine replicate test samples were leached in a 30 L tank of recirculating deionized water at ~ 20° C for 48 h. The slides were equilibrated in artificial seawater 1 h prior to the start of the experiments. Zoospores were released from fertile plants of *Ulva linza* and prepared for assay as described previously.[32] Ten mL of zoospore suspension (1×10^6 spores per mL), was pipetted into 12 compartments of Quadriperm polystyrene culture dishes (Greiner Bio-One), each containing a test slide. The test slides were incubated in the dark at ~ 20° C for 1 h and gently washed in seawater to remove zoospores that had not settled. Three slides were fixed using 2.5% glutaraldehyde in seawater and these replicates were used to quantify the density of zoospores attached to the surfaces as previously reported.[33]

Ulva sporelings (young plants) were cultured on 6 replicates of each coating.[34] After washing, the samples were transferred to dishes containing nutrient enriched seawater for 7 days. Growth was estimated by direct measurement of fluorescence from chlorophyll contained within the chloroplasts of the sporelings using a Tecan plate reader (GENios Plus).[35] Fluorescence was recorded as Relative Fluorescence Units (RFU) from direct readings. The slides (6 replicates) were read from the top, 300 readings per slide, taken in blocks of 30×10. The strength of attachment of the sporelings was determined by jet washing using a water jet.[36] The range of impact pressures used was chosen to provide maximum information on the strength of attachment of the sporelings. RFU readings (80 per slide) were taken from the central part of the slide that was exposed to the water jet. Percentage removal was calculated from the mean RFU reading before and after exposure to the water jet. From the percentage removal data, the critical water pressure required to remove 50% of the sporelings was derived.

Finally, due to the extremely high release of *Ulva* sporelings from some of the experimental surfaces in this study, an additional fouling release assay was run in which the strength of attachment of sporelings was assessed using a water flow channel to produce a wall shear stress of 52 Pa for a duration of 5 minutes. Biomass remaining was assessed using the fluorescent plate reader described previously. The percentage removal was calculated from readings taken before and after testing using the water channel.

Settlement and Strength of Attachment of *Navicula* Diatoms

Navicula cells were cultured in F/2 medium contained in 250 ml conical flasks. After 3 days the cells were in log phase growth. Cells were washed 3 times in fresh medium before harvesting and diluted to give a suspension with a chlorophyll a content of approximately 0.25 μg ml^{-1}. Cells were settled in individual dishes containing 10 mL of suspension at ~20° C on the laboratory bench. After 2 h the slides were gently washed in seawater to remove cells that had not properly attached (submerged wash). Slides were fixed using 2.5% glutaraldehyde in seawater. The density of cells attached to the surface was counted on each slide using an image analysis system attached to a fluorescence microscope. Counts were made for 30 fields of view (each 0.064 mm^2) on each slide.

Slides settled with Navicula were exposed to a shear stress of 23 Pa (32 US gall min^{-1}) in a water channel. The number of cells remaining attached was counted using the image analysis system described previously.

Results and Discussion:

Polymer Synthesis and Characterization

The synthesis of the ether-linked side chain SABC with pendent ethoxylated fluoroalkyl groups was followed using both infrared spectroscopy and ^{1}H NMR spectroscopy. Following the epoxidation reaction, ^{1}H NMR spectroscopy clearly showed that there was no longer evidence of any protons associated with unsaturated alkene groups on the polymer back-bone, and a significant peak at ca. ~ 2.7 ppm appeared indicating the presence of protons adjacent to the newly formed oxirane rings on the polyisoprene back-bone. Additionally, infrared spectroscopy clearly showed the appearance of a C-O-C stretching peak at roughly 880 cm^{-1} associated with the epoxide ring. This indicated that most of the residual unsaturated alkene groups were successfully converted to their epoxidized form. Subsequent catalytic ring-opening using ethoxylated fluoroalkyl alcohol led to the disappearance of the epoxide proton peak in the ^{1}H NMR spectra. Further analysis of the ^{1}H NMR spectra showed the appearance of peaks at ca. ~ 2.4, 3.6 and 3.8 ppm for the Zonyl functionalized sample demonstrating successful attachment of the side groups. These findings were supported by infrared spectroscopy which demonstrated the appearance of a strong C-O stretching peak at ca. ~ 1125 cm^{-1} indicating formation of ether and alcohol groups from ring opening of the epoxy in conjunction with a strong C-F stretching peak at ca ~ 1220 cm^{-1} suggesting the presence of the semifluorinated amphiphilic side chain moieties.

The percentage of attachment of ethoxylated fluoroalkyl side chain was estimated by ^{1}H NMR integration. Specifically, this was done by comparing the total amount of aromatic protons (associated with the PS block) in the ^{1}H NMR spectra with the number of protons associated with the PEGylated section of the amphiphilic side chain. The number of repeat units associated with the PEGylated section of the

attached Zonyl ethoxylated fluoroalkyl side chains were checked in an analogous fashion to and confirmed to be similar to those reported in Krishnan et al.[24] This analysis suggested attachment of side chains on the order of ca. ~ 45% relative to epoxy functionality. Using GPC, the polydispersity of the sample was found to increase from 1.06 for the PS-*b*-P(E/B)-*b*-PI precursors to ca. ~ 1.12 for its epoxidized form. Finished, substituted SABC samples containing ethoxylated fluoroalkyl side chains were found to have PDI values of ca. ~ 1.3. This rise in polydispersity combined with the observation of complete reaction of the epoxide despite less than 100% attachment suggested that some of the epoxide was most likely lost to intermolecular cross linking reactions. Additionally, intramolecular reactions in combination with epoxide ring-opening by any residual water molecules left in the reaction mixture may have contributed to this lowered observed attachment. Since this work spanned several batches of polymers, chemical characterization for each batch was done independently. Nevertheless, chemical analysis demonstrated very similar results from batch to batch. Thus values given here are representative of the several samples tested.

Dynamic Water Contact Angle Analysis

Dynamic water contact angle analysis of spun coat amphiphilic ethoxylated fluoroalkyl SABC samples on Si wafers indicated the presence of low surface energy, hydrophobic fluorinated moieties at the surface with $\theta_{w,\ advancing} = 107 \pm 2°$. High contact angle hysteresis was observed with $\theta_{w,\ receding} = 26 \pm 2°$. This suggests a dynamic surface capable of facile reordering of the side chains to readily orient the hydrophilic PEGylated groups at the surface. This is similar to what was observed for the ethoxylated fluoroalkyl polystyrene-*block*-poly(acrylic acid) derived SABC

reported on in Krishnan et al.,[24] but with significantly higher contact angle hysteresis (81° versus 60°) observed for the PS-*b*-P(E/B)-*b*-PI triblock derived SABC.

X-Ray Photoelectron Spectroscopy (XPS)

Figure 3.2 depicts a typical high resolution C 1s XPS spectra of amphiphilic SABC derived from the PS_{8K}-*b*-$P(E/B)_{25K}$-*b*-PI_{10K} precursor with ethoxylated fluoroalkyl side chains when spun directly on Si. The strong intensity peak near 284.5 eV associated with C-C and C=C bonds is most likely indicative of the presence of the polymer back-bone. The peak associated with C-O-C groups present at near 286.5 eV meanwhile is indicative of the PEGylated groups of the amphiphilic side chain. Finally, the peaks at 292 eV and 294 eV are indicative of CF_2 and CF_3 groups respectively, further suggesting successful segregation of the ethoxylated fluoroalkyl side chains to the surface of the polymer coating. One can also note that the peaks associated with the side chain (CF_3, CF_2, and C-O-C) show higher intensities at a 75° incidence angle than at a 0° incidence angle. This suggests the preferential segregation of the side chains to the surface as desired.

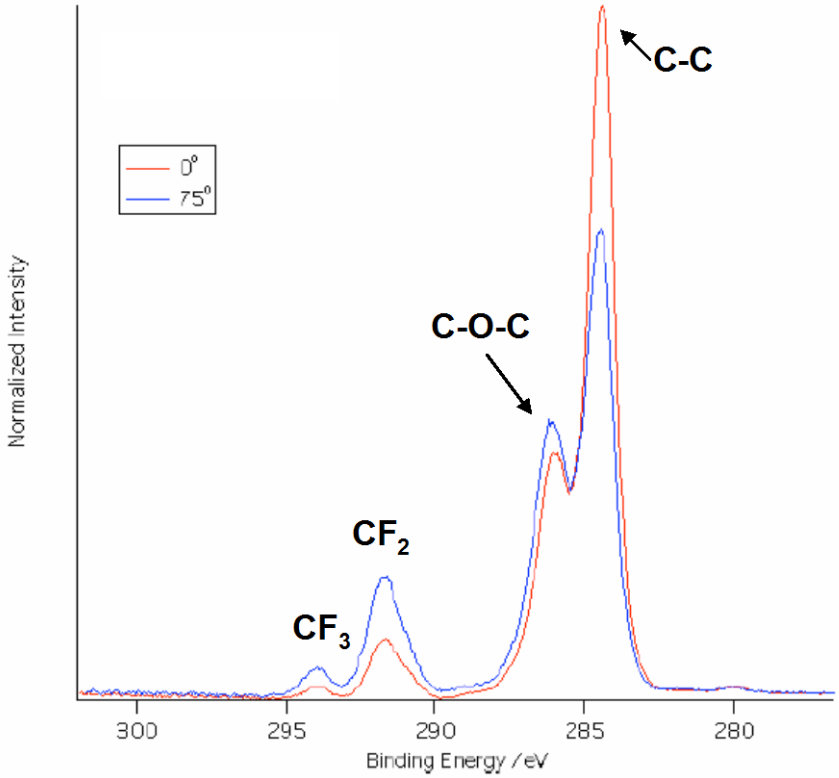

Figure 3.2. XPS C 1s spectra of the surface of the amphiphilic SABC with ethoxylated fluoroalkyl side chains derived from the PS_{8K}-*b*-$P(E/B)_{25K}$-*b*-PI_{10K} precursor polymer spun coat on Si taken at both 0° and 75° incidence angles.

Further characterization by XPS to determine if these model surfaces formed by spin coating were similar to those formed in the fabrication of samples for biofouling assays was performed. Figure 3.3 depicts a typical high resolution C 1s XPS spectra of amphiphilic SABC derived from the PS_{8K}-*b*-$P(E/B)_{25K}$-*b*-PI_{10K} precursor with ethoxylated fluoroalkyl side chains when sprayed on top of the MD6945 SEBS thermoplastic elastomer for biofouling assays. While the same set of chemical signatures is present for the spray coated samples as for the spun coat samples, peak intensities associated with the ethoxylated fluoroalkyl side chains greatly increased across the board. Particularly striking was that at the 75° incidence angle, the contribution from the polymer back-bone was so minimal that the C-C peak

simply appeared as a shoulder on the much stronger C-O-C peak. Initially, this led to concerns about residual ethoxylated fluoroalkyl side chain precursor alcohol being left in the sample due to incomplete purification. However, additional step-wise reprecipitations followed by bulk chemical characterization suggested that any loose ethoxylated fluoroalkyl alcohol molecules were already fully removed from the sample. This suggests that successful segregation of surface active groups may be highly dependent on the process conditions used—something that should be explored in future iterations of this work.

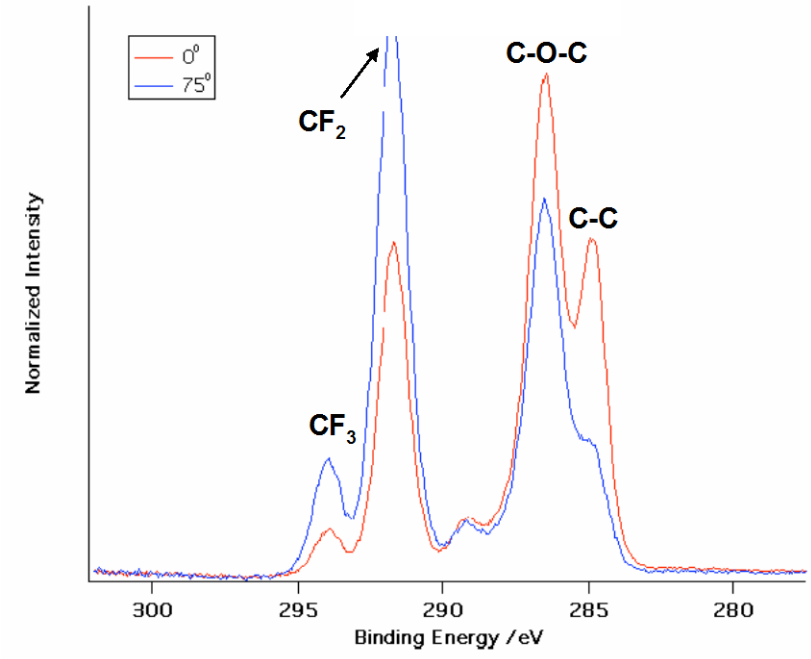

Figure 3.3. XPS C 1s spectra of the surface of the amphiphilic SABC with ethoxylated fluoroalkyl side chains derived from the PS_{8K}-*b*-$P(E/B)_{25K}$-*b*-PI_{10K} precursor polymer spray coated on MD6945 SEBS thermoplastic elastomer taken at both 0° and 75° incidence angles.

Determination of Elastic Modulus for SEBS Base Layers

Figure 3.4 shows the measured stress-strain curves for the Kraton G1652 and Kraton MD6945 SEBS thermoplastic elastomers. Kraton G1652 was found to have a

measured elastic modulus (E) of ca. ~ 18 MPa while the measured value of E for Kraton MD6945 was an order of magnitude less, ca. ~ 1.2 MPa. This demonstrates that MD6945 has a modulus much closer to that of PDMS, which is dependent on degree of polymerization and crosslinking, but is reported to be between 1.4-3.0 MPa for the commercial PDMS elastomers RTV11 and Intersleek.[37]

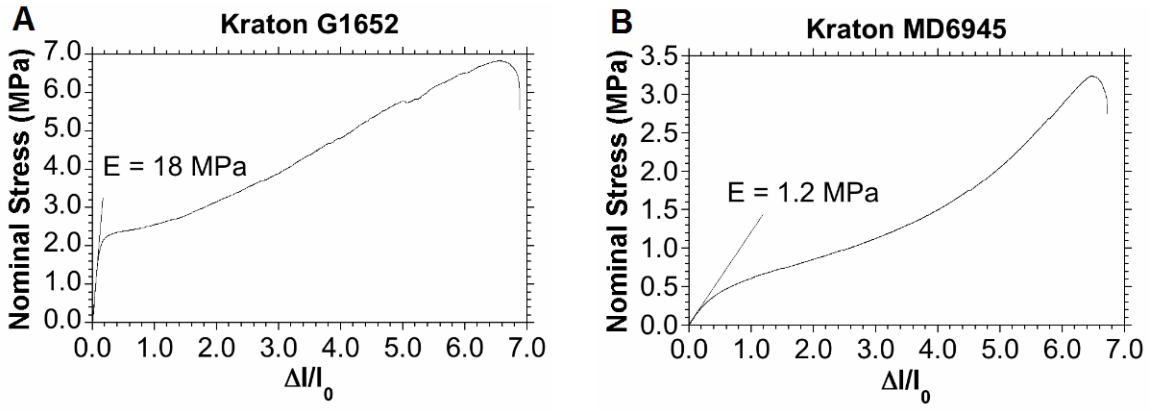

Figure 3.4. Measured stress-strain curves for SEBS thermoplastic elastomers A) Kraton G1652 and B) Kraton MD6945. Young's Modulus (E) values are estimated from the slope of the stress-strain curve during elastic deformation.

Settlement of *Ulva* Spores and Release of *Ulva* Sporelings

Figure 3.5A shows the settlement density of *Ulva* spores on glass, PDMS, G1652 SEBS and amphiphilic SABCs derived from the PS_{8K}-b-$P(E/B)_{25K}$-b-PI_{10K} precursor and the ethoxylated fluoroalkyl nonionic surfactant. For the experimental surfaces, the lowest spore settlement was recorded for the amphiphilic SABC. *Ulva* spores are known to preferentially settle on hydrophobic, low energy surfaces.[38] This was true for the PDMS control surface, which showed the greatest settlement of *Ulva* spores. The lower observed settlement on the amphiphilic SABC however suggests that the materials' apparent ability to readily reorganize in a polar environment likely deters settlement of spores. Also of note is the stark contrast between the high

observed settlement on the G1652 SEBS base layer and the low observed settlement for the amphiphilic SABC, clearly highlighting the ability of the thin layer of SABC to drastically modify the surface properties and settlement behavior of the multilayer coating system. Figure 3.5B meanwhile depicts *Ulva* sporeling growth on the experimental surfaces. *Ulva* growth generally scaled with settlement, with the least biomass recorded on the amphiphilic SABC.

Finally, the percentage removal of *Ulva* sporelings from the experimental surfaces at a range of applied water jet pressures is given in figure 3.5C. The amphiphilic SABC demonstrated extremely robust fouling release behavior with regards to *Ulva* sporelings, releasing ca. ~ 67% of *Ulva* biomass at an applied water jet pressure of 24 kPa, and over 95% biomass at an applied pressure of just 44 kPa. This contrasted to the PDMS control which only released 16% *Ulva* biomass at an applied water jet pressure of 24 kPa, and even at an applied water jet pressure of 132 kPa only released 84% of biomass. The combination of favorable settlement results with exceptional release results for *Ulva* in this initial assay led us to question what effect substituting the new, softer Kraton MD6945 thermoplastic elastomer in place of Kraton G1652 would have on the fouling release characteristics of the coating. While multiple studies have been published previously equating lower modulus with enhanced fouling release of calciferous “hard” macrofouling organisms such as barnacles,[13, 39, 40] minimal data has been reported on “soft” fouling organisms such as *Ulva* and *Navicula*. Chaudhury et al. examined a range of PDMS coatings with different degrees of polymerization and determined that there was a sharp drop off in fouling release performance at modulus values above 2 MPa.[34] This suggested that further reduction of the bulk modulus of the coating could prove advantageous to its fouling release performance.

Figure 3.5. Results of *Ulva* biofouling assays on glass, G1652 SEBS, PDMS and the PS_{8K}-*b*-$P(E/B)_{25K}$-*b*-PI_{10K} derived amphiphilic SABC with ethoxylated fluoroalkyl side chains. A) The settlement of *Ulva* spores. Each point is the mean from 90 counts on 3 replicate slides. Bars show 95% confidence limits. B) The growth of *Ulva* sporelings. Each point is the mean biomass from 6 replicate slides measured using a fluorescence plate reader. Bars show standard error of the mean. C) The removal of *Ulva* sporelings. Slides were exposed to a water jet over a range of pressures. One slide was used for each reported pressure.

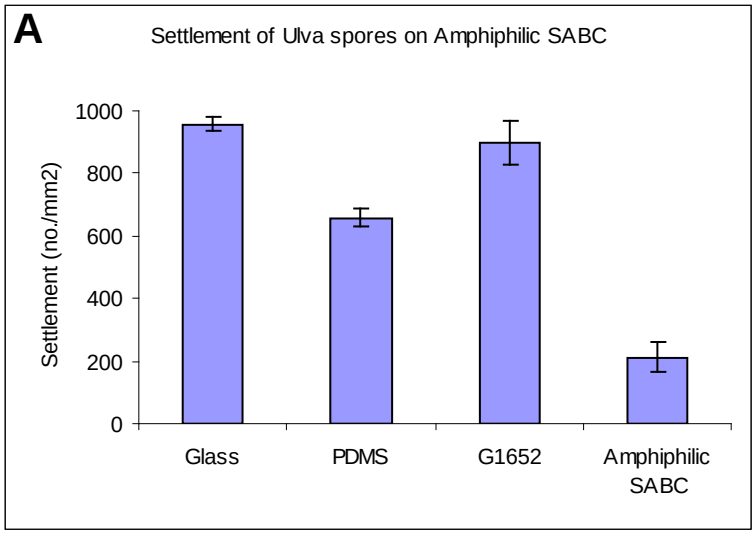
A
Settlement of Ulva spores on Amphiphilic SABC
Settlement (no./mm2)
1000
800
600
400
200
0
Glass
PDMS
G1652
Amphiphilic SABC

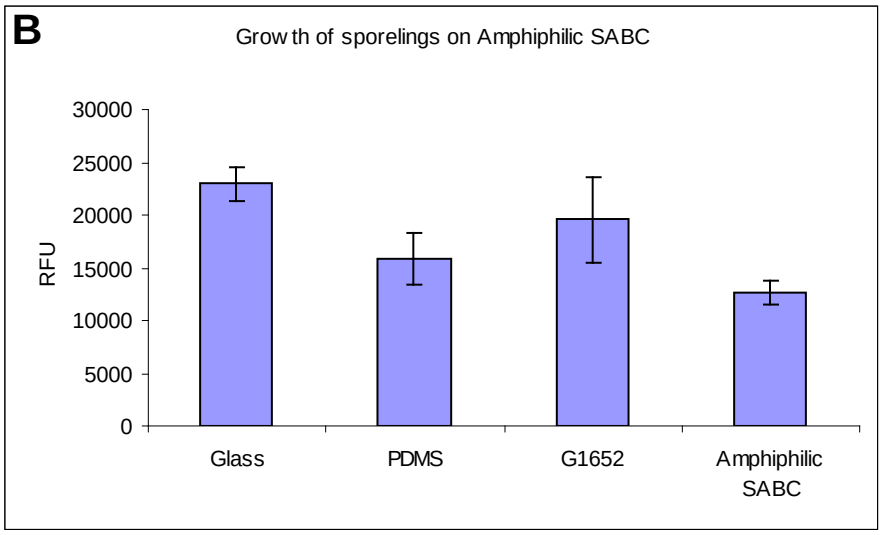
B
Grow th of sporelings on Amphiphilic SABC
RFU
30000
25000
20000
15000
10000
5000
0
Glass
PDMS
G1652
Amphiphilic SABC

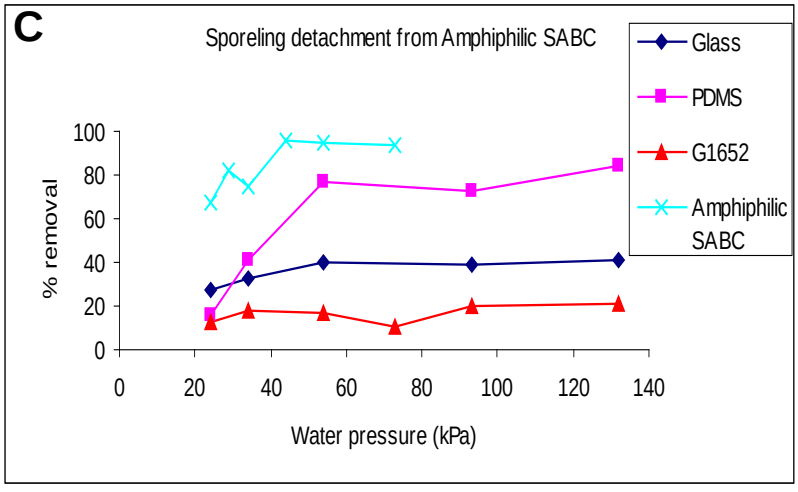
C
Sporeling detachment from Amphiphilic SABC
% removal
100
80
60
40
20
0
0
20
40
60
80
100
120
140
Water pressure (kPa)
Glass
PDMS
G1652
Amphiphilic SABC

To pursue this goal and also to check the repeatability of the initial *Ulva* testing, samples for biofouling assay of the amphiphilic SABC containing ethoxylated fluoroalkyl side chains were again prepared. In this experiment however, both the high modulus G1652 SEBS and the low modulus MD6945 SEBS were tested independently for their effect on settlement and release characteristics of *Ulva* spores and *Ulva* sporelings respectively when used as the base layer for the multilayer coating system. Figure 3.6A depicts the result of the *Ulva* spore settlement assay. Despite similar settlement performance for multilayer coatings of the amphiphilic SABC incorporating both G1652 and MD6945, the base layer controls on their own surprisingly showed very different settlement behavior with the low modulus MD6945 SEBS thermoplastic elastomer showing the lowest overall biomass of any of the five surfaces evaluated. The hydrophobic, low surface energy PDMS elastomer showed high settlement as expected. The growth of *Ulva* sporelings in the assay, given in Figure 3.6B, generally correlated to the amount of biomass settled, indicating no unexpected toxicity for any of the coatings as in the initial test. Meanwhile, Figure 3.6C depicts the percentage removal of *Ulva* sporelings from the experimental surfaces at a range of different applied water jet pressures in this additional iteration of testing. Again, the amphiphilic SABC demonstrated exceptional fouling resistance with both the high modulus G1652 and the low modulus MD6945 base layers, but the low modulus MD6945 base layer was particularly notable for imparting extremely robust release properties to the coating even at the lowest tested applied water jet pressures. Even at an applied water jet pressure of 19 kPa, the amphiphilic SABC coating on a base layer of the low modulus MD6945 demonstrated ca. ~ 87% removal of *Ulva* sporeling biomass. This contrasted to ca. ~ 17% removal for the amphiphilic SABC on a base layer of the high modulus G1652 at an applied pressure of 19 kPa, and ca. ~ 21% removal for the PDMS control at an applied pressure of 23 kPa. This

trend continued with greater than 99% of *Ulva* sporeling biomass removed from the amphiphilic SABC with the MD6945 base layer at an applied water jet pressure of 26 kPa. This contrasted the maximum observed biomass removal for PDMS (ca. ~ 89% at 63 kPa) and the amphiphilic SABC on the G1652 base layer (ca. ~ 94% at 46 kPa). This suggests clearly that the order of magnitude drop in modulus between the high modulus G1652 and the low modulus MD6945 resulted in a drastic increase in fouling release efficacy. Results are summarized in Table 3.1 which gives the critical applied water jet pressure to remove 50% of the *Ulva* sporeling biomass for each experimental surface. These results generally agree with the determination in Chaudhury et al. that the ease of *Ulva* sporeling removal greatly increases for substrates with a modulus below 2.7 MPa.[34] Care must be taken however since clearly the surface chemistry presented to fouling organisms by our amphiphilic SABC is significantly different than that of PDMS. Nevertheless, these findings taken in conjunction with those previously reported clearly support a hypothesis that the release of soft fouling organisms can greatly be facilitated through the use of very low modulus materials with an elastic modulus value on the order of 3 MPa or less.

Table 3.1. Estimated critical applied water jet surface pressure for 50% removal of *Ulva* sporeling biofilm derived from the curve in Figure 3.6C.

Sample	Est. Surface Pressure for 50% Removal (kPa)
PDMS	34
G1652	152
MD6945	>270
Amphiphilic SABC – G1652	26
Amphiphilic SABC - MD6945	<10

Figure 3.6. Results of *Ulva* biofouling assays on G1652 SEBS, MD6945 SEBS, PDMS and the PS_{8K}-*b*-$P(E/B)_{25K}$-*b*-PI_{10K} derived amphiphilic SABC with ethoxylated fluoroalkyl side chains on both thermoplastic elastomer base layers. A) The settlement of *Ulva* spores. Each point is the mean from 90 counts on 3 replicate slides. Bars show 95% confidence limits. B) The growth of *Ulva* sporelings. Each point is the mean biomass from 6 replicate slides measured using a fluorescence plate reader. Bars show standard error of the mean. C) The removal of *Ulva* sporelings. Slides were exposed to a water jet over a range of pressures. One slide was used for each reported pressure.

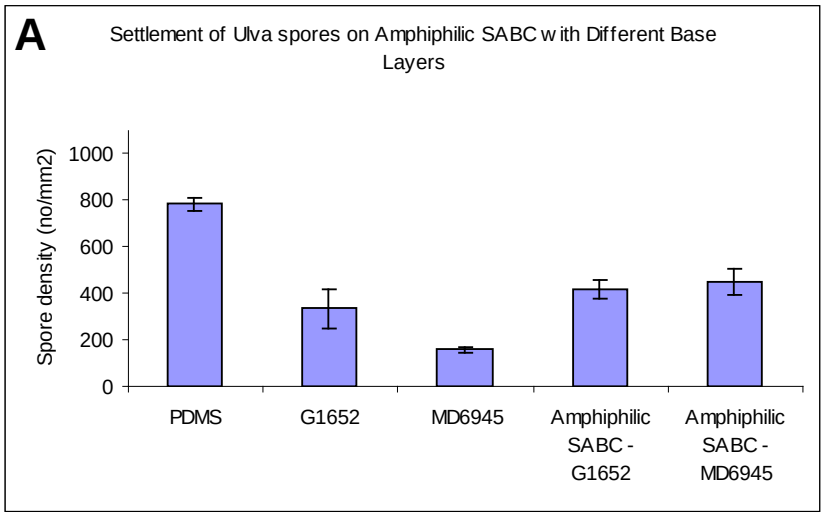
A
Settlement of Ulva spores on Amphiphilic SABC with Different Base Layers
Spore density (no/mm2)
1000
800
600
400
200
0
PDMS
G1652
MD6945
Amphiphilic SABC - G1652
Amphiphilic SABC - MD6945

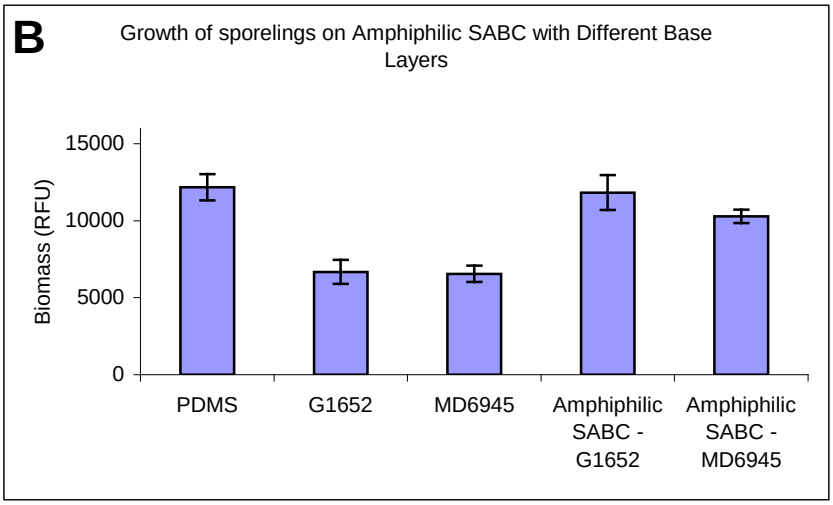
B
Growth of sporelings on Amphiphilic SABC with Different Base Layers
Biomass (RFU)
15000
10000
5000
0
PDMS
G1652
MD6945
Amphiphilic SABC - G1652
Amphiphilic SABC - MD6945

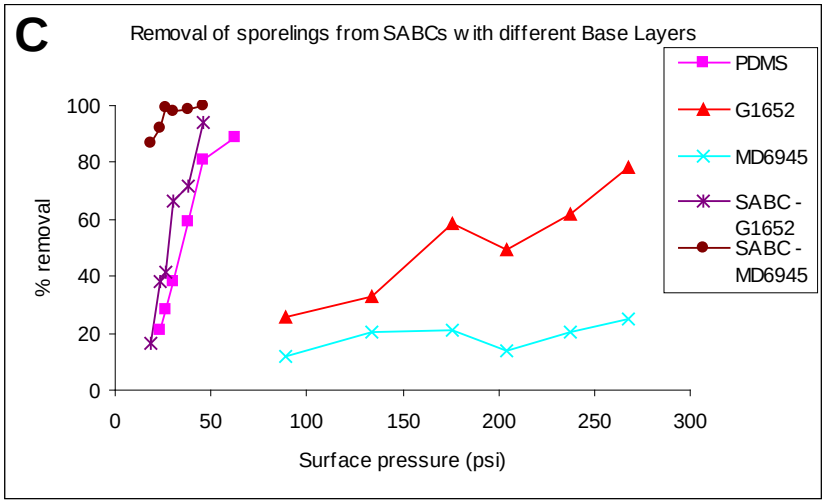
C
Removal of sporelings from SABCs with different Base Layers
% removal
100
80
60
40
20
0
0
50
100
150
200
250
300
Surface pressure (psi)
PDMS
G1652
MD6945
SABC - G1652
SABC - MD6945

Since the amphiphilic SABC released cultured *Ulva* sporelings at an efficiency of 87% or greater for every different applied water jet pressure tested, a decision was made to try an additional experiment using a water channel capable of producing much lower applied shear stress. The water jet runs perpendicular to the surface and produces a small central area with a high impact pressure surrounded by a radiating area of water flow parallel to the surface with an associated wall shear stress. While this technique does provide reliable information on the attachment strength of organisms to a surface, it does not model the flow of water around the hull of a ship at all accurately. A ship in motion does generate a turbulent boundary layer that creates a wall shear stress against the hull, but obviously there is no zone of central impact. Thus, testing with the specially designed water flow channel gives an opportunity to examine how different applied stresses vary removal characteristics of a coating. Additionally, since the applied shear stress generated is significantly less (52 Pa), the hope was that more statistically meaningful results could be generated for measuring the removal of *Ulva* sporelings from the amphiphilic SABCs using both the high modulus G1652 SEBS and the low modulus MD6945 SEBS.

For this additional round of testing, *Ulva* spore settlement was not analyzed. Figure3.7A depicts the growth of the sporelings which was similar for both amphiphilic SABC samples and all four control surfaces. Sporeling removal meanwhile is depicted in Figure 3.7B. Results here were quite surprising since while sporelings on the PDMS standards were readily detached by the applied 52 Pa shear stress generated in the water channel, removal from the two different sets of amphiphilic SABC samples was low, with no more than ca. ~ 25% removal observed. This ran completely counter to the expectations based on the water jet test data that suggested that removal from these surfaces would be equivalent to or better than that observed for PDMS. Natural variability in biological systems can sometimes produce

unexpected behavior in these assays, but removal was as expected from the PDMS, SEBS, and glass standards, suggesting the *Ulva* sporelings were indeed of good quality. As these samples were fabricated from a new batch of amphiphilic SABC that was produced from a more recent batch of the Zonyl FSO-100 fluorosurfactant, these findings suggested that the surface chemistry or these new samples may have been altered greatly despite them appearing to have very similar bulk chemical characteristics.

In order to try to confirm if the "new" amphiphilic SABC samples had similar properties to those supplied previously (the "old" amphiphilic SABC samples), one slide each from a set of spare samples from the "new" and "old" amphiphilic SABC sets were settled with *Ulva* spores and sporelings were grown out on them for 7 days by the standard method. Figure 3.8 demonstrates that exposure to a water jet pressure of 24 kPa easily removed sporelings from the "old" set of amphiphilic SABCs and the PDMS standard, but only yielded between ca. ~ 20-25% removal of *Ulva* sporelings for the "new" amphiphilic SABC samples. This further suggested that the surface properties of the "new" set of coatings were significantly different than those of the "old" set. An analysis of what we now know concerning the differences in performance of the two sample sets will be given in a later section of this chapter.

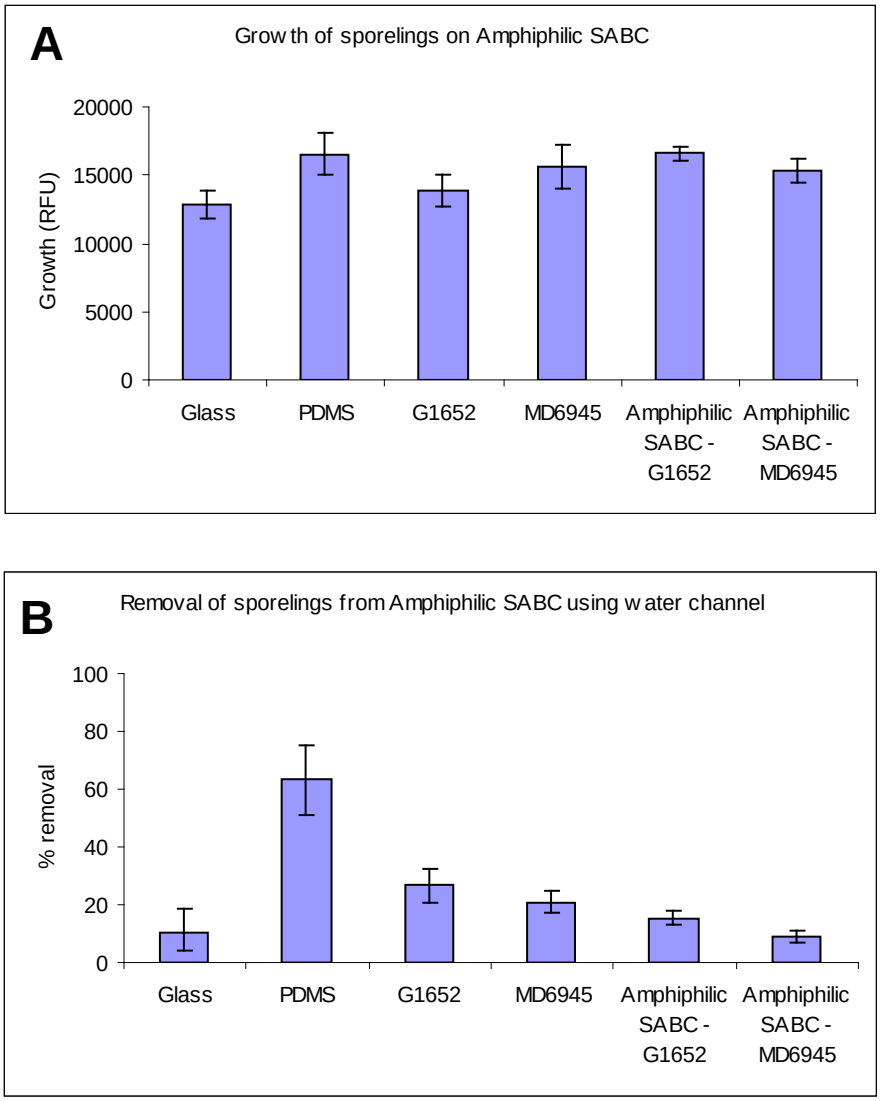

Figure 3.7. Results of additional *Ulva* biofouling assay designed to probe the release of sporelings in a water flow channel. Experimental surfaces consist of the amphiphilic fluoroalkyl SABC on both the high modulus G1652 SEBS thermoplastic elastomer base layer and the low modulus MD6945 SEBS base layer. Additionally, control surfaces of PDMS, glass, and both base layers are included for comparison purposes. A) Growth of *Ulva* sporelings on experimental surfaces after 7 days. Each point is the mean biomass measured from 6 replicate slides using a fluorescence plate reader (RFU; relative fluorescence unit). Bars show standard error of the mean. B) Detachment of *Ulva* sporelings from experimental surfaces. Slides were exposed to aw all shear stress of 52 Pa in a water flow channel. Points represent the mean percent removal from 6 slides with standard error of the mean derived from arsine transformed data.

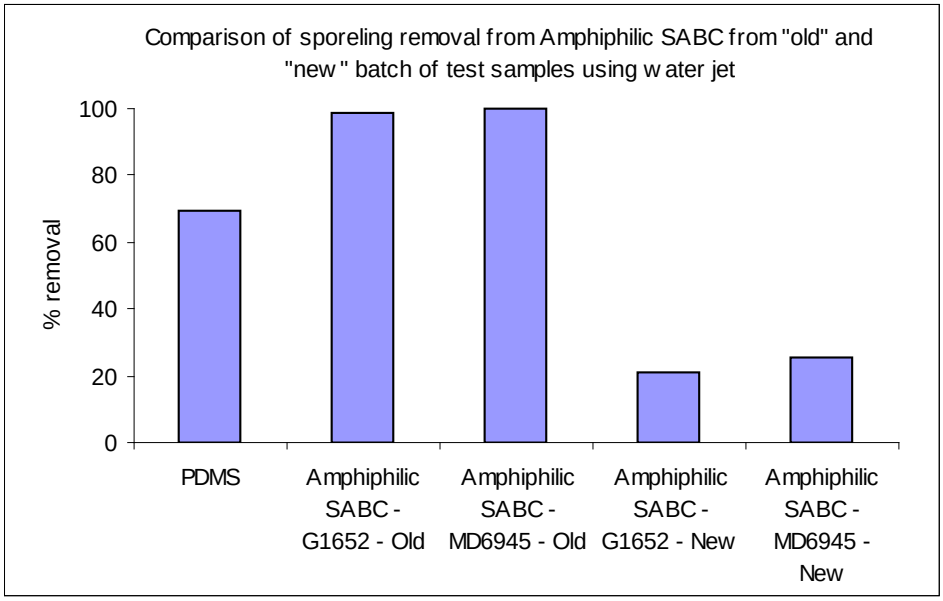

Figure 3.8. Comparison of *Ulva* sporeling removal from the "new" and "old" sets of samples using the water jet. Samples were exposed to a single surface pressure of 24 kPa from a water jet, and one slide was used for each measurement.

Settlement and Removal of *Navicula* Diatoms

Navicula diatom settlement is depicted in Figure 3.9A on the amphiphilic SABC with ethoxylated fluoroalkyl side chains in conjunction with glass, G1652 SEBS and PDMS controls. Since diatoms reach a fouling surface by sinking through the water column under the influence of gravity (they do not sample the surface like *Ulva*), measured attachment is more a function of differences in adhesion strength following gentle washing. Settlement of *Navicula* diatoms on the amphiphilic SABC was found to be noticeably lower than that on both the hydrophobic PDMS elastomer control, and the G1652 SEBS base layer control. As expected, glass showed lower settlement due to its hydrophilic nature. Removal results for *Navicula* diatoms, given in Figure 3.9B, inversely correlate to settlement as expected, with the highest removal being seen on the samples with the lowest settlement (where weak adhesion was implied). The most important thing to note here is that while the PDMS elastomer

only showed ca. ~ 5% removal of the *Navicula* diatoms, the amphiphilic SABC demonstrated ca. ~ 51% removal. This clearly demonstrates the ability of the amphiphilic SABC to also function as an effective antifouling and fouling-release coating for *Navicula* diatoms, despite their generally contrary settlement and release behavior relative to the green alga *Ulva*.[22] This highlights this approaches potential versus traditional PDMS derived fouling-release elastomers. Additional study is planned to examine what role reducing the base layer modulus through the incorporation of Kraton MD6945 will have on *Navicula* diatom settlement and release.

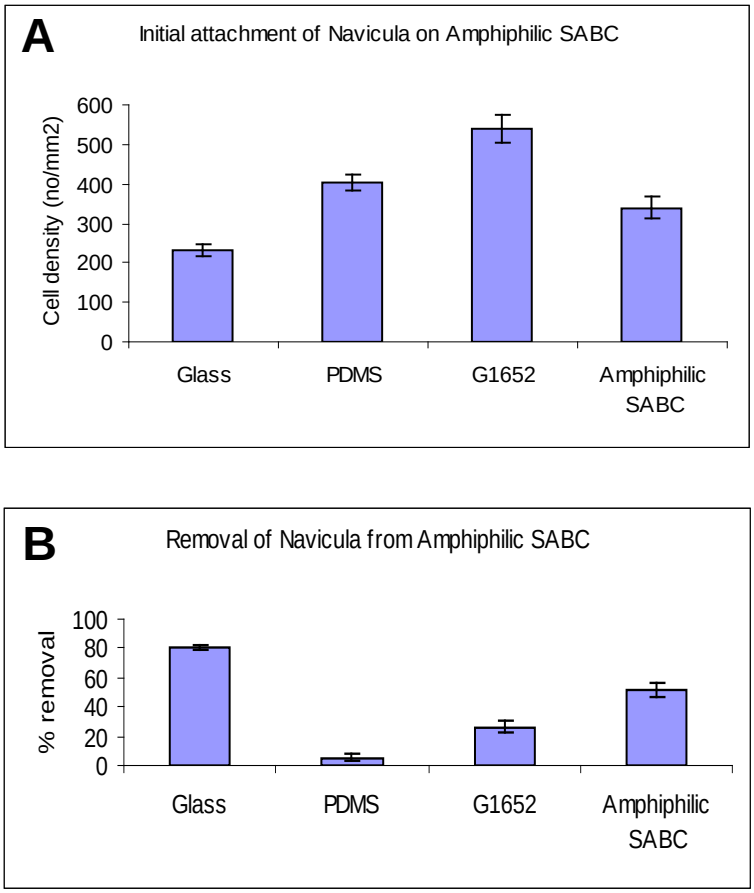

Figure 3.9. A) Initial attachment after gentle washing of *Navicula* diatoms to PS_{8K}-*b*-$P(E/B)_{25K}$-*b*-PI_{10K} derived amphiphilic SABC with ethoxylated fluoroalkyl side chains. B) Detachment of *Navicula* diatoms from same SABC as a result of exposure to a shear stress of 23 Pa. Each point is the mean from 90 counts on 3 replicate slides. Bars show 95% confidence limits.

Discussion of Conflicting Fouling-Results; Further Batch to Batch Analysis

The surprising lack of fouling release behavior observed for the amphiphilic SABCs in the *Ulva* sporeling release testing using the water flow channel left us extremely puzzled as to what had happened initially. There were two major factors in play that we initially suspected. One of them was the possible presence of silicone contamination in the samples as some sort of artifact of polymer and/or biofouling assay sample preparation. The second issue was that work with the ethoxylated fluoroalkyl SABC has spanned several different iterations of synthetic samples. While every possible attempt has been made to try to make sure that we are indeed testing polymers with a chemical structure as close to each other as possible from one sample iteration to the next, we now believe that certain factors outside of our control could have contributed to initially undetected subtle variability from sample to sample. The following section will aim to briefly discuss these issues, present what we have learned thus far in resolving them, and finally, propose what additional steps should be undertaken to try to reach a decisive outcome in preventing similar challenges in the future.

Figure 3.10 depicts a recent high resolution C 1s XPS spectrum taken on one of our amphiphilic SABC samples containing ethoxylated fluoroalkyl side chains. Clearly, if one compares this spectrum to those previously reported in this chapter, it quickly becomes obvious that the contribution from the ethoxylated fluoroalkyl side chains at the surface is negligible at best. The peak associated with CF_3 moieties at 294 eV is no longer visible, and the peak associated with CF_2 groups at 292 eV is drastically reduced in intensity. Additionally, the C-C peak at ca. ~ 284.5 eV is now dominant with very little contribution from the C-O-C peak at around 287 eV (it simply manifests itself as a shoulder). This led to the question: What happened to the ethoxylated fluoroalkyl groups at the surface? An initial concern was that side chain

attachment was no longer as robust as in the samples initially produced, but additional scrutiny by ^{1}H NMR spectroscopy indicated that attachment of side chains still was on the order of 40% or greater relative to epoxy in the epoxidized PS_{8K}-*b*-$P(E/B)_{25K}$-*b*-PI_{10K} precursor. Thus, our attention shifted to the XPS survey scans for the spun coat samples of the newly produced amphiphilic SABC. Figure 3.11 gives a representative survey scan taken at an incidence angle of 75° of a spun coat film of a "new" amphiphilic SABC on a Si wafer. Here, we see an extremely small contribution from the F 1s peak, suggesting minimal presence of fluorinated moieties at the surface. Additionally surprising was the relatively high intensity of the O 1s peak and the presence of a significant Si 2p contribution. This led us to believe that unwanted low molecular weight siloxane contamination was present in the sample, likely from some form of silicon based oil or grease introduced during synthesis or sample work up.

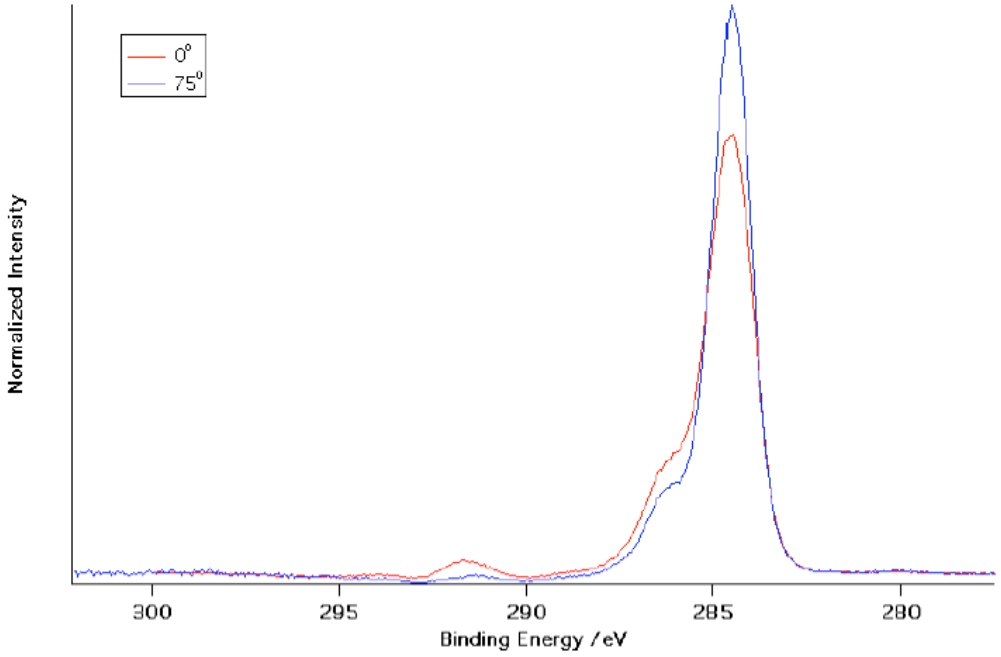

Figure 3.10. XPS C 1s spectra of the surface of the amphiphilic SABC with ethoxylated fluoroalkyl side chains derived from the PS_{8K}-*b*-$P(E/B)_{25K}$-*b*-PI_{10K} precursor polymer spun coat on silicon taken at both 0° and 75° incidence angles.

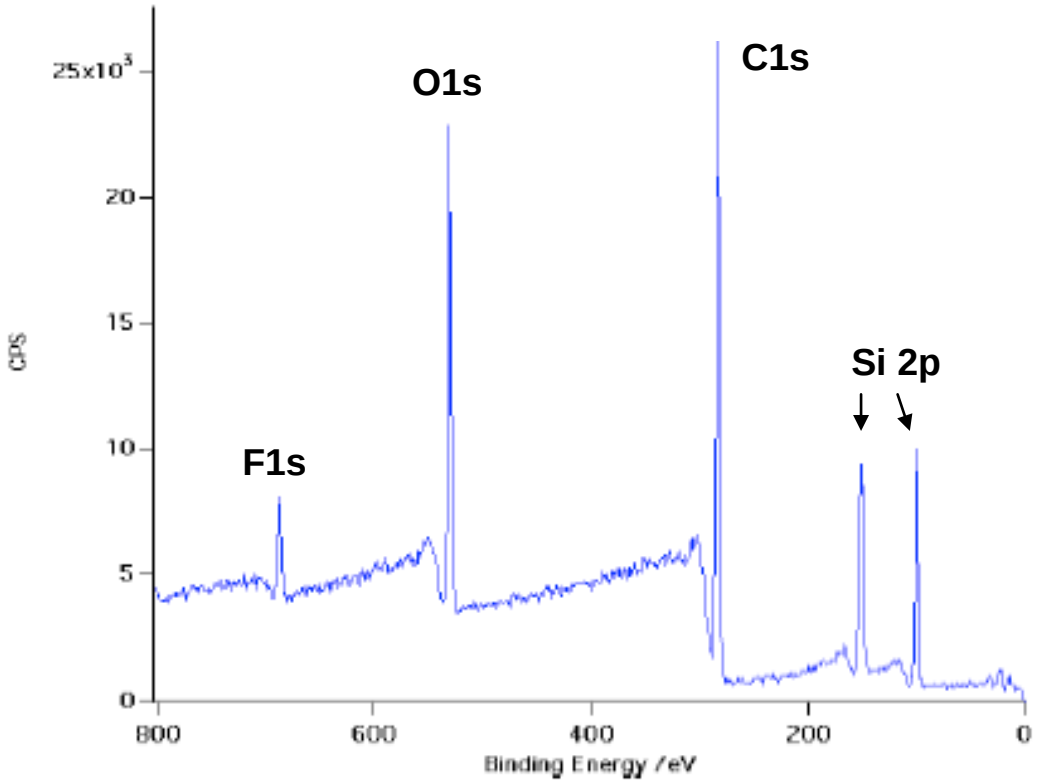

Figure 3.11. XPS survey scan of "new" amphiphilic SABC spun coat on Si wafer taken at an incidence angle of 75°.

This touched off a pain-staking attempt to eliminate all potential sources of contamination. Since the synthesis and ultimate fabrication of surfaces for either characterization o biofouling analysis is a many step process, there were quite a few potential areas of concern. First of all, we immediately cleaned and/or replaced all of the hosing in the laboratory hoods in which these samples were prepared. Another potential source of contamination was the oil pumps used both in the drying stage following synthesis and during the annealing phase following casting of the surface characterization and biofouling assay samples. The annealing setup was of particular concern due to many years of lax operating procedures where pump oil was often allowed to back into the oven through improper usage and carelessness. A new

annealing oven and pump were ordered, setup, and designated to be used for only antifouling research. Additionally, greater attention was paid to annealing with this oven, particularly with focus on preventing the liquid nitrogen, used both to keep solvents liberated by annealing from entering the pump and molecules in the pump from entering the oven, from evaporating; thus keeping the vacuum trap at low temperature always while annealing. To answer questions about the cleanliness of the drying oven meanwhile, a new oven was purchased and fitted with an oil free pump and designated also for use with only samples prepared as part of our antifouling work.

These fixes did not solve our problem however. This led us to the additional realization that we had purchased a different type of syringe in bulk that was either coated with silicon oil and/or leaching a silicon containing compound from a rubber plug in the plunger mechanism. These syringes were generally used in conjunction with syringe filters for removing fine particles that would otherwise interfere with film formation during spinning samples for surface analysis. Once this step was removed from the flow process for generating samples for surface analysis, we found that silicon contamination in the XPS traces was drastically reduced. This experience highlighted the extreme sensitivity of XPS to mobile, low surface energy species in a thin film however as the silicon impurity was able to effectively displace the expected ethoxylated fluoroalkyl surface functionality. Ultimately the silicon contamination served as a type of red herring however as subsequent analysis of various spray coated samples found that it was not present in any significant quantity (most likely due to the lack of use of syringes in that process flow).

Another area of concern was that while the samples for the first two sets of *Ulva* assays, and the *Navicula* assay were prepared by spraying solutions in TFT, the samples in the final *Ulva* assay involving the water flow channel were prepared from solutions in chloroform. However, significant effects from this processing change

were ruled out in a fourth *Ulva* assay (data not reported) in which a similar lack of fouling release of sporelings was observed.

At this point, our focus shifted to trying to confirm that very subtle chemical differences between the "old" batch of amphiphilic SABC and the "new" batch were not manifesting significant differences in surface chemistry. A particularly troubling point of information was that in late 2007, the physical characteristics of the Zonyl FSO-100 compound as commercially available from Sigma Aldrich changed. Until this point, previous batches of the FSO-100 were received as a waxy, brownish yellow solid at room temperature. For the new batch of material however, the Zonyl was now a brown liquid at room temperature. This suggested one of two things. First of all, the presence of some sort of low molecular weight impurity such as residual solvent in the "new" batch of Zonyl FSO-100 may have contributed to this change in physical characteristics. Secondly, since the Zonyl FSO-100 is inherently a dispersion of different molecular weight species, a change in the mode or mean of the dispersion could greatly influence its physical characteristics.

Figure 3.12 depicts the ^{1}H NMR spectra of the "new" batch of Zonyl FSO-100 nonionic fluorosurfactant, while figure 3.13 depicts the same spectra for the "old" batch of Zonyl FSO-100. Peak integrations of both the proton peak at ca. ~ 3.6 ppm associated with the $–CH_2CH_2O-$ repeat groups of the PEGylated sections of the molecules and the $-CH_2CF_2-$ protons at ca. ~ 2.4 ppm are given. These values were used in conjunction with the equations given in Krishnan et al. to calculate the average values of x and y for each batch of ethoxylated fluoroalkyl surfactant $(F(CF_2CF_2)_y(CH_2CH_2O)_xCH_2CH_2OH)$.[24] The "new" batch of Zonyl was found to have a value of $x \approx 6.7$, while the "old" batch was found to have a value of $x \approx 7.7$. Additionally, for the "new" batch of Zonyl it was determined that $y \approx 3.7$, while for the "old" batch $y \approx 3.5$. These values compared to $x \approx 5.9$ and $y \approx 3.4$ reported

previously.[24] This suggests that the average length of the fluorinated component of the Zonyl FSO-100 was very similar in all three cases. The PEGylated chain length was slightly longer for the "old" batch of material, but it would be surprising if this change (which only accounts to a 15% difference) would have resulted in such a drastic change in fouling release behavior. The large singlet peak that shows up at ca. ~ 3.2 ppm for the "new" material and ca. ~ 2.7 ppm for the "old" material is likely due to the presence of water in the starting material. Further examination of the spectra indicate some minor differences with trace peaks, but there is no major contribution that stands out in either spectra otherwise. This suggests that the mean size of the repeat units in the two separate Zonyl FSO-100 samples is not likely the cause of this discrepancy in fouling release behavior. Additional characterization using matrix assisted laser desorption ionization time of flight (MALDI-TOF) characterization will likely help with further determination of the structure of the "old" and "new" batches of Zonyl, but to date we have not been able to replicate the conditions used by Krishnan et al. to previously conduct this analysis.[24] Additionally, efforts are now being undertaken to try to get assistance from Dupont in isolating the differences between each batch of Zonyl.

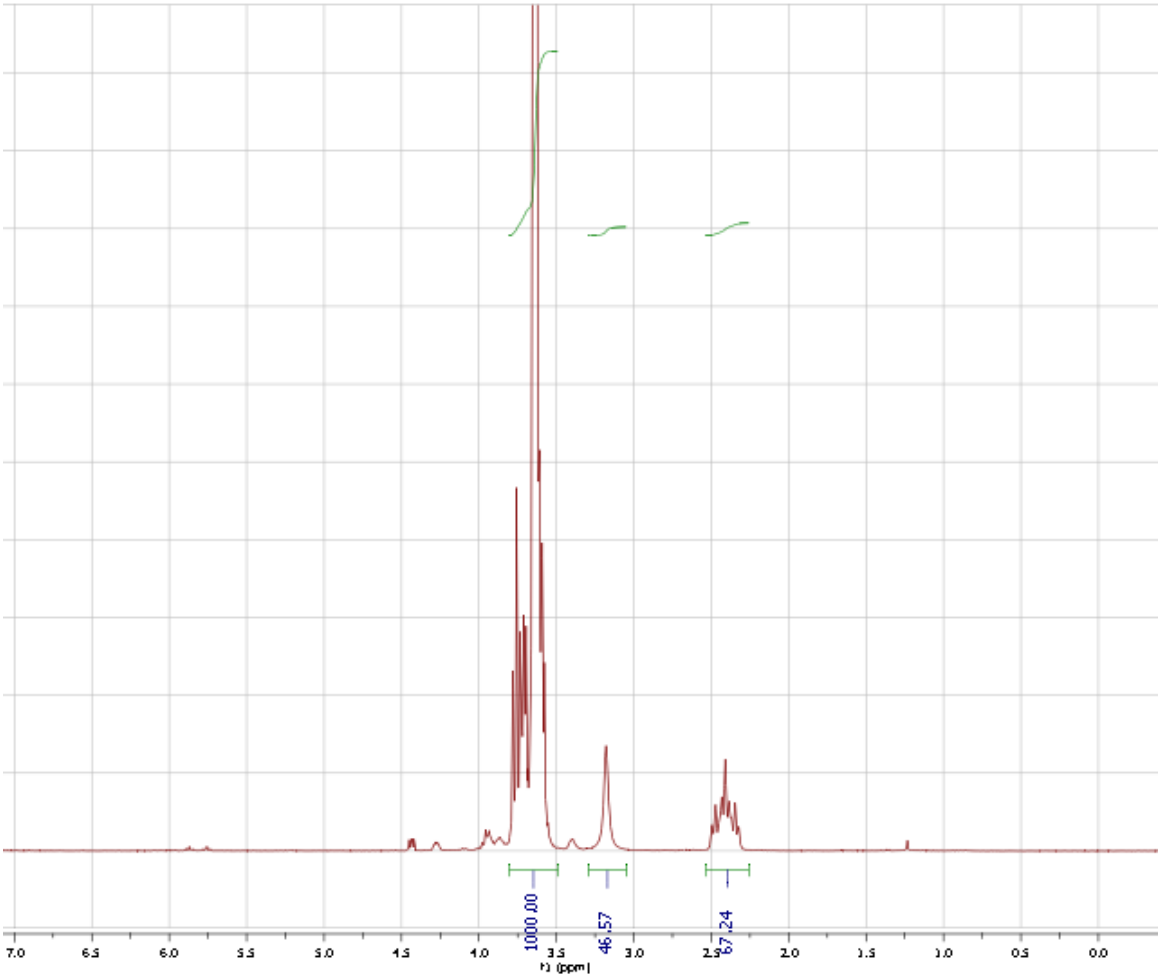

Figure 3.12. ^{1}H NMR spectra of the “new” batch of Zonyl FSO-100 non-ionic fluorosurfactant with major peaks integrated.

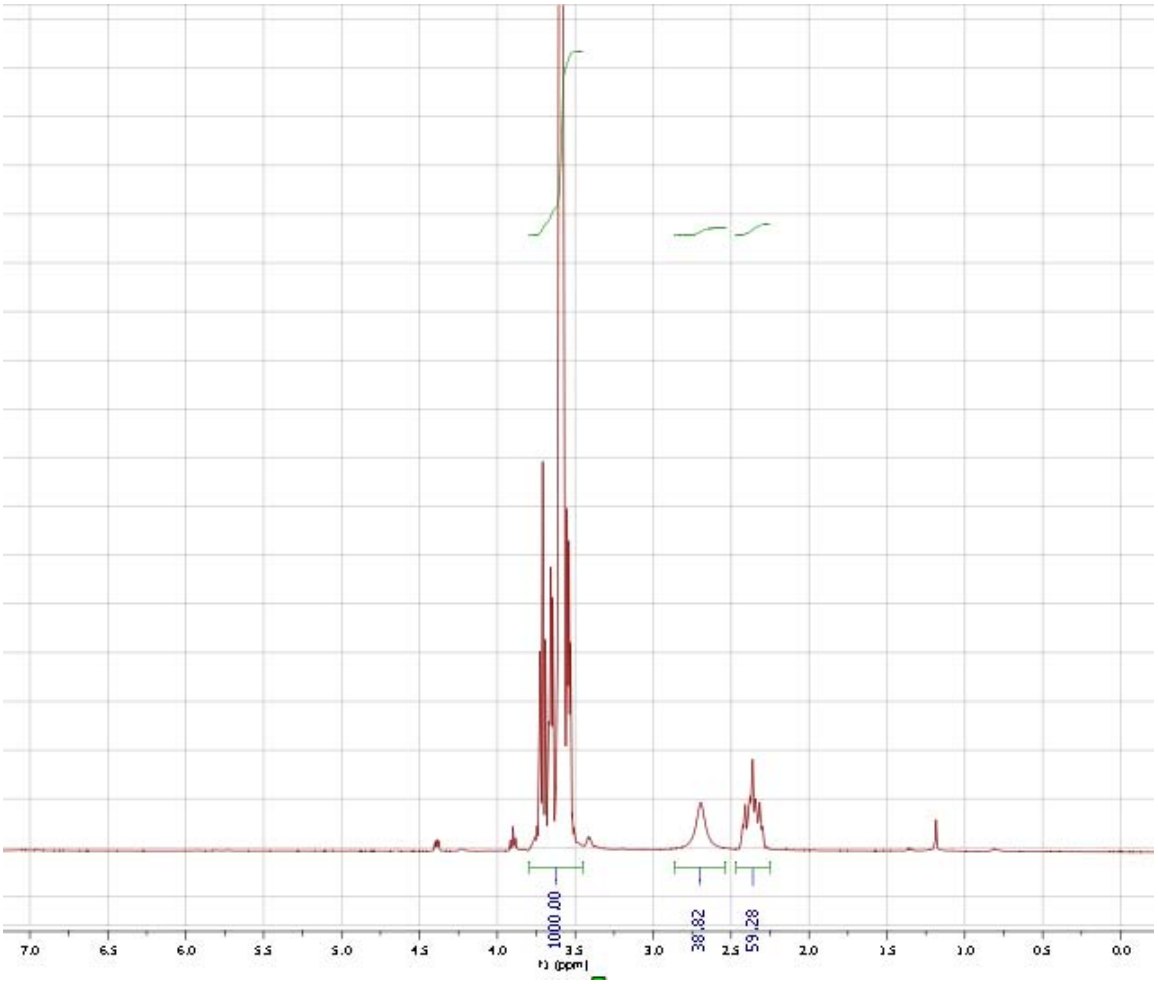

Figure 3.13. ^{1}H NMR spectra of the "old" batch of Zonyl FSO-100 non-ionic fluorosurfactant with major peaks integrated.

This led to a final effort to try to identify and hopefully isolate any batch to batch differences in the final amphiphilic SABCs produced by reviewing the ^{1}H NMR spectra of polymers produced with the "old" batch of Zonyl versus the "new" batch of Zonyl with attention focused on small differences that may not have initially been noticed. Figure 3.14 depicts the ^{1}H NMR spectra of the amphiphilic SABC produced recently from the "new" batch of Zonyl FSO-100 fluorosurfactant, while figure 3.15 depicts the ^{1}H NMR spectra of the amphiphilic SABC produced from the "old" batch. Major peaks have been integrated and normalized to the known value of 385 for the

aromatic protons of the polystyrene block. Analysis of the large peak at ca. ~ 3.6 ppm, indicative of the protons of the PEGylated part of the amphiphilic side chains, suggests slightly greater incorporation of the side chain into the “new” samples (especially considering the “new” Zonyl appears to have a slightly lower mean chain length for the oligo(ethylene glycol) groups). This is further supported by integration of the peak at ca. ~ 2.4 ppm indicative of the methylene group adjacent to the perfluorinated section of the amphiphilic side chain. Revisiting the two spectra further demonstrates three more subtle discrepancies between them. First of all, the magnitude of the integrated polymer back-bone when normalized to the aromatic polystyrene protons seems larger for the “new” sample versus the “old” sample (ca. ~ 5600 for the “old” sample versus ca. ~ 6300 for the “new”). Secondly, the aliphatic proton peak at ca. ~ 1.6 ppm appears much sharper for the “old” sample versus the “new” sample. Finally, the “old” sample appears to have evidence of unexpected protons bonded to silicon at ca. ~ 0.1 ppm. When these results are all taken into consideration, it seems that the “old” amphiphilic SABC likely had minor silicone oil contamination as an artifact of the synthetic work up. The additional aliphatic proton intensity meanwhile suggests some form of hydrocarbon contamination in the “new” amphiphilic SABCs. Nevertheless, this hydrocarbon contamination may be quite minimal however when the inherent lack of precision of ^{1}H NMR integration is taken into account.

Figure 3.14. ^{1}H NMR spectra of the amphiphilic SABC derived from the "new" batch of Zonyl FSO-100 non-ionic fluorosurfactant with major peaks integrated. Values are normalized to the known value of 385 protons for the aromatic protons of the polystyrene block.

Figure 3.15. ^{1}H NMR spectra of the amphiphilic SABC derived from the "old" batch of Zonyl FSO-100 non-ionic fluorosurfactant with major peaks integrated. Values are normalized to the known value of 385 protons for the aromatic protons of the polystyrene block.

Finally, the XPS survey scan taken at a 75° incident angle for the "old" amphiphilic SABC was double checked to confirm that there was no significant contribution of silicon contaminant at the surface. Figure 3.16 demonstrates the absence of any peaks associated with Si 2p, suggesting that despite the evidence of minor Si contamination in the ^{1}H NMR spectra, the surfaces were free of any silicon containing species. Thus, enhanced fouling release due to the presence of self polishing, low molecular weight silicon containing compounds was ruled out.

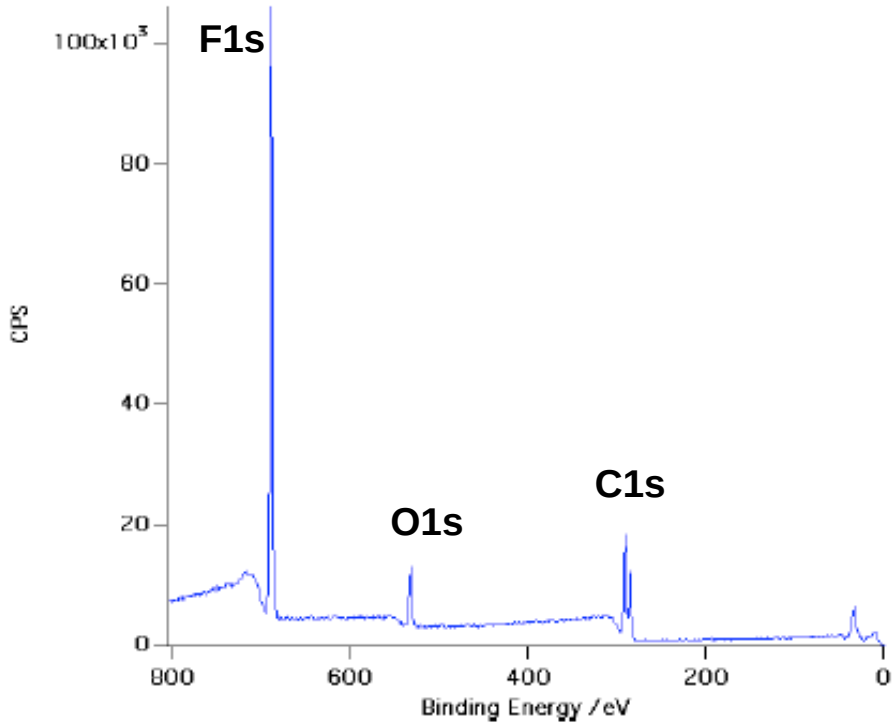

Figure 3.16. XPS survey scan for “old” amphiphilic SABC at an incident angle of 75°.

In summary, while a definitive statement about the differences in fouling release performance of the “old” and “new” amphiphilic SABCs cannot be made, silicone oil contamination can be ruled out. Furthermore, no drastic differences appear to be present in the chemical signatures of the “old” and “new” Zonyl FSO-100 fluorosurfactant samples despite their significantly different physical properties at room temperature. Obtaining more information from Dupont on differences between the batches in conjunction with completing MALDI-TOF analysis of the “new” Zonyl FSO-100 for comparison to the “old” are the next logical steps in solving this puzzle. It will also be advantageous to produce a fresh amphiphilic SABC for comparison purposes using the small amount of “old” Zonyl FSO-100 that was recently located.

Conclusions

Amphiphilic surface active block copolymers with ethoxylated fluoroalkyl side chains were successfully produced through polymer modification of a polystyrene-*block*-poly(ethylene-*ran*-butylene)-*block*-polyisoprene precursor. Resultant polymers were characterized using a combination of ^{1}H NMR spectroscopy and Fourier transform infrared spectroscopy, confirming the successful attachment of the amphiphilic surface active groups. Dynamic water contact angle analysis in conjunction with X-ray photoelectron spectroscopy suggested a surface highly populated by the amphiphilic moieties with hydrophobic fluorinated species present in an air (non-polar) environment that could readily reorient to bring PEGylated moieties to the surface upon immersion into a hydrophobic, polar environment such as water. The settlement and removal behavior of two types of ubiquitous marine "soft" fouling organisms, the green alga *Ulva* and *Navicula* diatoms were evaluated through a series of biofouling assays. Robust removal of both organisms from glass microscope slides coated with the multilayer marine antifouling/fouling-release surface active block copolymer was realized. Additional assays focusing on the effect of tuning the elastic modulus of the thermoplastic elastomer base layer used in the coating demonstrated a drastically reduced force of adhesion for *Ulva* sporelings to the multilayer coating system. This is unique since it demonstrates the first time that tuning of the modulus of a flexible coating system developed by Ober and coworkers over several years has been demonstrated.

Acknowledgements

This work was supported by the United States Department of Defense's Strategic Environmental Research and Development Program (SERDP), grant WP #1454 with additional support from the Office of Naval Research (ONR) through award # N00014-05-1-0134 (JAC and MEC) and N00014-02-1-0170 (CKO and EJK). KES and EJK acknowledge partial support from an NSF Graduate Fellowship and the NSF Polymers Program (DMR-0704539) as well as the use of facilities funded by the NSF-MRSEC program (UCSB MRL, DMR-0520415).

REFERENCES

1 M. E. Callow and J. A. Callow, *Biologist*, 2002, **49**, 1.

2 R. L. Townsin, *Biofouling*, 2003, **19 (Supplement)**, 9.

3 M. P. Schultz, *Biofouling*, 2007, **23**, 331.

4 L. Chromy and K. Uhacz, *Journal of the Oil and Colour Chemists' Association*, 1978, **61**, 39.

5 R. F. Brady, *Journal of Protective Coatings & Linings*, 2003, **20**, 33.

6 D. M. Yebra, S. Kiil, and K. Dam-Johansen, *Prog. Org. Coat.*, 2004, **50**, 75.

7 S. Krishnan, C. J. Weinman, and C. K. Ober, *J. Mater. Chem.*, 2008, **18**, 3405.

8 L. D. Chambers, K. R. Stokes, F. C. Walsh, and R. J. K. Wood, *Surf. Coat. Technol.*, 2006, **201**, 3642.

9 J. Genzer and K. Efimenko, *Biofouling*, 2006, **22**, 339.

10 T. Vladkova, *Journal of the University of Chemical Technology and Metallurgy*, 2007, **42**, 239.

11 A. O. Christine and R. Dalley, in 'Barnacle fouling and its prevention.' ed. A. J. Southward, Rotterdam, 1987.

12 N. L. Gray, W. C. Banta, and G. I. Loeb, *Biofouling*, 2002, **18**, 269.

13 R. F. Brady and I. L. Singer, *Biofouling*, 2000, **15**, 73.

14 A. Beigbeder, P. Degee, S. L. Conlan, R. J. Mutton, A. S. Clare, M. E. Pettitt, M. E. Callow, J. A. Callow, and P. Dubois, *Biofouling*, 2008, **24**, 291.

15 K. J. Wynne, G. W. Swain, R. B. Fox, S. Bullock, and J. Ulik, *Biofouling*, 2000, **16**, 277.

16 R. F. Brady, *Polymers Paint Colour Journal*, 2000, **190**, 18.

17 A. Terlizzi, E. Conte, V. Zupo, and L. Mazzela, *Biofouling*, 2000, **15**, 327.

18 K. L. Prime and G. M. Whitesides, *J. Am. Chem. Soc.*, 1993, **115**, 10714.

19 H. Ma, J. Hyun, P. Stiller, and A. Chilkoti, *Advanced Materials*, 2004, **16**, 338.

20 S. Schilp, A. Kueller, A. Rosenhahn, M. Grunze, M. E. Pettitt, M. E. Callow, and J. A. Callow, *Biointerphases*, 2007, **2**, 143.

21 J. P. Youngblood, L. Andruzzi, C. K. Ober, A. Hexemer, E. J. Kramer, J. A. Callow, J. A. Finlay, and M. E. Callow, *Biofouling*, 2003, **19**, 91.

22 S. Krishnan, N. Wang, C. K. Ober, J. A. Finlay, M. E. Callow, J. A. Callow, A. Hexemer, K. E. Sohn, E. J. Kramer, and D. A. Fischer, *Biomacromolecules*, 2006, **7**, 1449.

23 C. S. F. Gudipati, J. A.; Callow, J. A.; Callow, M. E.; Wooley, K. L., *Langmuir*, 2005, **21**, 3044.

24 S. Krishnan, R. Ayothi, A. Hexemer, J. A. Finlay, K. E. Sohn, R. Perry, C. K. Ober, E. J. Kramer, M. E. Callow, J. A. Callow, and D. A. Fischer, *Langmuir*, 2006, **22**, 5075.

25 C. J. K. Weinman, S.; Park, D.; Paik, M. Y.; Wong, K., Fischer, D. A.; Handlin, D. A., Kowalke, G. L.; Wendt, D. E.; Sohn, K. E.; Kramer, E. J.; Ober, C. K., *PMSE Preprints*, 2007, **96**, 597.

26 E. Martinelli, S. Agostini, G. Galli, E. Chiellini, A. Glisenti, M. E. Pettiitt, M. E. Callow, J. A. Callow, K. Graf, and F. W. Bartels, *Langmuir*, 2008, **24**, 13138.

27 S. Krishnan, R. J. Ward, A. Hexemer, K. E. Sohn, K. L. Lee, E. R. Angert, D. A. Fischer, E. J. Kramer, and C. K. Ober, *Langmuir*, 2006, **22**, 11255.

28 S. Krishnan, J. A. Finlay, A. Hexemer, N. Wang, C. K. Ober, E. J. Kramer, M. E. Callow, J. A. Callow, and D. A. Fischer, *Polym. Prepr. (Am. Chem. Soc., Div. Polym. Chem)*, 2005, **46**, 1248.

29 C. J. Weinman, J. A. Finlay, D. Park, M. Y. Paik, S. Krishnan, B. R. Fletcher, M. E. Callow, J. A. Callow, D. L. Handlin, C. L. Willis, D. A. Fischer, K. E. Sohn, E. J. Kramer, and C. K. Ober, *Polymeric Materials: Science & Engineering Preprints*, 2008, **98**, 639.

30 M. Berglin, Gatenholm, P., *J. Adhes. Sci. Tech.*, 1999, **13**, 713.

31 J. F. Schumacher, M. L. Carman, T. G. Estes, A. W. Feinberg, L. H. Wilson, M. E. Callow, J. A. Callow, J. A. Finlay, and A. B. Brennan, *Biofouling*, 2007, **23**, 55.

32 M. E. Callow, J. A. Callow, J. D. Pickett-Heaps, and R. Wetherbee, *Journal of Phycology*, 1997, **33**, 938.

33 M. E. Callow, A. R. Jennings, A. B. Brennan, C. E. Seegert, A. Gibson, L. Wilson, A. Feinberg, R. Baney, and J. A. Callow, *Biofouling*, 2002, **18**, 237.

34 M. K. Chaudhury, J. A. Finlay, J. Y. Chung, M. E. Callow, and J. A. Callow, *Biofouling*, 2005, **21**, 41.

35 F. Casse, E. Ribeiro, A. Ekin, D. C. Webster, J. A. Callow, and M. E. Callow, *Biofouling*, 2007, **23**, 267.

36 J. A. Finlay, M. E. Callow, M. P. Schultz, G. W. Swain, and J. A. Callow, *Biofouling*, 2002, **18**, 251.

37 F. T. Arce, R. Avci, I. B. Beech, K. E. Cooksey, and B. Wigglesworth-Cooksey, *J. Chem. Phys.*, 2003, **119**, 1671.

38 J. A. Finlay, S. Krishnan, M. E. Callow, J. A. Callow, R. Dong, N. Asgill, K. Wong, E. J. Kramer, and C. K. Ober, *Langmuir*, 2008, **24**, 503.

39 M. Berglin, N. Lonn, and P. Gatenholm, *Biofouling*, 2003, **19 (Supplement)**, 63.

40 J. Stein, K. Truby, C. Darkangelo-Wood, M. Takemori, M. Vallance, G. Swain, C. Kavanagh, B. Kovach, M. Schultz, D. Wiebe, E. Holm, J. Montemarano, D. Wendt, C. Smith, and A. Meyer, *Biofouling*, 2003, **19**, 87.

CHAPTER 4

TRIBLOCK SURFACE ACTIVE BLOCK COPOLYMERS WITH MIXED HYDROPHOBIC AND HYDROPHILIC SIDE CHAINS: DEVELOPMENT OF AMPHIPHILIC MARINE FOULING-RELEASE POLYMERS THROUGH TUNING OF HYDROPHOBIC AND HYDROPHILIC MOIETIES

Abstract

Two series of amphiphilic triblock surface active block copolymers (SABCs) were synthesized through chemical modification of two polystyrene-*block*-poly(ethylene-*ran*-butylene)-*block*-polyisoprene ABC triblock copolymer precursors. Poly(ethylene glycol) methyl ether with $M_n \approx 550$ g/mol (PEG550) and semifluorinated decyl alcohol (F10H10OH) were attached at different molar ratios to impart both hydrophobic and hydrophilic groups to the polymeric back-bone. Bilayer coatings on glass slides consisting of a thin layer of the amphiphilic SABC deposited on a thicker layer of a polystyrene-*block*-poly(ethylene-*ran*-butylene)-*block*-poly(styrene) thermoplastic elastomer were prepared for biofouling assays. Dynamic water contact angle analysis, X-ray photoelectron spectroscopy (XPS) and near-edge X-ray absorption fine structure (NEXAFS) measurements were utilized to characterize the surfaces. Clear differences in surface structure were realized as the composition of attached side chains was varied. In biofouling assays, spore settlement of the green alga *Ulva* was generally enhanced for surfaces incorporating a large proportion of the hydrophobic F10H10 side chains, whilst a large proportion of the PEG550 side chains inhibited settlement. *Ulva* sporeling release assays did not show such an obvious trend, however, amphiphilic SABCs incorporating a mixture of PEG550 and F10H10 side chains performed the best. There were no significant differences in the settlement of

Navicula diatoms (a unicellular alga) across the two sets of coatings. However, in fouling release assays, the removal of *Navicula* increased with increasing ratio of the hydrophobic F10H10 side chains, contrary behavior to what has generally been previously reported.

Introduction

The vast collection of fouling organisms and environmental conditions present in the world make the task of developing universal marine antifouling and/or fouling-release coatings extremely challenging. During the early 1970s, it was discovered that the prevention of marine biofouling could be achieved through the use of ablative coatings containing organometallic tributyl-tin (TBT). As the toxic organometallic biocide leached out of the coating, the growth of adhered microorganisms such as barnacles and algae was stunted and ultimately the organisms were killed. Unfortunately, the lack of selectivity of TBT proved extremely detrimental to other organisms in the environment. For instance, TBT was proven to cause deformations in oysters and lead to sex changes in the dog whelk (*Nucella lapillus*).[1] As a result, TBT based marine anti-fouling coatings have now been banned in most countries.[2] Finding alternative coatings has proved a challenging process. Some approaches have included the use of copper based ablative coatings, but they are also environmentally undesirable and concerns exist in the marine community that they may too be forced out of service.[3, 4] The incorporation of non-leaching biocidal moieties into coatings has also been a robust area of research to produce more environmentally friendly anti-fouling coatings.[5-8] Their reported use in marine applications however has been limited and thus far, produced mixed results.[9-13]

The primary mode of attachment of marine organisms to a surface involves the secretion of adhesives which frequently contain large proportions of proteins and

glycoproteins.[14, 15] Therefore, the design of minimally adhesive coatings capable of both preventing the attachment of marine organisms and promoting their release is required. One approach is the fabrication of protein repellant surfaces incorporating poly(ethylene-glycol) (PEG) based (co)polymers. PEG, an uncharged, water-soluble polymer has inherent extraordinary antifouling efficacy since it is hydrophilic and its long, flexible chains contribute to its ability to uniquely coordinate with surrounding water molecules. It is believed that this superior ability of PEG to be hydrated with water molecules in conjunction with steric exclusion effects are both crucial to protein adsorption resistance.[16-18] A multitude of protein resistant materials incorporating PEG have been reported in the literature, ranging from the combination with poly(methyl methacrylate) as a potential material for biomedical devices,[19] to PEG containing self assembled monolayers[20, 21] and polymer brushes[22] to form protein resistant functional coatings. In the area of marine anti-fouling, PEG monolayers,[23-25] PEGylated hydrogels,[26] and also multilayer coatings based on surface active block copolymers with grafted PEG side chains[27, 28] have been evaluated.

Another prevalent approach to marine biofouling control is to utilize hydrophobic coatings possessing low surface energy. The low surface energy reduces the polar and hydrogen bonding interactions with the marine organism's adhesive, effectively lowering adhesion strength. This leads to fouling release coatings capable of shedding marine fouling under low values of applied shear. Many studies on the fouling-release behavior of siloxanes,[2, 29-33] fluorosiloxanes,[34] and fluoropolymers[35] have been reported. In particular poly(dimethyl siloxane) (PDMS) elastomers with low surface energy are widely used as fouling-release coatings readily shedding fouling organisms under suitable hydrodynamic conditions.[36]

Recently, several amphiphilic fouling release coatings have been reported that combine hydrophobic, low surface energy fluorinated moieties with protein resistant

hydrophilic PEG containing groups. Gudipati et al. reported on the development of coatings consisting of an amphiphilic network of hyperbranched fluoropolymer groups combined with linear PEG moieties that showed better release of *Ulva* sporelings than PDMS controls.[37] Additionally, in two separate studies, Krishnan et al.[38] and Martinelli et al.[39] reported on side chain block copolymers containing grafted ethoxylated fluoroalkyl groups that were capable of facile release of both sporelings of the green alga *Ulva* and *Navicula* diatoms. This suggests that amphiphilic fouling release coatings have the potential to resist settlement and adhesion by a wider range of organisms than other coatings currently in use. Due to the significant global demand for a universal practical solution to marine fouling control, additional study in this area is desperately needed.

The following study will report the development of ambiguous amphiphilic polymeric antifouling coatings combining low surface energy with cell adhesion resistance through the random incorporation of discrete poly(ethylene glycol) and semifluorinated side chains with two specifically designed polystyrene-*block*-poly(ethylene-*ran*-butylene)-*block*-polyisoprene, PS-*b*-P(E/B)-*b*-PI, ABC triblock copolymer precursors. Chemical characterization of the resultant surface active block copolymers (SABCs) will be reported and correlated to surface characterization using near-edge X-ray adsorption fine structure (NEXAFS) analysis, X-ray photoelectron spectroscopy (XPS) and dynamic water contact angle analysis. Additionally, biofouling assays carried on two separate, but related sets of ambiguous amphiphilic SABCs will be described, charting these materials ability to resist and release fouling by both the green macroalga *Ulva* and the diatom *Navicula*. Specific trends in settlement and release behavior will be reported and areas of interest for additional work will be identified.

Experimental Section:

Materials

Both the polystyrene$_{8K}$-*block*-poly(ethylene-*ran*-butylene)$_{25K}$-*block*-polyisoprene$_{10K}$ (PS$_{8K}$-*b*-P(E/B)$_{25K}$-*b*-PI$_{10K}$) and the polystyrene$_{8K}$-*block*-poly(ethylene-*ran*-butylene)$_{25K}$-*block*-polyisoprene$_{20K}$ (PS$_{8K}$-*b*-P(E/B)$_{25K}$-*b*-PI$_{20K}$) triblock precursor copolymers were produced using anionic polymerization and subsequent catalytic hydrogenation by Kraton Polymers at large scale (~ 0.5 kg).

1-iodoperfluorodecane (I(CF$_2$)$_{10}$F, FW 648.98, 98%) was purchased from Synquest Labs and used as received. 9-decen-1-ol (H_2C=CH(CH$_2$)$_8$OH, FW 156.27, 97%), 2,2'-azobisisobutyronitrile (N≡CC(CH$_3$)$_2$N=NC(CH$_3$)$_2$C≡N, FW 164.21, 98%), and tributyltin hydride ((*n*-Bu)$_3$SnH, FW 291.06, 97%) were purchased from Sigma Aldrich and used as received in conjunction with the 1-iodoperfluorodecane to synthesize 10-perfluorodecyl-1-decanol (F10H10OH, F(CF$_2$)$_{10}$(CH$_2$)$_{10}$OH, FW 676.35).

3-*meta*-chloroperoxybenzoic acid (*m*CPBA, ClC$_6$H$_4$COOOH, FW 172.57, 77%), boron trifluoride diethyl etherate (BF$_3$•Et$_2$O, BF$_3$•O(CH$_2$CH$_3$)$_2$, FW 141.93, 99.9%), and poly(ethylene glycol) methyl ether (PEG550, CH$_3$(OCH$_2$CH$_2$)$_x$OH, average $M_n \approx 550$, $x \approx 12$) were also purchased from Sigma Aldrich and used as received in the modification of the PS-*b*-P(E/B)-*b*-PI triblock precursor polymers. Anhydrous chloroform (CHCl$_3$), anhydrous toluene, and anhydrous α,α,α-trifluorotoluene (TFT) were purchased from Sigma Aldrich and used with no further purification. Chloroform, dichloromethane (CH$_2$Cl$_2$), methanol, toluene, 6.25 N sodium hydroxide, 96% sulfuric acid, 30 wt % hydrogen peroxide in water, 95% ethanol and all other reagents were used as received.

3-(Glycidoxypropyl)-trimethoxysilane (GPS, 99%) was purchased from Gelest and used as received. Two separate polystyrene-*block*-poly(ethylene-*ran*-butylene)-

block-polystyrene (SEBS) triblock thermoplastic elastomers (Kraton G1652 and Kraton MD6945) and SEBS grafted with maleic anhydride (MA-SEBS, Kraton FG1901X) were generously provided by Kraton Polymers.

Synthesis of 10-perfluorodecyl-1-decanol (F10H10OH)

The semifluorinated alcohol, 10-perfluorodecyl-1-decanol (F10H10OH) was produced in a manner analogous to that reported in Hopken et al.[40] The reaction scheme is given in Figure 4.1. 9-decen-1-ol (14.07 g, 0.09 mol) and perfluorodecyliodide (38.76 g, 0.06 mol) were taken in a round bottom flask fitted with a condenser and septa. The reactants were purged with argon and the mixture was heated to 90° C while stirring. AIBN (300 mg) was added incrementally over a period of 45 minutes. After 5 hours, the reaction temperature was reduced to 80° C and 30 mL of anhydrous toluene was added, followed by additional AIBN (1.5 g) and tributyl tin hydride (52.38 g, 0.18 mol). The reaction mixture was stirred while heating at 80° C for 24 hours and then an additional 60 mL of anhydrous toluene was added to the reaction mixture, which was then allowed to cool to room temperature. The raw F10H10OH product crystallized out of solution as a white solid and was collected by filtration and subsequently recrystallized from hot toluene three times to remove residual starting products and tributyl tin impurities. Finally, the purified F10H10OH was dried under reduced pressure at room temperature for 48 hours.

^{1}H NMR for F10H10OH (300 MHz, $CDCl_3$, δ): 3.63 (q, 2H, HO**CH_2**CH_2-), 2.07 (m, 2H, -CH_2**CH_2**CF_2-), 1.58 (m, 2H, -CF_2CH_2**CH_2**CH_2-); 1.30 (br s, 12H, -CF_2-CH_2-CH_2-**$(CH_2)_6$**- and 1H, –**H**OCH_2-). IR (dry film) υ_{max} (cm^{-1}): 3250 (O-H stretching); 2925, 2850 (C-H stretching); 1470, 1452 (C-H bending); 1330-1095 (C-F stretching); 1055 (C-O stretch).

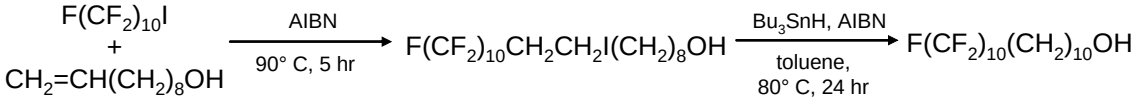

Figure 4.1. Synthesis of semifluorinated 10-perfluorodecyl-1-decanol (F10H10OH).

Polymer Synthesis and Characterization

Surface active block copolymers were produced through a straight-forward two step modification of the Kraton PS-*b*-P(E/B)-*b*-PI precursor polymers depicted in Figure 4.2, in similar fashion to that previously reported by Weinman et al.[41] Functionalization of the PI block was achieved through epoxidation of the residual alkene groups followed by subsequent catalytic ring-opening etherification reactions using alcohols carrying functionality.

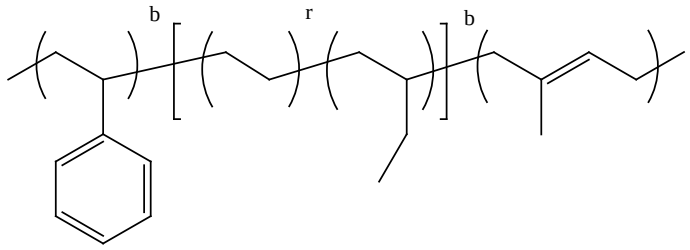

PS-*b*-P(E/B)-*b*-PI Triblock Copolymer

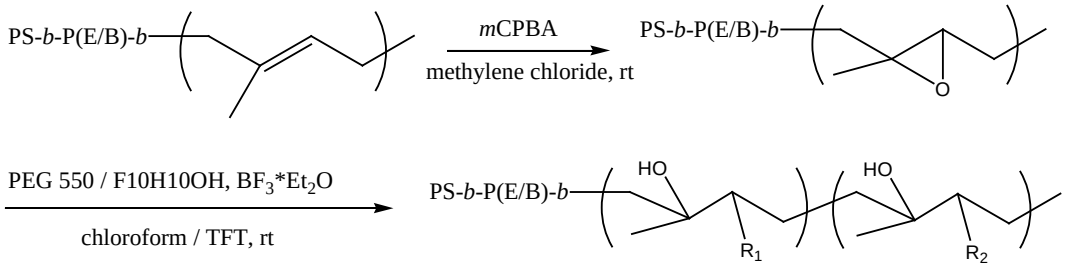

Figure 4.2. Synthesis of ether-linked surface active triblock copolymers containing PEG550 and/or F10H10 side chains; R_1 = -$O(CH_2)_{10}(CF_2)_{10}F$, R_2 = -$(OCH_2CH_2)_{12}OCH_3$.

In a typical epoxidation reaction, the PS_{8K}-*b*-$P(E/B)_{25K}$-*b*-PI_{10K} SABC precursor polymer (5 g, 14.5 mmol of reactive isoprene sites) was dissolved in 100 mL of dichloromethane in a round bottomed flask. 3-Chloroperoxybenzoic acid (*m*CPBA, 3.9 g, 17.4 mmol) was added to the mixture, and the solution was stirred vigorously for 5 hours at room temperature. Subsequently, the polymer was precipitated in methanol, collected by filtration, and reprecipitated from dichloromethane to remove residual *m*CPBA and its respective byproducts. The white, rubbery product was dried at room temperature under reduced pressure for 48 hours to remove remaining solvent. An analogous reaction and work-up was used to successfully epoxidized the PS_{8K}-*b*-$P(E/B)_{25K}$-*b*-PI_{20K} SABC precursor polymer, scaled to 25 mmol of reactive isoprene sites per 5 g of precursor polymer.

^{1}H NMR for epoxidized PS_{8K}-*b*-$P(E/B)_{25K}$-*b*-PI_{10K} (300 MHz, $CDCl_3$, δ): 6.57, 7.07, (5H, styrene), 2.66 (br s, 1H, epoxidized isoprene, -CH_2**HCOC(**CH_3)CH_2-), 0.80, 1.07, 1.22, 1.45, 1.57 (back-bone). IR (dry film) υ_{max} (cm $^{-1}$): 2925, 2850 (C-H stretching); 1470 (C-H bending); 1070 (C-O stretching); 880 (C-O-C stretching); 700 (C-H bending, aromatic).

To produce ether-linked side chain surface active block copolymers, 2.1 g of epoxidized PS_{8K}-*b*-$P(E/B)_{25K}$-*b*-PI_{10K} (5.8 mmol of epoxide) was taken in a round bottom flask in conjunction with a four times molar excess (23.2 mmol) of side-chain precursor alcohol (F10H10OH and/or PEG550). Seven different mixtures of F10H10OH relative to PEG550 were used in the feed to produce a range of different SABCs: 100% F10H10OH, 80% F10H10OH/20% PEG550, 60% F10H10OH/40% PEG550, 50% F10H10OH/50% PEG550, 40% F10H10OH/60% PEG550, 20% F10H10OH/80% PEG550 and 100% PEG550. The reactants were purged with argon, and subsequently dissolved in ca. ~ 150 mL of anhydrous chloroform. Anhydrous TFT was added as necessary to solvate the F10H10OH (indicated by the formation of a

clear solution). Activated molecular sieves were added to the reaction mixture and it was allowed to sit for ca. ~ 12 h. Etherification was performed through the addition of boron trifluoride diethyl etherate catalyst (0.345 g, 2.4 mmol) followed by vigorous stirring at room temperature for at least 48 hours. Following the reaction, 6.25 N sodium hydroxide was added to quench any residual boron catalyst and the reaction mixture was concentrated under reduced pressure using a rotary evaporator. The resultant surface active triblock copolymers were precipitated into methanol, with water added as necessary to help isolate the PEGylated samples. The SABCs were collected by filtration and subsequently reprecipitated twice from chloroform to remove additional residual surface active side-chain alcohol precursors. Finally, the finished samples were dried under reduced pressure at room temperature for 48 hours to fully remove residual solvent.

^{1}H NMR for PS_{8K}-*b*-$P(E/B)_{25K}$-*b*-PI_{10K} functionalized with PEG550 side chains (300 MHz, $CDCl_3$, δ): 6.56, 7.08, (5H, styrene), 3.63 (br s, 4H –O**CH_2CH_2**O-); 3.38 (s, 3H, -O**CH_3**); 2.24 (s, 1H, -**OH**); 0.83, 1.06, 1.24, 1.80 (back-bone). IR (dry film) υ_{max} (cm $^{-1}$): 3350 (O-H stretching); 2935, 2865 (C-H stretching); 1455, 1375 (C-H bending); 1120 (C-O stretching); 700 (C-H bending, aromatic). Elemental analysis: C (76.1 %), H (11.7 %).

^{1}H NMR for PS_{8K}-*b*-$P(E/B)_{25K}$-*b*-PI_{10K} functionalized with F10H10 side chains (300 MHz, $CDCl_3$, δ): 6.57, 7.07, (5H, styrene), 3.50 (br m, 2H –O**CH_2**CH_2-); 2.40 (br s, 2H –CH_2**CH_2**CF_2-); 0.82, 1.04, 1.24, 1.57, 2.03 (back-bone, -OCH_2**$(CH_2)_8$**CH_2CF_2). IR (dry film) υ_{max} (cm $^{-1}$): 3480 (O-H stretching); 2930, 2860 (C-H stretching); 1460, 1380 (C-H bending); 1220 (C-F stretching); 1090 (C-O stretching); 700 (C-H bending, aromatic). Elemental analysis: C (67.5%), H (9.4%), F (18.3%). Surface active block copolymers incorporating both types of side chain were

found to have a blend of peaks that correlated to the amount of incorporation of each moiety.

^{1}H NMR spectra were recorded using a Varian Gemini spectrometer with deuterated chloroform. The IR spectra of the polymers cast as films from THF solution on sodium chloride plates was collected using a Mattson 2020 Galaxy Series FTIR spectrometer. Elemental analysis for weight percent C, H, and F of the surface active block copolymers was performed by Quantitative Technologies, Inc. (QTI). Gel permeation chromatography of a THF solution of polymers (1 mg/mL) was carried out using four Waters Styragel HT columns operating at 40 °C in conjunction with Waters 490 ultraviolet (λ = 254 nm) and Waters 410 refractive index detectors. The molecular weight range of the columns was from 500 to 10^7 g/mol. THF was used as the eluent at a flow rate of 1 mL/min, and toluene was used as a marker for flow calibration.

Surface Preparation and Characterization

Surfaces for NEXAFS measurements, XPS, and dynamic water contact angle analysis were prepared on silicon wafers by spin-coating 3% (w/v) solutions of SABCs in TFT at 2000 rpm for 60 seconds. All surfaces prepared for study were annealed in a vacuum oven at reduced pressure at 120 °C for at least 12 h followed by slow cooling to room temperature.

XPS measurements were performed using a Kratos Axis Ultra Spectrometer (Kratos Analytical, Manchester, UK) with a monochromatic Al Kα X-ray source (1486.6 eV) operating at 225 W under a vacuum of 1.0 × 10-8 Torr. Charge compensation was carried out by injection of low-energy electrons into the magnetic lens of the electron spectrometer. The pass energy of the analyzer was set at 40 eV for high-resolution spectra and 80 eV for survey scans, with energy resolutions of 0.05 and 1 eV, respectively. The spectra were analyzed using CasaXPS v.2.3.12Dev4

software. The C-C peak at 285 eV was used as the reference for binding energy calibration.

NEXAFS experiments were carried out on the U7A NIST/Dow materials characterization end-station at the National Synchrotron Light Source at Brookhaven National Laboratory (BNL). The general underlying principles of NEXAFS and a description of the beam line at BNL have been previously reported.[42, 43] The X-ray beam was elliptically polarized (polarization factor = 0.85), with the electric field vector dominantly in the plane of the storage ring. The photon flux was about $1x10^{11}$ photons per second at a typical storage ring current of 500 mA. A spherical grating monochromator was used to obtain monochromatic soft X-rays at an energy resolution of 0.2 eV. The C 1s NEXAFS spectra were acquired for incident photon energy in the range 270–320 eV. The angle of incidence of the X-ray beam, measured from the sample surface, was 50°. The partial-electron-yield (PEY) signal was collected using a channeltron electron multiplier with an adjustable entrance grid bias (EGB). Data was reported for a grid bias of -150 V. The channeltron PEY detector was positioned in the equatorial plane of the sample chamber and at an angle of 36° relative to the incoming X-ray beam. The PEY C 1s spectra were normalized by subtracting a linear pre-edge baseline and setting the edge jump to unity at 320 eV.[44] The photon energy was calibrated by adjusting the peak position of the lowest π^* phenyl resonance from polystyrene to 285.5 eV.[45]

Water contact angles were measured using a contact angle goniometer (AST Products, Inc. model VCA Optima XE) at room temperature. Dynamic water contact angle measurements were performed through the addition and retraction of a small drop of water (ca. ~ 2 μL) on the surface. The advancing and receding contact angle behavior was digitally recorded and image analysis software was used to measure the angles.

Preparation of Surfaces for Biofouling Assays

Glass slides for biofouling assays with the green alga *Ulva* and *Navicula* diatoms were prepared as previously reported for SABCs based on the PS_{8K}-*b*-$P(E/B)_{25K}$-*b*-PI_{20K} precursor using Kraton G1652 SEBS as a thermoplastic elastomer base layer when forming the multilayer coating.[6] Glass slides coated with SABCs based on the PS_{8K}-*b*-$P(E/B)_{25K}$-*b*-PI_{10K} precursor for biofouling assays meanwhile were prepared in an analogous fashion using the newly released Kraton MD6945 SEBS in place of G1652. The rationale behind this change midstream was that the elastic modulus of MD6945 is very similar to that of PDMS, known to possess its excellent fouling release properties as a combination of both surface energy and its low modulus.[46-49] The elastic modulus of G1652 meanwhile is still roughly an order of magnitude greater than that of PDMS. For all biofouling assays, glass microscope slides coated with a polydimethylsiloxane elastomer (PDMS), Silastic® T2 (Dow Corning) prepared as described by Schumacher et al.[50] and either G1652 or MD6945 SEBS were used as standards. PDMS was used as a control due to excellent release properties against macrofouling organisms such as *Ulva* sporelings, while the G1652 or MD6945 base layers were used to highlight the differences in performance between the base layer when used alone and in the multilayer coatings.

Settlement and Strength of Attachment of *Ulva* Zoospores and Strength of Attachment of *Ulva* Sporelings (Young Plants)

Twelve replicate test samples (9 for SABCs based on the PS_{8K}-*b*-$P(E/B)_{25K}$-*b*-PI_{20K} precursor) were leached in a 30 L tank of recirculating deionized water at ~ 20° C for a minimum of 24 hours. The slides were equilibrated in artificial seawater 1 h

prior to the start of the experiments. Zoospores were released from fertile plants of *Ulva linza* and prepared for assay as described previously.[51] Ten mL of zoospore suspension (1×10^6 spores per mL), was pipetted into the compartments of Quadriperm polystyrene culture dishes (Greiner Bio-One), each containing a test slide. The test slides were incubated in the dark at ~ 20° C for 1 h and gently washed in seawater to remove zoospores that had not settled. Three replicate slides of each type were fixed using 2.5% glutaraldehyde in seawater and were used to quantify the density of zoospores attached to the surfaces as previously reported.[52]

Three slides, coated with the SABCs based on the PS_{8K}-*b*-$P(E/B)_{25K}$-*b*-PI_{10K} precursor, were settled with zoospores for 1 hour by the above method and exposed to a shear stress of 53 Pa created by the turbulent flow of seawater in a specially designed water channel. Following this, slides were fixed in glutaraldehyde as described above. The number of spores remaining attached was compared with unexposed control slides (the same as used to determine settlement).

Ulva sporelings (young plants) were cultured on 6 replicates of each coating.[53] Spores were settled on the coatings by the method described above. After washing, the samples were transferred to dishes containing nutrient enriched seawater and grown for 7 days with the culture medium being refreshed every 48 hours, under an18h:6h light:dark regime at 18^{o}C. Growth was estimated by direct measurement of fluorescence from chlorophyll contained within the chloroplasts of the sporelings using a Tecan plate reader (GENios Plus)[54] and recorded as Relative Fluorescence Units (RFU). The slides (6 replicates) were read from the top, 300 readings per slide, taken in blocks of 30×10. The strength of attachment of the sporelings was determined by washing using a water jet.[55] The range of impact pressures used was chosen to provide maximum information on the strength of attachment of the sporelings. RFU readings (80 per slide) were taken from the central part of the slide that was exposed

to the water jet. Percentage removal was calculated from the mean RFU reading before and after exposure to the water jet. From the percentage removal data, the critical water pressure required to remove 50% of the sporelings was derived.

Settlement and Strength of Attachment of *Navicula* Diatoms

Navicula cells were cultured in F/2 medium contained in 250 ml conical flasks. After 3 days the cells were in log phase growth. Cells were washed 3 times in fresh medium before harvesting and diluted to give a suspension with a chlorophyll *a* content of approximately 0.25 μg ml^{-1}. Cells were settled in individual dishes containing 10 mL of suspension at ~20° C on the laboratory bench. After 2 h the slides were gently washed in seawater to remove cells that had not properly attached (submerged wash). Slides were fixed using 2.5% glutaraldehyde in seawater. The density of cells attached to the surface was counted on each slide using an image analysis system attached to a fluorescence microscope. Counts were made for 30 fields of view (each 0.064 mm^2) on each slide.

Slides settled with *Navicula* were exposed to a shear stress of 23 Pa in a water channel. The number of cells remaining attached was counted using the image analysis system described above.

Results and Discussion:

Polymer Synthesis and Characterization

The synthesis of these two series of amphiphilic SABCs containing mixed discrete hydrophobic semifluorinated side-chains and hydrophilic PEGylated side chains was closely followed using both infrared spectroscopy and ^{1}H NMR. Following the epoxidation reaction, ^{1}H NMR studies clearly showed that there was no longer evidence of any alkene protons, and a significant peak at ca. ~ 2.7 ppm appeared

indicating the presence of protons adjacent to the newly formed oxirane rings on the PI backbone. Additionally, infrared spectroscopy clearly showed the appearance of a C-O-C stretching peak at roughly 880 cm^{-1} associated with the epoxide ring. This indicated that all of the residual unsaturated alkene groups were successfully converted to their epoxidized form. Subsequent catalytic ring-opening using F10H10OH and/or PEG550 alcohols led to the disappearance of the epoxide peak in the ^{1}H NMR spectra. Further analysis of the ^{1}H NMR spectra demonstrated the appearance of peaks at ca. ~ 3.3 and 3.6 ppm for the PEG550 functionalized sample in conjunction with the appearance of a peak at ca. ~ 3.5 ppm for the F10H10OH functionalized sample demonstrated successful attachment of the side groups. These findings were supported by infrared spectroscopy which demonstrated the appearance of a strong C-O stretching peak at 1120 cm^{-1} for samples functionalized with PEG550 and a strong C-F stretching peak at 1200 cm^{-1} for samples functionalized with F10H10OH. For mixed samples functionalized with both moieties, peak intensity generally varied with the amount of incorporation of the side chain.

Table 1 demonstrates the percentage of attachment of PEG550 and F10H10OH for each different molar feed ratio for both PS-*b*-P(E/B)-*b*-PI precursors. The percentage of PEG550 and F10H10OH successfully attached was calculated by ^{1}H NMR integration and elemental analysis of fluorine, respectively. Specifically, the percent attachment of PEG550 was obtained by comparing the total amount of aromatic protons (associated with the PS block) in the ^{1}H NMR spectra with the number of protons associated with the PEG side chain. Meanwhile, the weight percent of fluorine obtained by elemental analysis allowed the determination of F10H10OH attachment by comparing this value to that which would have been obtained assuming 100% attachment. The attachment of both PEG550 and F10H10OH generally depended on the molar ratios in the feed, and the overall attachment relative to

epoxidized isoprene was generally between 22 to 30 % for the PS_{8K}-*b*-$P(E/B)_{25K}$-*b*-PI_{20K} precursor and between 33 and 54% for the PS_{8K}-*b*-$P(E/B)_{25K}$-*b*-PI_{10K} precursor. Using GPC, the polydispersity of the samples was found to increase from 1.06 for both of the PS-*b*-P(E/B)-*b*-PI precursors to ca. ~ 1.12 for their epoxidized forms. Finished, substituted SABC samples containing F10H10 and/or PEG550 side chains generally had a polydispersity between 1.2 and 1.3. This rise in polydispersity combined with the observation of complete reaction of the epoxide despite less than 100% attachment suggested that some of the epoxide was most likely lost to intermolecular cross linking reactions. Additionally, intramolecular reactions in combination with epoxide ring-opening by any residual water molecules left in the reaction mixture may have contributed to this lowered observed attachment.

Table 4.1. The percentage of attachment of PEG550 and F10H10OH and fluorine content for both series of SABCs produced from different molar ratios of F10H10OH and PEG550 in the reaction feed.

PS_{8K}-*b*-$P(E/B)_{25K}$-*b*-PI_{20K} Precursor

Feed % F10H10	Feed % PEG550	Attach % F10H10	Attach % PEG550	Overall Attachment	Weight % F	Nomenclature
20	80	3	28	31	2.7	PS_{8K}-b-$P(E/B)_{25K}$-b-PI_{20K}-3F-28P
40	60	5	18	23	7.2	PS_{8K}-b-$P(E/B)_{25K}$-b-PI_{20K}-5F-18P
60	40	9	13	22	11.1	PS_{8K}-b-$P(E/B)_{25K}$-b-PI_{20K}-9F-13P
80	20	17	7	24	18.4	PS_{8K}-b-$P(E/B)_{25K}$-b-PI_{20K}-17F-7P

PS_{8K}-*b*-$P(E/B)_{25K}$-*b*-PI_{10K} Precursor

Feed % F10H10	Feed % PEG550	Attach % F10H10	Attach % PEG550	Overall Attachment	Weight % F	Nomenclature
0	100	0	33	33	0	PS_{8K}-b-$P(E/B)_{25K}$-b-PI_{10K}-0F-33P
20	80	22	27	49	8.4	PS_{8K}-b-$P(E/B)_{25K}$-b-PI_{10K}-22F-27P
40	60	19	28	47	6.9	PS_{8K}-b-$P(E/B)_{25K}$-b-PI_{10K}-19F-28P
50	50	24	24	48	9.2	PS_{8K}-b-$P(E/B)_{25K}$-b-PI_{10K}-24F-24P
60	40	28	19	47	10.4	PS_{8K}-b-$P(E/B)_{25K}$-b-PI_{10K}-28F-19P
80	20	41	13	54	15.2	PS_{8K}-b-$P(E/B)_{25K}$-b-PI_{10K}-41F-13P
100	0	50	0	50	18.3	PS_{8K}-b-$P(E/B)_{25K}$-b-PI_{10K}-50F-0P

Dynamic Water Contact Angles

For the samples derived from the PS_{8K}-*b*-$P(E/B)_{25K}$-*b*-PI_{20K} precursor polymer, advancing and receding water contact angles seemed largely dependent on the amount of hydrophobic F10H10 and hydrophilic PEG550 side chains that were incorporated in the SABC. As the amount of PEG550 incorporated in the coating increased in conjunction with a decrease in the amount of F10H10, water contact angles decreased from 128° to 103° (advancing) and from 67° to 28° (receding), suggesting that the presence of the surface active groups was greatly influencing wettability. The samples derived from the PS_{8K}-*b*-$P(E/B)_{25K}$-*b*-PI_{10K} precursor polymer did not show quite as clear a trend however, with all the coatings except for PS_{8K}-b-$P(E/B)_{25K}$-b-PI_{10K}-0F-33P showing an advancing water contact angle on the order of ca. ~ 125°. Receding angles did show a slight trend however, varying from 21° for PS_{8K}-b-$P(E/B)_{25K}$-b-PI_{10K}-0F-33P to 42° for PS_{8K}-b-$P(E/B)_{25K}$-b-PI_{10K}-50F-0P. High water contact angle hysteresis was demonstrated for both sets of SABCs, suggesting a dynamic surface capable of significant reorganization was realized in all cases. Contact angle hysteresis was generally a bit more pronounced for polymers derived from the PS_{8K}-b-$P(E/B)_{25K}$-b-PI_{10K} precursor however. These observed differences in wettability behavior between each set of SABCs can most likely be attributed to the combination of higher attachment and significantly higher side chain grafting density realized for the PS_{8K}-b-$P(E/B)_{25K}$-b-PI_{10K} derived samples.

Table 4.2. Advancing and receding dynamic water contact angle measurements for both sets of SABCs produced through the incorporation of different amounts of the F10H10 and PEG550 side chains.

PS_{8K}-*b*-$P(E/B)_{25K}$-*b*-PI_{20K} Precursor

Sample	Θw,a	Θw,r
PS_{8K}-b-$P(E/B)_{25K}$-b-PI_{20K}-3F-28P	103 ± 5	28 ± 3
PS_{8K}-b-$P(E/B)_{25K}$-b-PI_{20K}-5F-18P	118 ± 4	48 ± 3
PS_{8K}-b-$P(E/B)_{25K}$-b-PI_{20K}-9F-13P	124 ± 2	54 ± 2
PS_{8K}-b-$P(E/B)_{25K}$-b-PI_{20K}-17F-7P	128 ± 4	67 ± 4

PS_{8K}-*b*-$P(E/B)_{25K}$-*b*-PI_{10K} Precursor

Sample	Θw,a	Θw,r
PS_{8K}-b-$P(E/B)_{25K}$-b-PI_{10K}-0F-33P	104 ± 3	21 ± 4
PS_{8K}-b-$P(E/B)_{25K}$-b-PI_{10K}-22F-27P	125 ± 3	25 ± 3
PS_{8K}-b-$P(E/B)_{25K}$-b-PI_{10K}-19F-28P	128 ± 3	26 ± 4
PS_{8K}-b-$P(E/B)_{25K}$-b-PI_{10K}-24F-24P	128 ± 3	27 ± 4
PS_{8K}-b-$P(E/B)_{25K}$-b-PI_{10K}-28F-19P	127 ± 3	28 ± 3
PS_{8K}-b-$P(E/B)_{25K}$-b-PI_{10K}-41F-13P	127 ± 2	31 ± 2
PS_{8K}-b-$P(E/B)_{25K}$-b-PI_{10K}-50F-0P	126 ± 2	42 ± 4

X-Ray Photoelectron Spectroscopy (XPS)

Figure 4.3 shows high-resolution C 1s XPS spectra of amphiphilic SABCs derived from the PS_{8K}-*b*-$P(E/B)_{25K}$-*b*-PI_{10K} precursor with different attachment percents of PEG550 and F10H10. The percent attachment of F10H10 (F) and PEG550 (P) relative to epoxidized isoprene in the precursor is given in the legend. The spectra are normalized so that the total area under the carbon peaks is equal to unity. All polymers showed strong intensity peaks from C=C and C-C near 285 eV, most likely indicative of the block copolymer backbone. There was clear evidence for all but the PS_{8K}-*b*-$P(E/B)_{25K}$-*b*-PI_{10K}-0F-33P sample of peaks associated with -CF_2- and -CF_3 near 292 and 294 eV, respectively. As expected, the intensities of both -CF_2- and -CF_3 decreased with increasing attachment of PEG550 and decreasing attachment of F10H10 in the mixture. A pronounced shoulder at ca. ~ 287 eV associated with C-O

was present in many of the samples, which can be attributed to both the ether-linked groups of the PEG550 moiety and also the alcohol functionality resulting on the polyisoprene block after ring opening of the oxirane group.

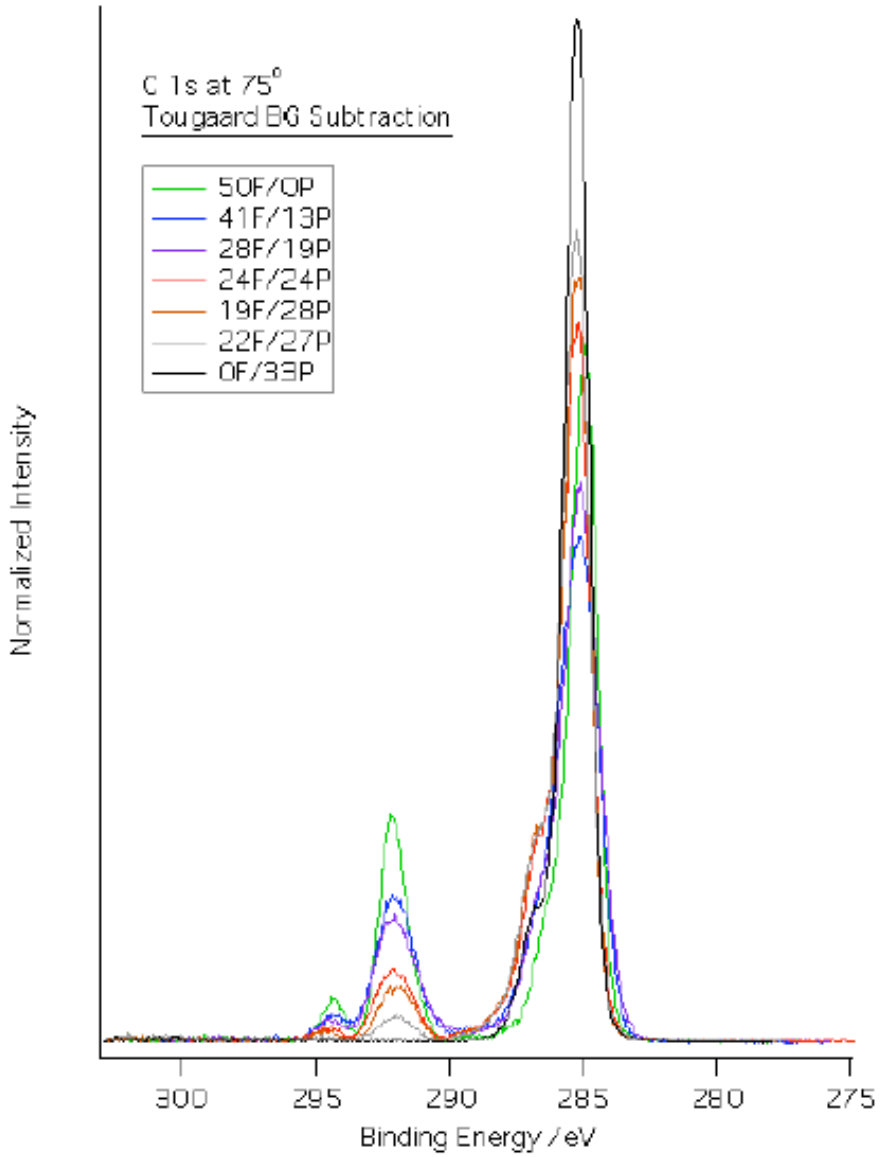

Figure 4.3. XPS C 1s spectra of the surfaces of amphiphilic SABCs containing mixed hydrophobic F10H10 and hydrophilic PEG550 side chains derived from the PS_{8K}-*b*-$P(E/B)_{25K}$-*b*-PI_{10K} precursor polymer taken at a 75° incident angle processed using Tougaard background subtraction. Sample labels give amounts of PEG550 (P) and F10H10 (F) side chains incorporated relative to epoxy functionality in the precursor polymer.

Near-Edge X-Ray Adsorption Fine Structure (NEXAFS) Analysis

Figure 4.4 depicts the normalized C 1s NEXAFS spectra of spin-coated surfaces of amphiphilic SABCs derived from the PS_{8K}-*b*-$P(E/B)_{25K}$-*b*-PI_{10K} precursor with different amounts of PEG550 and F10H10 side chains attached taken at an angle of 50˚ between the surface and the soft X-ray beam. The characteristic C 1s $\rightarrow \pi^*_{C=C}$ signals derived from the polystyrene block were observed near 285.5 eV for all seven of the spectra,[43] but the intensity of this peak was very low because the SABC surfaces were dominated by the PEG550 and F10H10 side chains. Other peak assignments can be based on calibrated NEXAFS spectra of poly(ethylene oxide) and poly(methyl methacrylate) as discussed in Krishnan et al.[38] The sharp resonance peak near 288 eV can be attributed to the C 1s $\rightarrow\sigma^*_{C-H}$ signal. This peak was particularly prevalent for the PS_{8K}-b-$P(E/B)_{25K}$-b-PI_{10K}-0F-33P sample, likely due to the absence of fluorinated moieties, indicating a surface dominated by the low surface energy poly(ethylene-*ran*-butylene) block, with possible contributions from the PEGylated moieties. The characteristic signals near 293 eV and 295.8 eV can be easily seen for the other six samples, and they are indicative of both the C 1s $\rightarrow\sigma^*_{C-F}$ and C 1s $\rightarrow\sigma^*_{C-O}$ resonances, demonstrating the presence of the semifluorinated groups on the surfaces with possible contributions from the PEG containing side chains. The intensity profiles of C 1s $\rightarrow\sigma^*_{C-F}$ signal were quite similar to the ones in XPS spectra which decreased with increasing incorporation of PEG550 and decreasing incorporation of F10H10OH in the mixture.

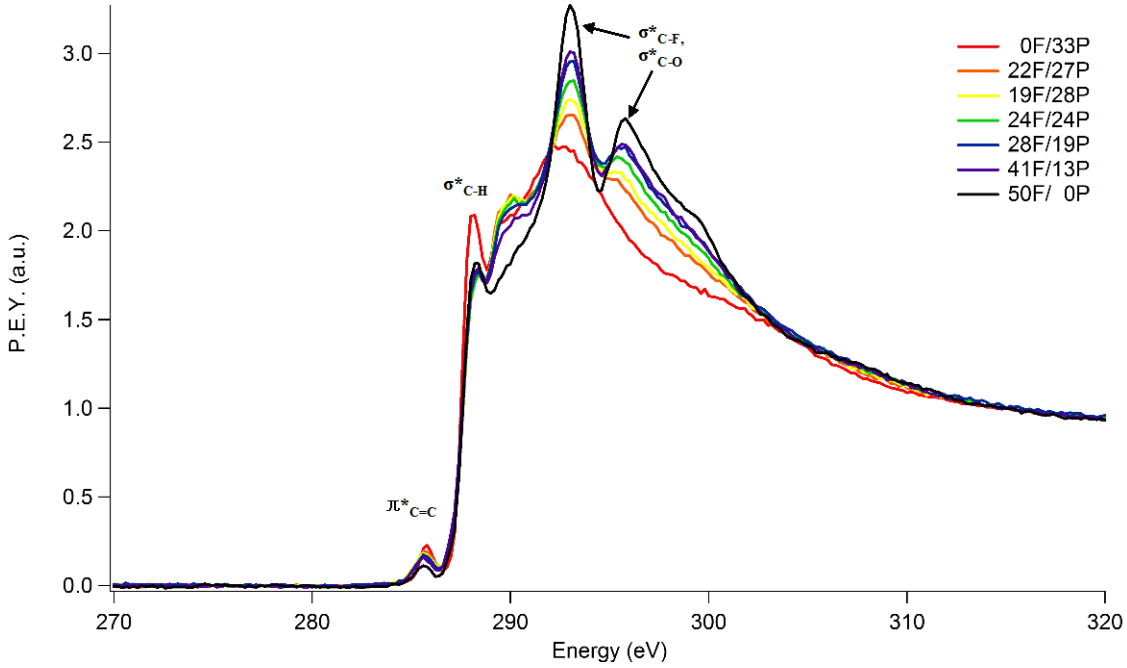

Figure 4.4. NEXAFS spectra of spin-coated surfaces of PS_{8K}-b-$P(E/B)_{25K}$-b-PI_{10K} derived SABCs on a silicon wafer after annealing at 120 °C for 12 hr at an angle of 50˚ between the surface and the soft X-ray beam with major resonance transition peaks labeled.

Settlement and Removal of *Ulva* Spores and Removal of *Ulva* Sporelings

Figure 4.5A shows the settlement density of *Ulva* spores on PDMS, G1652 SEBS and amphiphilic SABCs derived from the PS_{8K}-b-$P(E/B)_{25K}$-b-PI_{20K} precursor. For the experimental coatings, the lowest settlement was shown on the surface with 3% attachment of F10H10 and 28% attachment of PEG550. This was generally consistent with behavior reported in literature for spores preferring to settle on a hydrophobic surface.[24] The low settlement density on the hydrophobic PDMS control was surprising however. Meanwhile, the growth of *Ulva* sporelings, depicted in Figure 4.5B, largely reflected the number of spores settled, confirming no unexpected toxicity from the experimental coatings. The percentage removal of *Ulva* sporelings from the experimental coatings at a range of applied water jet pressures is shown in Figure 4.5C.

Sporelings were removed from the PDMS standard at low water jet pressures reflecting the fouling-release characteristics of this low surface energy elastomer.[28, 54] The applied water jet pressure required to remove *Ulva* sporelings from the amphiphilic SABCs surfaces derived from the PS_{8K}-b-$P(E/B)_{25K}$-b-PI_{20K} precursor largely depended on the incorporation of PEG550 and F10H10 side-chains. The surface with 3 % attachment of F10H10 and 28% attachment of PEG550, which demonstrated the lowest spore settlement, required the highest applied water jet pressure of the four surfaces. It was notable that the surfaces derived from the PS_{8K}-b-$P(E/B)_{25K}$-b-PI_{20K}-5F-18P and PS_{8K}-b-$P(E/B)_{25K}$-b-PI_{20K}-9F-13P SABCs required lower impact pressure than PDMS for effective *Ulva* sporeling release. This was especially true for the surface of PS_{8K}-b-$P(E/B)_{25K}$-b-PI_{20K}-5F-18P, for which ca. ~ 95% sporelings were removed from the surface with an applied water jet pressure of only 24kPa reflecting the excellent fouling-release properties of this polymer.

The set of SABCs derived from the PS_{8K}-*b*-$P(E/B)_{25K}$-*b*-PI_{10K} polymer were also evaluated for *Ulva* spore settlement, and *Ulva* sporeling growth and release to see if additional information regarding the fouling-release performance of these materials could be ascertained. Since this sample set was produced at a later date than that derived from the PS_{8K}-*b*-$P(E/B)_{25K}$-*b*-PI_{20K} polymer, we hoped that the inclusion of purely PEGylated and purely fluorinated SABCs in conjunction with the more symmetric attachment distribution of side chains would aid in optimization of this approach.

Figure 4.5. A) The settlement of *Ulva* spores on G1652 SEBS, PDMS and PS_{8K}-*b*-$P(E/B)_{25K}$-*b*-PI_{20K} derived amphiphilic SABCs. Each point is the mean from 90 counts on 3 replicate slides. Bars show 95% confidence limits. B) The growth of *Ulva* sporelings on G1652 SEBS, PDMS and PS_{8K}-*b*-$P(E/B)_{25K}$-*b*-PI_{20K} derived amphiphilic SABCs. Each point is the mean biomass from 6 replicate slides measured using a fluorescence plate reader. Bars show standard error of the mean. C) The removal of *Ulva* sporelings from G1652 SEBS, PDMS and PS_{8K}-*b*-$P(E/B)_{25K}$-*b*-PI_{20K} derived amphiphilic SABCs. Slides were exposed to a water jet over a range of pressures. One slide was used for each pressure.

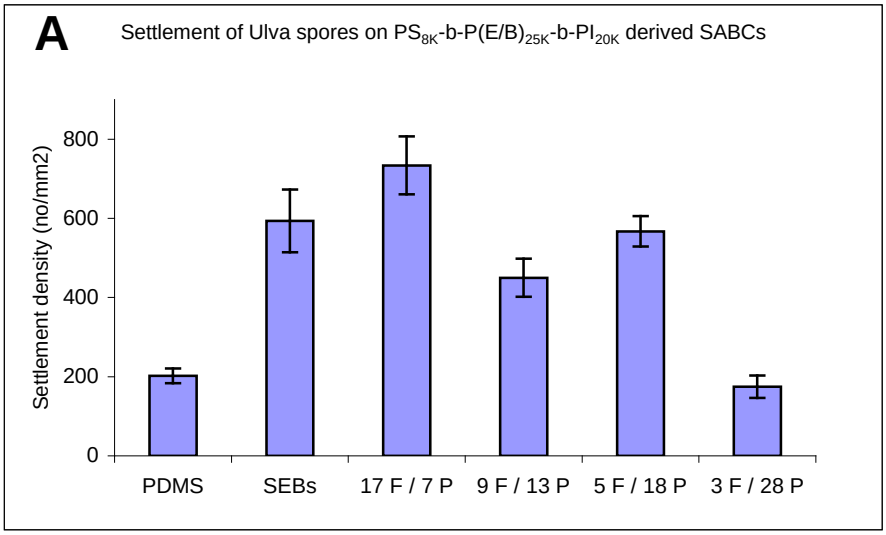
A
Settlement of Ulva spores on PS8K-b-P(E/B)25K-b-PI20K derived SABCs
Settlement density (no/mm2)
800
600
400
200
0
PDMS
SEBs
17 F / 7 P
9 F / 13 P
5 F / 18 P
3 F / 28 P

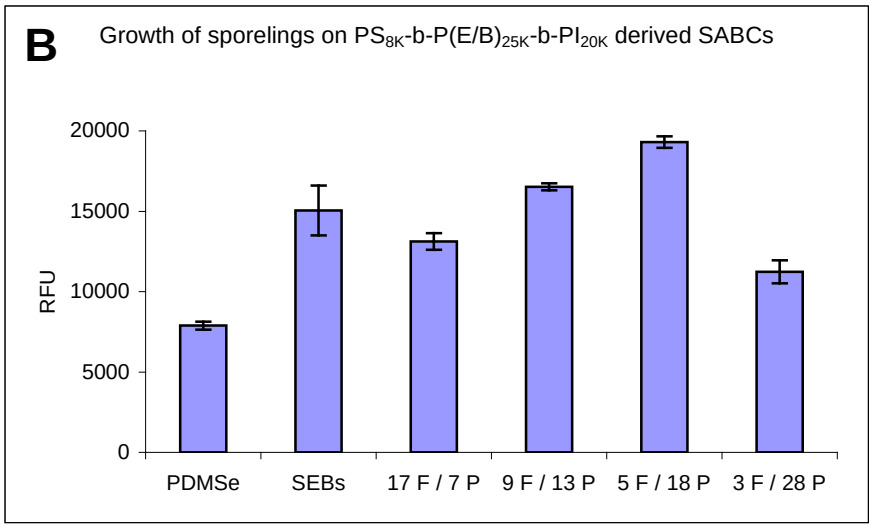
B
Growth of sporelings on PS8K-b-P(E/B)25K-b-PI20K derived SABCs
RFU
20000
15000
10000
5000
0
PDMSe
SEBs
17 F / 7 P
9 F / 13 P
5 F / 18 P
3 F / 28 P

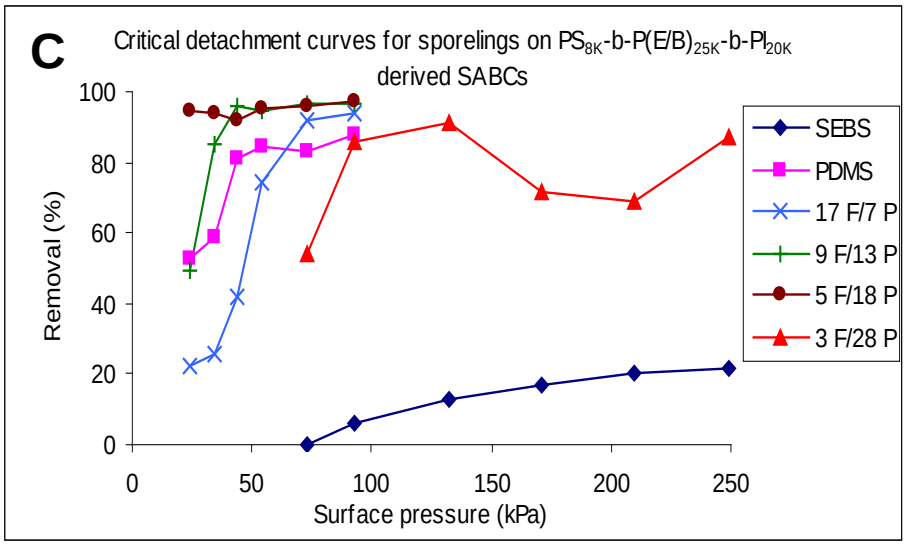
C
Critical detachment curves for sporelings on PS8K-b-P(E/B)25K-b-PI20K derived SABCs
Removal (%)
100
80
60
40
20
0
0
50
100
150
200
250
Surface pressure (kPa)
SEBS
PDMS
17 F/7 P
9 F/13 P
5 F/18 P
3 F/28 P

Figure 4.6A shows the settlement density of *Ulva* spores on PDMS, MD6945 SEBS and SABCs derived from the PS_{8K}-b-$P(E/B)_{25K}$-b-PI_{10K} precursor. Trends were generally as expected and correlated very closely with the PS_{8K}-b-$P(E/B)_{25K}$-b-PI_{20K} derived samples, with those samples containing the largest proportion of the PEG550 side chain showing the lowest settlement. As expected in this case, the hydrophobic PDMS control showed a high amount of settlement. The removal of *Ulva* spores for the PS_{8K}-b-$P(E/B)_{25K}$-b-PI_{10K} derived samples (Figure 4.6B) showed an interesting trend similar to that for *Ulva* sporeling release from the PS_{8K}-b-$P(E/B)_{25K}$-b-PI_{20K} derived samples with some optimal mixture of hydrophilic PEG550 and hydrophobic F10H10 side chains appearing to give exceptional release. In this case, the polymer with 19% attachment of F10H10 side chains and 28% attachment of PEG550 side chains show ca. ~ 51% removal of *Ulva* spores, better than the ca. ~ 42% removal demonstrated by the PDMS control. A very similar polymer in this test with regards to bulk and surface characterization (derived from 22% attachment of F10H10 side chains and 27% attachment of PEG550 side chains) only demonstrated ca. ~ 27% removal of *Ulva* spores however. This suggests that the optimal "mixture" of side chains for *Ulva* spore release may still benefit from further optimization. Again, the growth of *Ulva* sporelings (Figure 4.7A) was generally consistent with the settlement density of spores, suggesting no inherent coating toxicity. Figure 4.7B depicts the results of sporeling removal tests using a range of water jet pressures. Whilst the lower boundary for relative incorporation of PEG550 to F10H10 side chains was not as well pronounced as was seen for the PS_{8K}-b-$P(E/B)_{25K}$-b-PI_{20K} derived coatings, both of the samples incorporating slightly more PEGylated than fluorinated side chains, along with the purely PEGylated sample, showed extremely promising fouling-release characteristics. When taken with the previous experiment, in conjunction with the spore release data, the sample incorporating 19% F10H10 and 28% PEG550 side

chains appears to be particularly promising with regards to *Ulva* spore settlement and release, and growth and release of sporelings. These results also suggest that a further iteration of testing focusing on samples incorporating slightly more of the PEGylated moiety than the fluorinated component could lead to further optimization of the system.

Table 4.3 summarizes the estimated critical pressure to release 50% of the attached *Ulva* sporelings for both sets of coatings. The combination of the PS_{8K}-b-$P(E/B)_{25K}$-b-PI_{10K} derived SABCs with the MD6945 thermoplastic elastomer base layer led to a wide range of coatings that performed similarly, or better than, the PDMS control. This further suggests that a wide range of sample chemistries can be explored with regards to antifouling and fouling-release performance relative to other marine organisms while retaining robust performance against the green alga *Ulva*.

Table 4.3. Critical surface pressures for 50% removal of *Ulva* sporeling biofilm derived from *Ulva* sporeling removal curves in figure 4.5C and 4.6B.

PS_{8K}-b-$P(E/B)_{25K}$-b-PI_{20K} Precursor	
Sample	Est. Surface Pressure for 50% Removal (kPa)
PS_{8K}-b-$P(E/B)_{25K}$-b-PI_{20K}-3F-28P	70
PS_{8K}-b-$P(E/B)_{25K}$-b-PI_{20K}-5F-18P	<25
PS_{8K}-b-$P(E/B)_{25K}$-b-PI_{20K}-9F-13P	25
PS_{8K}-b-$P(E/B)_{25K}$-b-PI_{20K}-17F-7P	45
PDMSe	25
G1652M SEBS	>250
PS_{8K}-b-$P(E/B)_{25K}$-b-PI_{10K} Precursor	
Sample	Est. Surface Pressure for 50% Removal (kPa)
PS_{8K}-b-$P(E/B)_{25K}$-b-PI_{10K}-0F-33P	<21
PS_{8K}-b-$P(E/B)_{25K}$-b-PI_{10K}-22F-27P	<21
PS_{8K}-b-$P(E/B)_{25K}$-b-PI_{10K}-19F-28P	<21
PS_{8K}-b-$P(E/B)_{25K}$-b-PI_{10K}-24F-24P	29
PS_{8K}-b-$P(E/B)_{25K}$-b-PI_{10K}-28F-19P	31
PS_{8K}-b-$P(E/B)_{25K}$-b-PI_{10K}-41F-13P	165
PS_{8K}-b-$P(E/B)_{25K}$-b-PI_{10K}-50F-0P	250
PDMSe	31
MD 6945 SEBS	>288

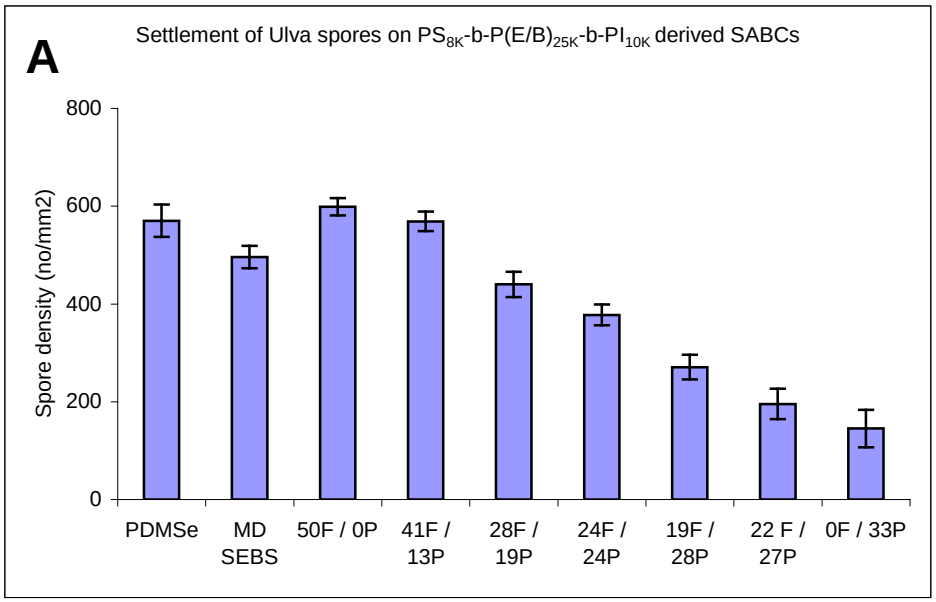

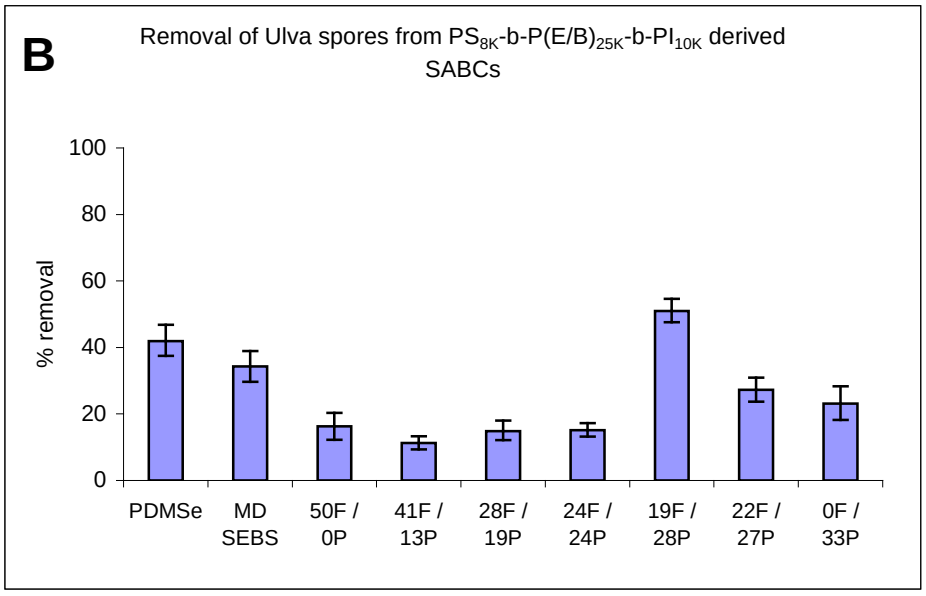

Figure 4.6. A) The settlement densities of *Ulva* spores on PS_{8K}-*b*-$P(E/B)_{25K}$-*b*-PI_{10K} derived SABCs. B) The removal of *Ulva* spores from PS_{8K}-*b*-$P(E/B)_{25K}$-*b*-PI_{10K} derived SABCs coatings. Each point is the mean from 90 counts on 3 replicate slides. Bars show 95% confidence limits.

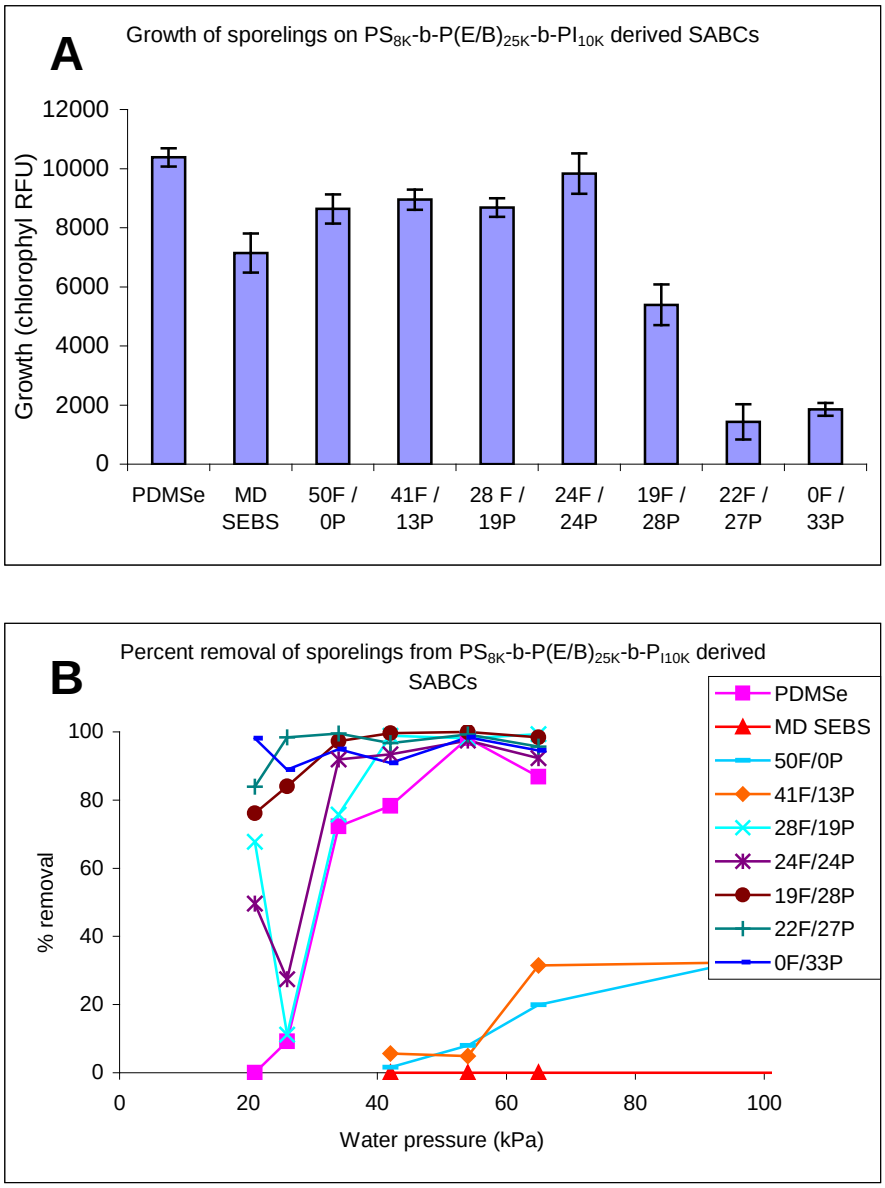

Figure 4.7. A) The growth of *Ulva* sporelings on PS_{8K}-*b*-$P(E/B)_{25K}$-*b*-PI_{10K} derived SABCs after 7 days. Each point is the mean biomass from 6 replicate slides measured using a fluorescence plate reader (RFU; relative fluorescence unit). Bars show standard error of the mean. B) Detachment of *Ulva* sporelings from PS_{8K}-*b*-$P(E/B)_{25K}$-*b*-PI_{10K} derived SABCs. Coated slides were exposed to the water jet over a range of water pressures. One slide was used at each pressure.

Settlement and Removal of *Navicula* Diatoms

The settlement and release behavior of *Navicula* diatoms on PDMS, G1652M SEBS and amphiphilic SABCs derived from PS_{8K}-*b*-$P(E/B)_{25K}$-*b*-PI_{20K} was different from that observed for *Ulva*. As a consequence of the passive nature by which the non-motile cells of *Navicula* settle under gravity (*Navicula* cells are not able to explore the surface in the same way that *Ulva* spores can), the settlement densities varied little between the surfaces (Figure 4.7A),. The detachment of *Navicula* in the water channel, depicted in Figure 4.7B, was dependent on the relative incorporation of PEG550 to F10H10 in the polymer. The removal steadily increased with increasing incorporation of F10H10 side-chains. The surface with 17% attachment of F10H10 and 7% attachment of PEG550 showed the highest removal of *Navicula* diatoms (ca. ~ 52%) among the experimental surfaces, higher than that for the PDMS control (ca. ~ 41%). This trend of increasing removal of *Navicula* cells with increasing incorporation of hydrophobic chemical moieties runs counter to the usual observations, which generally show increasing attachment strength with increasing hydrophobicity.[28] This suggests the ability of the coating surface to readily reorganize in an aqueous environment.

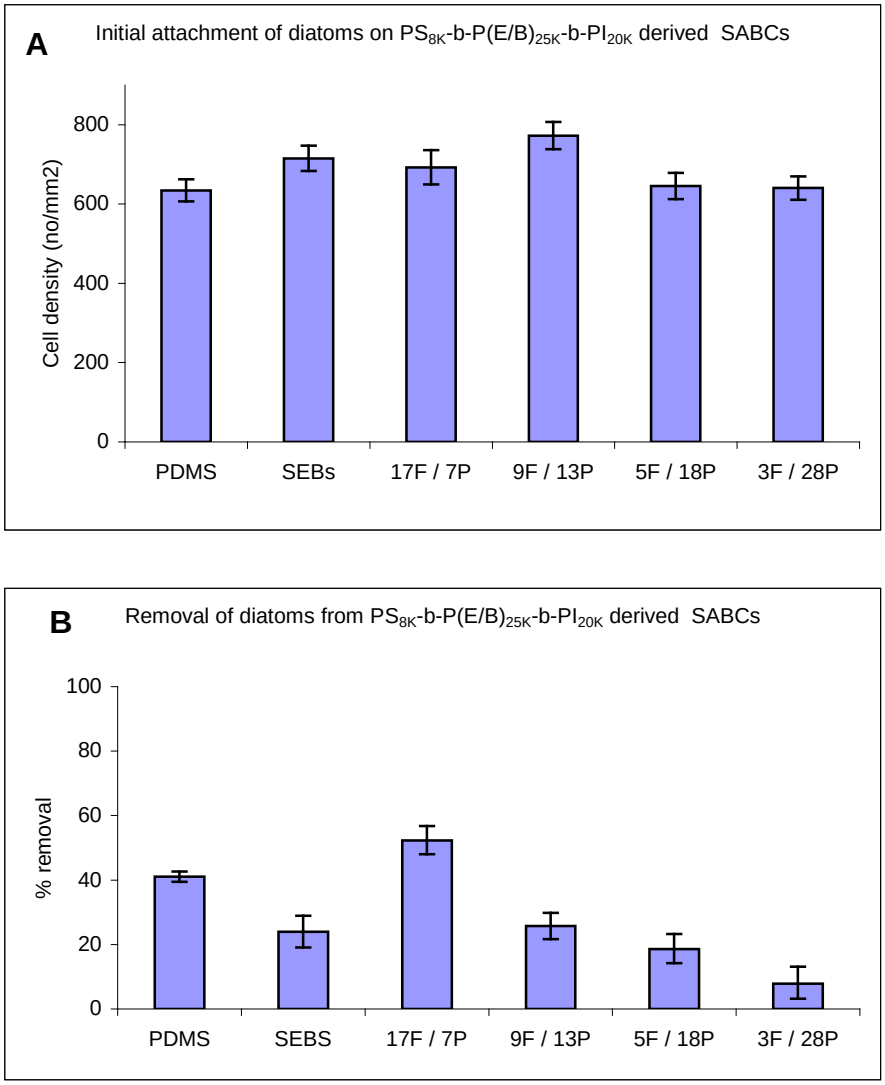

Figure 4.7. A) Initial attachment after gentle washing of *Navicula* diatoms to PS_{8K}-*b*-$P(E/B)_{25K}$-*b*-PI_{20K} derived amphiphilic SABCs. B) Detachment of *Navicula* diatoms from PS_{8K}-*b*-$P(E/B)_{25K}$-*b*-PI_{20K} derived amphiphilic SABCs as a result of exposure to a shear stress of 23 Pa. Each point is the mean from 90 counts on 3 replicate slides. Bars show 95% confidence limits.

Conclusions:

Amphiphilic marine antifouling/fouling-release coatings were developed by chemical modification of two different polystyrene-*block*-poly(ethylene-*ran*-butylene)-*block*-polyisoprene ABC triblock copolymers with different combinations of hydrophilic PEG550 and hydrophobic F10H10 side chains. Resultant polymers were

characterized using a combination of infrared spectroscopy, ^{1}H NMR spectroscopy and elemental analysis, confirming a broad range of different relative amounts of PEG550 and F10H10 incorporated. The surfaces of the polymers showed high water contact angle hysteresis suggesting a dynamic surface capable of significant reorganization. An increase in the incorporation of F10H10 side-chains to the polymer resulted in an increase in the intensity of the -CF_2- and –CF_3 peaks for C 1s XPS analysis and 1s $\rightarrow \sigma^*_{C\text{-}F}$ resonance for C 1s NEXAFS measurements, suggesting segregation of this low surface energy moiety to the surface. The settlement and removal of *Ulva* spores/sporelings and *Navicula* diatoms showed significantly different behavior. In general, the lowest settlement of *Ulva* spores was seen on coatings containing a large proportion of PEG550 side-chains. However, *Navicula* settlement densities were similar across all coatings tested. Analysis of *Ulva* spore removal using a flow channel and *Ulva* sporeling removal using a water jet suggested that some optimal mixture of hydrophobic and hydrophilic side chains, biased towards a majority incorporation of PEG550, existed. Of particular note was the potential to further optimize the coating system to obtain a fouling-release performance superior to that of PDMS, a known fouling-release material. *Navicula* diatoms showed more straightforward detachment results, with removal being favored from the coatings containing the greatest amount of hydrophobic F10H10 moieties.

Acknowledgement

This work was supported by United States Department of Defense's Strategic Environmental Research and Development Program (SERDP), grant WP #1454 with additional support from the Office of Naval Research (ONR) through award # N00014-05-1-0134 (JAC and MEC) and N00014-02-1-0170 (CKO and EJK). KES and EJK acknowledge partial support from an NSF Graduate Fellowship and the NSF Polymers Program (DMR-0704539) as well as the use of facilities funded by the NSF-MRSEC program (UCSB MRL, DMR-0520415).

REFERENCES

1 L. Chromy and K. Uhacz, *Journal of the Oil and Colour Chemists' Association*, 1978, **61**, 39.

2 R. F. Brady, *Journal of Protective Coatings & Linings*, 2003, **20**, 33.

3 A. Katranitsas, J. Castritsi-Catharios, and G. Persoone, *Marine pollution bulletin*, 2003, **46**, 1491.

4 A. Terlizzi, S. Fraschetti, P. Gianguzza, M. Faimali, and F. Boero, *Aquatic Conservation: Marine and Freshwater Ecosystems*, 2001, **11**, 311.

5 G. Sauvet, S. Dupond, K. Kazmierski, and J. Chojnowski, *Journal of Applied Polymer Science*, 2000, **75**, 1005.

6 S. Krishnan, R. J. Ward, A. Hexemer, K. E. Sohn, K. L. Lee, E. R. Angert, D. A. Fischer, E. J. Kramer, and C. K. Ober, *Langmuir*, 2006, **22**, 11255.

7 D. Park, J. Wang, and A. M. Klibanov, *Biotechnology Progress*, 2006, **22**, 584.

8 P. Kurt, L. Wood, D. E. Ohman, and K. J. Wynne, *Langmuir*, 2007, **23**, 4719.

9 D. Park, J. A. Finlay, R. J. Ward, C. J. Weinman, S. Krishnan, M. Y. Paik, K. E. Sohn, M. E. Callow, J. A. Callow, D. L. Handlin, C. L. Willis, D. A. Fischer, E. R. Angert, E. J. Kramer, and C. K. Ober, *manuscript in preparation*.

10 P. Majumdar, E. Lee, N. Patel, S. J. Stafslien, J. Daniels, and B. J. Chisholm, *Journal of Coatings Technology and Research*, 2008, **5**, 405.

11 P. Majumdar, E. Lee, N. Patel, K. Ward, S. J. Stafslien, J. Daniels, B. J. Chisholm, P. Boudjouk, M. E. Callow, J. A. Callow, and S. E. M. Thompson, *Biofouling*, 2008, **24**, 185.

12 S. Krishnan, J. A. Finlay, A. Hexemer, N. Wang, C. K. Ober, E. J. Kramer, M. E. Callow, J. A. Callow, and D. A. Fischer, *Polym. Prepr. (Am. Chem. Soc., Div. Polym. Chem)*, 2005, **46**, 1248.

13 S. Ye, A. McClelland, P. Majumdar, S. J. Stafslien, J. Daniels, B. Chisholm, and Z. Chen, *Langmuir*, 2008, **24**, 9686.

14 J. A. Finlay, M. E. Callow, L. K. Ista, G. P. Lopez, and J. A. Callow, *Integrative and Comparative Biology*, 2002, **42**, 1116.

15 H. Yamamoto, Y. Sakai, and K. Ohkawa, *Biomacromolecules*, 2000, **1**, 543.

16 L. D. Unsworth, H. Sheardown, and J. L. Brash, *Langmuir*, 2005, **21**, 1036.

17 L. Li, S. Chen, J. Zheng, B. D. Ratner, and S. Jiang, *J. Phys. Chem. B*, 2005, **109**, 2934.

18 Y.-Y. Luk, M. Kato, and M. Mrksich, *Langmuir*, 2000, **16**, 9604.

19 D. G. Walton, P. P. Soo, A. M. Mayes, S. J. S. Allgor, J. T. Fujii, L. G. Griffith, J. F. Ankner, H. Kaiser, J. Johansson, and G. D. Smith, *Macromolecules*, 1997, **30**, 6947.

20 M. Mrksich and G. M. Whitesides, *ACS Symposium Series*, 1997, **680**, 361.

21 K. L. Prime and G. M. Whitesides, *J. Am. Chem. Soc.*, 1993, **115**, 10714.

22 H. Ma, J. Hyun, P. Stiller, and A. Chilkoti, *Advanced Materials*, 2004, **16**, 338.

23 S. Schilp, A. Kueller, A. Rosenhahn, M. Grunze, M. E. Pettitt, M. E. Callow, and J. A. Callow, *Biointerphases*, 2007, **2**, 143.

24 J. A. Finlay, S. Krishnan, M. E. Callow, J. A. Callow, R. Dong, N. Asgill, K. Wong, E. J. Kramer, and C. K. Ober, *Langmuir*, 2008, **24**, 503.

25 M. E. Callow, J. A. Callow, L. K. Ista, S. E. Coleman, A. C. Nolasco, and G. P. Lopez, *Applied and Environmental Microbiology*, 2000, **66**, 3249.

26 T. Ekblad, G. Bergstrom, T. Ederth, S. L. Conlan, R. Mutton, A. S. Clare, S. Wang, Y. Liu, Q. Zhao, F. D'Souza, G. T. Donnelly, P. R. Willemsen, M. E. Pettitt, M. E. Callow, J. A. Callow, and B. Liedberg, *Biomacromolecules*, 2008, **9**, 2775.

27 J. P. Youngblood, L. Andruzzi, C. K. Ober, A. Hexemer, E. J. Kramer, J. A. Callow, J. A. Finlay, and M. E. Callow, *Biofouling*, 2003, **19**, 91.

28 S. Krishnan, N. Wang, C. K. Ober, J. A. Finlay, M. E. Callow, J. A. Callow, A. Hexemer, K. E. Sohn, E. J. Kramer, and D. A. Fischer, *Biomacromolecules*, 2006, **7**, 1449.

29 A. Beigbeder, P. Degee, S. L. Conlan, R. J. Mutton, A. S. Clare, M. E. Pettitt, M. E. Callow, J. A. Callow, and P. Dubois, *Biofouling*, 2008, **24**, 291.

30 D. E. Wendt, G. L. Kowalke, J. Kim, and I. L. Singer, *Biofouling*, 2006, **22**, 1.

31 R. J. Pieper, A. Ekin, D. C. Webster, F. Casse, J. A. Callow, and M. E. Callow, *Journal of Coatings Technology and Research*, 2007, **4**.

32 A. Ekin, D. C. Webster, J. W. Daniels, S. J. Stafslien, F. Casse, J. A. Callow, and M. E. Callow, *Journal of Coatings Technology and Research*, 2007, **4**, 435.

33 M. E. Callow and J. A. Callow, *Biofouling*, 2000, **13**, 157.

34 M. A. Grunlan, N. S. Lee, G. Cai, T. Gaedda, J. M. Mabry, F. Mansfield, E. Kus, D. E. Wendt, G. L. Kowalke, J. A. Finlay, J. A. Callow, M. E. Callow, and W. P. Weber, *Chemistry of Materials*, 2004, **16**, 2433.

35 J. C. Yarbrough, J. P. Rolland, J. M. DeSimone, M. E. Callow, J. A. Finlay, and J. A. Callow, *Macromolecules*, 2006, **39**, 2521.

36 C. J. Kavanagh, R. D. Quinn, and G. W. Swain, *Journal of Adhesion*, 2005, **81**, 843.

37 C. S. F. Gudipati, J. A.; Callow, J. A.; Callow, M. E.; Wooley, K. L., *Langmuir*, 2005, **21**, 3044.

38 S. Krishnan, R. Ayothi, A. Hexemer, J. A. Finlay, K. E. Sohn, R. Perry, C. K. Ober, E. J. Kramer, M. E. Callow, J. A. Callow, and D. A. Fischer, *Langmuir*, 2006, **22**, 5075.

39 E. Martinelli, S. Agostini, G. Galli, E. Chiellini, A. Glisenti, M. E. Pettiitt, M. E. Callow, J. A. Callow, K. Graf, and F. W. Bartels, *Langmuir*, 2008, **24**, 13138.

40 J. Hopken, M. Moller, and S. Boileau, *New Polymeric Materials*, 1991, **2**, 339.

41 C. J. Weinman, J. A. Finlay, D. Park, M. Y. Paik, S. Krishnan, B. R. Fletcher, M. E. Callow, J. A. Callow, D. L. Handlin, C. L. Willis, D. A. Fischer, K. E. Sohn, E. J. Kramer, and C. K. Ober, *Polymeric Materials: Science & Engineering Preprints*, 2008, **98**, 639.

42 M. Y. Paik, S. Krishnan, F. You, X. Li, A. Hexemer, Y. Ando, S. H. Kang, D. A. Fischer, E. J. Kramer, and C. K. Ober, *Langmuir*, 2007, **23**, 5110.

43 J. Genzer, E. Sivaniah, E. J. Kramer, J. Wang, H. Köerner, K. Char, C. K. Ober, B. M. DeKoven, R. A. Bubeck, D. A. Fischer, and S. Sambasivan, *Langmuir*, 2000, **16**, 1993.

44 M. G. Samant, J. Stöhr, H. R. Brown, and T. P. Russell, *Macromolecules*, 1996, **29**, 8334.

45 Y. Liu, T. P. Russell, M. G. Samant, J. Stöhr, H. R. Brown, A. Cossy-Favre, and J. Diaz, *Macromolecules*, 1997, **30**, 7768.

46 T. Vladkova, *Journal of the University of Chemical Technology and Metallurgy*, 2007, **42**, 239.

47 M. Berglin, Gatenholm, P., *J. Adhes. Sci. Tech.*, 1999, **13**, 713.

48 K. J. Wynne, G. W. Swain, R. B. Fox, S. Bullock, and J. Ulik, *Biofouling*, 2000, **16**, 277.

49 R. F. Brady and I. L. Singer, *Biofouling*, 2000, **15**, 73.

50 J. F. Schumacher, M. L. Carman, T. G. Estes, A. W. Feinberg, L. H. Wilson, M. E. Callow, J. A. Callow, J. A. Finlay, and A. B. Brennan, *Biofouling*, 2007, **23**, 55.

51 M. E. Callow, J. A. Callow, J. D. Pickett-Heaps, and R. Wetherbee, *Journal of Phycology*, 1997, **33**, 938.

52 M. E. Callow, A. R. Jennings, A. B. Brennan, C. E. Seegert, A. Gibson, L. Wilson, A. Feinberg, R. Baney, and J. A. Callow, *Biofouling*, 2002, **18**, 237.

53 M. K. Chaudhury, J. A. Finlay, J. Y. Chung, M. E. Callow, and J. A. Callow, *Biofouling*, 2005, **21**, 41.

54 F. Casse, E. Ribeiro, A. Ekin, D. C. Webster, J. A. Callow, and M. E. Callow, *Biofouling*, 2007, **23**, 267.

55 J. A. Finlay, M. E. Callow, M. P. Schultz, G. W. Swain, and J. A. Callow, *Biofouling*, 2002, **18**, 251.

CHAPTER 5

SETTLEMENT AND RELEASE PROPERTIES OF THE GREEN ALGA *ULVA* AND THE DIATOM *NAVICULA* ON HYDROPHOBIC FLUORINATED AND HYDROPHILIC PEGYLATED SELF ASSEMBLED MONOLAYERS AND POLYMER BRUSHES

Abstract

A series of model test surfaces on glass slides were produced to probe the settlement and release of the green alga *Ulva* and *Navicula* diatoms, two prominent marine fouling organisms. Surfaces of a PEGylated self assembled monolayer (SAM) consisting of 8 oligoethylene glycol groups in conjunction with surfaces functionalized with polymer brushes of a PEGylated acrylate were produced to probe the hydrophilic side of the wettability spectrum. To examine hydrophobic surfaces meanwhile, substrates coated with a fluorinated SAM were produced in conjunction with polymer brushes grown from a fluorinated methacrylate. Surface characterization techniques including dynamic water contact angle analysis, X-ray photoelectron spectroscopy (XPS) and near-edge X-ray adsorption fine structure (NEXAFS) were employed to confirm that the surfaces were functionalized as intended. Settlement of *Ulva* spores was reduced on both the hydrophilic PEGylated SAMs and hydrophilic PEGylated brushes, while settlement of *Navicula* diatoms was only reduced on the PEGylated SAMs. Release of *Ulva* spores was only significant on the PEGylated SAMs. This contrasted with the release of *Navicula* diatoms, which followed an inverse trend of wettability, with the best release observed from the PEGylated SAMs and the least removal from the fluorinated SAMs. This suggested that factors beyond

chemical surface functionality greatly influenced the settlement and release behavior of these marine fouling organisms.

Introduction

The formation of self-assembled monolayers (SAMs) and grafting of polymer brushes are both routes to producing a robustly functionalized surface. SAMs are produced by a "grafted to" approach through the chemisorption of a reactive "head group" of a short chain amphiphilic molecule from either the vapor or liquid phase[1]. Meanwhile, polymer brushes, consisting of a polymeric chain tethered at one end to a surface or interface,[2] can either be formed by chemisorption to a substrate through a solution based "grafted to" approach or by surface initiated polymerization through a "grafted from" approach.[3] Polymer brushes are characterized by a height significantly greater than the molecule's radius of gyration due to the dense packing of the brushes causing them to stretch away from the substrate to which they are tethered. Due to the unique properties realized by these surface treatments, studies of adhesion, lubrication, wetting, nucleation and crystal growth, and molecular recognition in conjunction with applied work in nanotechnology and biotechnology have been realized.[4, 5]

One area where these surface treatments have been utilized is in the study of marine biofouling, the undesirable accumulation of microbial bioslimes, macroalgae, and calciferous macroscopic organisms such as barnacles on a surface immersed in seawater.[6] The extra friction realized by the accumulation of biofouling leads to higher operational and maintenance costs to industrial and defense interests, and also increases global carbon emissions.[7, 8] Since traditional fouling control coatings leach environmentally sensitive biocides, alternative coating systems are now being explored.[9-12] Fundamental studies of fouling settlement and release behaviors using

model surfaces such as SAMs and polymer brushes present an opportunity to explore fouling behavior using extremely well defined surface properties.

The green seaweed *Ulva* is a ubiquitous marine fouling alga. Distribution is primarily by microscopic zoospores, pear-shaped cells approximately 5-7 μm in length, that swim using four flagella at their anterior end.[13] Colonization of a surface by a spore involves surface sensing, subsequent commitment to settlement and ultimately the exocytotic secretion of a hydrophilic glycoprotein adhesive.[13-15] Zoospores are known to exhibit selectivity during settlement and respond to surface cues including surface chemistry and wettability,[16-19] topography[20, 21], and the presence of preexisting biofilms.[22] While several studies have suggested the preferential settlement of *Ulva* zoospores on hydrophobic surfaces relative to hydrophilic surfaces,[16-18, 23] the strength of attachment of settled spores is typically stronger on the hydrophilic surfaces.[24] Exceptions to this rule have been reported in the literature however, with hydrophilic surfaces of both mPEG-DOPA$_3$[23] and oligo(ethylene glycol) SAMs[19] demonstrating only weak adhesion of spores.

The study of diatoms is also of great interest to the marine fouling community since bioslimes dominated by these organisms contribute significantly to the fouling present on both biocidal and nonbiocidal fouling control coatings, suggesting that further optimization of antifouling coatings towards these organisms is needed.[25, 26] Diatoms are non-motile organisms that rely on water currents and movement to transport them to the substrates on which they ultimately attach. They are unicellular algae characterized by the presence of an elaborate silica cell wall known as the frustule. Raphid diatoms posses one or two slits in the frustule, called raphes, that allow secretion of sticky extracellular polymeric substances (EPS) that are responsible for both adhesion and motility.[25, 27, 28] The EPS is a multicomponent, mucilaginous bioadhesive, primarily composed of a complex mixture of proteoglycans.[29] The

adhesion of diatoms is greatly influenced by surface chemistry and wettability and they are a particular nuisance on hydrophobic siloxane coatings which are currently being explored to replace traditional biocidal coatings.[19, 30, 31]

This work will examine the settlement and release of both *Ulva* spores and *Navicula* diatoms on both hydrophilic and hydrophobic SAM and polymer brush surfaces. While similar work has been reported that focused on the settlement and release of *Ulva* and *Navicula* from SAMs with different wettabilities,[19] to the best of our knowledge this is the first time that a direct comparison of polymer brushes and SAMs has been reported on in the literature. Hydrophilic poly(ethylene glycol) (PEG) based materials have previously shown exceptional biofouling resistance with regards to both biomedical[4] and marine applications.[11] When a surface is functionalized with grafted PEG moieties, a close affinity exists between water molecules and the PEG arising from hydrogen bonding. Consequently, a hydration layer is formed that hinders the nonspecific adsorption of proteins[32] and can deter the settlement and adhesion of cells or microorganisms.[33] Thus, a SAM consisting of 8 ethylene glycol repeat groups (PEG-8 SAM, figure 5.1A) in conjunction with a polymer brush formed via surface initiated atom transfer radical polymerization (ATRP) of an acrylate consisting of side chains with ca. ~9 ethylene glycol repeat groups (PEG-9 Brush, figure 5.1B) were selected as model hydrophilic surfaces. Meanwhile, to form model hydrophobic surfaces, a SAM consisting of 8 perfluorinated carbons in conjunction with a two carbon alkyl spacer (F8H2 SAM, figure 5.1C) was selected in conjunction with a polymer brush also grown via surface initiated ATRP of a methacrylate with an identical side chain as the SAM (F8H2 Brush, figure 5.1D). Formation of the intended surfaces will be confirmed through the use of several surface characterization techniques including dynamic water contact angle analysis, X-ray photoelectron spectroscopy (XPS) and near-edge X-ray adsorption fine structure (NEXAFS). Finally,

the settlement and release behavior of the green alga *Ulva* and the diatom *Navicula* will be examined on the set of model surfaces.

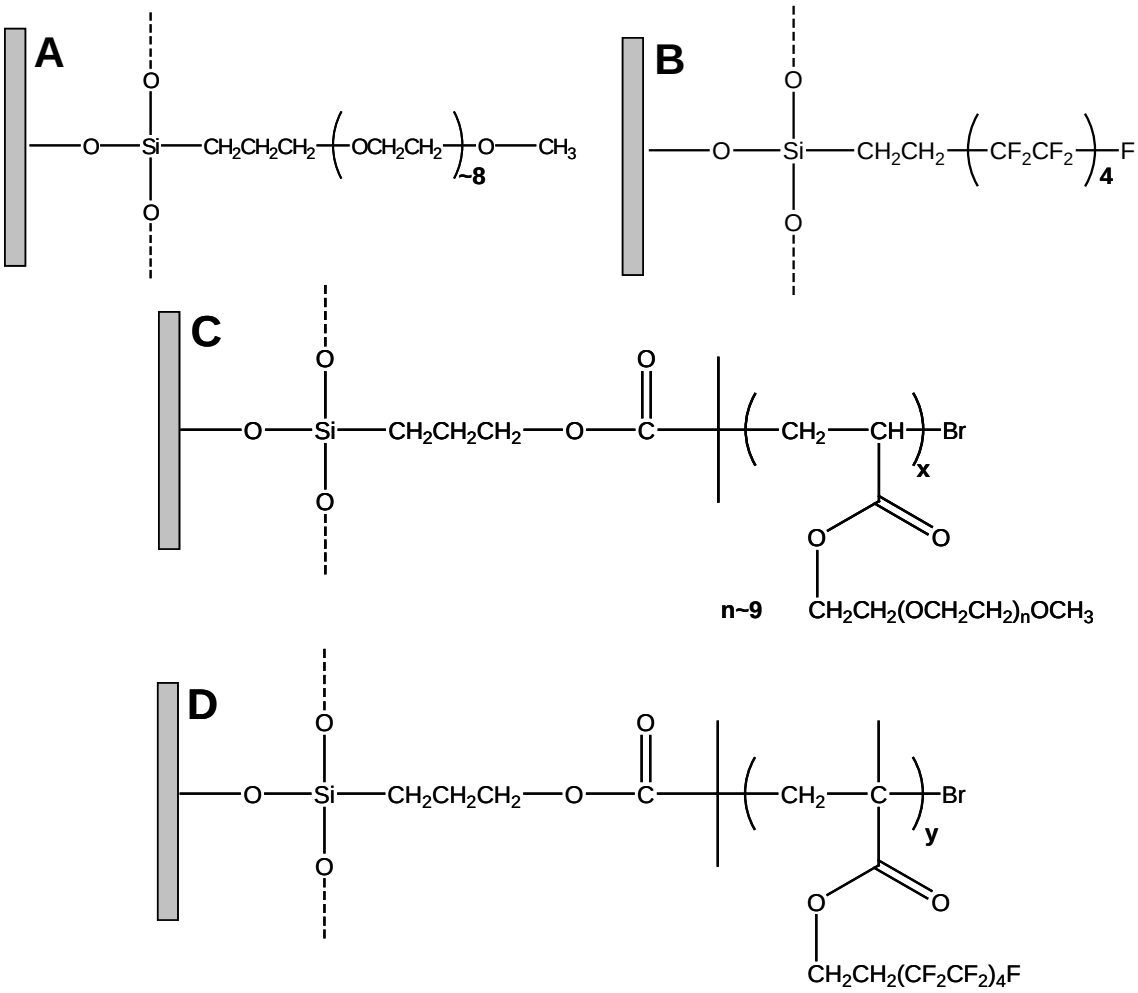

Figure 5.1. Structures of (A) PEG-8 SAM, (B) F8H2 SAM, (C) PEG-9 brush, and (D) F8H2 Brush.

Experimental Section:

Materials

2-[Methoxy(polyethyleneoxy)propyl]trimethoxysilane (PEG-8 silane, $CH_3O(CH_2CH_2O)_{6\text{-}9}(CH_2)_3Si(OCH_3)_3$, FW 460-590) and heptadecafluoro-1,1,2,2-tetrahydrodecyl trichlorosilane (F8H2 silane, $F(CF_2)_8CH_2CH_2SiCl_3$, FW 581.56)

were purchased from Gelest and used as received. Acetic acid, anhydrous pyridine, anhydrous toluene, 96% sulfuric acid (H_2SO_4), 30 wt % hydrogen peroxide in water (30% H_2O_2 in H_2O) and all other reagents were purchased from Sigma Aldrich or Fisher Scientific and used as received.

Allyl 2-bromo-2-methylpropionate (CH_2=$CHCH_2OCOC(CH_3)_2Br$, FW 207.7, 98%), dimethylchlorosilane ($(CH_3)_2SiHCl$, FW 94.62, 98%), platinum on carbon (Pt/C, 10%), triethylamine ($N(CH_2CH_3)_3$, FW 101.19, 99%), and anhydrous toluene were purchased from Sigma Aldrich and used as received to synthesize the [3-(2-bromoisobutyrl)propyl]dimethyl-chlorosilane and immobilize it on glass microscope slides.

Poly(ethylene glycol) methyl ether acrylate (CH_2=$CHCOO(CH_2CH_2O)_nCH_3$, average M_n ~480, n~9), heptadecafluoro-1,1,2,2-tetrahydrodecyl methacrylate (CH_2=$CHCOOCH_2CH_2(CF_2)_8F$, FW 532.19, 97%), copper(I) bromide (CuBr, FW 143.15, 99.999%), copper(II) bromide ($CuBr_2$, FW 223.35, 99.999%), and 2,2'-bipyridyl (FW 156.18, 99%) were also purchased from Sigma Aldrich and used as received to grow polymer brushes of F8H2 methacrylate and PEG-9 acrylate. Anhydrous α,α,α-trifluorotoluene and all other reagents were purchased from either Sigma Aldrich or Fisher and used as received.

All reactions were run in a custom air-free reactor designed to hold twelve glass microscope slides suspended in the reaction mixture. Microscope slides were cleaned with piranha solution (7:3 H_2SO_4:30% H_2O_2 in H_2O), rinsed with copious distilled water, and dried under a stream of argon prior to all surface functionalization reactions.

Synthesis of PEG-8 and F8H2 SAMs on Glass Slides

To form slides functionalized with the PEG-8 silane, twelve microscope slides were first placed in the dried reactor and purged with argon. The glass slides were then immersed in a toluene solution consisting of 8 mL of PEG-8 silane, 250 mL of anhydrous toluene, 50 μL of pyridine, and 20 μL of acetic acid for approximately 24 hours. Subsequently the slides were removed from the reaction, extracted with toluene under sonication, dried under a stream of nitrogen, and ultimately annealed in a vacuum oven at 120 °C for 12 hours. F8H2 silane functionalized glass slides were formed in an analogous fashion from the F8H2 chlorosilane without the use of pyridine and acetic acid.

Synthesis and Immobilization of ATRP Surface Initiator

The procedure outlined in Ramakrishnan et al. was closely followed to produce and immobilize the ATRP surface initiator.[34] Allyl 2-bromo-2-methylpropionate (2 mL) was mixed with 20 mL of freshly distilled dimethylchlorosilane in a round bottom flask. 20 mg of Pt/C (10% Pt) was added and the mixture was refluxed for ca. ~ 15 h. Subsequently, the excess dimethylchlorosilane was removed under reduced pressure, yielding the initiator chlorosilane as an oil. The oil was quickly filtered over anhydrous sodium sulfate to remove the residual Pt/C catalyst yielding [3-(2-bromoisobutyrl)propyl]dimethyl-chlorosilane as a colorless oil.

Twelve microscope slides were placed in the dried reactor and purged with argon. 250 mL of a toluene solution containing the initiator (concentration ≈ 1 mL initiator chlorosilane/1L toluene) was added to the reactor and the contents were allowed to stand for at least 18 h. Subsequently, the glass slides were removed from the reaction solution, extracted with dichloromethane under sonication, dried under a nitrogen stream, and used for grafting reactions to synthesize polymer brushes.

ATRP Surface Initiated Polymerization of PEG-9 and F8H2 Brushes

To produce PEG-9 acrylate brushes, a mixture of 54.5 g (0.12 mol) of poly(ethylene glycol) methyl ether acrylate, 200 mL of water, 55 mg (0.4 mmol) CuBr, 5.5 mg ($CuBr_2$, 0.02 mmol), and 125 mg (0.8 mmol) of 2,2'-bipyridyl was degassed by purging with argon and cumulated into the reactor containing twelve glass slides functionalized with the ATRP surface initiator. The reaction was lightly heated at 30° C for 48 h. Subsequently the slides were removed from the reaction solution, and extracted with acetone under sonication and dried under a nitrogen stream. F8H2 methacrylate brushes were made in an analogous fashion in α,α,α-trifluorotoluene with 79.8 g (50 mL, 0.15 mol) of the heptadecafluoro-1,1,2,2-tetrahydrodecyl methacrylate. Due to the slower polymerization kinetics of the fluorinated methacrylate, the reaction was heated at 90° C for 48 h. For the F8H2 methacrylate brushes, the slides were extracted with α,α,α-trifluorotoluene, and subsequently dichloromethane, under sonication and subsequently dried under a nitrogen stream. All surface grafted brushes were annealed under reduced pressure at 120° C for 12 h.

Surface Characterization

XPS measurements were performed using a Kratos Axis Ultra Spectrometer (Kratos Analytical, Manchester, UK) with a monochromatic Al Kα X-ray source (1486.6 eV) operating at 225 W under a vacuum of 1.0 × 10-8 Torr. Charge compensation was carried out by injection of low-energy electrons into the magnetic lens of the electron spectrometer. The pass energy of the analyzer was set at 40 eV for high-resolution spectra and 80 eV for survey scans, with energy resolutions of 0.05 and 1 eV, respectively. The spectra were analyzed using CasaXPS v.2.3.12Dev4

software. The C-C peak at 285 eV was used as the reference for binding energy calibration.

NEXAFS experiments were carried out on the U7A NIST/Dow materials characterization end-station at the National Synchrotron Light Source at Brookhaven National Laboratory (BNL). The general underlying principles of NEXAFS and a description of the beam line at BNL have been previously reported on.[35, 36] The X-ray beam was elliptically polarized (polarization factor = 0.85), with the electric field vector dominantly in the plane of the storage ring. The photon flux was about $1x10^{11}$ photons per second at a typical storage ring current of 500 mA. A spherical grating monochromator was used to obtain monochromatic soft X-rays at an energy resolution of 0.2 eV. The C 1s NEXAFS spectra were acquired for incident photon energy in the range 270–320 eV. The angle of incidence of the X-ray beam, measured from the sample surface, was 50°. The partial-electron-yield (PEY) signal was collected using a channeltron electron multiplier with an adjustable entrance grid bias (EGB). Data was reported for a grid bias of -150 V. The channeltron PEY detector was positioned in the equatorial plane of the sample chamber and at an angle of 36° relative to the incoming X-ray beam. The PEY C 1s spectra were normalized by subtracting a linear pre-edge baseline and setting the edge jump to unity at 320 eV.[37] The photon energy was calibrated by adjusting the peak position of the lowest π^* phenyl resonance from polystyrene to 285.5 eV.[38]

Water contact angles were measured using a contact angle goniometer (AST Products, Inc. model VCA Optima XE) at room temperature. Dynamic water contact angle measurements were performed through the addition and retraction of a small drop of water (ca. ~ 2 μL) on the surface. The advancing and receding contact angle behavior was digitally recorded and image analysis software was used to measure the angles.

Settlement and Strength of Attachment of *Ulva* Zoospores

Six replicate glass slides of each test sample were equilibrated in artificial seawater 1 h prior to the start of the experiments. Zoospores were released from fertile plants of *Ulva linza* and prepared for assay as described previously.[13] Ten mL of zoospore suspension (1×10^6 spores per mL), was pipetted into the compartments of Quadriperm polystyrene culture dishes (Greiner Bio-One), each containing a test slide. The test slides were incubated in the dark at ~ 20° C for 1 h and gently washed in seawater to remove zoospores that had not settled. Three slides were fixed using 2.5% glutaraldehyde in seawater and these replicates were used to quantify the density of zoospores attached to the surfaces as previously reported.[39]

Three slides surface functionalized with either the SAMs or Brushes settled with zoospores for 1 hour by the above method, were exposed to a shear stress of 53 Pa created by the turbulent flow of seawater in a specially designed water channel. Following this, slides were fixed in gluteraldehyde as described above. The number of spores remaining attached was compared with unexposed control slides (the same as used to determine settlement).

Settlement and Strength of Attachment of *Navicula* Diatoms

Six replicate test slides of each sample were again equilibrated in artificial sea water 1 h prior to the experiment. *Navicula* cells were cultured in F/2 medium contained in 250 ml conical flasks. After 3 days the cells were in log phase growth. Cells were washed 3 times in fresh medium before harvesting and diluted to give a suspension with a chlorophyll *a* content of approximately 0.25 μg ml^{-1}. Cells were settled in individual dishes containing 10 mL of suspension at ~20° C on the laboratory bench. After 2 h the slides were gently washed in seawater to remove cells

that had not properly attached (submerged wash). Slides were fixed using 2.5% glutaraldehyde in seawater. The density of cells attached to the surface was counted on each slide using an image analysis system attached to a fluorescence microscope. Counts were made for 30 fields of view (each 0.064 mm^2) on each slide.

Slides settled with *Navicula* were exposed to a shear stress of 22.1 Pa in a water channel. The number of cells remaining attached was counted using the image analysis system described above.

Results and Discussion:

Dynamic Water Contact Angles

Dynamic water contact angle results are given in table 1. Advancing contact angles for both the F8H2 SAM and F8H2 Brush were on the order of 110° or greater, indicating a hydrophobic surface. This suggests a significant surface contribution from the low surface energy fluorinated moieties as expected. Meanwhile, both the PEG-8 SAM and PEG-9 Brush samples had significantly lower advancing and receding contact angles due to the hydrophilicity of the oligoethylene glycol groups. Contact angle hysteresis, which was significant for all four samples, was likely to have been increased by the inherent roughness of the glass slide substrates and possibly also by the roughness of the polymer brushes.[40]

Table 5.1. Advancing and receding dynamic water contact angle measurements for fluorinated and PEGylated SAMs and polymer brushes.

Sample	$\theta_{w, adv.}$	$\theta_{w, rec.}$
F8H2 SAM	128 ± 2	77 ± 3
F8H2 Brush	107 ± 2	49 ± 3
PEG-8 SAM	70 ± 3	40 ± 3
PEG-9 Brush	71 ± 3	28 ± 4

X-Ray Photoelectron Spectroscopy (XPS)

Figure 5.2A depicts the C 1s high resolution XPS scan of the F8H2 SAM while Figure 5.2B gives the C 1s high resolution XPS scan of the F8H2 brush. Two different incident angles (0° and 75°) were used in both cases to explore if there was a difference in chemical structure between the immediate surface (75°) and slightly deeper (0°) in the brush or SAM. Both samples showed the characteristic peaks associated with -CF_2- and –CF_3 near 292 eV and 294 eV respectively. The strong intensity peak near ca. ~ 285 eV was indicative of C-C bonds, and the relative intensity of this peak was greater for the F8H2 brush than the F8H2 SAM due to the additional contribution of the polymer brush back-bone. A significant shoulder associated with the C-O peak was also seen at ca. ~ 286 eV, in conjunction with a peak representative of O=C-O at ca. ~ 289 eV for the F8H2 brush due to the larger amount of ester groups present. A minor, unexpected peak indicative of O=C-O also appears to be present for the F8H2 SAM, which is likely an artifact of sample preparation. Comparison of the spectra produced at different incident angles for both the F8H2 SAM suggests very little difference between the scans with a bit larger proportion of fluorinated moieties detected for the 0° scan. If a similar comparison is done for the F8H2 brush, it is apparent that the -CF_2- and C-C groups appear to be more prevalent in the 75° scan, likely indicating that the fluorinated side chains are preferentially segregating to the surface.

Meanwhile, Figure 5.3A depicts the C 1s high resolution XPS scans of the PEG-8 SAM taken at both 0° and 75° incident angles, while Figure 5.3B depicts the C 1s high resolution XPS scans for the PEG-9 brush. Both scans show very strong peaks indicative of C-C and C-O near 284 eV and 286 eV respectively. The PEG-9 brush sample also shows the characteristics peak indicative of the ester groups associated with the acrylate back-bone at ca. ~ 289 eV. The PEG-8 SAM sample demonstrates a

greater intensity C-C peak and a lower intensity C-O peak for the 75° incident angle scan, suggesting that the high surface energy PEG groups are being suppressed from the surface. The PEG-9 brush meanwhile showed very little difference between the scans taken at 0° and 75°.

Near Edge X-ray Adsorption Fine Structure (NEXAFS) Analysis

To determine the orientation of molecules at the brush surfaces, the angle of incidence of the polarized synchrotron X-ray beam was varied and the intensity of Auger electrons was measured for X-ray photons with energy ranging from 270 eV to 320 eV. As can be seen in Figure 5.4, the semifluorinated alkyl side chains of the F8H2 Brush were highly oriented at the surface. In contrast, the PEGylated side chains did not show any orientation at the surface (Figure 5.5). It is also evident that the polymer brushes and SAMs exhibited qualitatively similar NEXAFS spectra. As expected, the C1s $\rightarrow \pi^*_{C=O}$ peak is seen in the NEXAFS spectra of the polymer brushes, while this resonance is absent in the spectra of the SAM surfaces as the latter do not contain the carbonyl group.

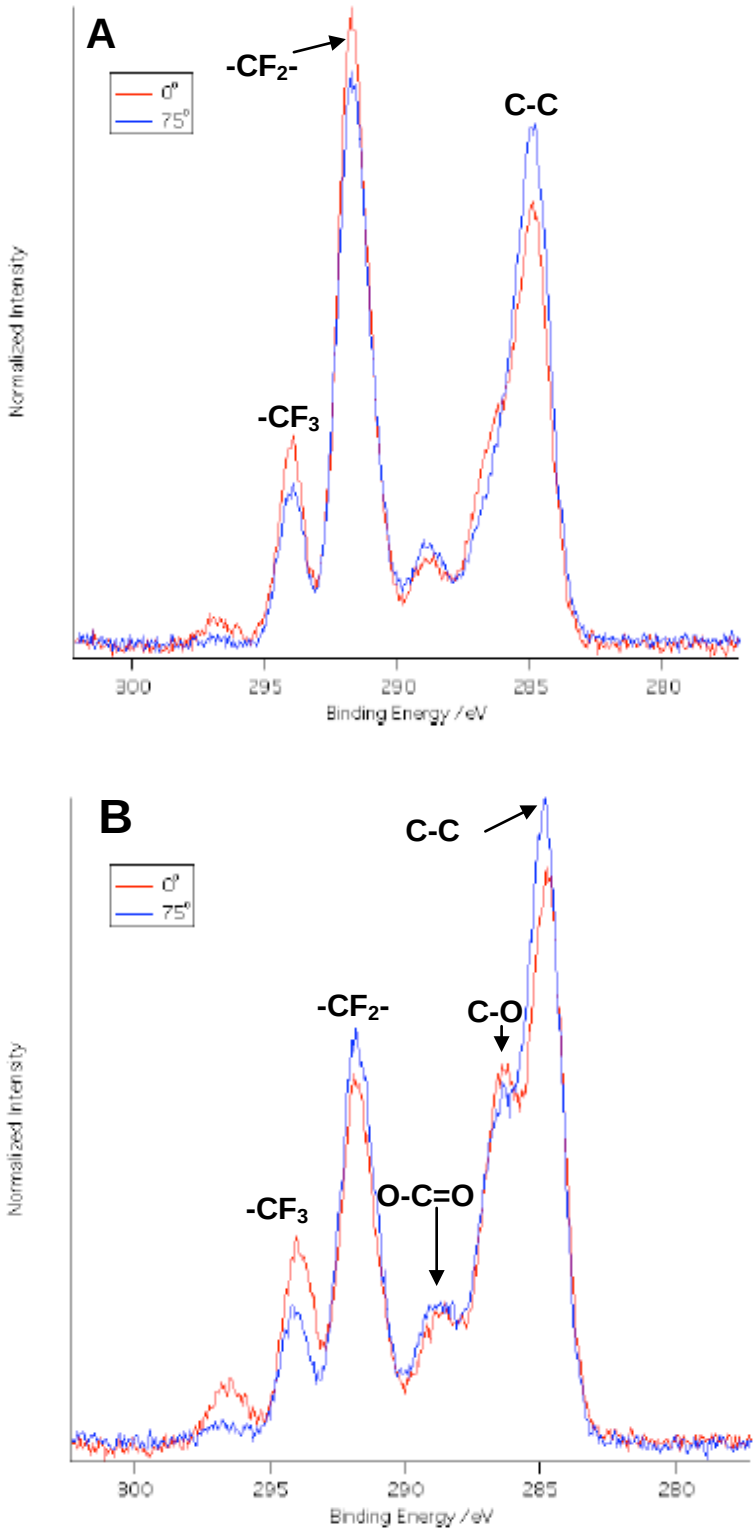

Figure 5.2. C 1s high resolution XPS scans of A) the F8H2 SAM and B) the F8H2 brush. Scans taken at two different incident angles (0° and 75° are given).

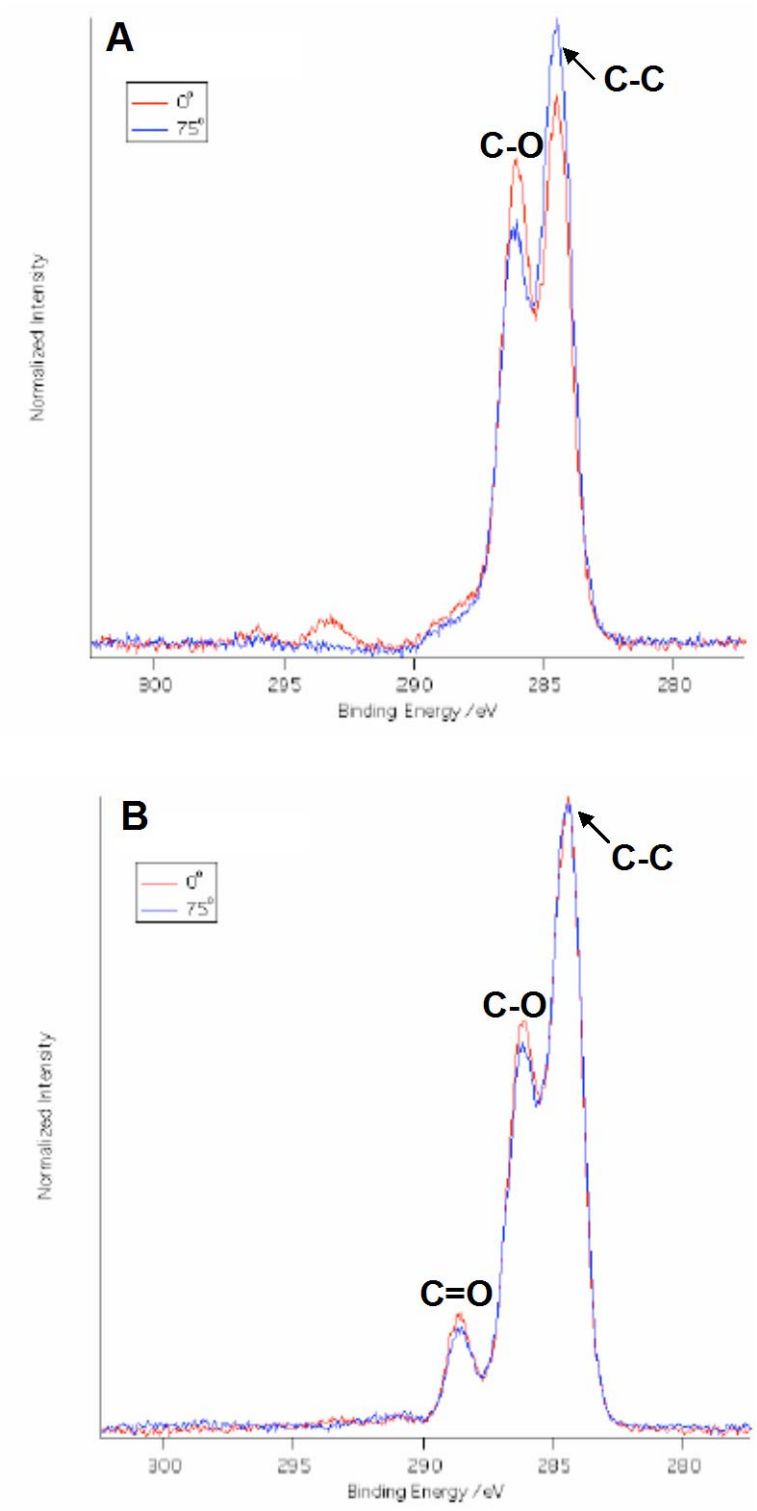

Figure 5.3. C 1s high resolution XPS scans of A) the PEG-8 SAM and B) the PEG-9 brush. Scans taken at two different incident angles (0° and 75° are given).

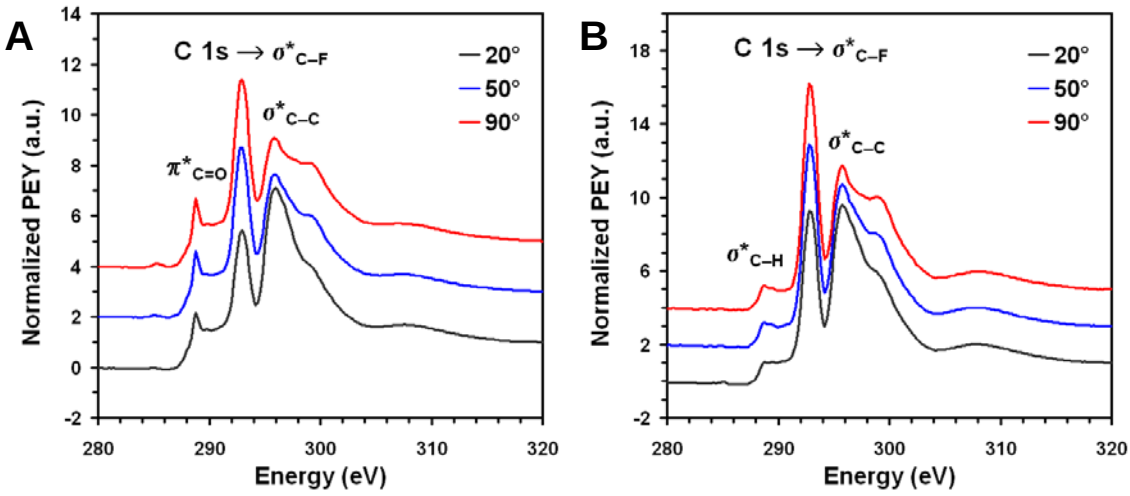

Figure 5.4. A) C1s NEXAFS spectra of the F8H2 brush and B) F8H2 SAM obtained at three different emission angles. Major resonance transition peaks are labeled.

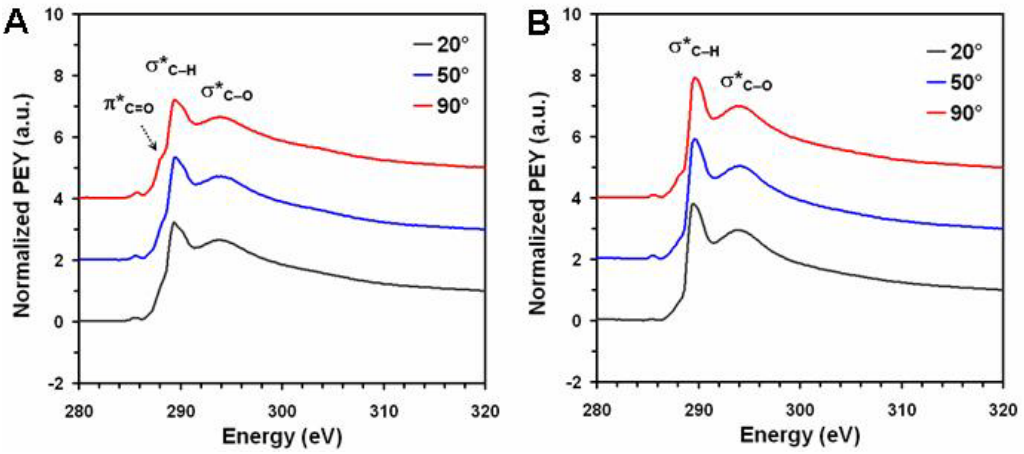

Figure 5.5. A) C1s NEXAFS spectra of the PEG-9 brush and B) the PEG-8 SAM acquired at three different emission angles. Major resonance transition peaks are labeled.

Settlement and Removal of *Ulva* Spores

Ulva spore settlement density (depicted in Figure 5.6) was slightly higher on the F8H2 SAM samples than on the F8H2 brush samples. Settlement was significantly higher on both of the fluorinated samples versus the PEGylated surfaces. On the F8H2

SAM, spore settlement density was ca. ~ 60% that on glass. Although spore settlement densities on the fluorinated SAMs and brushes were close in value, a one way analysis of variance supported by a Tukey test showed that there was a significant difference between them ($F_{3, 356} = 750$ $P<0.05$). The slightly lower settlement density on the F8H2 brush sample versus the F8H2 SAM probably reflects the difference in wettabilities between these surfaces and the fluorinated SAM samples as shown by the contact angles in table 1. Settlement densities on both of the PEGylated samples was very low being less than 12% of that on the glass standard; settlement results were not statistically different between them. These observations generally followed the expected trend of increasing spore settlement with increasing hydrophobicity of the surface.[16, 18, 23] Furthermore, the similar spore settlement densities on the fluorinated SAM and polymer brush surfaces taken in conjunction with the close similarity between settlement densities on the PEGylated SAM and polymer brush surfaces suggests that the SAMs and brushes are functioning in a similar way to each other with regards to *Ulva* zoospore settlement behavior.

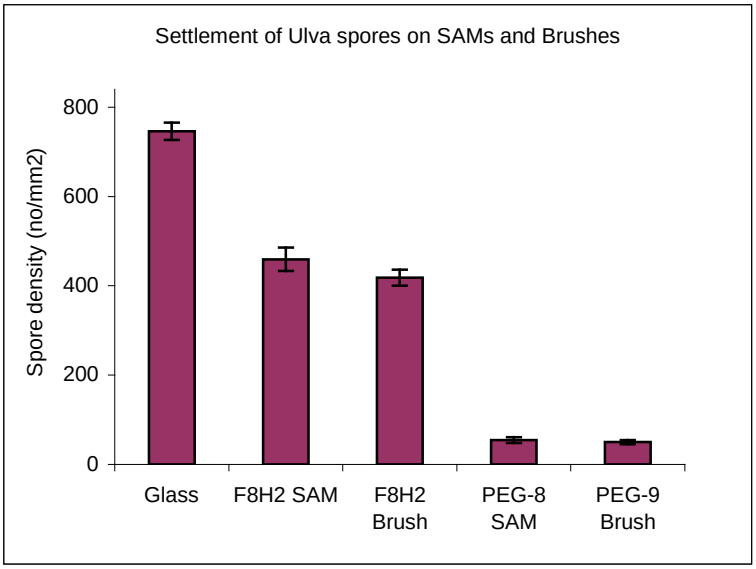

Figure 5.6. The settlement of *Ulva* spores on fluorinated and PEGylated SAMs and brushes. Each point is the mean from 90 counts on 3 replicate slides. Bars show 95% confidence limits.

Spore removal from all the samples was low (Figure 5.7). The only appreciable removal was from the PEG-8 SAMs (ca. ~ 22%). The stronger attachment of spores to the PEGylated brush compared with the PEGylated SAM suggests that the thicker layer of PEGylated groups may have a negative effect on spore-release properties. It can be hypothesized that this might be due to increased roughness and surface area at the molecular level. The observation of enhanced spore removal from a hydrophilic surface however is interesting, since when taken in conjunction with similar observations reported in the literature,[19, 23] this runs counter to the observation of enhanced spore removal from a hydrophobic elastomeric surface reported in Youngblood et al.[41] Clearly, additional factors including coating thickness and modulus appear to influence *Ulva* spore strength of adhesion and should be further investigated.

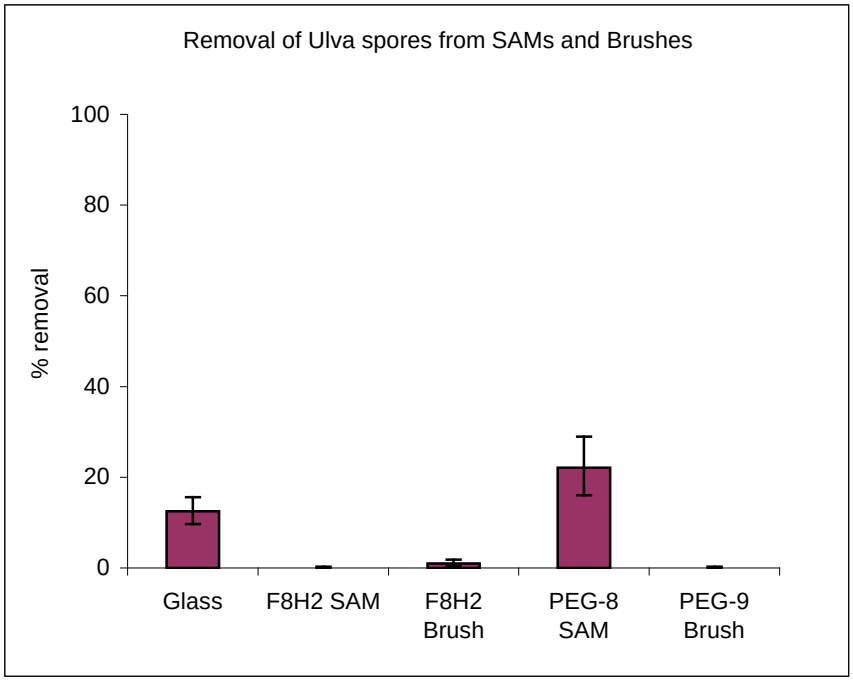

Figure 5.7. Detachment of *Ulva* spores from fluorinated and PEGylated SAMs and brushes. Each point represents the mean percentage removal from 90 counts from 3 replicate slides. Bars represent 95% confidence limits derived from arcsine transformed data.

Settlement and Removal of *Navicula* Diatoms

Diatoms are non-motile and reach the substrate surface by sinking through the water column. Thus, at the end of the assay, every surface supports the same number of cells. Differences in settlement (attachment) after gentle washing thus reflect differences in the ability of cells to adhere. Cell settlement (attachment) was broadly similar on all the surfaces except for the PEG-8 SAMs (Figure 8). On these surfaces, the cells clumped together and detached. The attachment strength of the cells was so weak that even slight movement of the assay dish caused some cells to detach from the surface. When the slides were gently washed by dipping in water, even more of the cells were removed, leaving only about half as many attached to the PEG-8 SAM

as on the other surfaces. This clearly demonstrated a difference in the adhesion of diatoms to the PEG-8 SAM and PEG-9 Brush.

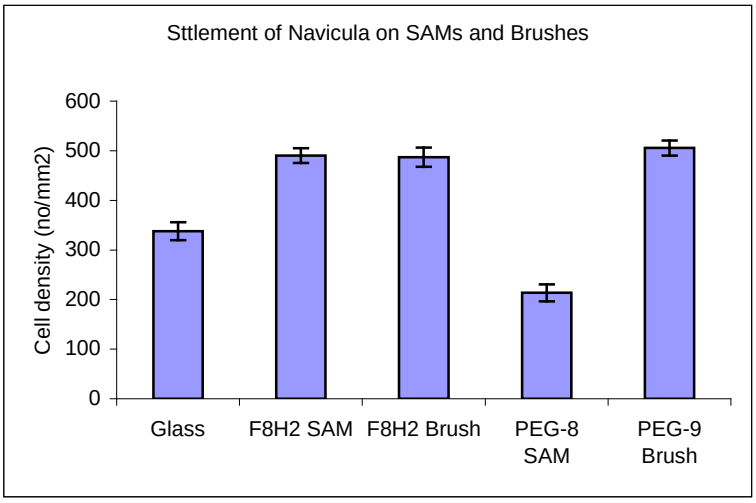

Figure 5.8. The settlement of *Navicula* diatoms on fluorinated and PEGylated SAMs and brushes. Each point is the mean from 90 counts on 3 replicate slides. Bars show 95% confidence limits.

Strength of attachment was greater on the fluorinated than on the PEGylated surfaces (Figure 5.9). Attachment strength was particularly high on the F8H2 SAMs with less than 5% removal. Detachment was greatest from the PEG-8 SAM which, as described previously, lost cells at the washing stage. These results were generally consistent with those previously reported showing that *Navicula* removal increases with increasing wettability of a surface.[23, 31]

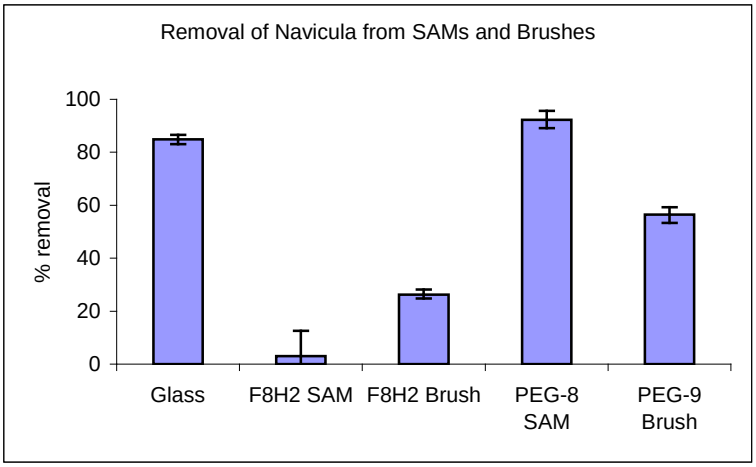

Figure 5.9. Detachment of *Navicula* diatoms from fluorinated and PEGylated SAMs and brushes. Each point represents the mean percentage removal from 90 counts from 3 replicate slides. Bars represent 95% confidence limits derived from arcsine transformed data.

Conclusions:

A series of test surfaces were produced on glass slides to compare and contrast the influences of hydrophobic and hydrophilic SAMs and polymer brushes on the settlement and attachment of spores of the green alga *Ulva* and the diatom *Navicula*. Surface characterization techniques demonstrated that the surfaces were functionalized as intended. Settlement of *Ulva* spores was found to be minimized on the hydrophilic PEGylated SAMs and brushes, while settlement of *Navicula* diatoms was only minimized on the PEGylated SAMs. Release of *Ulva* spores was significant on the PEGylated SAMs while release of the *Navicula* diatoms generally followed an inverse trend of wettability, with the best release for the PEGylated SAMs and the least removal observed on the fluorinated, F8H2 SAMs. This suggested that despite similarities in the surface characterization of the fluorinated SAMs and brushes and PEGylated SAMs and brushes, the interaction of these two test organisms with the surfaces was significantly different. More striking is the obvious differences observed here versus thick, elastomeric polymer coatings which have previously demonstrated

the best removal of *Ulva* spores from hydrophobic substrates.[41] This suggests that factors beyond surface chemical functionality greatly influence the settlement and release behavior of these marine algae.

Acknowledgement

This work was supported by the Office of Naval Research (ONR) through award # N00014-05-1-0134 (JAC and MEC) and N00014-02-1-0170 (CKO and EJK). Additional supported was provided by the United States Department of Defense's Strategic Environmental Research and Development Program (SERDP), grant WP #1454. KES and EJK acknowledge partial support from an NSF Graduate Fellowship and the NSF Polymers Program (DMR-0704539) as well as the use of facilities funded by the NSF-MRSEC program (UCSB MRL, DMR-0520415).

REFERENCES

1 D. K. Schwartz, *Annual Review of Physical Chemistry*, 2001, **52**, 107.

2 P. G. d. Gennes, *Maromolecules*, 1980, **13**, 1069.

3 B. Zhao and W. J. Brittain, *Progress in Polymer Science*, 2000, **25**, 677.

4 W. Senaratne, L. Andruzzi, and C. K. Ober, *Biomacromolecules*, 2005, **6**, 2427.

5 A. Ulman, *Chemical Reviews*, 1996, **96**, 1533.

6 M. E. Callow and J. A. Callow, *Biologist*, 2002, **49**, 1.

7 R. L. Townsin, *Biofouling*, 2003, **19 (Supplement)**, 9.

8 M. P. Schultz, *Biofouling*, 2007, **23**, 331.

9 D. M. Yebra, S. Kiil, and K. Dam-Johansen, *Prog. Org. Coat.*, 2004, **50**, 75.

10 T. Vladkova, *Journal of the University of Chemical Technology and Metallurgy*, 2007, **42**, 239.

11 S. Krishnan, C. J. Weinman, and C. K. Ober, *J. Mater. Chem.*, 2008, **18**, 3405.

12 J. Genzer and K. Efimenko, *Biofouling*, 2006, **22**, 339.

13 M. E. Callow, J. A. Callow, J. D. Pickett-Heaps, and R. Wetherbee, *Journal of Phycology*, 1997, **33**, 938.

14 J. A. Callow, M. P. Osborne, M. E. Callow, F. Baker, and A. M. Donald, *Collids and Surfaces B: Biointerfaces*, 2003, **27**, 315.

15 M. S. Stanley, M. E. Callow, and J. A. Callow, *Planta*, 1999, **210**, 61.

16 L. K. Ista, M. E. Callow, J. A. Finlay, S. E. Coleman, A. C. Nolasco, R. H. Simons, J. A. Callow, and G. P. Lopez, *Applied and Environmental MIcrobiology*, 2004, **66**, 4151.

17 J. A. Finlay, S. Krishnan, M. E. Callow, J. A. Callow, R. Dong, N. Asgill, K. Wong, E. J. Kramer, and C. K. Ober, *Langmuir*, 2008, **24**, 503.

18 M. E. Callow, J. A. Callow, L. K. Ista, S. E. Coleman, A. C. Nolasco, and G. P. Lopez, *Applied and Environmental Microbiology*, 2000, **66**, 3249.

19 S. Schilp, A. Kueller, A. Rosenhahn, M. Grunze, M. E. Pettitt, M. E. Callow, and J. A. Callow, *Biointerphases*, 2007, **2**, 143.

20 J. F. Schumacher, M. L. Carman, T. G. Estes, A. W. Feinberg, L. H. Wilson, M. E. Callow, J. A. Callow, J. A. Finlay, and A. B. Brennan, *Biofouling*, 2007, **23**, 55.

21 M. L. Carman, T. G. Estes, A. W. Feinberg, J. F. Schumacher, W. Wilkerson, L. H. Wilson, M. E. Callow, J. A. Callow, and A. B. Brennan, *Biofouling*, 2006, **22**, 11.

22 J. A. Callow and M. E. Callow, *Progress in Molecular and Subcellular Biology*, 2006, **42**, 141.

23 A. Statz, J. A. Finlay, J. Dalsin, M. E. Callow, J. A. Callow, and P. B. Messersmith, *Biofouling*, 2006, **22**, 391.

24 J. A. Finlay, M. E. Callow, M. P. Schultz, G. W. Swain, and J. A. Callow, *Biofouling*, 2002, **18**, 251.

25 M. E. Callow, in 'Algal Biofilms', ed. L. V. Evans, Amsterdam, 2000.

26 J. H. Bishop, S. R. Silva, and V. M. Silva, *J. Oil Colour Chem. Assoc.*, 1974, **57**, 30.

27 M. J. Higgins, P. Molino, P. Mulvaney, and R. Wetherbee, *J. Phycol.*, 2003, **39**, 1181.

28 R. Wetherbee, J. L. Lind, J. Burke, and R. S. Quatrano, *J. Phycol.*, 1998, **34**, 9.

29 T. M. Dugdale, R. Dagastine, A. Chiovitti, and R. Wetherbee, *Biophysical Journal*, 2006, **90**, 2987.

30 R. Holland, T. M. Dugdale, R. Wetherbee, A. B. Brennan, J. A. Finlay, J. A. Callow, and M. E. Callow, *Biofouling*, 2004, **20**, 323.

31 S. Krishnan, N. Wang, C. K. Ober, J. A. Finlay, M. E. Callow, J. A. Callow, A. Hexemer, K. E. Sohn, E. J. Kramer, and D. A. Fischer, *Biomacromolecules*, 2006, **7**, 1449.

32 P. Harder, M. Grunze, R. Dahint, G. M. Whitesides, and P. E. Laibinis, *J. Phys. Chem. B*, 1998, **102**, 426.

33 L. Andruzzi, W. Senaratne, A. Hexemer, E. D. Sheets, B. Ilic, D. Holowka, E. J. Kramer, B. Baird, and C. K. Ober, *Langmuir*, 2005, **21**, 2495.

34 A. Ramakrishnan, R. Dhamodharan, and J. Ruhe, *Macromolecular Rapid Communications*, 2002, **23**, 612.

35 M. Y. Paik, S. Krishnan, F. You, X. Li, A. Hexemer, Y. Ando, S. H. Kang, D. A. Fischer, E. J. Kramer, and C. K. Ober, *Langmuir*, 2007, **23**, 5110.

36 J. Genzer, E. Sivaniah, E. J. Kramer, J. Wang, H. Köerner, K. Char, C. K. Ober, B. M. DeKoven, R. A. Bubeck, D. A. Fischer, and S. Sambasivan, *Langmuir*, 2000, **16**, 1993.

37 M. G. Samant, J. Stöhr, H. R. Brown, and T. P. Russell, *Macromolecules*, 1996, **29**, 8334.

38 Y. Liu, T. P. Russell, M. G. Samant, J. Stöhr, H. R. Brown, A. Cossy-Favre, and J. Diaz, *Macromolecules*, 1997, **30**, 7768.

39 M. E. Callow, A. R. Jennings, A. B. Brennan, C. E. Seegert, A. Gibson, L. Wilson, A. Feinberg, R. Baney, and J. A. Callow, *Biofouling*, 2002, **18**, 237.

40 D. Quere, *Annual Review of Materials Research*, 2008, **38**, 71.

41 J. P. Youngblood, L. Andruzzi, C. K. Ober, A. Hexemer, E. J. Kramer, J. A. Callow, J. A. Finlay, and M. E. Callow, *Biofouling*, 2003, **19**, 91.

CHAPTER 6

SETTLEMENT AND RELEASE OF THE GREEN ALGA *ULVA* ON TRIBLOCK SURFACE ACTIVE BLOCK COPOLYMERS BASED ON THREE UNIQUE NON-IONIC SURFACTANTS

Abstract

A series of three amphiphilic triblock surface active block copolymers (SABCs) were synthesized through chemical modification of a polystyrene-*block*-poly(ethylene-*ran*-butylene)-*block*-polyisoprene ABC triblock copolymer precursor with three different amphiphilic non-ionic surfactants. Amphiphilicity was imparted by a hydrophobic aliphatic or silicon containing chemical group combined with a hydrophilic poly(ethylene glycol) (PEG) containing moiety. Bilayer coatings on glass slides consisting of a thin layer of the amphiphilic SABC deposited on a thick layer of a polystyrene-*block*-poly(ethylene-*ran*-butylene)-*block*-poly(styrene) (SEBS) thermoplastic elastomer were prepared for biofouling assays using the green alga *Ulva*, a ubiquitous marine fouling organism. Dynamic water contact angle analysis and X-ray photoelectron spectroscopy (XPS) were utilized to characterize the surfaces. Despite similar wettability parameters for all three SABCs, significant differences in surface chemistry were realized depending on which non-ionic surfactant was incorporated. Additionally, characterization of samples produced by both spin coating and spray coating suggested significant process dependent differences in surface functionality. In biofouling assays, spore settlement of the green alga *Ulva* was significantly reduced relative to a PDMS control for SABCs derived from two of the three non-ionic surfactants, with the non-ionic surfactant combining an PEG group with an aliphatic moiety demonstrating the best performance (least settlement).

Additionally, a fouling release assay using *Ulva* sporelings suggested that the SABC derived from the PEG and aliphatic containing non-ionic surfactant also out-performed PDMS as a fouling release material. Similar facile release of *Ulva* sporelings was not demonstrated for the other two coatings. This suggests that small differences in chemical surface functionality likely impart much more significant changes to fouling settlement and release performance of materials than overall wettability behavior.

Introduction

Marine biofouling is a worldwide problem caused by the adhesion and accumulation of microbial slimes, fouling algae, and calcariferous organisms such as barnacles on a surface immersed in sea water.[1] Various methods have been used to combat this problem, but to date the most effective has been the use of ablative biocide containing tributyl-tin (TBT) containing coatings. Unfortunately, TBT coatings were found to not exhibit sufficient selectivity towards target organisms,[2] and they have already been banned most places in the world due to their potential for environmental damage.[3] Consequently, a great deal of research is currently on-going to find alternative methods to achieve antifouling and/or fouling-release surfaces.[4-7] Additional interest in this area has been generated by the many applications of antifouling surfaces to the biomedical community.[8-11] Two recent reviews have even managed to unify these approaches into one coherent discussion of antifouling and fouling-release properties.[12, 13]

Due to this wide range of ongoing research, the base of knowledge concerning fouling organisms and methods to deter their settlement and facilitate their release is constantly evolving. A great deal of focus has been on controlling the wettability of coatings through tuning of surface chemistry, with successful antifouling and/or

fouling-release behavior demonstrated for both hydrophobic and hydrophilic coatings. Hydrophobic poly(dimethyl siloxane) (PDMS) coatings have demonstrated excellent fouling release properties as a result of their low surface energy in conjunction with their low modulus and elasticity.[14-16] Other promising hydrophobic coatings for fouling control applications have included perfluoropolyether-based random terpolymers[17] and poly(styrene)-*block*-poly(isoprene) block copolymers containing fluorinated side chains.[18] Hydrophilic coatings for fouling prevention meanwhile have generally focused on either the use of poly(ethylene glycol) (PEG), known for its exceptional resistance to protein adsorption and cell adhesion,[19-21] in various applications. Zwitterionic materials have also demonstrated exceptional fouling resistance.[22, 23]

This leads us to the question: Is fouling control simply a question of selecting the correct hydrophobic or hydrophilic surface treatment for the application? Unfortunately, a recent study documented a limitation in pursuing a strictly hydrophobic or hydrophilic approach to marine fouling control. Krishnan et al. profiled the fouling settlement and release of two complementary ubiquitous types of marine algae against a range of hydrophobic and hydrophilic coating surfaces.[24] While hydrophilic block copolymer coatings containing PEG side chains were found to perform extremely well with regards to the release of *Navicula* diatoms, hydrophobic fluorinated block copolymer and PDMS coatings were found to perform much better with respect to removal of sporelings of the green alga *Ulva*. Thus, much recent work has focused on the production of ambiguous amphiphilic coatings able to present both hydrophobic and hydrophilic moieties at the surface. Gudipati et al. produced hyperbranched polymers containing both fluorinated and PEGylated groups that achieved both low protein adsorption and high fouling release at an optimal composition of hydrophobic and hydrophilic monomers.[25] More recently, Ober and

coworkers reported the development of several surface active block copolymers with amphiphilic side chains derived from a non-ionic ethoxylated fluorosurfactant capable of both resisting and releasing *Ulva* and *Navicula*, and also deterring barnacle settlement.[26-28] Additionally, similar fluorinated side chain surface active block copolymers reported by Martinelli et al. also demonstrated exceptional fouling release properties with regards to algal marine fouling.[29]

These results clearly demonstrate the potential of using amphiphilic coatings to combat marine fouling. All the systems described however relied on fluorinated moieties to impart hydrophobicity to the amphiphilic system however. This observation led us to the question: What antifouling and/or fouling-release performance would be realized for coatings based on amphiphilic groups containing a hydrophobic moiety that was not fluorinated? Thus, we will report the synthesis, characterization and biofouling performance with respect to the green alga *Ulva* of three different surface active block copolymers (SABCs) derived from the grafting of various nonionic surfactants to a specially designed polystyrene-*block*-poly(ethylene-*ran*-butylene)-*block*-poly(isoprene) (PS-*b*-P(E/B)-*b*-PI) ABC triblock precursor copolymer. Particular attention will be given to surface characterization of the resultant SABCs using X-ray photoelectron spectroscopy (XPS) and dynamic water contact angle analysis.

Experimental Section:

Materials

The polystyrene$_{8K}$-*block*-poly(ethylene-*ran*-butylene)$_{25K}$-*block*-polyisoprene$_{10K}$ (PS_{8K}-*b*-$P(E/B)_{25K}$-*b*-PI_{10K}) triblock precursor copolymer was produced using anionic polymerization and subsequent catalytic hydrogenation by Kraton Polymers at large scale (~ 0.5 kg) to facilitate preparation of SABCs.

3-*meta*-Chloroperoxybenzoic acid (*m*CPBA, ClC_6H_4COOOH, FW 172.57, 77%), boron trifluoride diethyl etherate ($BF_3•Et_2O$, $BF_3•O(CH_2CH_3)_2$, FW 141.93, 99.9%), Brij 56 (registered trademark of Croda International PLC, $CH_3(CH_2)_{15}(OCH_2CH_2)_nOH$, n ~ 10, $M_n \approx 683$), Tergitol NP-9 (registered trademark of Union Carbide Chemicals and Plastics Technology Corporation, $CH_3(CH_2)_8C_6H_4(OCH_2CH_2)_9OH$, FW 616.82), and anhydrous chloroform ($CHCl_3$) were purchased from Sigma Aldrich and used as received with no further purification. Silwet L-408 ($[(CH_3)_3SiO]_2CH_3Si(CH_2)_3(OCH_2CH_2)_nOH$, n ~ 11, $M_n \approx 720$) was generously provided by Momentive Performance Materials and used as received. Chloroform, dichloromethane (CH_2Cl_2), methanol (CH_3OH), toluene, 6.25 N sodium hydroxide (NaOH), 96% sulfuric acid (H_2SO_4), 30 wt % hydrogen peroxide (H_2O_2) in water, 95% ethanol (CH_3CH_2OH) and all other reagents were used as received.

3-(Glycidoxypropyl)-trimethoxysilane (GPS, 99%) was purchased from Gelest and used as received. Polystyrene-*block*-poly(ethylene-*ran*-butylene)-*block*-polystyrene (SEBS) triblock thermoplastic elastomers (Kraton G1652M) and SEBS grafted with maleic anhydride (MA-SEBS, Kraton FG1901X) were generously provided by Kraton Polymers.

Polymer Synthesis and Characterization

Surface active block copolymers were produced through a straight-forward two step modification of the Kraton PS_{8K}-*b*-$P(E/B)_{25K}$-*b*-PI_{10K} precursor polymer depicted in Figure 6.1, in similar fashion to that previously reported in Weinman et al.[28] Functionalization of the PI block of the triblock precursor was achieved through epoxidation of the residual alkene groups followed by subsequent catalytic ring-opening etherification reactions using non-ionic surfactant alcohols carrying amphiphilic functionality.

In a typical epoxidation reaction, the PS_{8K}-*b*-$P(E/B)_{25K}$-*b*-PI_{10K} SABC precursor polymer (5 g, 14.5 mmol of reactive isoprene sites) was dissolved in 100 mL of dichloromethane in a round bottomed flask. 3-chloroperoxybenzoic acid (*m*CPBA, 3.9 g, 17.4 mmol) was added to the mixture, and the solution was stirred vigorously for 5 hours at room temperature. Subsequently, the polymer was precipitated in methanol, collected by filtration, and reprecipitated from dichloromethane to remove residual *m*CPBA and its respective byproducts. The white, rubbery product was dried at room temperature under reduced pressure for 48 hours to remove remaining solvent.

^{1}H NMR for epoxidized PS_{8K}-*b*-$P(E/B)_{25K}$-*b*-PI_{10K} (300 MHz, $CDCl_3$, δ): 6.57, 7.07, (5H, styrene), 2.66 (br s, 1H, epoxidized isoprene, -CH_2**H**$COC(CH_3)CH_2$-), 0.80, 1.07, 1.22, 1.45, 1.57 (back-bone). IR (dry film) υ_{max} (cm^{-1}): 2925, 2850 (C-H stretching); 1470 (C-H bending); 1070 (C-O stretching); 880 (C-O-C stretching); 700 (C-H bending, aromatic).

To produce ether-linked side chain surface active block copolymers, 2.1 g of epoxidized PS_{8K}-*b*-$P(E/B)_{25K}$-*b*-PI_{10K} (5.8 mmol of epoxide) was taken in a round bottom flask in conjunction with a four times molar excess (23.2 mmol) of side-chain precursor non-ionic surfactant alcohol (Brij 56, Tergitol NP-9, or Silwet L-408; figure 6.2). The reactants were purged with argon, and subsequently dissolved in ca. ~ 150 mL of anhydrous chloroform. Activated molecular sieves were added to the reaction mixture and it was allowed to sit for ca. ~ 12 h to optimize the adsorption of water. Etherification was performed through the addition of boron trifluoride diethyl etherate catalyst (0.345 g, 2.4 mmol) followed by vigorous stirring at room temperature for at least 48 hours. Following the reaction, 6.25 N sodium hydroxide was added to quench any residual boron catalyst and the reaction mixture was concentrated under reduced pressure using a rotary evaporator. The resultant surface active triblock copolymers were precipitated into methanol. The SABCs were collected by filtration and

subsequently reprecipitated twice from chloroform to remove additional residual surface active side-chain alcohol precursors. Finally, the finished samples were dried under reduced pressure at room temperature for 48 hours to fully remove residual solvent.

^{1}H NMR for PS_{8K}-*b*-$P(E/B)_{25K}$-*b*-PI_{10K} functionalized with Brij 56 side chains (300 MHz, $CDCl_3$, δ): 6.58, 7.10, (5H, styrene), 3.65 (br s, 40H, -(O**CH_2CH_2)$_{10}$**-; 3.43 (t, 2H, -$(CH_2CH_2O)_{10}$**CH_2**$(CH_2)_{14}$-); 0.82, 1.06, 1.24, 1.82 (31H, **$CH_3(CH_2)_{14}$**CH_2- of Brij 56 side chain, and back-bone). IR (dry film) υ_{max} (cm^{-1}): 3480 (O-H stretching); 2930, 2855 (C-H stretching); 1460, 1380 (C-H bending); 1115 (C-O stretching); 765, 700 (C-H bending, aromatic).

^{1}H NMR for PS_{8K}-*b*-$P(E/B)_{25K}$-*b*-PI_{10K} functionalized with Tergitol NP-9 side chains (300 MHz, $CDCl_3$, δ): 6.56, 6.84, 7.10, (5H, styrene; 4H, Tergitol NP-9 side chain), 4.10 (t, 2H, -C_6H_4O**CH_2**CH_2O-); 3.85 (t, 2H, -$C_6H_4OCH_2$**CH_2**O-); 3.66 (br m, -$C_6H_4OCH_2CH_2(O$**CH_2CH_2**$)_8$-); 0.84, 1.06, 1.24, 1.75 (19H, **$CH_3(CH_2)_8$**- of Tergitol NP-9 side chain, and back-bone). IR (dry film) υ_{max} (cm^{-1}): 3510 (O-H stretching); 2925, 2860 (C-H stretching); 1460, 1380 (C-H bending); 1120 (C-O stretching); 770, 700 (C-H bending, aromatic).

^{1}H NMR for PS_{8K}-*b*-$P(E/B)_{25K}$-*b*-PI_{10K} functionalized with Silwet L-408 side chains (300 MHz, $CDCl_3$, δ): 6.58, 7.08, (5H, styrene), 3.65 (br s, 44H, -(O**CH_2CH_2**$)_{11}$-); 3.40 (t, 2H, -$(CH_2)_2$**CH_2**$(OCH_2CH_2)_{11}$-); 0.83, 1.06, 1.25, 1.81 (back-bone), 0.43 (m, 2H, $[(CH_3)_3SiO]_2CH_3Si$**CH_2**$(CH_2)_2$-); 0.08 (br s, 18H, [**$(CH_3)_3$**$SiO]_2CH_3Si(CH_2)_3$-); 0.00 (s, 3H, $[(CH_3)_3SiO]_2$**CH_3**$Si(CH_2)_3$-). IR (dry film) υ_{max} (cm^{-1}): 3480 (O-H stretching); 2925, 2855 (C-H stretching); 1460, 1360 (C-H bending); 1110 (C-O stretching); 765, 700 (C-H bending, aromatic).

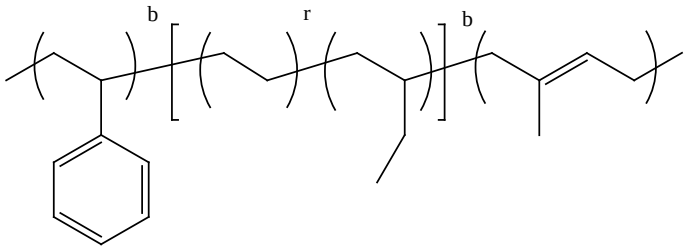

PS-*b*-P(E/B)-*b*-PI Triblock Copolymer

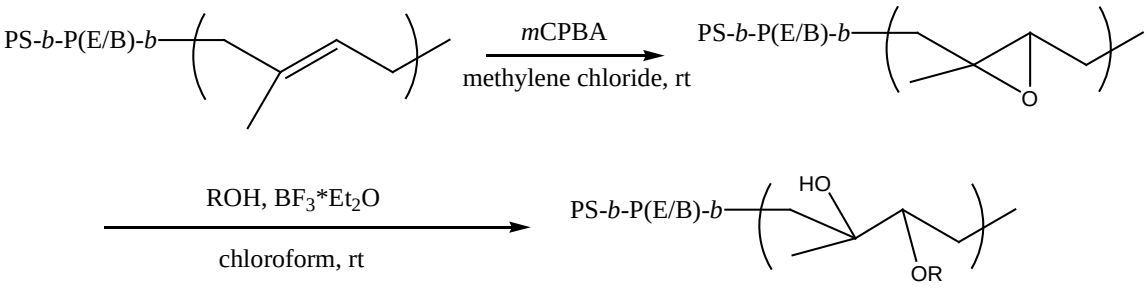

Figure 2.1. Synthesis of ether-linked surface active triblock copolymers containing Brij 56, Tergitol NP-9, or Silwet L-408 derived side chains. ROH = $CH_3(CH_2)_{15}(OCH_2CH_2)_nOH$, n ~ 10 (Brij 56), $CH_3(CH_2)_8C_6H_4(OCH_2CH_2)_9OH$ (Tergitol NP-9), or $[(CH_3)_3SiO]_2CH_3Si(CH_2)_3(OCH_2CH_2)_nOH$, n ~ 11 (Silwet L-408).

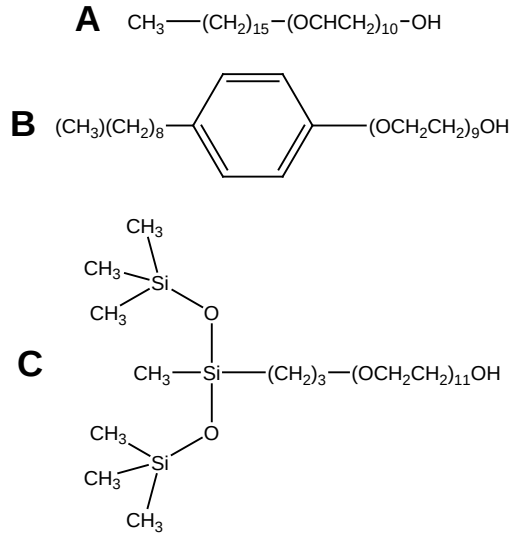

Figure 6.2. Chemical structures of A) Brij 56, B) Tergitol NP-9, and C) Silwet L-408 non-ionic surfactant starting materials.

^{1}H NMR spectra were recorded using a Varian Gemini spectrometer with deuterated chloroform. The IR spectra of the polymers cast as films from tetrahydrofuran (THF) solution on sodium chloride plates was collected using a Mattson 2020 Galaxy Series FTIR spectrometer. Gel permeation chromatography of a THF solution of polymers (1 mg/mL) was carried out using four Waters Styragel HT columns operating at 40 °C in conjunction with Waters 490 ultraviolet (λ = 254 nm) and Waters 410 refractive index detectors. The molecular weight range of the columns was from 500 to 10^{7} g/mol. THF was used as the eluent at a flow rate of 1 mL/min, and toluene was used as a marker for flow calibration.

Surface Preparation and Characterization

Surfaces for XPS and dynamic water contact angle analysis were prepared on silicon wafers by spin-coating 3% (w/v) solutions of SABCs in toluene at 2000 rpm for 60 seconds. All surfaces prepared for study were annealed in a vacuum oven at reduced pressure at 120 °C for at least 12 h followed by slow cooling to room temperature.

XPS measurements were performed using a Kratos Axis Ultra Spectrometer (Kratos Analytical, Manchester, UK) with a monochromatic Al Kα X-ray source (1486.6 eV) operating at 225 W under a vacuum of 1.0 × 10-8 Torr. Charge compensation was carried out by injection of low-energy electrons into the magnetic lens of the electron spectrometer. The pass energy of the analyzer was set at 40 eV for high-resolution spectra and 80 eV for survey scans, with energy resolutions of 0.05 and 1 eV, respectively. The spectra were analyzed using CasaXPS v.2.3.12Dev4 software. The C-C peak at 285 eV was used as the reference for binding energy calibration.

Water contact angles were measured using a contact angle goniometer (AST Products, Inc. model VCA Optima XE) at room temperature. Dynamic water contact angle measurements were performed through the addition and retraction of a small drop of water (ca. ~ 2 μL) on the surface. The advancing and receding contact angle behavior was digitally recorded and image analysis software was used to measure the angles.

Preparation of Surfaces for Biofouling Assays

Glass slides for biofouling assays with the green alga *Ulva* were prepared as previously reported.[30] Kraton G1652M was used as the thermoplastic elastomer base layer in the multilayer coating to control bulk modulus. For the biofouling assay, glass microscope slides coated with a polydimethylsiloxane elastomer (PDMS), Silastic® T2 (Dow Corning) prepared as described in Schumacher et al.[31] and G1652M SEBS were used as standards. PDMS was used as a control due to its excellent release properties against macrofouling organisms such as *Ulva* sporelings, while the G1652M base layers were used to highlight the differences in performance between the base layer when used alone and when used in the multilayer coating formulations.

Settlement of *Ulva* Zoospores and Strength of Attachment of *Ulva* Sporelings

Nine replicate test samples were leached in a 30 L tank of recirculating deionized water at ~ 20° C for 48 h. The slides were equilibrated in artificial seawater 1 h prior to the start of the experiments. Zoospores were released from fertile plants of *Ulva linza* and prepared for assay as described previously.[32] Ten mL of zoospore suspension (1×10^6 spores per mL), was pipetted into 12 compartments of Quadriperm polystyrene culture dishes (Greiner Bio-One), each containing a test slide. The test slides were incubated in the dark at ~ 20° C for 1 h and gently washed in

seawater to remove zoospores that had not settled. Three slides were fixed using 2.5% glutaraldehyde in seawater and these replicates were used to quantify the density of zoospores attached to the surfaces as previously reported.[33]

Ulva sporelings (young plants) were cultured on 6 replicates of each coating.[34] After washing, the samples were transferred to dishes containing nutrient enriched seawater for 7 days. Growth was estimated by direct measurement of fluorescence from chlorophyll contained within the chloroplasts of the sporelings using a Tecan plate reader (GENios Plus).[35] Fluorescence was recorded as Relative Fluorescence Units (RFU) from direct readings. The slides (6 replicates) were read from the top, 300 readings per slide, taken in blocks of 30×10. The strength of attachment of the sporelings was determined by jet washing using a water jet.[36] The range of impact pressures used was chosen to provide maximum information on the strength of attachment of the sporelings. RFU readings (80 per slide) were taken from the central part of the slide that was exposed to the water jet. Percentage removal was calculated from the mean RFU reading before and after exposure to the water jet. From the percentage removal data, the critical water pressure required to remove 50% of the sporelings was derived.

Results and Discussion:

Polymer Synthesis and Characterization

The synthesis of this series of nonionic surfactant derived amphiphilic SABCs was monitored using both infrared spectroscopy and ^{1}H NMR spectroscopy. Following the epoxidation reaction, ^{1}H NMR spectroscopy clearly showed that there was no longer evidence of any alkene protons, and a significant peak at ca. ~ 2.7 ppm appeared indicating the presence of protons adjacent to the newly formed oxirane rings on the PI backbone. Additionally, infrared spectroscopy clearly showed the

appearance of a C-O-C stretching peak at roughly 880 cm^{-1} associated with the epoxide ring. This indicated that all of the residual unsaturated alkene groups were successfully converted to their epoxidized form. Subsequent catalytic ring-opening using Brij 56, Tergitol NP-9, or Silwet L-408 non-ionic surfactant alcohol led to the disappearance of the epoxide peak in the ^{1}H NMR spectra. Further analysis of the ^{1}H NMR spectra demonstrated the appearance of peaks at ca. ~ 3.6 and 3.4 ppm indicating the presence of oligoethylene glycol groups for the Brij 56 functionalized sample, indicating successful attachment of the amphiphilic side chain. For the Tergitol NP-9 sample, similar peaks for the oligoethylene glycol groups of the side chain were scene at ca. ~ 4.1, 3.9, and 3.7 ppm, in addition to the appearance of a third aromatic proton peak at ca. ~ 6.8 ppm corresponding to the aromatic protons of the Tergitol NP-9 side chain. Finally, the Silwet L-408 sample showed oligoethylene glycol protons at ca. ~ 3.6 and 3.4 ppm (similar to the Brij 56 derived sample), but additional peaks at 0.43 and 0.08 ppm were present from the $–CH_3$ groups attached to Si atoms present in the side chain. These findings were supported by infrared spectroscopy which demonstrated the appearance of a strong O-H stretching peak between 3300 and 3500 cm^{-1}, formed during ring-opening of the epoxy, and a C-O stretching peak at ca ~ 1115 cm^{-1}, formed from the etherification attachment of side chains, for all three samples.

Table 6.1 demonstrates the percentage of attachment of the three non-ionic surfactants relative to epoxy functionality in the epoxidized PS-*b*-P(E/B)-*b*-PI precursor. The percentage of non-ionic surfactant successfully attached was calculated by integration of ^{1}H NMR spectra. Specifically, this value was obtained by comparing the total amount of aromatic protons (associated with the PS block, or in the case of Tergitol NP-9, the PS block and the attached side chain) in the ^{1}H NMR spectra with the number of protons associated with the PEGylated part of the amphiphilic non-ionic

surfactant derived side chain. The percent attachment of side chain relative to the amount of epoxy groups in the PS_{8K}-*b*-$P(E/B)_{25K}$-*b*-PI_{10K} precursor was found to be 18% for Brij 56, 26% for Silwet L-408, and 50% for Tergitol NP-9. Using GPC, the dispersity index (DI) of the samples was found to increase from 1.06 for the PS-*b*-P(E/B)-*b*-PI precursors to 1.12 when epoxidized. Finished, substituted SABC containing Brij 56 and Tergitol NP-9 side chains generally had a PDI between 1.2 and 1.3. The sample produced from Silwet L-408 experienced a rise in PDI to ca. ~ 1.6. This rise in PDI for all three samples combined with the observation of complete reaction of the epoxide despite less than 100% attachment of non-ionic surfactant side chain suggests that some of the epoxide was most likely lost to intermolecular cross linking reactions between epoxide rings. Additionally, intramolecular reactions in combination with epoxide ring-opening by any residual water molecules left in the reaction mixture may have contributed to this relatively low observed attachment. The additional increase in DI for the Silwet L-408 sample suggests that an additional undesirable side reaction likely enhanced cross linking.

Dynamic Water Contact Angle Analysis

Dynamic water contact angle analysis of spun coat SABC samples on Si wafers indicated the presence of low surface energy, hydrophobic moieties at the surface for all three side chain polymers with $\theta_{w,\ advancing}$ ranging from 102° to 108°. High contact angle hysteresis was seen for all three samples, with $\theta_{w,\ receding}$ measured between 22° and 25°, suggesting the facile reordering of the side chains to orient the hydrophilic PEGylated groups at the surface. It was notable that both advancing and receding water contact angle measurements for all three samples were not statistically different, demonstrating that all three non-ionic surfactant derived samples had very similar wettability characteristics.

Table 6.1. Percent attachment of each non-ionic surfactant side chain relative to epoxy in the precursor polymer, and the measured advancing and receding water contact angles for each sample.

Grafted Side Chain	% Attachment	$\theta_{w,a}$	$\theta_{w,r}$
Brij 56	18	102 ± 3	25 ± 2
Tergitol NP-9	50	108 ± 3	22 ± 1
Silwet L-408	26	107 ± 2	22 ± 3

X-ray Photoelectron Spectroscopy (XPS)

Figure 6.3 shows high-resolution C 1s XPS spectra of the amphiphilic SABC derived from the PS_{8K}-*b*-$P(E/B)_{25K}$-*b*-PI_{10K} precursor with attached Brij 56 non-ionic surfactant side chains taken at two different incident angles (0° and 75°). The spectra are normalized so that the total area under the carbon peaks is equal to unity. All samples showed a strong intensity peak from C=C and C-C near 285 eV, most likely indicative of a combination of the polymer backbone and the low surface energy aliphatic section of the Brij 56 derived side chain. Additionally, a pronounced shoulder at ca. ~ 287 eV associated with C-O became increasingly apparent in the spray coated samples, suggesting the presence of the PEGylated moieties of the Brij 56 side-chain near the surface. Analysis of the XPS survey scans given in figure 6.4 show the surfaces dominated by the peaks associated with C 1s and O 1s, located at ca. ~ 285 eV and ca. ~ 535 eV respectively. The spray coated samples depicted in figures 6.4C and 6.4D also showed unexpected trace contamination of fluorine (indicated by F 1s, ca. ~ 685 eV) and additional contamination from Si (indicated by Si 2p, ca. ~ 150 eV and ca. ~ 100 eV). This was likely an artifact due to a combination of laboratory glassware and/or Schlenk line contamination coupled with an annealing oven setup

contaminated with small molecules and pump oil. Nevertheless, the similarities in the C 1s high resolution spectra between the samples produced by spray and spin coating suggests that this contamination did not play a major role in influencing ultimate surface characteristics.

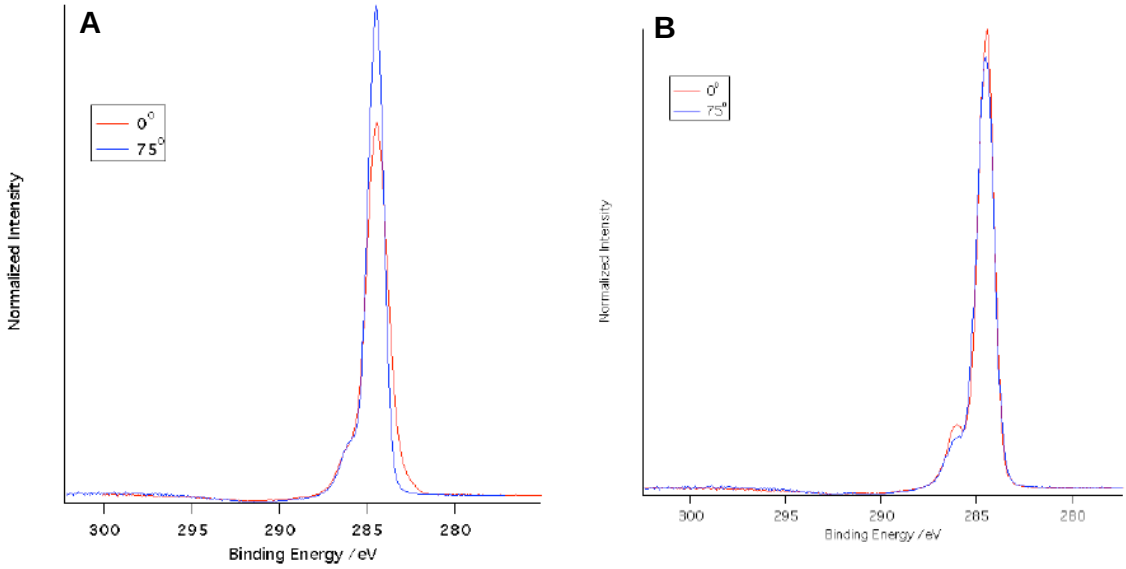

Figure 6.3. High resolution C 1s XPS spectra of PS_{8K}-*b*-$P(E/B)_{25K}$-*b*-PI_{10K} SABC precursor polymer with attached Brij 56 non-ionic surfactant side chains for: A) sample spun on Si wafer and B) spray coated multi-layer coating for biofouling assay on glass slides.

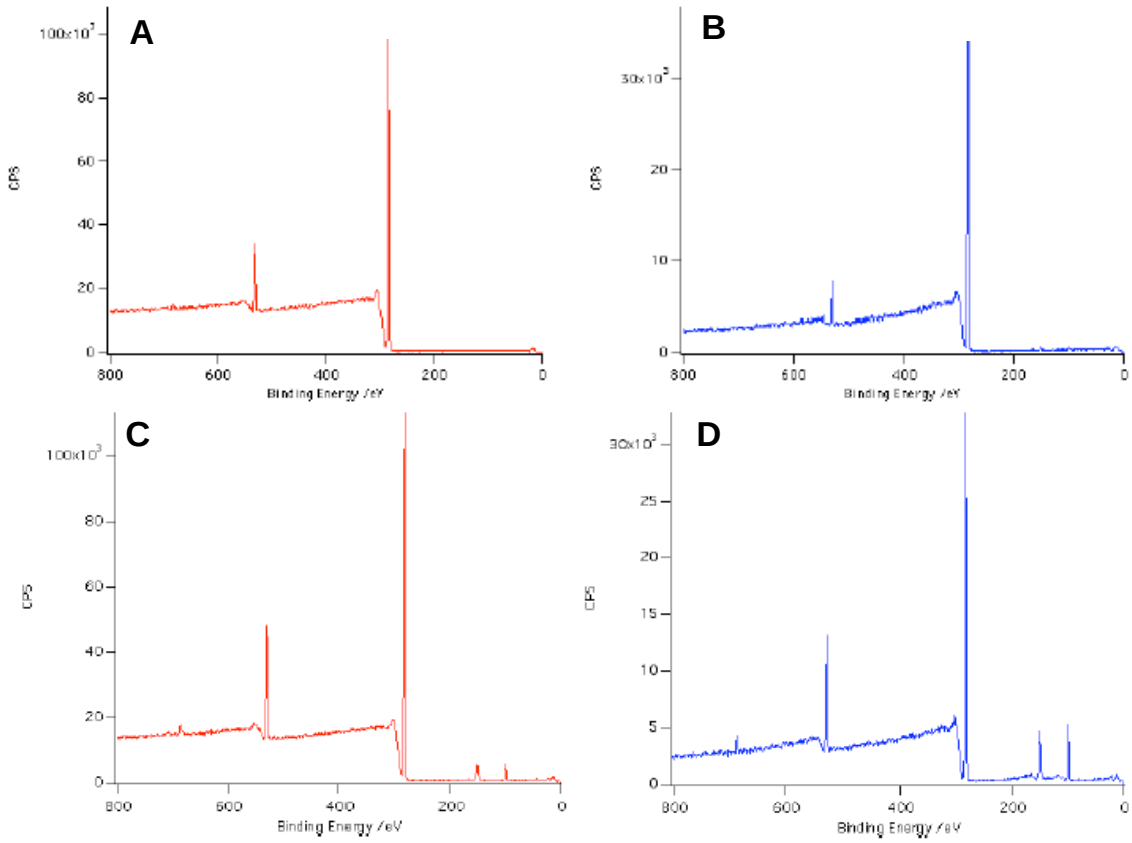

Figure 6.4. XPS survey scans of PS_{8K}-*b*-$P(E/B)_{25K}$-*b*-PI_{10K} SABC precursor polymer with attached Brij 56 non-ionic surfactant side chains for: A) sample spun on Si wafer, 0° incident angle and B) 75° incident angle; C) spray coated multi-layer coating for biofouling assay on glass slides, 0° incident angle and D) 75° incident angle.

Meanwhile, figure 6.5 shows high-resolution C 1s XPS spectra of the amphiphilic SABC derived from the PS_{8K}-*b*-$P(E/B)_{25K}$-*b*-PI_{10K} precursor with attached Tergitol NP-9 non-ionic surfactant side chains taken at two different incident angles (0° and 75°). The spectra are normalized so that the total area under the carbon peaks is equal to unity. Again, similar to the Brij 56 derived sample, all samples showed a strong intensity peak from C=C and C-C near 285 eV, most likely indicative of a combination of the polymer backbone and the low surface energy aliphatic section of the Tergitol NP-9 derived side chain. Additionally, a pronounced shoulder at ca. ~ 287 eV indicative of C-O again became increasingly apparent in the spray coated

samples, suggesting the presence of the PEGylated moieties of the Tergitol NP-9 side-chain near the surface. While the intensity of this shoulder associated with the C-O peak was very similar to what was seen for the Brij 56 derived sample, the peak intensity was noticeably higher for the spray coated samples of the Tergitol NP-9 derived SABC than for the Brij 56 derived SABC, suggesting that the spray coating process had an unique effect on the segregation of the oligo(ethylene glycol) moieties of the Tergitol NP-9 side chains to the surface. Analysis of the XPS survey scans given in figure 5 again showed the surfaces dominated by the peaks associated with the C 1s and O 1s peaks, at ca. ~ 285 eV and ca. ~ 535 eV respectively. Again, the spray coated samples depicted in figures 5C and 5D also showed unexpected trace contamination from F 1s (ca. ~ 685 eV) and Si 2p (ca. ~ 150 eV and ca. ~ 100 eV). This was likely due to the same reasons previously proposed in the discussion of the Brij 56 side chain SABC analysis.

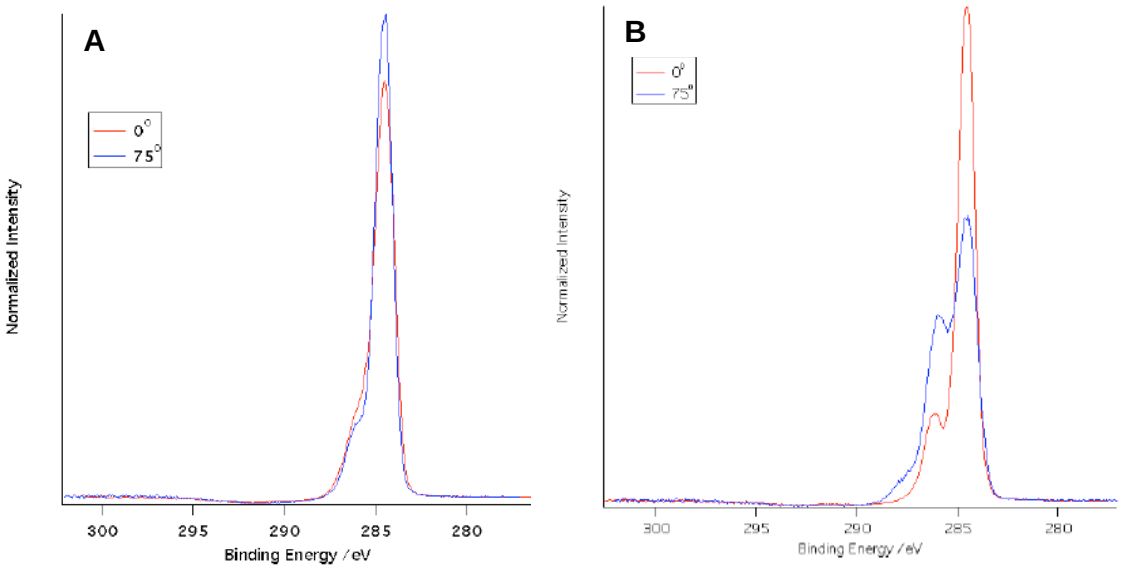

Figure 6.5. High resolution C 1s XPS spectra of PS_{8K}-*b*-$P(E/B)_{25K}$-*b*-PI_{10K} SABC precursor polymer with attached Tergitol NP-9 non-ionic surfactant side chains for: A) sample spun on Si wafer and B) spray coated multi-layer coating for biofouling assay on glass slides.

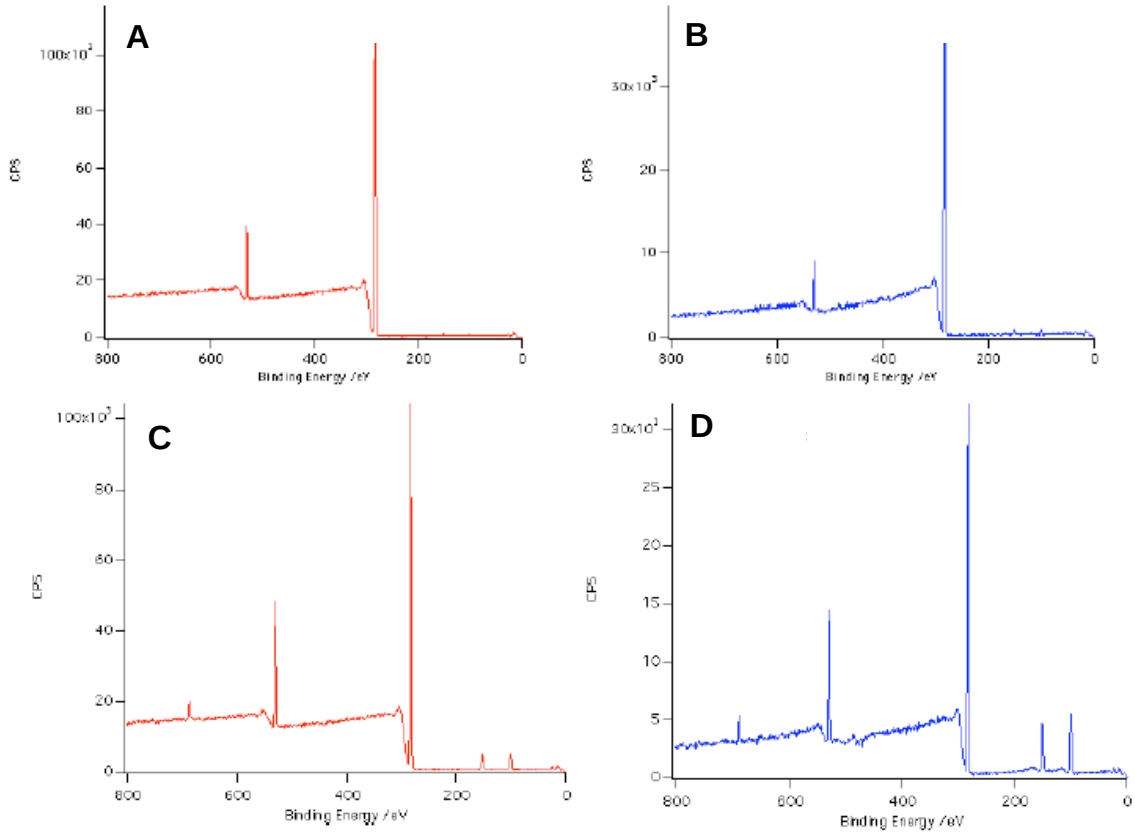

Figure 6.6. XPS survey scans of PS_{8K}-*b*-$P(E/B)_{25K}$-*b*-PI_{10K} SABC precursor polymer with attached Tergitol NP-9 non-ionic surfactant side chains for: A) sample spun on Si wafer, 0° incident angle and B) 75° incident angle; C) spray coated multi-layer coating for biofouling assay on glass slides, 0° incident angle and D) 75° incident angle.

Finally, figure 6.7 shows high-resolution C 1s XPS spectra of the amphiphilic SABC derived from the PS_{8K}-*b*-$P(E/B)_{25K}$-*b*-PI_{10K} precursor with attached Silwet L-408 non-ionic surfactant side chains taken at two different incident angles (0° and 75°). The spectra are normalized so that the total area under the carbon peaks is equal to unity. Again, similar to the Brij 56 and Tergitol NP-9 derived samples, both the sample spun coat on Si and spray coated on glass slides showed a strong intensity peak from C=C and C-C near 285 eV. In this case, this is likely due primarily to the polymer back bone, with a possible minor contribution form the aliphatic -CH_2-

groups in the Silwet L-408 side chain. The same pronounced shoulder at ca. ~ 287 eV associated with C-O, suggesting the presence of PEG groups, was present for the sample produced by spin coating (at a much higher intensity than was seen for other samples), but appeared to be nearly completely absent from the spray coated sample. This was in stark contrast to the other two samples derived from the Brij 56 and Tergitol NP-9 non-ionic surfactants that had clear evidence of this peak in the spray coated samples, but much less contribution in those formed by spin coating. This again suggests that the surface formed from all three of these SABC samples may be extremely dependent on the route of formation, with different processing capable of producing surfaces with significantly different functionality. Analysis of the XPS survey scans given in figure 6.8 show the surfaces dominated by the peaks associated with the C 1s and O 1s peaks, located at ca. ~ 285 eV and ca. ~ 535 eV respectively, as expected. Additionally, silicon 2p peaks at ca ~ 150 eV and ca. ~ 100 eV were present in all samples as expected, due to the presence of Si in the Silwet L-408 side chain. The spectra of the spray coated samples depicted in Figures 6.8C and 6.8D showed a minor unexpected peak at ca. ~ 500 eV, again likely an artifact of a trace impurity introduced during sample preparation.

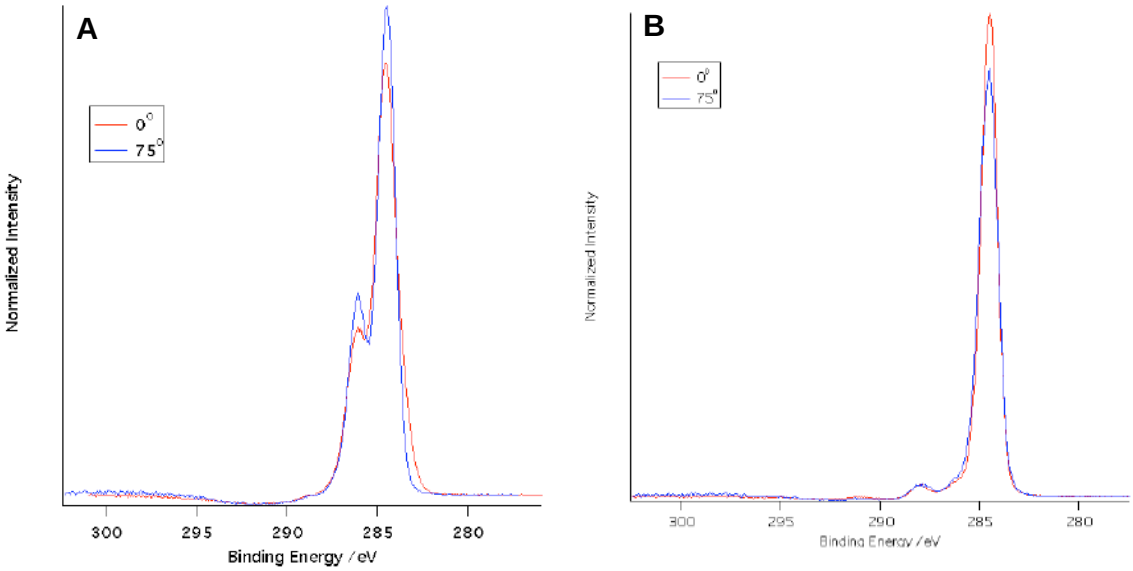

Figure 6.7. High resolution C 1s XPS spectra of PS_{8K}-*b*-$P(E/B)_{25K}$-*b*-PI_{10K} SABC precursor polymer with attached Silwet L-408 non-ionic surfactant side chains for: A) sample spun on Si wafer and B) spray coated multi-layer coating for biofouling assay on glass slides.

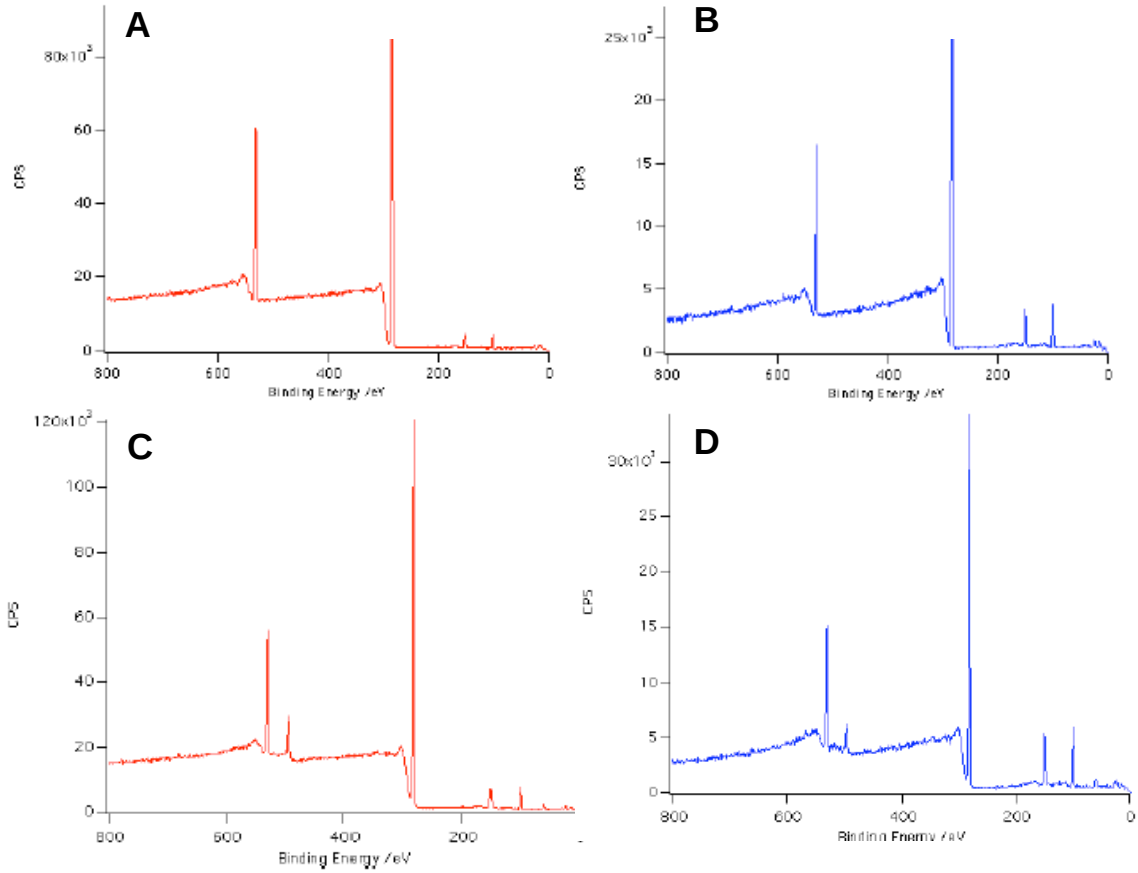

Figure 6.8. XPS survey scans of PS_{8K}-*b*-$P(E/B)_{25K}$-*b*-PI_{10K} SABC precursor polymer with attached Silwet L-408 non-ionic surfactant side chains for: A) sample spun on Si wafer, 0° incident angle and B) 75° incident angle; C) spray coated multi-layer coating for biofouling assay on glass slides, 0° incident angle and D) 75° incident angle.

Settlement of *Ulva* Spores and Release of *Ulva* Sporelings

Figure 6.9A shows the settlement density of *Ulva* spores on PDMS, G1652M SEBS and amphiphilic SABCs derived from the PS_{8K}-b-$P(E/B)_{25K}$-b-PI_{10K} precursor and Brij 56, Tergitol NP-9, or Silwet L-408 non-ionic surfactants. For the experimental coatings, the lowest settlement was shown on the surface incorporating the Brij 56 non-ionic surfactant. *Ulva* spores are known to preferentially settle on hydrophobic, low energy surfaces.[37] This was true for the PDMS control surface, which showed the greatest settlement of *Ulva* spores. Dynamic water contact angle

analysis indicated that all three non-ionic surfactant derived SABCs had similar advancing and receding water contact angles, indicating a hydrophobic surface in a non-polar environment, capable of reordering and becoming hydrophilic once placed in a polar environment such as water. The amount of *Ulva* spore settlement was dependent on the type non-ionic surfactant incorporated in the SABC coating however despite the similar wettability parameters of all three samples. Settlement of *Ulva* spores was minimized on the Brij 56 derived SABC, with greatest settlement observed for the Tergitol NP-9 derived SABC. The SABC derived from Silwet L-408 experienced settlement intermediate to the two other coatings. This clearly indicates that factors beyond wettability and contact angle hysteresis played a significant role in dictating *Ulva* spore settlement in this study. Meanwhile, the growth of *Ulva* sporelings, depicted in Figure 6.9B, largely reflected the number of spores settled, confirming no unexpected toxicity from the experimental coatings. Finally, the percentage removal of *Ulva* sporelings from the experimental coatings at a range of applied water jet pressures is shown in figure 6.9C in conjunction with critical applied water jet stress values for 50% removal of *Ulva* sporelings given in table 6.2. Sporelings were removed from the PDMS standard at low water jet pressures reflecting the fouling-release characteristics of this low surface energy elastomer.[24, 35] More remarkable however was the extreme difference in fouling release observed for the Brij 56 derived multi-layer SABC coating versus those derived from Silwet L-408 and Tergitol NP-9. The SABC derived from the Brij 56 non-ionic surfactant demonstrated more robust release of *Ulva* sporelings than the PDMS control. The coatings derived from both Silwet L-408 and Tergitol NP-9 meanwhile demonstrated removal only on the order of the SEBS control, indicating that these two experimental coatings were not functioning as effective foul release materials with regards to *Ulva* sporelings. This observation when taken in conjunction with the settlement results for

these coatings clearly indicates that non-ionic surfactant structure appears to have a much greater effect on fouling release behavior than overall surface wettability parameters. These preliminary results suggest that this is an area worth additional exploration due to the large range of commercial non-ionic surfactants available incorporating different ratios of PEGylated and hydrocarbon moieties. Room for further optimization of these potential hybrid marine anti-fouling/fouling-release materials may exist. Furthermore, this suggests that excellent fouling release behavior for amphiphilic materials not incorporating fluorinated moieties can be realized.

Table 6.2. Applied critical surface pressures for 50% removal of *Ulva* sporeling biofilm derived from curves in figure 6.9C.

Grafted Side Chain	Estimated surface pressure (kPa) for 50% removal
PDMS	34
G1652M SEBS	152
Brij 56	22
Silwet L-408	185
Tergitol NP-9	160

Figure 6.9. A) The settlement of *Ulva* spores on G1652M SEBS, PDMS and PS_{8K}-*b*-$P(E/B)_{25K}$-*b*-PI_{10K} non-ionic surfactant derived amphiphilic SABCs. Each point is the mean from 90 counts on 3 replicate slides. Bars show 95% confidence limits. B) The growth of *Ulva* sporelings on G1652M SEBS, PDMS and PS_{8K}-*b*-$P(E/B)_{25K}$-*b*-PI_{10K} non-ionic surfactant derived amphiphilic SABCs. Each point is the mean biomass from 6 replicate slides measured using a fluorescence plate reader. Bars show standard error of the mean. C) The removal of *Ulva* sporelings from G1652M SEBS, PDMS and PS_{8K}-*b*-$P(E/B)_{25K}$-*b*-PI_{10K} non-ionic surfactant derived amphiphilic SABCs. Slides were exposed to a water jet over a range of pressures. One slide was used for each pressure.

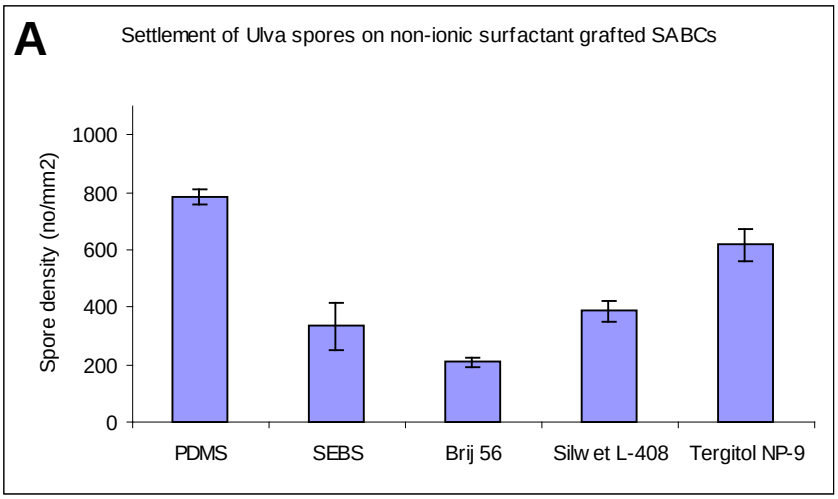
A
Settlement of Ulva spores on non-ionic surfactant grafted SABCs
Spore density (no/mm2)
1000
800
600
400
200
0
PDMS
SEBS
Brij 56
Silw et L-408
Tergitol NP-9

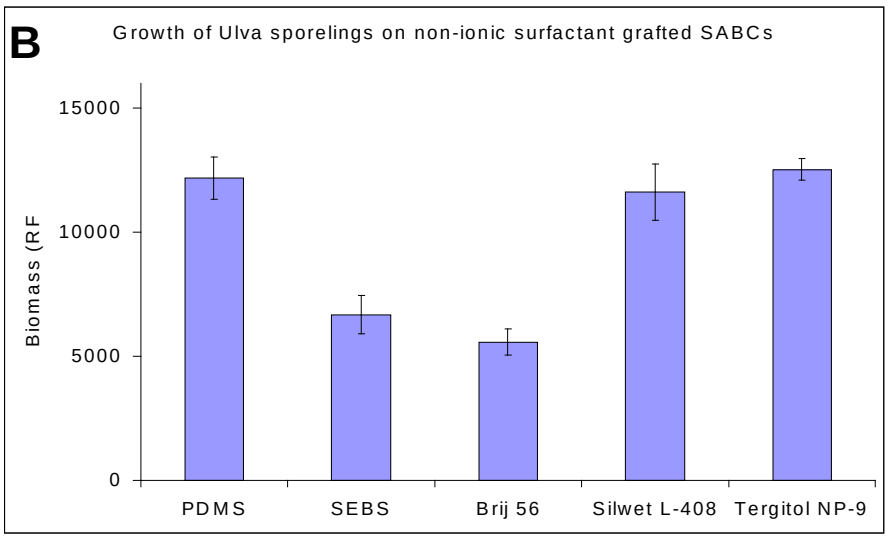
B
Growth of Ulva sporelings on non-ionic surfactant grafted SABCs
Biomass (RF
15000
10000
5000
0
PDMS
SEBS
Brij 56
Silwet L-408
Tergitol NP-9

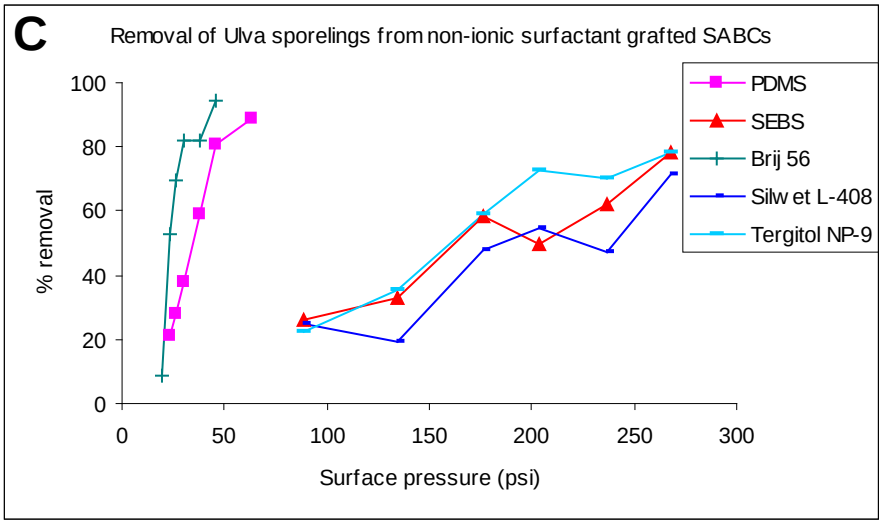
C
Removal of Ulva sporelings from non-ionic surfactant grafted SABCs
% removal
100
80
60
40
20
0
0
50
100
150
200
250
300
Surface pressure (psi)
PDMS
SEBS
Brij 56
Silw et L-408
Tergitol NP-9

Conclusions

Potential coatings for marine antifouling and/or fouling-release applications were developed through chemical modification of a polystyrene-*block*-poly(ethylene-*ran*-butylene)-*block*-polyisoprene ABC triblock copolymers with three different non-ionic surfactants (Brij 56, Silwet L-408, and Tergitol NP-9). Resultant SABCs were obtained through the grafting of these amphiphilic molecules consisting of a low surface energy aliphatic or silicon containing species combined with a hydrophilic PEG group to the polyisoprene block of the precursor polymer. SABC samples were characterized using a combination of infrared spectroscopy and ^{1}H NMR spectroscopy to confirm the successful attachment of the amphiphilic groups. The surfaces of all three polymers showed high water contact angle hysteresis suggesting a dynamic surface capable of significant reorganization. Surface characterization using XPS suggested successful segregation of the amphiphilic side chain to the surface for all three samples. Further analysis comparing samples prepared by spin coating of the SABC on Si wafers to ones prepared by spray coating of the SABC on a SEBS base layer as part of a multilayer coating suggested significant process specific differences in resultant surface chemistry. The SABC prepared from grafted Brij 56 non-ionic surfactant showed both lower settlement and better fouling release of the green alga *Ulva* than the PDMS control samples, but this behavior was not duplicated for the Silwet L-408 or Tergitol NP-9 containing materials. This suggests that despite similarities in wettability based on dynamic water contact angle analysis measurements taken for all three coatings, the chemical structure and/or surface chemistry realized for the different non-ionic surfactants played a much more significant role in both deterring the settlement of and encouraging the release biofouling organisms. The presence of minor surface contamination in the biofouling assay test samples also appeared to have little effect on settlement and release

characteristics since there was no apparent correlation between performance and the amount of contamination present. Additional work should be conducted exploring a wider range of commercially available non-ionic surfactants to try to further understand the correlation between chemical structure of the surface active group and fouling resistance and release.

Acknowledgement

This work was supported by the Office of Naval Research (ONR) through award #N00014-02-1-0170 (CKO and EJK) and N00014-05-1-0134 (JAC and MEC). Additional support was provided by the United States Department of Defense's Strategic Environmental Research and Development Program (SERDP), grant WP #1454. Additionally, EJK acknowledges support from the NSF Polymers Program (DMR-0704539) as well as the use of facilities funded by the NSF-MRSEC program (UCSB MRL, DMR-0520415).

REFERENCES

1 M. E. Callow and J. A. Callow, *Biologist*, 2002, **49**, 1.

2 L. Chromy and K. Uhacz, *Journal of the Oil and Colour Chemists' Association*, 1978, **61**, 39.

3 R. F. Brady, *Journal of Protective Coatings & Linings*, 2003, **20**, 33.

4 D. M. Yebra, S. Kiil, and K. Dam-Johansen, *Prog. Org. Coat.*, 2004, **50**, 75.

5 J. Genzer and K. Efimenko, *Biofouling*, 2006, **22**, 339.

6 L. D. Chambers, K. R. Stokes, F. C. Walsh, and R. J. K. Wood, *Surf. Coat. Technol.*, 2006, **201**, 3642.

7 T. Vladkova, *Journal of the University of Chemical Technology and Metallurgy*, 2007, **42**, 239.

8 C. Werner, M. F. Maitz, and C. Sperling, *J. Mater. Chem.*, 2007, **17**, 3376.

9 N. Wisniewski and M. Reichert, *Colloids and Surfaces B: Biointerfaces*, 2000, **18**, 197.

10 H. Otsuka, Y. Nagasaki, and K. Kataoka, *Advanced Drug Delivery Reviews*, 2003, **55**, 403.

11 J. M. Harris and R. B. Chess, *Nature Reviews Drug Discovery*, 2003, **2**, 214.

12 S. Chen and S. Jiang, *Advanced Materials*, 2008, **20**, 335.

13 S. Krishnan, C. J. Weinman, and C. K. Ober, *J. Mater. Chem.*, 2008, **18**, 3405.

14 A. Beigbeder, P. Degee, S. L. Conlan, R. J. Mutton, A. S. Clare, M. E. Pettitt, M. E. Callow, J. A. Callow, and P. Dubois, *Biofouling*, 2008, **24**, 291.

15 K. J. Wynne, G. W. Swain, R. B. Fox, S. Bullock, and J. Ulik, *Biofouling*, 2000, **16**, 277.

16 R. F. Brady, *Polymers Paint Colour Journal*, 2000, **190**, 18.

17 J. C. Yarbrough, J. P. Rolland, J. M. DeSimone, M. E. Callow, J. A. Finlay, and J. A. Callow, *Macromolecules*, 2006, **39**, 2521.

18 J. P. Youngblood, L. Andruzzi, C. K. Ober, A. Hexemer, E. J. Kramer, J. A. Callow, J. A. Finlay, and M. E. Callow, *Biofouling*, 2003, **19**, 91.

19 K. L. Prime and G. M. Whitesides, *J. Am. Chem. Soc.*, 1993, **115**, 10714.

20 H. Ma, J. Hyun, P. Stiller, and A. Chilkoti, *Advanced Materials*, 2004, **16**, 338.

21 S. Schilp, A. Kueller, A. Rosenhahn, M. Grunze, M. E. Pettitt, M. E. Callow, and J. A. Callow, *Biointerphases*, 2007, **2**, 143.

22 H. Kitano, A. Kawasaki, H. Kawasaki, and S. Morokoshi, *Journal of Colloid and Interface Science*, 2005, **282**, 340.

23 Z. Zhang, T. Chao, S. Chen, and S. Jiang, *Langmuir*, 2006, **22**, 10072.

24 S. Krishnan, N. Wang, C. K. Ober, J. A. Finlay, M. E. Callow, J. A. Callow, A. Hexemer, K. E. Sohn, E. J. Kramer, and D. A. Fischer, *Biomacromolecules*, 2006, **7**, 1449.

25 C. S. F. Gudipati, J. A.; Callow, J. A.; Callow, M. E.; Wooley, K. L., *Langmuir*, 2005, **21**, 3044.

26 S. Krishnan, R. Ayothi, A. Hexemer, J. A. Finlay, K. E. Sohn, R. Perry, C. K. Ober, E. J. Kramer, M. E. Callow, J. A. Callow, and D. A. Fischer, *Langmuir*, 2006, **22**, 5075.

27 C. J. K. Weinman, S.; Park, D.; Paik, M. Y.; Wong, K., Fischer, D. A.; Handlin, D. A., Kowalke, G. L.; Wendt, D. E.; Sohn, K. E.; Kramer, E. J.; Ober, C. K., *PMSE Preprints*, 2007, **96**, 597.

28 C. J. Weinman, J. A. Finlay, D. Park, M. Y. Paik, S. Krishnan, B. R. Fletcher, M. E. Callow, J. A. Callow, D. L. Handlin, C. L. Willis, D. A. Fischer, K. E. Sohn, E. J. Kramer, and C. K. Ober, *Polymeric Materials: Science & Engineering Preprints*, 2008, **98**, 639.

29 E. Martinelli, S. Agostini, G. Galli, E. Chiellini, A. Glisenti, M. E. Pettiitt, M. E. Callow, J. A. Callow, K. Graf, and F. W. Bartels, *Langmuir*, 2008, **24**, 13138.

30 S. Krishnan, R. J. Ward, A. Hexemer, K. E. Sohn, K. L. Lee, E. R. Angert, D. A. Fischer, E. J. Kramer, and C. K. Ober, *Langmuir*, 2006, **22**, 11255.

31 J. F. Schumacher, M. L. Carman, T. G. Estes, A. W. Feinberg, L. H. Wilson, M. E. Callow, J. A. Callow, J. A. Finlay, and A. B. Brennan, *Biofouling*, 2007, **23**, 55.

32 M. E. Callow, J. A. Callow, J. D. Pickett-Heaps, and R. Wetherbee, *Journal of Phycology*, 1997, **33**, 938.

33 M. E. Callow, A. R. Jennings, A. B. Brennan, C. E. Seegert, A. Gibson, L. Wilson, A. Feinberg, R. Baney, and J. A. Callow, *Biofouling*, 2002, **18**, 237.

34 M. K. Chaudhury, J. A. Finlay, J. Y. Chung, M. E. Callow, and J. A. Callow, *Biofouling*, 2005, **21**, 41.

35 F. Casse, E. Ribeiro, A. Ekin, D. C. Webster, J. A. Callow, and M. E. Callow, *Biofouling*, 2007, **23**, 267.

36 J. A. Finlay, M. E. Callow, M. P. Schultz, G. W. Swain, and J. A. Callow, *Biofouling*, 2002, **18**, 251.

37 J. A. Finlay, S. Krishnan, M. E. Callow, J. A. Callow, R. Dong, N. Asgill, K. Wong, E. J. Kramer, and C. K. Ober, *Langmuir*, 2008, **24**, 503.